

GENERAL INFORMATION

The 6th International Symposium on Frontiers in Materials Science (FMS 2022) will be held in Phu Quoc Island, Vietnam, from November 21st to 23rd, 2022. This event, which continues from a delayed FMS 2021 (Hsin-chu, Taiwan, 2021) due to Covid-19, covers a broad range of research activities in all areas of modern materials science.

The FMS 2022 is based on the success of the previous FMS - NANOMATA 2019 in Danang, NANOMATA 2009, 2014 in Hanoi, and FMS 2013, 2015, 2016, 2017 in Hanoi, Tokyo and Greifswald. It is co-organized by the University of Engineering and Technology (Vietnam National University Hanoi), Institute of Physics (Vietnam Academy of Science and Technology), Osaka University, Waseda University, National Yang Ming Chiao Tung University, and Goethe University with participants from Vietnam, Taiwan, South Korea, Japan, US, Germany, and many other countries world-wide.

Among the main supporters and sponsors of this event belong SG Service, Horiba Scientific, Metrohm, Merck, Core, and Zaiken.

The FMS 2022 meeting showcases leading interdisciplinary research in both fundamental and applied fields presented by scientists from around the world. It will be organized as a hybrid symposium with online and offline meetings in parallel, providing possibilities to exchange research ideas, experiences, and results, and promoting the international collaborations in education and research in the fields of:

- Multiferroics and magnetic materials
- Materials for energy and environment
- Photonics and hybrid Materials
- Theory and computation
- Spintronic materials and devices

Symposium venue

The venue is Building A2, in Novotel Phu Quoc Resort, located at Duong Bao Hamlet, Duong To Commune, 922273 Phu Quoc City Kien Giang Province, Vietnam

(<https://goo.gl/maps/gPKg3rBDNPzFWnWj9>)

This site is about 8.2 km far from the Phu Quoc International Airport.

The temperature in November in Phu Quoc is around 30 degrees Celcius.

Manuscript submission and publications

The participants are invited to submit their manuscripts to the following journals:

- Materials Transactions (Q2) journal
- Optical Materials: X (OMX) (Q1) journal

All manuscripts submitted to ISI journal will be peer-reviewed according to the standards applied to the Thompson-Reuters indexing SCI-journals for originality and scientific quality.

The detailed instructions for the manuscript submission can be found at the FMS 2022 website: <http://fms.uet.vnu.edu.vn/submissions.html>

Presentation

All presentations must be in English. The plenary presentations will be limited to 30-minute talk (including 5-minute Q&A). The invited will be limited to 20-minute talk (including

5-minute Q&A) and the oral to 15-minute talk (including 3-minute Q&A). Please contact the Symposium staff before starting each session for using laptop and projectors.

The presentation schedule will be strictly enforced by each session Chair, to allow the audience to switch between sessions.

The poster session begins on Tuesday, November 22nd from 13:30 to 14:30. All posters are requested to be the A1 format and put on each panel from afternoon of November 22nd and removed from the panel before lunch time of November 23rd. The poster frame and tools will be provided at the poster session.

Hotel

Novotel Phu Quoc Resort is the official host location of FMS 2022. We highly recommend this hotel and negotiated a good price for all the participants.

Flights to Phu Quoc

Phu Quoc Airport (PQC) is a medium-sized airport in Vietnam. It is an international airport. In total there are 14 airports around the world that have direct flights to Phu Quoc, spread around 14 cities in 3 countries (Malaysia, Singapore, and Korea). So, for passengers from Japan, Taiwan, the US, Europe, and other countries, you need to use transit flights with at least one stop at Ho Chi Minh City (SGN) or Hanoi (HAN), Vietnam.

Currently, from May 15th, 2022, there are 6 airlines (VietJet Air, Vietnam Airlines, Bamboo Airways, Veca Airlines, Asiana Airlines, and AirAsia) that fly to Phu Quoc.

Visa

Most European countries, the USA, Canada, Japan, Korea, Russia do not need a visa to enter Vietnam for a short period. The Symposium Secretary provides support for the other countries where visa is needed. Please contact the Symposium Secretary at fms2022.phuquoc@gmail.com.

Exhibition

An exhibition of equipment, services, software, materials, journals, and books will be held as a part of the Symposium. The purchasing of space is closed on 10th November 2022. Please contact the Symposium Secretary at fms2022.phuquoc@gmail.com for details and help.

Sponsors

- VNU-University of Engineering and Technology (<https://uet.vnu.edu.vn>)
- VNU-Hanoi University of Science (<https://hus.edu.vn>)
- VAST-Institute of Physics (<https://iop.vast.ac.vn>)
- Scientific Gear Service Co., Ltd. (<https://www.sgservice.com.tw>)
- Horiba Vietnam Co., Ltd. (<https://horiba.com.vn>)
- Metrohm Vietnam Co., Ltd. (<https://metrohm.com>)
- Merck Vietnam Co., Ltd. (<https://www.merck-lifescience.com.vn>)
- Kagami Memorial Research Institute for Materials Science and Technology, Waseda University (<https://www.waseda.jp/fsci/zaiken>)
- “Crystal Defect Core” Project, Nagoya University (<https://www.core.mp.pse.nagoya-u.ac.jp/en>)
- National Yang Ming Chiao Tung University, Taiwan (<https://en.nycu.edu.tw/>)
- Goethe University, Frankfurt, Germany (<https://www.goethe-university-frankfurt.de/>)

Covid-19 Important Note

As released on May 13th, 2022 by Vietnamese Government under the Official Dispatch No. 416/CD-TTg, the travelers to Vietnam (including tourists) DO NOT need to enter any kind of quarantine from May 15th, 2022. All the restrictions are removed.

More detail is in the following links:

<https://www.vietnamairlines.com/fr/en/covid-19/chuan-bi-truoc-chuyen-bay/hanh-trinh-quoc-te>

<https://xuatnhapcanh.gov.vn/en/tin-tuc/notice-7>

Covid-19 Testing Service at Phu Quoc

At International Hospital Vinmec Phu Quoc (35 km from the symposium venue, <https://www.vinmec.com/en/?province-location=phu-quoc>), you can take both COVID-19 RT-PCR test and antigen test services. It is possible for you to take the test from 8 am to 4 pm everyday and receive the PCR test within 24 hours. This could suit your strict timetable, especially when you are in need of a fit-to-fly certificate for departure.

The sample of a Covid-19 test result certificate is shown here:

<http://fms.uet.vnu.edu.vn/documentation/Form%20covid%20PCR.pdf>

Please register using a website (<https://www.vinmec.com/en/?province-location=phu-quoc>) of the hospital or calling +84 297 398 5588.

If you need any help for the Covid-19 Test, please contact the Secretary of Symposium.



Faculty of Engineering Physics and Nanotechnology
University of Engineering and Technology
Vietnam National University, Hanoi



History

1999-2004:

Starting from Dept. Engineering Physics of the Faculty of Technology, Vietnam National University (VNU) in Hanoi.

September 9, 2004:

Faculty of Engineering Physics and Nanotechnology (FEPN) was officially established under the University of Engineering and Technology (UET).

Locations: 144 Xuan Thuy St., Cau Giay Dist., Hanoi, Vietnam

Website: <http://fepn.uet.vnu.edu.vn/>

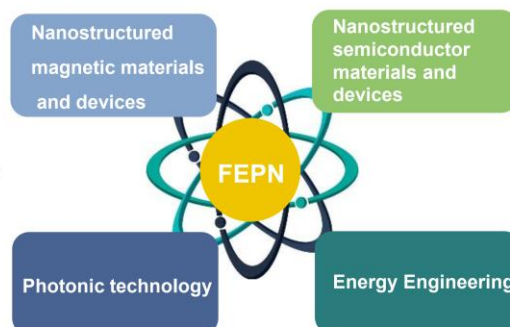
Phone: (024) 3754 9429

Fax: (024) 3754 9429



Organization

Departments



Staffs

- 21 faculties and supporting staffs: 2 full professors, 5 assistant professors, 11 PhD, 5 masters
- 10 adjunct professors from partner institutions.
(*Institute of Materials Science, Institute of Physics, Institute of Chemistry, Institute of Biotechnology, VAST*)



Program

Undergraduate program

Bachelor in Engineering Physics

(4 years): ~ 220 students.

Engineer in Energy Engineering

(4.5 years): ~ 220 students.

Graduate program

Master in Nanomaterials and devices

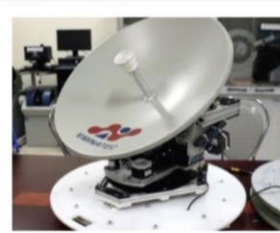
(2 years): ~ 10 students / year

PhD in Nanomaterials and devices

(4 year): ~ 10 students (in total)

Main topics

- Micro-nanostructured magnetic materials and devices.
- Micro-nanostructured semiconductor materials and devices.
- Catalysis materials
- Advanced optoelectronic materials and devices
- Physics of low dimensional systems, computational materials science.
- Photonics and lasers





Faculty of Engineering Physics and Nanotechnology
University of Engineering and Technology
Vietnam National University, Hanoi



Publications

Academic year 2021-2022: ~ 22 ISI/Sopus (> 1.0 / year / faculty).

Selected Publications:

- Nguyen, K.T., Hiep Vuong, V., Nguyen, T.N. et al. Unusual hydrogen implanted gold with lattice contraction at increased hydrogen content. *Nat Commun* 12, 1560 (2021).
<https://doi.org/10.1038/s41467-021-21842-9>
- Nguyen, D.T., Tran, M.D., Van Hoang, T. et al. Experimental and numerical study on photocatalytic activity of the ZnO nanorods/CuO composite film. *Sci Rep* 10, 7792 (2020).
<https://doi.org/10.1038/s41598-020-64784-w>
- D. T. Huong Giang, D. X. Dang, N. X. Toan, N. V. Tuan, A. T. Phung, and N. H. Duc, "Distance magnetic nanoparticle detection using a magnetoelectric sensor for clinical interventions", *Review of Scientific Instruments* 88, 015004 (2017).
<https://doi.org/10.1063/1.4973729>

Labs

- Practical labs. for undergraduate training and research
- Specialized labs. for final-year undergraduate training and research
- Central lab for graduate training and research (*Fabrication and characterization of advanced materials and devices*)
- Sharing facilities of UET, VNU (for IT, electronics practices, library, etc.)



Main facilities

Micro-nano material and device fabrication:

Sputtering systems, electron deposition system, spin coaters, Electrospinning, Langmuir-Blodgett system. Mask aligner, wet bench and fume hood, optical and biological microscopes, multipurpose digital thermosonic wire bonder, multipurpose bonding platform, hot-plate, furnace, and so on.

Micro-nano materials and devices characterisation:

AFM, MFM, SEM, XRD, VSM, MR/GMR and Hall effect systems, ME system. Semiconductor analyzer, UV-Vis, ferroelectric tester, solar simulator, fluorescence, centrifuge, and so on

Cooperation

In Vietnam:

- IMS, IoP, IoC, IBT, IAPSI - Vietnam Academy of Science and Technology
- Lab. for Nanotechnology, Univ. Natural Science (VNU in HCM city)

International:

- France: Univ. Paris-Sud, Néel Institute (*MSc and PhD, staff exchange*)
- Germany: Univ. Göttingen, Frankfurt Univ. (*staff exchange*)
- Japan: JAIST, NAIST, Osaka Univ, Waseda Univ. (*internship, MSc and PhD*);
IMRA Japan Co. Ltd. (*staff exchange*)
- Korea: Pusan Natl. Univ., Chungbuk Natl. Univ., Univ. of Ulsan (*MSc and PhD, staff exchange*)
- Singapore: NUS, NTU (*internship, PhD*)



**Trung tâm Vật lý ứng dụng & Thiết bị khoa học
Viện Vật lý**

PELICAN-VB



Thông số kỹ thuật cơ bản:

- Sải cánh: 2,5m
- Trọng lượng: 10kg (gồm tải có ích)
- Chiều dài: 1,8m
- Trần bay: 2300m
- Bán kính hoạt động (max): 50km; Chịu gió: 14m/s
- Năng lượng: Pin Lipo
- Cất cánh: giàn phóng;
- Hạ cánh: dù (không cần đường băng)

Mô tả sản phẩm

- Quan sát từ trên không ngày và đêm; Đo thám không cho các nghiên cứu khoa học.
- Tuần tra rừng, biển và đường giao thông bao gồm đường bộ, đường thủy.
- Thám không phục vụ cảnh báo thiên tai; Tìm kiếm cứu nạn cứu hộ.
- Tiếp cận những vùng nguy hiểm mà con người không thể vào trực tiếp.



Kagami Memorial Research Institute for Materials Science and Technology, Waseda University, Tokyo, JAPAN

早稲田大学 各務記念材料技術研究所

On October 21, 1938, Kagami Memorial Research Institute for Materials Science and Technology was established as the Casting Research Laboratory—the first laboratory attached to private universities in Japan—by a donation from the prominent business leader, Koichiro Kagami and his son, Yoshiyuki. Until 1980s, the laboratory played an important role both in academic and industrial circles as a unique institute focusing on metal processing such as casting, forging, welding and surface treatment. However, the laboratory had expanded its research field to cover a wider range of materials and in 1988, on the 50th anniversary of its founding, the Casting Research Laboratory was renamed Kagami Memorial Research Institute for Materials Science and Technology (ZAIKEN, which is the abbreviation of its Japanese name).

Since then, researchers studying structural materials and processes, functional materials, material properties, and material design and evaluation have joined ZAIKEN and have enhanced the quality and quantity of the research. Based on the research funding from outside the university, many professors and researchers are conducting various research projects.

ZAIKEN has been (1) acting as a leading academic research hub for fundamental technologies on a wide range of materials; (2) managing a joint use of the equipment for cutting-edge analysis and sample preparation and (3) sharing information and know-how with researchers and engineers in a wide range of material fields and constructing networks. Recently, a variety of global-scale environmental and energy problems have emerged, and solving these problems are advocated in the United Nations' Sustainable Development Goals and the Society 5.0 framework of the Japanese government. We believed that ZAIKEN can substantially contribute to solving these problems through fundamental materials technology, and accordingly, ZAIKEN applied to the program of “Joint Usage/Research Center” by MEXT, Japan, and was accepted and started in April 2018 the “Joint Research Center for Environmentally Conscious Technologies in Materials and Science”.

The objectives of the Joint Research Center for Environmentally Conscious Technologies in Materials and Science are:

- (a) to develop fundamental technology for environmentally conscious materials, to establish scientific principles of environmentally conscious materials, to create innovative environmentally conscious materials, and to incorporate them into society;
- (b) to promote joint research and joint use for researchers in a variety of research fields and to contribute to the development of the material technologies in Japan by providing them with facilities, equipment, and know-how at ZAIKEN.
- (c) to provide researchers in a variety of research fields with academic interaction with other researchers and to promote the fusion of different fields of material technologies.

Open for the international collaboration research

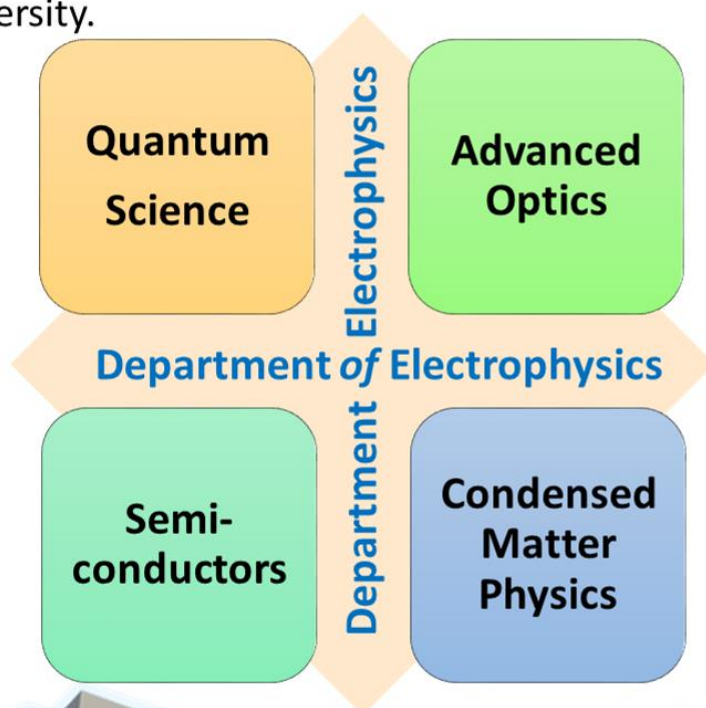
<https://www.waseda.jp/fsci/zaiken/>



國立陽明交通大學 電子物理系 National Yang Ming Chiao Tung University Department of Electrophysics

National Yang Ming Chiao Tung University is a university of academic excellency, global networking, and cultivation of high tech industrial leaders.

Department of Electrophysics was established in 1964, one of the first two departments in the university.



World's top university

Department of Electrophysics:

Faculty Members
32

Jointly Faculty
23

Graduate Students
213

Undergraduate
195



<https://ep.nycu.edu.tw/>

USEFUL FACTS

Airport	Phu Quoc International Airport (Phu Quoc, KienGiang, Vietnam)
Languages	Vietnamese, English can be converse in tourism.
Currency	Dong (VND). 1 US dollar = 24,800 Vietnam Dong (subject to change)
Time zone, dial code	GMT + 7. Press 00 before calling from Vietnam to overseas and Vietnam code is +84
Electricity	2 flat vertical pin or 2 round pin plug, 220 V
Water	It is not advisable to drink water directly from the tap. We recommend you buy bottled drinking water.
Food	Spring Roll (Nem), Soup of Noodle (Phở), Kebab rice noodles (Bún chả), Grilled fish (Chả cá), Snail rice noodles (Bún ốc), fried ground fish noodles (Bun Ken), Crab rice noodles (Bún riêu), Stuffed pancake (Bánh cuốn), Vietnamese crepes (Bánh xèo)
Religions	Majority Buddhism
Shopping	Silk, ceramic, wooden carvings
VAT	10%
Others	Information about tours and sightseeing can be found on the Symposium website

When traveling the 20 km distance from Phu Quoc Airport to Phu Quoc city center and vice versa, you have 2 options: you can take a shuttle bus with fares from 20,000 VND (\$0.80) or a taxi for around 200,000 VND (\$8). Travel time is 10 to 30 minutes, depending on your hotel's location on the island.

About Novotel Phu Quoc Resort

- Address: Duong Bao Hamlet, Duong To Commune, 922273 Phu Quoc City, KienGiang Province, Vietnam

- Tel.: +84 297 626 0999 Fax: +84 297 626 0888

- Website: <https://www.novotelphuquoc.com>

- **Wifi: Free access (no password)**

Banks & Exchange

Banking services on the Phu Quoc Island are concentrated in Duong Dong Town, providing comprehensive services that include cashing of traveler's cheques, currency exchange and ATM machines that are compatible with most international cards (Mastercard, Visa, Cirrus, etc).

- Vietcombank:

Address: No.1 Hung Vuong St., Duong Dong, Phu Quoc

Hours: Mon - Sat: 7am - 11am & 1pm - 4pm

- Kien Long Bank

Address: No.139 30/4 St., Duong Dong, Phu Quoc

Hours: Mon-Fri: 7.30am - 5pm & Sat 7.30am - 12pm

- Agribank*Address:* No. 2, Quarter 2, Tran Hung Dao St., Duong Dong Town,*Hours:* Mon - Fri 7.30am - 11:30am & 1.30pm - 5pm**- Vietinbank***Address:* No.100 30/4 St., Duong Dong, Phu Quoc*Hours:* Mon - Fri 7.30am - 11:30am & 1.30pm - 5pm**- Sacombank***Address:* No.52 30/4 St., Duong Dong, Phu Quoc*Hours:* Mon - Fri 7.30am - 11:30am & 1.30pm - 5pm**- BIDV***Address:* No.196 Nguyen Trung Truc St., Duong Dong, Phu Quoc*Hours:* Mon - Fri 7.30am - 11:30am & 1.30pm - 5pm**Taxi services**

The price ranges from 10,000 to 15,000 VND/km for 4-seaters and 11,000 to 17,000 VND/km for 7-seaters depending on the number of kilometers.

Taxi Mai Linh	Contact: 0297 3 97 97 97
----------------------	--------------------------

Taxi Phu Quoc	Contact: 0297 3 757 575
----------------------	-------------------------

Taxi Sasco	Contact: 0297 3 76 76 76
-------------------	--------------------------

Taxi Saigon Phu Quoc	Contact: 0297 3737 373
-----------------------------	------------------------

Taxi Vinasun Phu Quoc	Contact: 0297 38 27 27 27
------------------------------	---------------------------

Taxi Dang Quang	Contact: 0297 3 789 789
------------------------	-------------------------

Where to Eat?**- Gop Gio Restaurant Phu Quoc***Dishes:* Seafood, beef fried rice*Address:* Block 4-5-7 Phu Quoc Night Market, Bach Dang St., Duong Dong, Phu Quoc*Opening hours:* 5pm - 12am *Price range:* \$4.5 - \$22**- Bun Ken Ut Luom***Dishes:* “Bun Ken” which is a type of mixed noodles topping with fried ground fish, sprouts, chilies, papaya salad, herbs, and a little fish broth*Address:* No.40 30/4 St., Duong Dong, Phu Quoc*Opening hours:* 6am - 10pm *Price range:* \$0.8 - \$1.1**- Khanh Ly Vegetarian Restaurant***Dishes:* Vietnamese style vegan foods*Address:* No. 35 Nguyen Trai St., Duong Dong, Phu Quoc*Opening hours:* 9am - 9pm *Price range:* \$1.5 - \$2.5**- Crab House Phu Quoc***Dishes:* Western-style crab, seafood

Address: No. 26 Nguyen Trai St., Duong Dong Town, Phu Quoc

Opening hours: 11am - 10pm *Price range:* \$4.5 - \$70

- On The Rocks Restaurant

Dishes: European - Asian dishes, tropical fruits, pancakes, wines, cocktails

Address: Mango Bay Resort, Ong Lang Beach, Cua Duong, Phu Quoc

Opening hours: 6.30am - 10.30pm *Price range:* \$4.5 - \$180

- Winston's Burgers Restaurant Phu Quoc

Dishes: Fast-food

Address: No. 121 Tran Hung Dao St., Duong Dong, Phu Quoc

Opening hours: 11am - 9pm *Price range:* \$1.5 - \$16

- Vuon Tao Restaurant

Dishes: Coconut steamed shrimp, herring salad, fried red snapper, mixed hot pot

Address: No.1 Tran Hung Dao St., Cua Lap, Phu Quoc

Opening hours: 9am - 10pm *Price range:* \$6.5 - \$14.5

- Bun Quay Kien Xay

Dishes: Stirred noodles

Address: No.28 Bach Dang St., Duong Dong, Phu Quoc

Opening hours: 7am - 11.45pm *Price range:* \$1.5 - \$2.5

- The Home Pizza Phu Quoc

Dishes: Italian pizzas

Address: No. 127C Tran Hung Dao St., Duong Dong, Phu Quoc

Opening hours: 11am - 22.30pm *Price range:* \$2.5 - \$15

Further information

For additional information, please contact the Symposium Secretary: Faculty of Engineering Physics and Nanotechnology, VNU University of Engineering and Technology, Room 2.2, building E4, 144 Xuan Thuy road, Cau Giay district, Hanoi, Vietnam.

Tel.: +84 24 3754 9429

Hotline: +84 986 370 170

Email: fms2022.phuquoc@gmail.com

Conference website: <http://fms.uet.vnu.edu.vn>

NOVOTEL PHU QUOC RESORT MAP



SYMPOSIUM COMMITTEES

Conference Chairmen

Wu-ching Chou, National Yang Ming Chiao Tung University (Taiwan)

Michael Lang, Goethe University Frankfurt (Germany)

Chairmen of Plenary Session

Masato Yoshiya, Osaka University (Japan)

Nguyen Nang Dinh, VNU-University of Engineering and Technology (Vietnam)

Tomoyuki Yamamoto, Waseda University (Japan)

Hyung Kook Kim, Pusan National University (S. Korea)

Chairmen of Sessions

Andreas Honecker, University Cergy-Pontoise (France)

Huan Tran, Georgia Institute of Technology (United States)

Mikhail Brik, Jan Dlugosz University (Poland)

Michal Piasecki, Jan Dlugosz University (Poland)

Phan The Long, Hankuk University (S. Korea)

Masato Yoshiya, Osaka University (Japan)

Takashi Kimura, Kyushu University (Japan)

Akihide Kuwabara, Japan Fine Ceramics Center (Japan)

Kei Nakayama, Japan Fine Ceramics Center (Japan)

Jenh-Yih Juang, National Yang Ming Chiao Tung University (Taiwan)

Ray-Hua Horng, National Yang Ming Chiao Tung University (Taiwan)

Chun-Liang Lin, National Yang Ming Chiao Tung University (Taiwan)

Chung Li Dong, Tamkang University (Taiwan)

Bach Thanh Cong, VNU-University of Science (Vietnam)

Nguyen Quang Bau, VNU-University of Science (Vietnam)

Ngac An Bang, VNU-University of Science (Vietnam)

Nguyen Kien Cuong, VNU-University of Engineering and Technology (Vietnam)

Nguyen Dinh Lam, VNU-University of Engineering and Technology (Vietnam)

Do Thi Huong Giang, VNU-University of Engineering and Technology (Vietnam)

Bui Dinh Tu, VNU-University of Engineering and Technology (Vietnam)

Vu Ngoc Tuoc, Hanoi University of Science and Technology (Vietnam)

Nguyen Trong Tinh, VAST-Institute of Physics (Vietnam)

Phan Bach Thang, VNU-Ho Chi Minh University of Science (Vietnam)

Vu Thanh Tra, College of Natural Sciences, Can Tho University (Vietnam)

Yoon-Hwae Hwang, Pusan National University (S. Korea)

Way-Faung Pong, Tamkang University (Taiwan)

Jin Young Kim, Ulsan National University (S. Korea)

Tetsuya Yokoi, Nagoya University (Japan)

Bernd Wolf, Goethe University (Germany)

Ho Won Jang, Seoul National University (S. Korea)

Matthijs Jansen, University of Göttingen (Germany)

Kazunori Sato, Osaka University (Japan)

Susumu Fujii, Osaka University (Japan)

Sungkyun Park, Pusan National University (S. Korea)

Thi Ngoc Anh Nguyen, VAST - Institute of Materials Science (Vietnam)

Bae Ho Park, Konkuk university (S. Korea)

Best poster Awards Committee

Yoon-Hwae Hwang (chairman), Pusan National University (S. Korea)

Do Thi Huong Giang, VNU-University of Engineering and Technology (Vietnam)

Nguyen Dinh Lam, VNU-University of Engineering and Technology (Vietnam)

Phan Bach Thang, VNU-Ho Chi Minh University of Science (Vietnam)

Chun-Liang Lin, National Yang Ming Chiao Tung University (Taiwan)

Ray-Hua Horng, National Yang Ming Chiao Tung University (Taiwan)

Chung-Li Dong, Tamkang University (Taiwan)

Susumu Fujii, Osaka University (Japan)

Kei Nakayama, Japan Fine Ceramics Center (Japan)

Tetsuya Yokoi, Nagoya University (Japan)

Jin Young Kim, Ulsan National University (S. Korea)

Ho Won Jang, Seoul National University (S. Korea)

Bernd Wolf, Goethe University (Germany)

Matthijs Jansen, University of Göttingen (Germany)

International Advisory Board

Markus Muenzenberg, Greifswald University (Germany)

Michael Lang, Goethe University Frankfurt (Germany)

Andreas Honecker, University Cergy-Pontoise (France)

Mikhail Brik, Jan Dlugosz University (Poland)

Johan Akerman, Gothenburg University (Sweden)

Ekkes Bruck, Delft University of Technology (Netherlands)

Takashi Kimura, Kyushu University (Japan)

Hirofumi Wada, Kyushu University (Japan)

Tomoyuki Yamamoto, Waseda University (Japan)

Masato Yoshiya, Osaka University (Japan)

Hidekazu Ikeno, Osaka University (Japan)
Yoshitada Morikawa, Osaka University (Japan)
Fumiyasu Oba, Tokyo Institute of Technology (Japan)
Teruyasu Mizoguchi, University of Tokyo (Japan)
Katsuyuki Matsunaga, Nagoya University (Japan)
Wataru Norimatsu, Nagoya University (Japan)
Masashi Akabori, Japan Advance Institute of Science and Technology (Japan)
Dong-Hyun Kim, Chungbuk National University (Korea)
Bae Ho Park, Konkuk University (Korea)
Phan The Long, Hankuk University (Korea)
Sung-lae Cho, University of Ulsan (Korea)
Yong Soo Kim, University of Ulsan (Korea)
Han Young Woo, Pusan National University (Korea)
Wu-ching Chou, National Yang Ming Chiao Tung University (Taiwan)
Edward Yi Chang, National Yang Ming Chiao Tung University (Taiwan)
Shiuan-Huei Lin, National Yang Ming Chiao Tung University (Taiwan)
Jenh-Yih Juang, National Yang Ming Chiao Tung University (Taiwan)
Wen-Bin Jian, National Yang Ming Chiao Tung University (Taiwan)
Shun-Jen Cheng, National Yang Ming Chiao Tung University (Taiwan)
Jen-Sue Chen, National Cheng Kung University (Taiwan)
Jih-Jen Wu, National Cheng Kung University (Taiwan)
Ji-Lin Shen, Chung Yuan Christian University (Taiwan)
Meng-Jiy Wang, National Taiwan University of Science and Technology (Taiwan)
Hoang Nam Nhat, VNU-University of Engineering and Technology (Vietnam)
Nguyen Nang Dinh, VNU-University of Engineering and Technology (Vietnam)
Nguyen Linh Trung, VNU-University of Engineering and Technology (Vietnam)
Bach Thanh Cong, VNU-University of Science (Vietnam)
Ngac An Bang, VNU-University of Science (Vietnam)
Nguyen Trong Tinh, VAST-Institute of Physics (Vietnam)
Vu Ngoc Tuoc, Hanoi University of Science and Technology (Vietnam)
Phan Bach Thang, VNU-Ho Chi Minh University of Science (Vietnam)
Nguyen Thanh Tien, College of Natural Sciences, Can Tho University (Vietnam)
Vu Thanh Tra, College of Natural Sciences, Can Tho University (Vietnam)

Key Scientific Program Committee Members

Masato Yoshiya, Osaka University (Japan)
Tomoyuki Yamamoto, Waseda University (Japan)

Michael Lang, Goethe University (Germany)

Markus Muenzenberg, Greifswald University (Germany)

Wu-Ching Chou, National Yang Ming Chiao Tung University (Taiwan)

Hyung Kook Kim, Pusan National University (Korea)

Vu Ngoc Tuoc, Hanoi University of Science and Technology (Vietnam)

Dinh Van Trung, Vietnam Academy of Science and Technology (Vietnam)

Hoang Nam Nhat, VNU-University of Engineering and Technology (Vietnam)

Bach Thanh Cong, VNU-University of Science (Vietnam)

Program Committee

Chung-Li Dong, Tamkang University (Taiwan)

Chi-Tsu Yuan, Chung Yuan Christian University (Taiwan)

Chu-Shou Yang, Tatung University (Taiwan)

Ching-Shun Ku, National Synchrotron Radiation Research Center-NSRRC (Taiwan)

Chih-Wei Luo, National Yang Ming Chiao Tung University (Taiwan)

Atsushi Yabushita, National Yang Ming Chiao Tung University (Taiwan)

Chun-Liang Lin, National Yang Ming Chiao Tung University (Taiwan)

Nguyen Nang Dinh, VNU-University of Engineering and Technology (Vietnam)

Nguyen The Toan, VNU-University of Science (Vietnam)

Local Organizing Committee

Hoang Nam Nhat, VNU-University of Engineering and Technology (Head)

Tomoyuki Yamamoto, Waseda University (Co-Head)

Bui Dinh Tu, VNU-University of Engineering and Technology (Depute Head)

Nguyen Dinh Lam, VNU-University of Engineering and Technology

Le Viet Cuong, VNU-University of Engineering and Technology

Nguyen The Toan, VNU-University of Science

Ngac An Bang, VNU-University of Science

Vu Ngoc Tuoc, Hanoi University of Science and Technology

Nguyen Trong Tinh, VAST-Institute of Physics

Vu Thanh Tra, College of Natural Sciences, Can Tho University

Secretariat

Bui Dinh Tu, VNU-University of Engineering and Technology (Head)

Nguyen Dinh Lam, VNU-University of Engineering and Technology

Nguyen Duc Cuong, VNU-University of Engineering and Technology

Le Viet Cuong, VNU-University of Engineering and Technology (Webmaster)

Nguyen Tuan Canh, VNU-University of Engineering and Technology (Foreign Affairs)

Nguyen Huy Tiep, VNU-University of Engineering and Technology

Nguyen Thanh Tung, VNU-University of Engineering and Technology

Tran Thi Nguyet, VNU-University of Engineering and Technology

Vuong Van Hiep, VNU-University of Science Financial Secretary

Map of Conference Rooms

Notations for Posters

EE 1 : EE-P01 → EE-P13

EE 2 : EE-P14 → EE-P26

EE 3 : EE-P27 → EE-P30

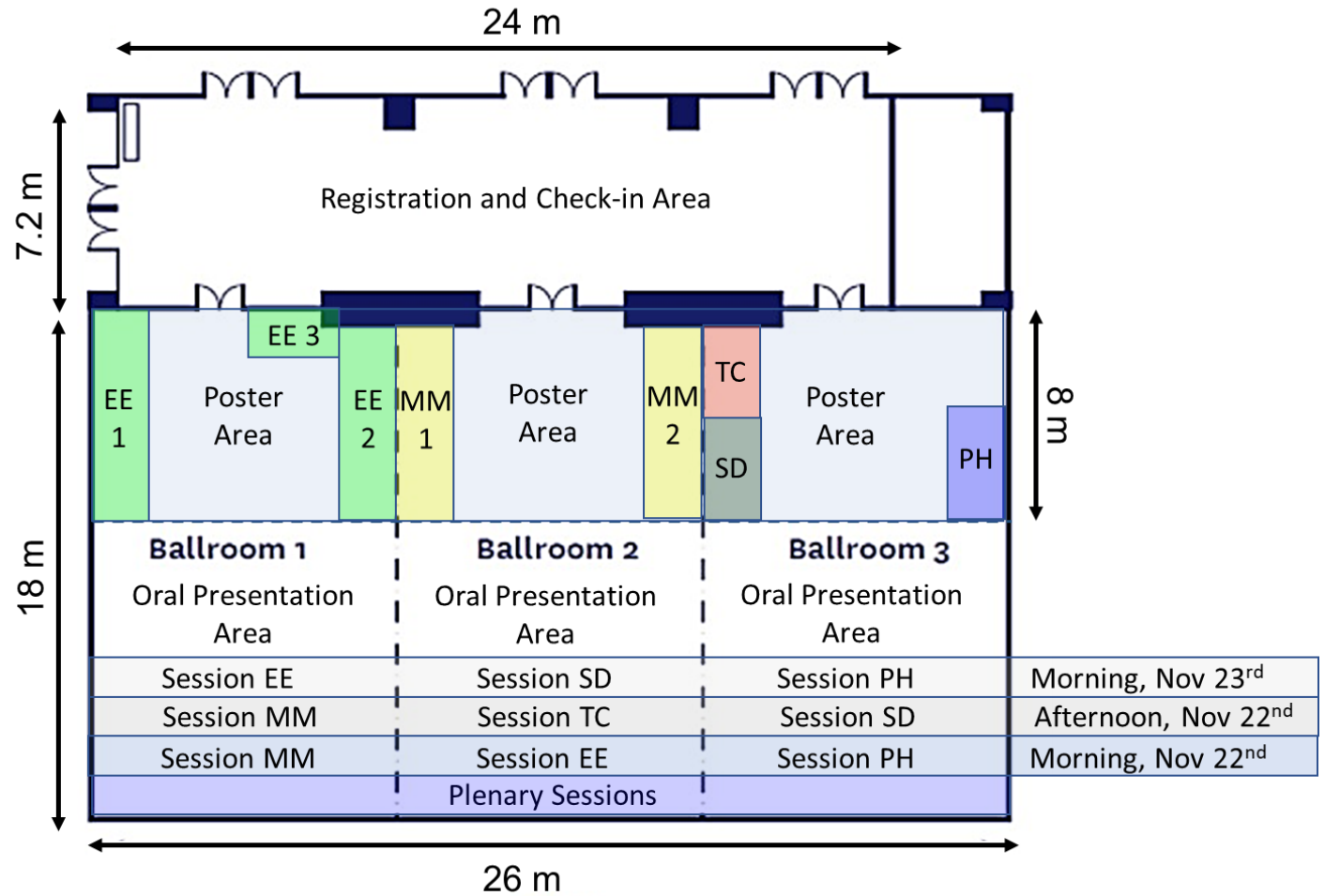
MM 1 : MM-P01 → MM-P14

MM 2 : MM-P15 → MM-P30

TC : TC-P01 → TC-P07

PH : PH-P01 → PH-P07

SD : SD-P01 → SD-P09



PROGRAM TIME TABLE

Day 1 (21/11/2022)	Arrivals at the Conference Venue
13:00 - 17:00	<ul style="list-style-type: none"> ▪ Registration ▪ Meeting of the International Advisory Board and the Key Scientific Program Committee
18:00 - 20:00	Welcome party for Invited speakers and International Advisory Board
Day 2 (22/11/2022)	Conference (1/2)
8:00 - 8:30	Registration
8:30 - 9:00	<p>Opening ceremony Chairmen: Wu-Ching Chou, Michael Lang</p> <ul style="list-style-type: none"> ▪ Sponsors remarks: 8:30 - 8:40: Nguyen Dang Khoa, Energy and Environment – LiB applications with PSA and XGT, Horiba Viet Nam ▪ Organizers remarks 8:40 - 8:50: Nguyen Huu Duc ▪ Keynote speeches by Chairmen 8:50 - 9:00: Wu-Ching Chou, Michael Lang
	Opening Plenary Session Chairmen: Masato Yoshiya, Nguyen Nang Dinh
9:00 - 9:30	<p>Plenary talk <u>PL1</u> <i>Akihide Kuwabara</i> <i>Japan Fine Ceramics Center</i> First-principles calculations of defect formation behavior and ion dynamics in solid state ionics materials</p>
9:30 - 10:00	<p>Plenary talk <u>PL2</u> <i>Yoon-Hwae Hwang, Hyung-Kook Kim and Dong-Myeong Shin</i> <i>Pusan National University</i> Nanogenerators: self-powered energy for technology innovation</p>

10:00 - 10:30	<p>Plenary talk PL3 Cancel <i>Nguyen The Toan</i> VNU University of Science Molecular understanding of protein structure and interaction related to Covid-19 and gout diseases by using computational biophysics</p>		
10:30 - 11:00	<p>Coffee break (1/3) Group photographs/photography of participant</p>		
11:00 - 12:30	Parallel sessions 1 (15)		
Time	<p>Section MM Multiferroics and magnetic materials (1/3) Chairmen: Bach Thanh Cong, Jehn Yih Juang</p>	<p>Section EE Materials for energy and environment (1/2) Chairmen: Yoon-Hwae Hwang, Masato Yoshiya</p>	<p>Section PH Photonics and Hybrid Materials (1/2) Chairmen: Mikhail Brik, Way-Faung Pong</p>
11:00 - 11:20	<p>MM-I01 (Invited) <i>Michael Lang, Christian Thurn, Paul Eibisch, et al.</i> PbCuTe₂O₆ – a quantum spin liquid candidate showing ferroelectric order close to a quantum critical point</p>	<p>EE-I01 (Invited) <i>Nguyen Hoang Nam, Do Quang Loc, Phi Thi Huong et al.</i> CD4⁺ T cell counting using anti-CD4 antibody conjugated magnetic nanoparticles and microfluidic counter</p>	<p>PH-I01 (Invited) <i>Tomoyuki Yamamoto</i> Local environment of emission center ions in phosphor materials</p>
11:20-11:40	<p>MM-I02 (Invited) <i>Yoshifuru Mitsui and Keiichi Koyama</i> Application of magnetic field for selective reaction in magnetic alloys</p>	<p>EE-I02 (Invited) <i>Kei Nakayama, Ryo Ishikawa and Yuichi Ikuhara</i> Structural analysis of battery materials by atomic-resolution scanning transmission electron microscopy</p>	<p>PH-I02 (Invited) <i>Michal Piasecki, Galyna Muronchuk, Andrzej Suchocki et al.</i> Luminescence and non-linear optical properties at mid-infrared spectral range</p>
11:40-12:00	<p>MM-I03 (Invited) <i>Hajime Yamamoto</i> Crystal structures and electronic properties of vanadium oxides</p>	<p>EE-I03 (Invited) <i>Ho Won Jang</i> Si-based photoelectrodes for water splitting</p>	<p>PH-I03 (Invited) <i>Huu-Quang Nguyen, My-Chi Nguyen and Jaebeom Lee</i> Magnetoplasmonic core-shell nanowires: synthesis and self-assembly for structural colors and chiral metasurfaces</p>

12:00-12:15	MM-O01 (Oral) <i>Jiunn-Yuan Lin</i> An emergent quasi-2D metallic state derived from the Mott insulator framework		EE-O01 (Oral) <i>Thi Thao Vu, Xuan Tung Nguyen, Dinh Tu Bui, et al.</i> Review of Langmuir-Blodgett films of octadecylamine: Fabrication, properties, and application		PH-O01 (Oral) <i>Viet Tuyen Nguyen, Thi Ha Tran, Van Tan Tran, et al.</i> Boosting surface enhanced Raman scattering from ZnO/Au nanorods by UV excitation
12:15-12.30	MM-O02 (Oral/Online) <i>Yoyo Hinuma</i> Deriving maximally orthogonalized supercells with given size		EE-O02 (Oral) <i>My-Chi Nguyen, Huu-Quang Nguyen and Jaebeom Lee</i> Lanthanide-based magnetoplasmonic probes for highly sensitive aqueous copper(II) sensing		PH-O02 (Oral) <i>Chia-Chun Wei, Tung-Han Wu and Wen-Bin Jian</i> Preparation of nanoparticulate WO ₃ /MoO ₃ films for making electrochromic devices
12:30 - 13:30	Lunch				
13:30 - 14:30	Poster sessions Note: (i) All posters are requested to be in the A1 format; (ii) to be put on each panel from afternoon of Nov 21 st and (iii) removed from the panel before lunch time of Nov 23 rd				
- Best posters: 02 - Silver: 03 - Bronze: 05	Section EE Materials for energy and environment <i>Chairmen: Nguyen Dinh Lam, Chun-Liang Lin, Jin Young Kim</i> <i>Codes: EE-P01 - EE-P30</i> <i>Location: Ballroom 1</i>	Section MM Multiferroics and magnetic materials <i>Chairmen: Phan Bach Thang, Chung-Li Dong, Tetsuya Yokoi</i> <i>Codes: MM-P01 - MM-P30</i> <i>Online: MM-P01, P03, P08, P09, P13, P15</i> <i>Location: Ballroom 2</i>	Section SD Spintronic materials and devices <i>Chairman: Do Thi Huong Giang, Bernd Wolf</i> <i>Codes: SD-P01 - SD-P09</i> <i>Location: Ballroom 3</i>	Section PH Photonics and Hybrid Materials <i>Chairman: Nguyen Kien Cuong, Ho Won Jang</i> <i>Codes: PH-P01 - PH-P07</i> <i>Location: Ballroom 3</i>	Section TC Theory and computation <i>Chairman: Nguyen Quang Bau, Matthijs Jansen</i> <i>Codes: TC-P01 - TC-P07</i> <i>Location: Ballroom 3</i>
	Best poster Awards Committee - Chairman: Prof. Yoon-Hwae Hwang - Members: Do Thi Huong Giang, Nguyen Dinh Lam, Phan Bach Thang, Chun-Liang Lin, Ray-Hua Horng, Chung-Li Dong, Susumu Fujii, Kei Nakayama, Tetsuya Yokoi, Jin Young Kim, Ho Won Jang, Bernd Wolf, Matthijs Jansen				

14:30 - 16:30	Parallel sessions 2 (18)		
Time	Section MM Multiferroics and magnetic materials (2/3) Chairmen: Kazunori Sato, Ray-Hua Horng	Section TC Theory and computation (1/2) Chairmen: Vu Ngoc Tuoc, Susumu Fujii	Section SD Spintronic materials and devices (1/3) Chairmen: Takashi Kimura, Sungkyun Park
14:30-14:50	MM-I04 (Invited) <i>Jeehoon Kim</i> Anomalous transport properties in a Weyl metal	TC-I01 (Invited) <i>Andreas Honecker</i> Thermodynamic properties of the Shastry-Sutherland model for SrCu ₂ (BO ₃) ₂	SD-I01 (Invited) <i>Wataru Norimatsu</i> Observation of flat band in millimeter-scale magic-angle twisted bilayer graphene
14:50-15:10	MM-I05 (Invited) <i>Bernd Wolf, Felix Spathelf, Jan Zimmermann et al.</i> Tuning the ground state of strongly correlated EuPd ₂ (Si _{1-x} Ge _x) ₂ using He-gas pressure	TC-I02 (Invited) <i>Koun Shirai</i> The Activation Energy of Glass Transition	SD-I02 (Invited) <i>Chanyong Hwang</i> Towards Magnetic Skyrmionics
15:10-15:30	MM-I06 (Invited) <i>Ivan Skorvanek, Branislav Kunc, Jozef Marcin et al.</i> Soft magnetic Fe(Co)-based high Bs nanocrystalline alloys for applications at elevated temperatures	TC-I03 (Invited) <i>Masato Yoshiya, Tomofumi Hara, Wataru Sekimoto et al.</i> Selective control of propagation-conduction of two different quantum waves by lattice imperfections: electrons and phonons	SD-I03 (Invited) <i>Bae Ho Park</i> Neuromorphic devices based on electrochemical metallization and charge trapping
15:30-15:50	MM-I07 (Invited) <i>Way-Faung Pong</i> X-ray spectro- and microscopic-techniques on novel materials	TC-I04 (Invited / Online) <i>Manh-Thuong Nguyen</i> Computational approaches to study heavy element materials	SD-I04 (Invited) <i>Teruo Ono</i> Superconducting diode effect in Rashba superlattice
15:50-16:10	MM-I08 (Invited) <i>Tahta Amrillah, My Ngoc Duong and Jenh-Yih Juang</i>	TC-I05 (Invited) <i>Tatsuya Yokoi, Yu Oshima and Katsuyuki Matsunaga</i>	SD-I05 (Invited / Online) <i>Takeshi Seki</i> Enhanced anomalous Nernst effect in metallic superlattices

	Substrate polarity, phase stability, electronic structure and magnetic properties of multiferroic YMnO ₃ thin films	Artificial-neural-network descriptor and interatomic potential for molecular simulations of lattice defects	
16:10-16:30	MM-I09 (Invited) <i>Masanobu Shiga, Takurou Harada, Tsubasa Teramoto et al.</i> Point contact Andreev reflection spectroscopy on topological Kondo insulator SmB ₆	TC-O01 (Oral) <i>Katsuhiro Suzuki, Takao Kotani and Kazunori Sato</i> The first-principles analysis of multiplet excitations using QSGW	SD-I06 (Invited) <i>Hieu Ho, Hai Hoang, Minh-Hanh Pham and Hai Tran</i> Extended X-ray absorption spectroscopy and Debye–Waller factor under pressure
16:30 - 16:45	Coffee break (2/3)		
16:50 - 18:30	Parallel sessions 3 (21)		
Time	Section MM Multiferroics and magnetic materials (3/3) Chairmen: Kei Nakayama, Thi Ngoc Anh Nguyen	Section TC Theory and computation (2/2) Chairmen: Tatsuya Yokoi, Vu Thanh Tra	Section SD Spintronic materials and devices (2/3) Chairmen: Nguyen Trong Tinh, Bae Ho Park
16:50-17:10	MM-I10 (Invited) <i>Sungkyun Park and Sehwan Song</i> Searching for the origin of magnetic inhomogeneity of FeRh film	TC-I06 (Invited) <i>Tien Quang Nguyen, Yusuke Nanba, Michihisa Koyama et al.</i> Accelerating materials discovery using universal neural network potential and ab-initio calculations	SD-I07 (Invited) <i>Ray Hua Horng</i> Material properties and growth mechanism of β -Ga ₂ O ₃ epilayers grown on sapphire by metal organic chemical vapor deposition
17:10-17:30	MM-I11 (Invited) <i>Yoshishige Suzuki, Soma Miki, Ryo Ishikawa et al.</i> Magnetic skyrmion for the Brownian computing	TC-I07 (Invited) <i>Susumu Fujii, Yuta Shimizu, Junji Hyodo et al.</i> Exploration for non-perovskite proton-conducting oxides using high-throughput computation and machine learning	SD-I08 (Invited/Online) <i>Masashi Akabori</i> Fabrication of quantum devices by fine sputtering using a focused ion beam with nitrogen gas field ion source

17:30-17:45	MM-O03 (Oral) <i>Yuichi Okazaki, Yushi Fujita, Hidenobu Murata et al.</i> Bayesian optimization design of high entropy oxide for oxygen evolution catalysis	TC-I08 (Invited) (17:30-17:50) <i>Kazunori Sato, Genta Hayashi, Kazuma Ogushi et al.</i> Computational materials design of high-entropy alloys based on FPKKR-CPA calculations and machine learning techniques	SD-O01 (Oral) <i>Ngoc Nam Ho, Katsuhiro Suzuki, Akira Masago et al.</i> Solid-liquid structure of Cu ₂ S: theoretical acanthite-like model for electronic and transport properties investigations
17:45-18:00	MM-O04 (Oral) <i>Ba Hung Tran and Yu-ichiro Matsushita</i> Magnetocaloric effect from first-principles calculations and Monte Carlo simulations	TC-I09 (Invited) (17:50-18:10) <i>Huan Tran</i> Accelerating materials science with artificial intelligence	SD-O02 (Oral) <i>Shiuanhuei Lin, Stefan Petrov and Vera Marinova</i> Graphene supported liquid crystal phase retarders on rigid glass and flexible polydimethylsiloxane substrates
18:00-18:15	MM-O05 (Oral) <i>Phi Thi Huong, Bui Duc Tri, Nguyen Thi Thanh Van et al.</i> Synthesis of bifunctional magnetic-plasmonic Fe ₃ O ₄ @SiO ₂ -Au nanoparticles by an ultrasound assisted chemical method	TC-I10 (Invited) (18:10-18:30) <i>Hirofumi Tanaka</i> Material intelligence: in-materio reservoir computing devices composed by random network of nanoparticles	SD-O03 (Oral) <i>Chung Li Dong</i> Advantages, Challenges and Opportunities of X-ray Absorption spectroscopy for advanced investigation of energy materials
18:15-18:30	MM-O06 (Oral) <i>Nguyen Duy Thien, Nguyen Quang Hoa, Vuong Van Hiep et al.</i> Thermal evaporation synthesis and some properties of WO ₃ /ITO electrochromic thin films		SD-O04 (Oral) <i>Canh Tuan Nguyen, Nam Nguyen Phuong Hoai, Cuong Nguyen Duc et al.</i> Fabricate electrospun nanofiber for rechargeable batteries
18:30-18:45	MM-O07 (Oral) <i>Thi Van Anh Nguyen and Duong Vu</i> Fabrication of RuO ₂ thin film for spin orbit torque – induced magnetization switching	TC-O02 (Oral) <i>Sena Hoshino, Yu Oshima, Tatsuya Yokoi et al.</i> Carrier-trapping induced transformation of dislocation core structures in Zn compounds	SD-O05 (Oral) <i>Minh Nhat Dang, Surinder Singh, Thomas G. Pattison, et al.</i> Is it possible to electropolish tungsten carbides?

19:30-21.30	Banquet		
Day 3 (23/11/2022):	Conference (2/2)		
08:00 - 09:45	Parallel sessions 4 (18)		
Time	Section EE Materials for energy and environment (2/2) Chairmen: Yoon-Hwae Hwang, Akihide Kuwabara	Section SD Spintronic materials and devices (3/3) Chairmen: Bui Dinh Tu, Huan Tran	Section PH Photonics and Hybrid Materials (2/2) Chairmen: Michal Piasecki, Ngac An Bang
08:00-08:20	EE-I04 (Invited) <i>Jessiel Siaron Gueriba, Nur Ellina Annisa Salehuddin, Wilson Agerico Dino et al.</i> Defluorination and adsorption of tetrafluoroethylene (TFE) on TiO ₂ (110) and Cr ₃ O ₃ (0001)	SD-I09 (Invited/Online) <i>Takashi Kimura</i> Study of nano-scale heat transports using magneto-thermoelectric effects	PH-I04 (Invited) <i>Jin Young Kim</i> High-performance colorful semitransparent organic solar cells with etalon electrodes
08:20-08:40	EE-I05 (Invited) <i>Moongyu Jang</i> Single cell capacitance measurement of NIH 3T3 cell using impedance biosensor	SD-I10 (Invited/Online) <i>Tho Duc Nguyen</i> Sub-second and ppm-level optical sensing of hydrogen using templated control of nano-hydride geometry and magnetic composition	PH-I05 (Invited) <i>Matthijs Jansen</i> Probing the exciton wavefunction in low-dimensional materials by photoemission momentum microscopy
08:40-08:55	EE-O03 (Oral) <i>Cong Doanh Sai, Van-Phu Vu, Viet Tuyen Nguyen et al.</i> Fast synthesis of ZnO/Ag heterostructure nanoparticles for enhanced photocatalytic	SD-O06 (Oral) <i>Tan Le Hoang Doan</i> Tandem cyclooxidative reaction of anthranilamide and alcohols over Fe(III)-based MOFs: effect of structure on catalytic efficiency	PH-O03 (Oral) <i>Chun-Liang Lin</i> Studying Defects in TMD Materials and Devices by STM

08:55-09:10	EE-O04 (Oral) Pham Ngoc Thanh, Yuji Hamamoto, Kouji Inagaki et al. Van der Waals density functional study of NO-H ₂ O coadsorption on Cu(111)	SD-I11 (Invited) Thi Ngoc Anh Nguyen, Quang Ngan Pham, Van Thanh Chu et al. Detection of weak, low-frequency magnetic field using single nanoscale MgO magnetic tunnel junctions	PH-O04 (Oral) Heongkyu Ju, Saikiran Kosame, Than Thi Nguyen and Jun-Ho Lee Abnormal spectral shift of surface plasmon resonance
09:10-09:30	EE-I06 (Invited) Ngoc Dinh Nguyen, Vinh Thang Tran, Van Thanh Pham et. al Development of a 3D bio-printing system for tubular tissue creation using umbilical cord-derived stem cell spheroids as bio-ink	SD-I12 (Invited) Dang Ngoc Toan Neutron diffraction study of state-of-the-art 2D materials	PH-I06 (Invited) Cancel Nguyen Thanh Tung Metamaterials: plasmonic properties, ultrafast dynamics, heat transfer, and tuneability
09:30-09:45	EE-O05 (Oral) Ngo Tran, Ruey-Bin Yang and B. W. Lee Development of high-efficient multi-layer microwave absorbers using Co-doped BaMnFe ₁₁ O ₁₉ nanoparticles	SD-O07 (Oral) Thi Thuy Nguyen, Tatsuaki Hirata and Shin-Ichiro Kuroki Nanowire single crystal grain field effect transistors and their applications	PH-O05 (Oral) Der-Hsien Lien Electronics and optoelectronics of atomically thin semiconductors
09:45 - 10:15	Coffee break (3/3)		
	Closing Plenary Session Chairmen: Tomoyuki Yamamoto, Hyung Kook Kim		
10:15 - 10:45	Plenary talk PL4 Ssu Kuan Wu, Nhu Quynh Diep, Hua Chiang Wen, Wu-Ching Chou and Thanh Tra Vu <i>National Yang Ming Chiao Tung University</i> Growth dynamics and physical properties of III-VI two dimensional semiconductors grown by molecular beam epitaxy		
10:45 - 11:15	Plenary talk PL5 Ekkas Bruck <i>Delft University of Technology</i> Fe ₂ P type alloys: an intriguing magnetic playground		

11:15 - 11:45	<p>Plenary talk PL6 <i>Mikhail Brik</i> <i>Jan Dlugosz University, Poland</i> Optical and electronic properties of crystalline solids from the first-principles and semiempirical methods</p>
11:45 - 12:00	<p>Final remarks Chairmen: Wu-Ching Chou, Michael Lang - Introduction of the next FMS - Publication notes: available journals, manuscript submission deadlines</p>
Conference closes	

TABLE OF CONTENTS

Code	Type	Room	Presenter	Title	Page
Sponsor-01	Sponsor	Grand Ballroom	Dang Khoa Nguyen	Particle size analysis & X-ray fluorescence analysis in Li-battery materials	43
PL1	Plenary	Grand Ballroom	Akihide Kuwabara	First-principles calculations of defect formation behavior and ion dynamics in solid state ionics materials	44
PL2	Plenary	Grand Ballroom	Yoon-Hwae Hwang	Nanogenerators: self-powered energy for technology innovation	45
PL3 Cancel	Plenary	Grand Ballroom	Nguyen The Toan	Molecular understanding of protein structure and interaction related to Covid-19 and Gout diseases by using computational biophysics	46
PL4	Plenary	Grand Ballroom	Wu-Ching Chou	Growth dynamics and physical properties of III-VI two dimensional semiconductors grown by molecular beam epitaxy	47
PL5	Plenary	Grand Ballroom	Ekkas Bruck	Fe ₂ P type alloys an intriguing magnetic playground	48
PL6	Plenary	Grand Ballroom	Mikhail Brik	Optical and electronic properties of crystalline solids from the first-principles and semiempirical methods	49
EE-I01	Invited	Ballroom 2	Nguyen Hoang Nam	CD4 ⁺ T cell counting using anti-CD4 antibody conjugated magnetic nanoparticles and microfluidic counter	50
EE-I02	Invited	Ballroom 2	Kei Nakayama	Structural analysis of battery materials by atomic-resolution scanning transmission electron microscopy	51
EE-I03	Invited	Ballroom 2	Ho Won Jang	Si-based photoelectrodes for water splitting	52
EE-I04	Invited	Ballroom 1	Wilson Agerico Dino	Defluorination and adsorption of tetrafluoroethylene (TFE) on TiO ₂ (110) and Cr ₂ O ₃ (0001)	53

Code	Type	Room	Presenter	Title	Page
EE-I05	Invited	Ballroom 1	Moongyu Jang	Single cell capacitance measurement of NIH 3T3 cell using impedance biosensor	54
EE-I06	Invited	Ballroom 1	Ngoc Dinh Nguyen	Development of a 3D bio-printing system for tubular tissue creation using umbilical cord-derived stem cell spheroids as bio-ink	55
EE-O01	Oral	Ballroom 2	Thi Thao Vu	Review of Langmuir-Blodgett films of octadecylamine: Fabrication, properties, and application	95
EE-O02	Oral	Ballroom 2	My-Chi Nguyen	Lanthanide-based magnetoplasmonic probes for highly sensitive aqueous Copper(II) sensing	96
EE-O03	Oral	Ballroom 1	Cong Doanh Sai	Fast synthesis of ZnO/Ag heterostructure nanoparticles for enhanced photocatalytic	97
EE-O04	Oral	Ballroom 1	Ngoc Thanh Pham	Van der Waals density functional study of NO-H ₂ O coadsorption on Cu(111)	98
EE-O05	Oral	Ballroom 1	Ngo Tran	Development of high-efficient multi-layer microwave absorbers using Co-doped BaMnFe ₁₁ O ₁₉ nanoparticles	99
EE-P01	Poster	Ballroom 1	Sohwi Kim	Progressive and stable synaptic plasticity with attojoule energy consumption by the interface engineering of a metal/ferroelectric	121
EE-P02	Poster	Ballroom 1	Anh-Quan Hoang	Silver nanoparticles synthesis using chromolaena odorata (L.) Extract in thermosensitive polymer solutions and evaluation of wound healing capability	122
EE-P03	Poster	Ballroom 1	Cong Doanh Sai	Construction of highly condensed Cu ₂ O/CuO composites on Cu sheet and its photocatalytic in photodegradation of hazardous colouring agent rose bengal	123
EE-P04	Poster	Ballroom 1	Tran Cong Thang	Chemical expansivity and oxygen transport in oxide perovskite ceramics	124

Code	Type	Room	Presenter	Title	Page
EE-P05	Poster	Ballroom 1	Linh Ho Thuy Nguyen	Zr and Hf-based metal-organic frameworks used as efficient heterogeneous catalysts for the synthesis of heterocyclic compounds	125
EE-P06	Poster	Ballroom 1	Nam-Nhat Hoang	Modeling inductance of a coil dipping in solution	126
EE-P07	Poster	Ballroom 1	Thi Thao Vu	The Langmuir-Blodgett and Langmuir-Schaefer film of stearic acid: preparation and characterization	127
EE-P08	Poster	Ballroom 1	Thi Thuong Huyen Tran	Preparation, photocatalytic degradation of pollutants and self-cleaning performance of TiO ₂ based-nanomaterials (TiO ₂ , TiO ₂ -ZnO, TiO ₂ -Au)	128
EE-P09	Poster	Ballroom 1	Thi Phuong Thao Ha	Application of SiO ₂ nano-spheres embedded in polypropylene matrix for the analytical blood filtering processes	129
EE-P10	Poster	Ballroom 1	Son Thanh Bach	Effects of surfactants on dispersion of expanded graphite in polyurethane foam	130
EE-P11	Poster	Ballroom 1	Huong Le Thi Thu	Study and characterization of betulin encapsulated by liquid compounds to improve its solubility in water	131
EE-P12	Poster	Ballroom 1	Ngoc Quang Tran	Coupling amorphous Ni hydroxide nanoparticles with single atom Rh on Cu nanowire arrays for highly efficient alkaline seawater electrolysis	132
EE-P13	Poster	Ballroom 1	Lieu Nguyen	Pre-irradiation-induced grafting acrylamide onto polypyrrolidone matrix and evaluating combined copolymers with graphene oxide for high-temperature offshore oilfield application	133
EE-P14	Poster	Ballroom 1	Nguyen Dang Phu	Synthesis of cobalt sulfide nanopowders for non-enzyme urea sensors	134
EE-P15	Poster	Ballroom 1	Tinh Nguyen Trong	Evaluation of antioxidant capacity by in vitro methods for some biologically-active natural compounds	135
EE-P16	Poster	Ballroom 1	Thi Thao Vu	Nanostructured stable floating layers and Langmuir-Schaefer films of 5,10,15,20-tetraphenylporphine	136

Code	Type	Room	Presenter	Title	Page
EE-P17	Poster	Ballroom 1	Nguyen Tran Truc Phuong	Sensitive detection of rhodamine B (RhB) in condiments using surface-enhanced Raman scattering (SERS) silver particles as substrate	137
EE-P18	Poster	Ballroom 1	Thi Thao Vu	Effect of glycerol, gelatin and stearic acid on physical and mechanical properties of native cassava starch thin film	138
EE-P19	Poster	Ballroom 1	Manh Quynh Luu	Size sorting and hydrophilic functionalization of fly ash from a thermal power plant toward to latent fingerprint development	139
EE-P20	Poster	Ballroom 1	Van Tan Tran	Active colloidal photonic arrays of Ag@Fe ₃ O ₄ nanoparticles as colorimetric sensing platforms for on-site environmental and food safety monitoring	140
EE-P21	Poster	Ballroom 1	Viet Tuyen Nguyen	Preparation and characterisitics of SnO ₂ nanomaterials by Joule heating effect	141
EE-P22	Poster	Ballroom 1	Dang Thi My Nga	Cu-doped effect on structural and optical properties of ZnO nanoparticles towards the application of maize growth	142
EE-P23	Poster	Ballroom 1	Viet Tuyen Nguyen	Preparation and characterisitics of CuO nanowires by Joule heating effect	143
EE-P24	Poster	Ballroom 1	Kazuma Midorikawa	Corrosion evaluation of carbonate apatite-coated pure magnesium by electrochemical measurement	144
EE-P25	Poster	Ballroom 1	Trung Thanh Le	SVM based-metal ion detection and identification in contaminated water sources	145
EE-P26	Poster	Ballroom 1	Ngoc Xuan Dat Mai	Biodegradable periodic mesoporous phenylene and tetrasulfide-based organosilica nanoparticles for controlled release of chemotherapeutic drug	146
EE-P27	Poster	Ballroom 1	Thi Thao Vu	Thin films of triphenylcorrole: Fabrication methods, properties, and their potential applications in the fields of sensing and catalysis	147

Code	Type	Room	Presenter	Title	Page
EE-P28	Poster	Ballroom 1	Nguyen Thi Mai Huong	Evaluation of stability and in vitro anticancer activity of dihydroquercetin nanoemulsion	148
EE-P29	Poster	Ballroom 1	Manh Quynh Luu	A novel water-ethanol based modified inverse emulsion method for nanoparticles silica-coating in Si QDs/SiO ₂ and NiFe ₂ O ₄ /SiO ₂ core-shell submicron spheres synthesis	149
EE-P30	Poster	Ballroom 1	Viet Cuong Le	Arrays of Nd ₂ Fe ₁₄ B clusters in PDMS background used to levitate human cells	150
MM-I01	Invited	Ballroom 1	Michael Lang	PbCuTe ₂ O ₆ – a quantum spin liquid candidate showing ferroelectric order close to a quantum critical point	56
MM-I02	Invited	Ballroom 1	Yoshifuru Mitsui	Application of magnetic field for selective reaction in magnetic alloys	57
MM-I03	Invited	Ballroom 1	Hajime Yamamoto	Crystal structures and electronic properties of vanadium oxides	58
MM-I04	Invited	Ballroom 1	Jecheon Kim	Anomalous transport properties in a Weyl metal	59
MM-I05	Invited	Ballroom 1	Bernd Wolf	Tuning the ground state of strongly correlated EuPd ₂ (Si _{1-x} Ge _x) ₂ using He-Gas pressure	60
MM-I06	Invited	Ballroom 1	Ivan Skorvanek	Soft magnetic Fe(Co)-based high Bs nanocrystalline alloys for applications at elevated temperatures	61
MM-I07	Invited	Ballroom 1	Way-Faung Pong	X-ray spectro- and microscopic-techniques on novel materials	62
MM-I08	Invited	Ballroom 1	Jenh-Yih Juang	Substrate polarity, phase stability, electronic structure and magnetic properties of multiferroic YMnO ₃ thin films	63
MM-I09	Invited	Ballroom 1	Masanobu Shiga	Point contact Andreev reflection spectroscopy on topological Kondo insulator SmB ₆	64
MM-I10	Invited	Ballroom 1	Sungkyun Park	Searching for the origin of magnetic inhomogeneity of FeRh film	65

Code	Type	Room	Presenter	Title	Page
MM-I11	Invited	Ballroom 1	Yoshishige Suzuki	Magnetic skyrmion for the Brownian computing	66
MM-O01	Oral	Ballroom 1	Jiunn-Yuan Lin	An emergent quasi-2D metallic state derived from the Mott insulator framework	100
MM-O02	Oral	Ballroom 1	Yoyo Hinuma	Deriving maximally orthogonalized supercells with given size	101
MM-O03	Oral	Ballroom 1	Yuichi Okazaki	Bayesian optimization design of high entropy oxide for oxygen evolution catalysis	102
MM-O04	Oral	Ballroom 1	Ba Hung Tran	Magnetocaloric effect from first-principles calculations and Monte Carlo simulations	103
MM-O05	Oral	Ballroom 1	Phi Thi Huong	Synthesis of bifunctional magnetic-plasmonic Fe ₃ O ₄ @SiO ₂ -Au nanoparticles by an ultrasound assisted chemical method	104
MM-O06	Oral	Ballroom 1	Nguyen Duy Thien	Thermal evaporation synthesis and some properties of WO ₃ /ITO electrochromic thin films	105
MM-O07	Oral	Ballroom 1	Thi Van Anh Nguyen	Fabrication of RuO ₂ thin film for spin orbit torque – induced magnetization switching	106
MM-P01	Poster	Ballroom 2	Kota Nakamoto	In-magnetic-field annealing effects on the phase growth of Mn-Bi-Sn ternary system	151
MM-P02	Poster	Ballroom 2	Yuta Kato	The crystal structure and magnetoelectronic properties in Mn-doped YCu ₃ Fe ₄ O ₁₂	152
MM-P03	Poster	Ballroom 2	Ryota Kobayashi	Magnetic properties of Ni ₂ MnAl by prepared in high magnetic field	153
MM-P04	Poster	Ballroom 2	Ippo Aoki	Crystal structure and magnetic property of magnetoplumbite-structured BaFe _{12-x} Rh _x O ₁₉	154

Code	Type	Room	Presenter	Title	Page
MM-P05	Poster	Ballroom 2	Asuka Ochi	High-pressure synthesis and oxygen evolution reaction activity of Fe ⁴⁺ -Mn ⁴⁺ -mixed perovskite oxide CaFe _{1-x} Mn _x O ₃	155
MM-P06	Poster	Ballroom 2	Tatsuki Watanabe	Brownian motion of depinned skyrmion under applying in-plane alternating electric current	156
MM-P07	Poster	Ballroom 2	Masaya Oshita	Crystal structure and thermochromism of a high-pressure phase of YIn _{1-x} Mn _x O ₃	157
MM-P08	Poster	Ballroom 2	Sachiko Kamiyama	V-V dimerization and its effect on magnetism in ilmenite-type CoVO ₃	158
MM-P09	Poster	Ballroom 2	Moriharu Nagano	Magnetic and structural properties of Cr _x Mn _{1-x} ZnSb with tetragonal Cu ₂ Sb-type structure	159
MM-P10	Poster	Ballroom 2	Manami Goto	Negative thermal expansion in Mn-doped CaCu ₃ Fe ₄ O ₁₂	160
MM-P11	Poster	Ballroom 2	Ryohei Oonaga	Stabilization of α -FAPbI ₃ by addition of dopamine hydrochloride	161
MM-P12	Poster	Ballroom 2	Yuta Kizawa	Evaluation of structural stability of quadruple perovskites RMn ₃ Al ₄ O ₁₂ (R = Ce, Pr, Eu, Dy, Y, Yb)	162
MM-P13	Poster	Ballroom 2	Akari Onaka	Magnetic and Hyperfine properties of MnCoGe-MnFeGe system	163
MM-P14	Poster	Ballroom 2	Harutaka Saito	Systematic QSGW analysis of excited states and model construction of 3d transition metal luminescent centers in α -Al ₂ O ₃	164
MM-P15	Poster	Ballroom 2	Taisei Takaoka	Site selectivity of Cu or Fe in Cu-doped or Fe-doped MnCoGe	165
MM-P16	Poster	Ballroom 2	Amane Morimura	Structures and magnetic properties of novel quadruple perovskite oxides LaMn ₃ Ru ₂ Mn ₂ O ₁₂ and LaMn ₃ Ru ₂ Fe ₂ O ₁₂	166
MM-P17	Poster	Ballroom 2	Woohyeon Ryu	The epitaxially grown ferroelectric Hf _{0.5} Zr _{0.5} O ₂ thin film using pulsed laser deposition method	167

Code	Type	Room	Presenter	Title	Page
MM-P18	Poster	Ballroom 2	Trung Hieu Nguyen	Effect of annealing on the exchange interaction between magnetic phases and the exchange bias effect in Co/CoO nanocomposite	168
MM-P19	Poster	Ballroom 2	Bach Thanh Cong	Thermodynamic properties of bilayer honeycomb spin lattice	169
MM-P20	Poster	Ballroom 2	Dang Co Nguyen	Design and experimental investigation of piezoelectric ceramic element PZT application for high-power ultrasonic welding transducer	170
MM-P21	Poster	Ballroom 2	Thu Le Thi Anh	Study of metal-insulator transition in complex perovskite for sensing application	171
MM-P22	Poster	Ballroom 2	Van Cuong Giap	Tuning independently the exchange bias and coercivity in top-pinned and bottom-pinned Co/Pd multilayers by FeMn film	172
MM-P23	Poster	Ballroom 2	Quang Hoa Nguyen	Correlation between structure and electromagnetic properties of some high permeability amorphous Fe and Co based alloys	173
MM-P24	Poster	Ballroom 2	Vi Vo	Tunable electronic properties of novel 2D Janus MSiGeN ₄ (M = Ti, Zr, Hf) monolayers by strain and external electric field	174
MM-P25	Poster	Ballroom 2	The-Long Phan	Critical exponents of La _{2/3} Ca _{1/3} MnO ₃ nanoparticles	175
MM-P26	Poster	Ballroom 2	Vu Nguyen Thuc	Electric field control of magnetization in artificial microporous magnetic structure based multiferroics	176
MM-P27	Poster	Ballroom 2	Ho Anh Tam	Micro-patterned configuration controlling GMI effect in magnetic artificial system	177
MM-P28	Poster	Ballroom 2	W.-B Wu	Fundamentally different magnetoresistance mechanisms in related Co/Pd and Co/Pt multilayers for spintronic applications	178
MM-P29	Poster	Ballroom 2	Seong-Cho Yu	Spin dynamics in ferromagnetic thin films	179

Code	Type	Room	Presenter	Title	Page
MM-P30	Poster	Ballroom 2	Nguyen Huy Tiep	Growth and multiferroics property of hybrid organic-inorganic perovskite single crystals	180
PH-I01	Invited	Ballroom 3	Tomoyuki Yamamoto	Local environment of emission center ions in phosphor materials	67
PH-I02	Invited	Ballroom 3	Michal Piasecki	Luminescence and non-linear optical properties at mid-infrared spectral range	68
PH-I03	Invited	Ballroom 3	Huu-Quang Nguyen	Magnetoplasmonic core-shell nanowires: synthesis and self-assembly for structural colors and chiral metasurfaces	69
PH-I04	Invited	Ballroom 3	Jin Young Kim	High-performance colorful semitransparent organic solar cells with etalon electrodes	70
PH-I05	Invited	Ballroom 3	Matthijs Jansen	Probing the exciton wavefunction in low-dimensional materials by photoemission momentum microscopy	71
PH-I06	Invited	Ballroom 3	Nguyen Thanh Tung	Metamaterials: plasmonic properties, ultrafast dynamics, heat transfer, and tuneability	72
PH-O01	Oral	Ballroom 3	Viet Tuyen Nguyen	Boosting surface enhanced Raman scattering from ZnO/Au nanorods by UV excitation	107
PH-O02	Oral	Ballroom 3	Chia-Chun Wei	Preparation of nanoparticulate WO ₃ /MoO ₃ films for making electrochromic devices	108
PH-O03	Oral	Ballroom 3	Chun-Liang Lin	Studying defects in TMD materials and devices by STM	109
PH-O04	Oral	Ballroom 3	Heongkyu Ju	Abnormal spectral shift of surface plasmon resonance	110
PH-O05	Oral	Ballroom 3	Der-Hsien Lien	Electronics and optoelectronics of atomically thin semiconductors	111

Code	Type	Room	Presenter	Title	Page
PH-P01	Poster	Ballroom 3	Fuma Samejima	Influence of co-dopings of alkaline metal ions in Er-doped CaSnO ₃ on its up-conversion emission intensity	181
PH-P02	Poster	Ballroom 3	Duy Thien Nguyen	Influence of oxygen ratio on growth and optical properties of ZnO thin film prepared by pulse electron deposition method	182
PH-P03	Poster	Ballroom 3	La Thi Ngoc Mai	Enhancing the absorption figure of merit on solution-based CuO thin films by Ni doping	183
PH-P04	Poster	Ballroom 3	Huu-Quang Nguyen	Chiropticality of magnetoplasmonic nanoparticle-doped titania hydrogels and aerogels	184
PH-P05	Poster	Ballroom 3	Viet Tuyen Nguyen	Effect piezo electric on surface enhanced Raman scattering from ZnO/Au nanorods	185
PH-P06	Poster	Ballroom 3	Kien-Cuong Nguyen	Raman-enhanced signal of rhodamine 6G molecules on SERS substrate in application of detecting chemical residues	186
PH-P07	Poster	Ballroom 3	Thi Ngoc Anh Mai	Influence of hydrothermal temperatures on characteristics of rare earth upconversion NaYF ₄ (Yb, Tm) nanoparticles	187
SD-I01	Invited	Ballroom 3	Wataru Norimatsu	Observation of flat band in millimeter-scale magic-angle twisted bilayer graphene	73
SD-I02	Invited	Ballroom 3	Chanyong Hwang	Towards magnetic skyrmionics	74
SD-I03	Invited	Ballroom 3	Bae Ho Park	Neuromorphic devices based on electrochemical metallization and charge trapping	75
SD-I04	Invited	Ballroom 3	Teruo Ono	Superconducting diode effect in Rashba superlattice	76
SD-I05	Invited	Ballroom 3	Takeshi Seki	Enhanced anomalous Nernst effect in metallic superlattices	77

Code	Type	Room	Presenter	Title	Page
SD-I06	Invited	Ballroom 3	Hieu Ho	Extended X-ray absorption spectroscopy and Debye–Waller factor under pressure	78
SD-I07	Invited	Ballroom 3	Ray Hua Horng	Material properties and growth mechanism of β -Ga ₂ O ₃ epilayers grown on sapphire by metal organic chemical vapor deposition	79
SD-I08	Invited	Ballroom 3	Masashi Akabori	Fabrication of quantum devices by fine sputtering using a focused ion beam with nitrogen gas field ion source	80
SD-I09	Invited	Ballroom 2	Takashi Kimura	Study of nano-scale heat transports using magneto-thermoelectric effects	81
SD-I10	Invited	Ballroom 2	Duc-Tho nguyen	Sub-second and ppm-level optical sensing of hydrogen using templated control of nano-hydride geometry and magnetic composition	82
SD-I11	invited	Ballroom 2	Thi Ngoc Anh Nguyen	Detection of weak, low-frequency magnetic field using single nanoscale MgO magnetic tunnel junctions	83
SD-I12	invited	Ballroom 2	Toan Dang	Neutron diffraction study of state-of-the-art 2D materials	84
SD-O01	Oral	Ballroom 3	Ngoc Nam Ho	Solid-liquid structure of Cu ₂ S: theoretical acanthite-like model for electronic and transport properties investigations	112
SD-O02	Oral	Ballroom 3	Shiuanhuei Lin	Graphene supported liquid crystal phase retarders on rigid glass and flexible polydimethylsiloxane substrates	113
SD-O03	Oral	Ballroom 3	Chung-Li Dong	Advantages, challenges and opportunities of X-ray absorption spectroscopy for advanced investigation of energy materials	114
SD-O04	Oral	Ballroom 3	Canh Tuan Nguyen	Fabricate electrospun nanofiber for rechargeable batteries	115
SD-O05	Oral	Ballroom 3	Minh Nhat Dang	Is it possible to electropolish tungsten carbides?	116
SD-O06	Oral	Ballroom 2	Tan Le Hoang Doan	Tandem cyclooxidative reaction of anthranilamide and alcohols over Fe(III)-based MOFs: effect of structure on catalytic efficiency	117

Code	Type	Room	Presenter	Title	Page
SD-O07	Oral	Ballroom 2	Thi Thuy Nguyen	Nanowire single crystal grain field effect transistors and their applications	118
SD-P01	Poster	Ballroom 3	Gwangtaek Oh	Gate-tunable photodetector and high-mobility ambipolar transistor	188
SD-P02	Poster	Ballroom 3	Chansoo Yoon	Neuromorphic devices based on the electrochemical metallization in the ferroelectric material	189
SD-P03	Poster	Ballroom 3	Hoa Lai	Thermoelectric properties of magnesium tin alloy thin films	190
SD-P04	Poster	Ballroom 3	Tran Van Hiep	Fabrication of the ion-selective field-effect transistor array for determine the pH of solutions	191
SD-P05	Poster	Ballroom 3	Thanh Pham	Design and fabrication of wireless contactless liquid level sensor based on LC passive circuit	192
SD-P06	Poster	Ballroom 3	Minh Nhat Dang	Plasma-assisted exfoliation of graphene from graphite: Is graphene truly exfoliated?	193
SD-P07	Poster	Ballroom 3	Tahereh Parvini	Ultrafast and precessional magnetization dynamics in magnetic tunnel junctions (MTJ) for neuromorphic computing	194
SD-P08	Poster	Ballroom 3	Minjeong Shin	Charge trapping memory device based on heterostructure of MoS ₂ FET and CrPS ₄	195
SD-P09	Poster	Ballroom 3	Manh Xuan Vu	Development of the high sensitive measurement system to investigate the characteristics of magnetic fluids	196
TC-I01	Invited	Ballroom 2	Andreas Honecker	Thermodynamic properties of the Shastry-Sutherland model for SrCu ₂ (BO ₃) ₂	85
TC-I02	Invited	Ballroom 2	Koun Shirai	The Activation Energy of Glass Transition	86
TC-I03	Invited	Ballroom 2	Masato Yoshiya	Selective control of propagation-conduction of two different quantum waves by lattice imperfections: electrons and phonons	87

Code	Type	Room	Presenter	Title	Page
TC-I04	Invited	Ballroom 2	Manh-Thuong Nguyen	Computational Approaches to Study Heavy Element Materials	88
TC-I05	Invited	Ballroom 2	Tatsuya Yokoi	Artificial-neural-network descriptor and interatomic potential for molecular simulations of lattice defects	89
TC-I06	Invited	Ballroom 2	Tien Quang Nguyen	Accelerating materials discovery using universal neural network potential and <i>ab-initio</i> calculations	90
TC-I07	Invited	Ballroom 2	Susumu Fujii	Exploration for non-perovskite proton-conducting oxides using high-throughput computation and machine learning	91
TC-I08	Invited	Ballroom 2	Kazunori Sato	Computational materials design of high-entropy alloys based on FPKKR-CPA calculations and machine learning techniques	92
TC-I09	Invited	Ballroom 2	Huan Tran	Accelerating materials science with artificial intelligence	93
TC-I10	Invited	Ballroom 2	Hirofumi Tanaka	Material intelligence: in-materio reservoir computing devices composed by random network of nanoparticles	94
TC-O01	Oral	Ballroom 2	Katsuhiro Suzuki	The first-principles analysis of multiplet excitations using QSGW	119
TC-O02	Oral	Ballroom 2	Sena Hoshino	Carrier-trapping induced transformation of dislocation core structures in Zn compounds	120
TC-P01	Poster	Ballroom 3	Kaiyuan Yao	Water molecular behavior at solid/liquid interfaces examined by ab initio molecular dynamics	197
TC-P02	Poster	Ballroom 3	Megumi Higashi	Extraction of local structural information from X-ray absorption spectra: machine learning approaches	198
TC-P03	Poster	Ballroom 3	Thong Nguyen-Minh Le	First-principles study on hydrogen adsorption and dissociation on Palladium clusters embedded in Zr-UiO-67 metal-organic frameworks	199

Code	Type	Room	Presenter	Title	Page
TC-P04	Poster	Ballroom 3	Ngoc Tuoc Vu	Novel few-layer nanosheets from layer structured gallium chalcogenides: structural, electronic and mechanical properties	200
TC-P05	Poster	Ballroom 3	Bui Hoi	Magneto-optical absorption in a borophene monolayer with titled Dirac cones: effect of electron - optical phonon coupling	201
TC-P06	Poster	Ballroom 3	Chuong V. Nguyen	Controllable electronic properties and contact types of metal/semiconductor MoSH/MoSi ₂ N ₄ heterostructure	202
TC-P07	Poster	Ballroom 3	Anh Tuan Tran	Quantum theory of the effect of increasing weak electromagnetic wave by a strong laser radiation in 2D graphene	203

ABSTRACTS

Sponsor-01

Particle size analysis & X-ray fluorescence analysis in Li-battery materials

Dang Khoa Nguyen

HORIBA VIETNAM CO., LTD, Lot 3-4, 16th Floor, Detech Tower II, 107 Nguyen Phong Sac Street, Dich Vong Hau Ward, Cau Giay District, Hanoi, Vietnam

Abstract

This topic focuses mainly on particle size analysis & EDXRF analysis in battery. Battery technology is improving, keeping up with the demand for more portable devices and the desire for better power storage for longer periods between charging and changing batteries. Batteries production also requires fast, easy, and accurate QC monitoring, which provides fast detection of faults in safety and performances issues, along with fast decision making when fault is suspected. This will save time and money, while providing perfect traceability. Particle size analyzer from Horiba was used to perform particle size distribution measurements on various materials used in the creation of lithium-ion batteries. Additionally, non-destructive analytical technique which can inspect defects, even non-visible ones, inside a sample because of the high penetration of X-rays by using XGT-9000. HORIBA analytical instruments provide unprecedented levels of reliability, reproducibility and sensitivity, combined with advanced data sciences, to contribute in the development of renewable source of energy, and making energy production and consumption more efficient.

Introduction

The particle size distribution (PSD) of the materials used to make these batteries is tested in both R&D environments and in QC for product acceptance since a PSD specification typically exists for the material. Particle size influences both capacity and coulombic efficiency. Reducing the PSD will increase the specific surface area, increasing reaction rates, and changing the size of the voids between electrode particles, which can reduce battery capacity. Thus, tracking PSD during battery development and manufacture is important to optimizing performance. A few examples for using laser scattering (LA series & SZ-100V2) and centrifuge (CN-300) are presented in this introduction. On the other hand, some applications for the use of XGT-9000 in materials battery testing and fabrication will be included in this topic.

Contact Us: Sales - ngoc.hoang@horiba.com & Technical Service - dangkhoa.nguyen@horiba.com



PL1 (Plenary)**First-principles calculations of defect formation behavior and ion dynamics in solid state ionic materials**

Akihide Kuwabara*

Nanostructures Research Laboratory, Japan Fine Ceramics Center, Aichi, 456-8587, Japan

* Corresponding author's e-mail: kuwabara@jfcc.or.jp

Solid state ionic devices are widely utilized as battery, fuel cell, gas sensor, and so on. Functional properties of these devices are originated from ionic conduction in ionic crystals. Therefore, we need to control optimally the formation and diffusion of the point defects in order to improve the performance of the solid state ionic devices. First principles calculation is powerful method for analysis of the defect structures because it can theoretically optimize atomic positions around defects and can evaluate quantitatively energy states of defective systems without empirical information. In this presentation, we report formation behavior and dynamics of point defects in solid state ionic devices such as Li ion batteries (LIB) and proton-conductive ceramics fuel cells (PCFC).

$\text{Li}_2\text{MnO}_3\text{-LiTMO}_2$ (TM = Ni, Co, Mn) solid solution systems is promising materials for use cathodes of LIBs with higher energy density and capacity. However, the $\text{Li}_2\text{MnO}_3\text{-LiTMO}_2$ system has a problem regarding lower mobility of charge carriers. We investigated Li ion migration behavior in $\text{Li}_{1.2}\text{Mn}_{0.567}\text{Ni}_{0.167}\text{Co}_{0.067}\text{O}_2$ by combination of first-principles calculations and scanning transmission electron microscopy. Our calculations reveal that the energy barrier against Li-ion diffusion across the domain boundary is 0.2~0.3 eV higher compared to that in the crystal bulk. In addition, Ni segregation suppresses Li-ion migration.

PCFC is regarded as one of clean energy resources in the next generation because PCFC can convert chemical energies of water generation from H_2 and O_2 gases to electric power. It is necessary to find oxides having high protonic conductivity used for a solid electrolyte of the PCFC. Several kinds of acceptor-doped BaZrO_3 systems were systematically studied using first principles calculations. Hydration and association energies are least negative for Er and Y, whose ionic radii are around 0.89-0.9 Å, whereas the oxygen affinity of the strongest proton trapping site is most negative for Lu, with an ionic radius of 0.86 Å. The results reveal that the compound with the highest proton conductivity has the most negative hydration energy and the least negative association energy, in other words, the most negative oxygen affinity.

Keywords: first-principles calculation, solid state ionic, point defect, diffusion, interface

References

- [1] H. Yu, Y. -G. So, A. Kuwabara, E. Tochigi, N. Shibata, T. Kudo, H. Zhou, and Y. Ikuhara, *Nano Lett.* 2016, 16, 2907–2915.
- [2] Y. Yamazaki, A. Kuwabara, J. Hyodo, Y. Okuyama, C. A. J. Fisher, and S. M. Haile, *Chem. Mater.* 2020, 32, 7292–730

PL2 (Plenary)**Nano generators: Self powered energy for technology innovation**Yoon-Hwae Hwang^{1, *}, Hyung-Kook Kim¹, Dong-Myeong Shin²¹ Department of Nanoenergy Engineerings, Pusan National University, Busan 46232, South Korea² Department of Mechanical Engineerings, The University of Hong Kong, Pokfulam 999077, Hong Kong, China

* Corresponding author's e-mail: yhwang@pusan.ac.kr

Recently, self powered electric devices attract much attentions due to the future technology trend of IoT based mobile, portable, patchable and even implantable nanodevices in the 4th industrial revolution. The energy harvesting is the process by which an electric energy is delivered from external sources such as solar power, thermal energy, wind energy, mechanical energy, etc. The energy harvesting, also called energy scavenging, is the promising sustainable, safe, and environmentally friendly technology for the next generation because it harvests electric power directly from the nature without any pollution problems. Nanogenerators are the one of the representative self powered energy harvesting devices which can be used for various nanoelectronic devices. In this talk, I would like to deliver the importance of the nanogenerators in future technology innovation and the underlying interesting physics such as flexoelectricity, contact electrification and etc. which can enhance the output power of nanogenerators

Keywords: Nanogenerators, Self Powered, Flexoelectricity, Triboelectricity, Piezoelectricity

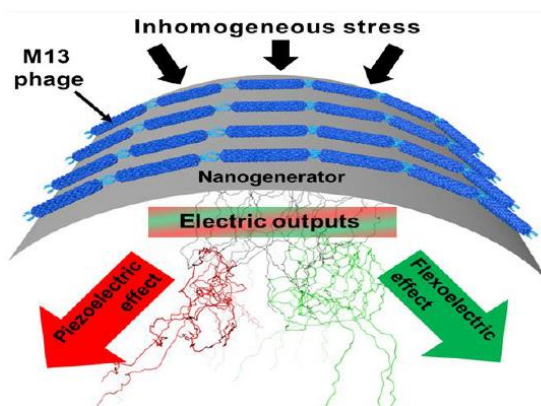


FIG. 1. Schematic explanation of flexoelectric effect in flexible devices.

References

- [1] Dong-Myeong Shin et al., Energy Environ. Sci. 8 (2015) 3198.
- [2] Hai Phan et al., Nano Energy. 33 (2017) 476.
- [3] Taewoo Kim et al., Nano Energy. 54 (2018) 209.
- [4] Yan Yan et al., Nano Energy. 81 (2021) 105607.

PL3 (Plenary) Cancel**Molecular understanding of protein structure and interaction related to Covid-19 and Gout diseases by using computational biophysics**

Toan T. Nguyen^{1, *}

¹ Key Laboratory for Multiscale Simulation of Complex Systems, and Department of Theoretical Physics, University of Science, Vietnam National University Hanoi, 334 Nguyen Trai, Thanh Xuan, Ha Noi, Viet nam

*Corresponding author's e-mail: toannt@hus.edu.vn

In this talk, I will give an overview of Multidisciplinary computational biomolecules research at the Key Laboratory for Multiscale Simulation of Complex Systems. By using and integrating an extensive array of bioinformatics, computational quantum and classical modelling and simulation methods, we can have comprehensive understanding of biomolecules, their structure and functions. Particular focus in this talk will be new research about Gout and Covid-19 being done at the KeyLAB. Unlike biochemical studies, we focus significantly more on understanding the physic picture of viral molecules' structure and interaction. For covid-19 disease, it is found that

(i) the SARS-CoV-2 Spike is more structural stable and has higher binding energy to the human ACE2 receptor than SARS-CoV Spike;

(ii) SARS-CoV-2 RBD-ACE2 binding interface is more stable, has higher binding area, and has more interactions than in SARS-CoV;

(iii) the mutation -PPA469-471/GVEG482-485 in Spike structure has most important and favorable impact for SARS-CoV-2 Spike binding to the ACE2 receptor;

(iv) the SARS-CoV-2 Mpro has hot-spots in the binding pocket of both covalent and non-covalent compounds: His41, Cys145, His163, Glu166 and GLN189.

The results assist in in-silico screening of phytocompounds found in Vietnam plants for finding potential natural compounds against SARS-CoV-2 virus. For Gout disease, the protein NLRP3 is targeted with some potential phytocompounds are found and in-vitro and in-vivo testing being conducted by our experimental colleagues. SCAR reaction to the allopurinol Gout drug due to HLA protein polymorphism in Vietnamese patients are studied. Other active researches are also briefly presented such as those involving biased and unbiased painkiller targeting mu-opioid, brain inflammation, etc.

Keywords: bioinformatics, covid-19, Multiscale, Gout, disease

PL4 (Plenary)**Growth dynamics and physical properties of III-VI two dimensional semiconductors grown by molecular beam epitaxy**

Ssu Kuan Wu¹, Nhu Quynh Diep¹, Hua Chiang Wen¹, Wu-Ching Chou^{1,*}, Thanh Tra Vu²

¹ Department of Electrophysics, National Yang Ming Chiao Tung University, Hsinchu, 30010, Taiwan

² Department of Physics Education, Can Tho University, Can Tho City, Vietnam

*Corresponding author's e-mail: wcchou957@nycu.edu.tw

III-VI two dimensional (2D) semiconductors were grown by molecular beam epitaxy (MBE) on GaN, GaAs, mica or glass substrates. The in-situ reflective high energy electron diffraction (RHEED) was used to monitor the surface epitaxy dynamics. High crystal quality of 2D III-VI semiconductors, InSe [1], GaSe [2-4], or GaTe [5] was revealed by the photoluminescence (PL), X-ray diffraction, Raman scattering, and transmission electron micrographs (TEM).

Raman scattering spectra, X-ray diffraction, and high-resolution transmission electron microscopy reveal that 2D InSe phase can be fabricated under both indium-rich and -poor conditions [1]. Strong red-shifts in the energy of in-plane E_{2g}^2 vibration modes and bound exciton emissions observed from Raman scattering and PL spectra in GaSe samples are attributed to the unintentionally biaxial in-plane tensile strains, induced by the dissimilarity of symmetrical surface structure between the 2D-GaSe layers and the substrates during the epitaxial growth [3]. The temporal in-situ RHEED patterns illustrate the transition from 2D hexagonal GaTe to one dimensional (1D) monoclinic GaTe growth mode at different growth temperatures [5]. Current investigation on the growth dynamics and physical properties of III-VI 2D semiconductors pave the way for future fabrication and device application of the hetero-structures made of these III-VI 2D semiconductors.

Keywords: two dimensional semiconductors, molecular beam epitaxy, InSe, GaSe, GaTe

References

- [1] Sheng-Wei Hsiao et al., *Frontiers in Materials* 9, 871003 (2022).
- [2] Nhu Quynh Diep et al., *Scientific Reports* 9, 17781 (2019).
- [3] Cheng-Wei Liu et al., *Scientific Reports* 10, 12972 (2020).
- [4] Nhu Quynh Diep et al., *Scientific Reports* 11, 19887 (2021).
- [5] Sa Hoang Huynh et al., *ACS Applied Nano Materials* 4, 8913 (2021).

PL5 (Plenary)**Fe2P type alloys: an intriguing magnetic playground**Ekkes Bruck^{1,*}¹ Delft University of Technology, The Netherlands

* Corresponding author's e-mail: E.H.Bruck@tudelft.nl

The Fe₂P intermetallic compound, is a prototypical example of a first order ferromagnetic phase transition, known since the 1980s to exhibit a sharp, but weak, FOMT at 216 K (-57°C) [1]. In this hexagonal system, the Fe atoms occupy two inequivalent atomic positions, referred to as 3f (in a tetrahedral environment of non-metallic atoms) and 3g (in a pyramidal environment). Also, for P we find two distinct lattice sites 1a and 2b. One intriguing aspect is the large uniaxial magnetic anisotropy leading to an anisotropy field of about 7T at 5K [2]. This anisotropy is quite unique for a mainly itinerant electron system as evidenced by the reduction (partial quenching) in the magnetic moments of the iron atoms on the 3f sites when TC is crossed from the ferromagnetic to the paramagnetic state, whereas there is only a limited decrease on the 3g site. This observation has led to a cooperative description of the FOMT, linking the loss of long-range magnetic order at TC with the loss of local moments on the 3f site [3]. Replacing Fe and/or P by other elements leads to a rich variety of phenomena. Magnetic ordering temperature and first order character of the phase transition can be either enhanced or reduced. The anisotropy is strongly reduced on reduction of the c lattice parameter and a wide range of compositions display easy-plane anisotropy rather than easy axis, which is favourable for magnetocaloric applications. We will discuss both theoretical and experimental results for a wide range of elements substituting either Fe or P and combined substitutions on both Fe and P sites, while maintaining the hexagonal Fe₂P type of structure. Most prominent results are achieved when partially replacing Fe with Mn or Co, and simultaneously Si substituting P. This leads for Mn to soft magnetic materials with excellent magnetocaloric properties [4]. Conversely, hard magnetic properties and Curie temperatures up to 640 K are found for Co substitutions [5].

Keywords: Magneto-caloric materials, gap magnets, transition-metal magnets**References**

- [1] O. Beckman et al., Specific Heat of the Ferromagnet Fe₂P, *Physica Scripta* 25 (1982) 679-681.
- [2] L. Caron, et al., Magnetocrystalline anisotropy and the magnetocaloric effect in Fe₂P, *Phys. Rev. B* 88 (2013) 094440.
- [3] H. Yamada and K. Terao, First-Order Transition of Fe₂P and Anti-Metamagnetic Transition, *Phase Transitions* 75 (2002) 231–242.
- [4] X. You et al., Magnetic Phase Diagram of the Mn_xFe_{2-x}P_{1-y}Si_y System. *Entropy* (2022), 24, 2. <https://doi.org/10.3390/e24010002>.
- [5] Y. He et al., Intrinsic Magnetic Properties of a Highly Anisotropic Rare-Earth-Free Fe₂P-Based Magnet. *Adv. Funct. Mater.* (2021), 2107513.

PL6 (Plenary)**Optical and electronic properties of crystalline solids from the first-principles and semiempirical methods**Mikhail Brik^{1, 2, 3, 4, *}¹ College of Sciences & CQUP-T-BUL Innovation Institute, Chongqing University of Posts and Telecommunications, Chongqing 400065, China² Institute of Physics, University of Tartu, W. Ostwald Str. 1, Tartu 50411, Estonia³ Faculty of Science and Technology, Jan Długosz University, 42200 Częstochowa, Poland⁴ Centre of Excellence for Photoconversion, Vinca Institute of Nuclear Sciences - National Institute of the Republic of Serbia, University of Belgrade, P.O. Box 522, Belgrade, 11001, Serbia

* Corresponding author's e-mail: mikhail.brik@ut.ee

Smart design and efficient search for new effective optical materials implies understanding of their physical parameters, such as structural, electronic, optical etc properties. Various first-principles and semiempirical models have been developed so far to elucidate relations between structure and properties of crystalline materials and between their various properties. In this presentation several examples of consistent application of the first-principles calculations to the large families of isostructural compounds, pure [1, 2] and doped [3, 4] will be discussed in detail with an emphasis of relations between the chemical composition, structure and properties. In addition, a semiempirical model that allows to make predictions of positions of emission maxima in the Eu²⁺-doped ternary sulfides will be presented (Fig. 1) [5].

Keywords: First-principles calculations; Mn⁴⁺-based phosphors; Eu²⁺-based phosphors

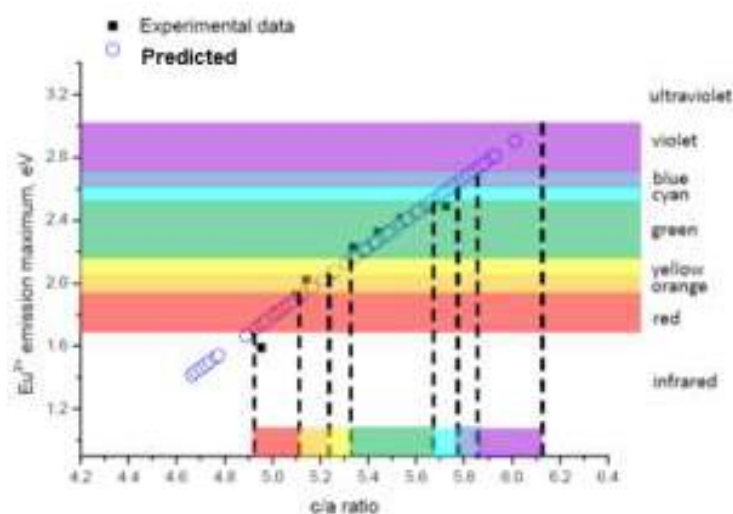


FIG. 1. Experimental and predicted Eu²⁺ emission maxima in the ternary sulfides with indication of emission color.

References

- [1] Y. Wang et al., Res. Phys. 13 (2019) 102180.
- [2] B. Wu et al., J. Am. Ceram. Soc. 104 (2021) 1489.
- [3] M.G. Brik et al., Opt. Mater. 113 (2021) 110843.
- [4] M. Subhoni et al., Materials 15 (2022) 613.
- [5] M.G. Brik et al., Chem. Eng. J. 418 (2021) 129380.

Session: Materials for energy and environment (EE)

EE-I01 - EE-I06

EE-I01 (Invited)

CD4⁺ T cell counting using anti-CD4 antibody conjugated magnetic

Nguyen Hoang Nam^{1, 2, *}, Do Quang Loc¹, Phi Thi Huong¹, Luu Manh Quynh¹, Pham Thi Thu Huong¹, Nguyen Thi Van Anh¹, Bui Thanh Tung³, Chu Duc Trinh³, Nguyen Hoang Luong^{1, 2}

¹ VNU University of Science, Vietnam National University, Hanoi, Vietnam

² Vietnam Japan University, Vietnam National University, Hanoi, Vietnam

³ VNU University of Engineer and Technology, Vietnam National University, Hanoi, Vietnam

* Corresponding author's email: namnh@hus.edu.vn

The CD4⁺ T-cell counting device was developed to be used in detection and treatment process of some immunodeficiency diseases, such as HIV, to reduce costs and increase accessibility due to its simplicity and compactness. Magnetic nanoparticles functionalized with carboxyl groups of 100-200 nm in size are conjugated to anti-CD4 antibodies to ensure specific interaction with the CD4 receptor on CD4⁺ T cells. The antibody conjugated magnetic nanoparticles were incubated with 50 μ L of blood sample, then the CD4⁺ T cells were captured by a magnet before being pumped through a microfluidic system with a three-electrode differential capacitance counter. Total CD4⁺ T cells were counted by considering the electrical peaks generated when the cells passed through the electrodes and analyzed using in-built software. The counting results then were compared with the gold standard test of cell counting using the FACS Canto system. The test results show that the developed device gives stable results over a wide range of CD4⁺ T cell concentrations tested (1000–200 CD4⁺ T cells/ μ L blood) and correlates well with the results on the FACS system.

Keywords: CD4⁺ T cell counter, magnetic nanoparticles, microfluidic system

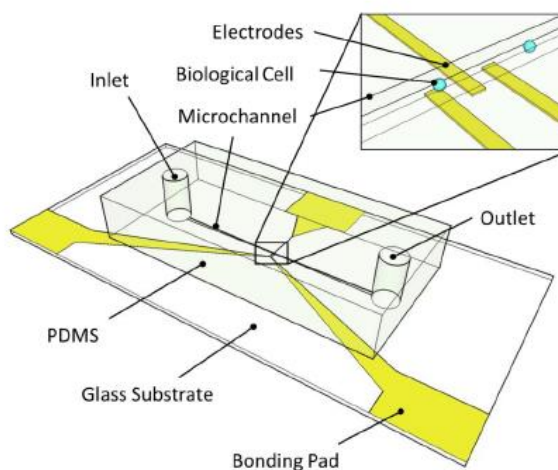


FIG. 1. Schematic design of Microfluidic cell counting system.

EE-I02 (Invited)**Structural analysis of battery materials by atomic-resolution scanning transmission electron microscopy**Kei Nakayama^{1,*}, Ryo Ishikawa², Yuichi Ikuhara^{1,2}¹ Nanostructures Research Laboratory, Japan Fine Ceramics Center, Nagoya, Aichi 456-8587, Japan² Institute of Engineering Innovation, University of Tokyo, Bunkyo, Tokyo 113-8656, Japan

* Corresponding author's e-mail: kei_nakayama@jfcc.or.jp

The performance of rechargeable batteries is greatly influenced by the microstructure of the electrode materials. However, in many cases, the specific structure-performance relationships are unclear owing to the difficulty of the structural analysis at the atomic scale and nanoscale. Here, we elucidate the microstructures of two kinds of electrode materials by scanning transmission electron microscopy (STEM) and discuss the relationships to the battery performance. The first material is Li_2MnO_3 , a cathode material for Li-ion batteries [1]. The extraction of Li-ions is accompanied by the release of oxygen, Mn/Li cation-mixing, and the introduction of dislocations. These irreversible structural changes could decrease the available number of Li-ions and shorten the cycle life of batteries. The second material is LaNi_5 , a cathode material for fluoride-ion batteries [2]. As shown in FIG. 1, the fluorination reaction in the early stage of the first charging process decomposes LaNi_5 into LaF_3 and Ni nanocrystals, forming nanoscale networks of F^- -ion- and electron-conducting paths, respectively. This nanoscale network can facilitate the fluorination and defluorination of Ni in the subsequent charge and discharge processes, which increases the practical capacity of batteries.

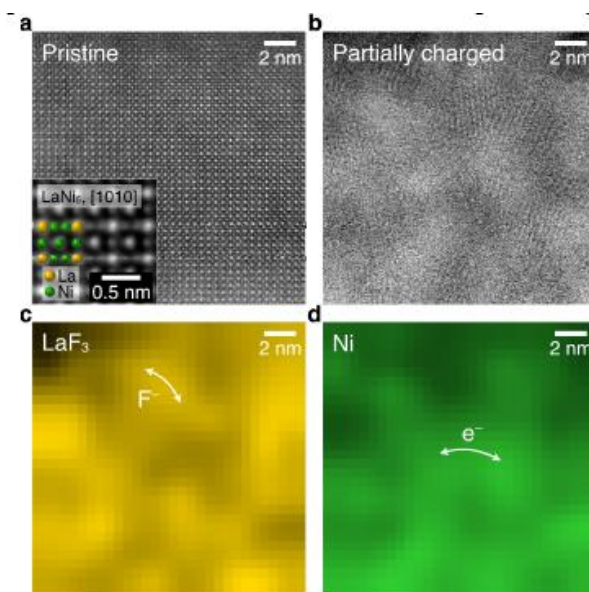
Keywords: Scanning transmission electron microscopy, STEM, Battery materials

FIG. 1. (a) Annular dark-field (ADF) STEM image of the pristine LaNi_5 sample. (b) ADF STEM image, (c) LaF_3 distribution map, and (d) Ni distribution map obtained from a partially charged sample.

Acknowledgement: This work was supported by the RISING2 (JPNP16001) and RISING3 (JPNP21006) projects from the New Energy and Industrial Technology Development Organization (NEDO), Japan.

References

- [1] K. Nakayama et al., Nat. Commun. 11 (2020) 4452.
- [2] K. Nakayama et al., J. Mater. Chem. A 10 (2022) 3743.

EE-I03 (Invited)**Si-based photoelectrodes for water splitting**Ho Won Jang^{1,*}¹ Department of Materials Science and Engineering, Seoul National University, Seoul, Korea* Corresponding author's email: hwjang@snu.ac.kr; <https://sites.google.com/view/onnl>

The development of a carbon-free hydrogen production method by photoelectrochemical water splitting is a promising pathway to deal with the increased energy demands and deleterious environmental issues derived from the usage of fossil fuels. Silicon, which is the second most earth-abundant element and a small band-gap material, is an applicable candidate for an efficient solar water splitting photoelectrode. However, the stability of Si-based photoelectrode hampers efficient water splitting because of its thermodynamic instability and etching of silicon surface. Until now, much research has been conducted to deal with the challenges of using Si to fabricate efficient and stable photoelectrodes. Over the decades, cheap and earth-abundant transition metal-based electrocatalysts have been investigated. In this presentation, we briefly introduce the photoelectrochemistry and important parameters for evaluating the performance of the Si photoelectrodes. We introduce transition metal-based catalysts, focusing on Ni-, Fe-, Co-, Mo-, W-, and Fe-based oxygen and hydrogen evolving catalysts. Then, we present various strategies to overcome the challenges of silicon by combining the advantages of transition metal-based co-catalysts, which are cost-effective, stable, and highly active for oxygen evolution reaction. Finally, to realize spontaneous water splitting, we introduce Si-based tandem cells combined with transition metal-based materials.

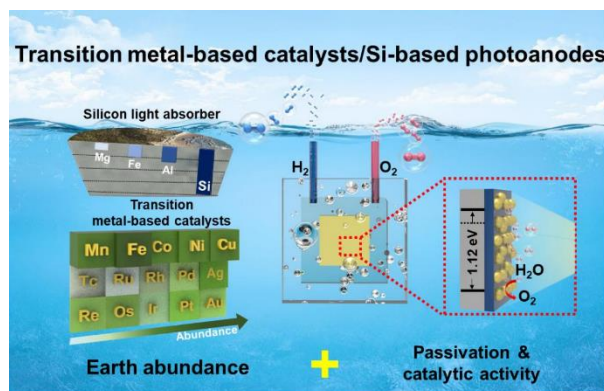


FIG. 1. Si-based photoanodes with cost-effective and high-performance transition-metalcatalysts.

EE-I04 (Invited)**Defluorination and adsorption of tetrafluoroethylene (TFE) on TiO₂(110) and Cr₃O₃ (0001)**

Jessiel Siaron Gueriba^{1,2,3}, Nur Ellina Annisa Salehuddin^{1,4}, Wilson Agerico Dino^{1,5,*}, Kiminori Washika⁶, Hiroshi Nakamura⁷, Tatsumi Kawafuchi⁶

¹ Department of Applied Physics, Osaka University, Suita, Osaka 565-0871, Japan

² Department of Physics, De La Salle University, 2401 Taft Ave., 0922 Manila, Philippines

³ Institute of Laser Engineering, Osaka University, Suita, Osaka 565-0871, Japan

⁴ Department of Chemical Sciences, Faculty of Science and Technology, Universiti Kebangsaan Malaysia, 43600 Bangi, Selangor, Malaysia

⁵ Center for Atomic and Molecular Technologies, Osaka University, Suita, Osaka 565-0871, Japan

⁶ Laser Technology Laboratory, Hirotec Co., Ltd., Saeki-ku, Hiroshima 731-5197, Japan

⁷ Research and Development Division, Technology and Development Department, Charmant, Inc., Sabae, Fukui 916-0088, Japan

* Corresponding author's e-mail: wilson@dyn.ap.eng.osaka-u.ac.jp

The capability to join dissimilar materials (cf., e.g., [1-4] and references therein) is a key enabling technology to innovative and sustainable materials design for industrial applications. Some notable examples include polymer-metal composites used in various specialized applications (cf., eg., [1,2] and references therein). All of these applications fundamentally start with polymer adhesion on metal surfaces. Recently, we report that metal oxide surfaces catalyze the formation of intermediate defluorinated tetrafluoroethylene (TFE) radicals, resulting in enhanced binding on the corresponding metal oxide surfaces [5]. As expected, reactivity of the corresponding metal oxide surfaces depends on the oxygen coordination of metal surface atoms. Thus, introducing oxygen vacancies and non-ionizing radiations to form intermediate radicals could promote binding of polymers to metals and metal-oxide surfaces, allowing for better materials design. This could find significant applications not only in joining dissimilar materials, but also allow for flexibilities in realizing materials with the desired (pre-determined) characteristic properties. Further details will be presented at the meeting.

Keywords: Dissimilar materials, Joining, Metal oxide surface, Catalysis, Materials design

References

- [1] A. Li, P.K. Chu, J. Sun, Appl. Surf. Sci. 515 (2020) 146065.
- [2] S.S. Anjum, J. Rao, J.R. Nicholls, IOPConf. Ser. Mater. Sci. Eng. 40 (2012) 012006.
- [3] D.W. Kim, K.T. Kim, D.U. Lee, S.H. Jung, J. Yu, Sci. Rep. 10 (2020) 14560.
- [4] Y. Ohkubo, K. Endo, K. Yamamura, Sci. Rep. 8 (2018) 18058.
- [5] J.S. Gueriba *et al.*, Sci. Rep. 11 (2021) 21551.

EE-I05 (Invited)**Single cell capacitance measurement of NIH 3T3 cell using impedance biosensor**Dahyun Kang¹, Yeeun Kim¹, Jungmok Yang¹, Jisoo Choi¹ and Moongyu Jang^{1, 2, *}¹ School of Nano Convergence Technology, Hallym University, Chuncheon 24252, Korea² Center of Nano Convergence Technology, Hallym University, Chuncheon 24252, Korea

* Corresponding author's e-mail: jangmg@hallym.ac.kr

The change of capacitance as a function of time is measured using impedance biosensor for the monitoring of NIH-3T3 cell growth. The capacitance value increased with the growth of NIH-3T3 cell. However, the capacitance behavior showed different tendency between early (from 0 to 140 minutes) and later stage. Therefore, to analyze the difference, we observed the change in the number of cells with real-time images measured using NanoEnTek JuLiTmBr. In addition, the cell counting result was compared with the capacitance measured with various frequencies from 1 kHz upto 800 kHz. As a result, it was confirmed that in the early stage (from 0 to 140 minutes), the cells floating in the medium started to sink to the sensor's surface, and after 140 minutes, cells on the sensor's surface started growth and division. Finally, the average capacitance values of one cell in the early stage and the later stage are presented for each frequency. For example, at 300 kHz, the average capacitance of the cell in the early stage was 0.11 fF, and in the later stage was 0.53 fF. Also, we confirmed that, the measured capacitance increased linearly with the increase of cell numbers, confirming that the parallel arrangement of cells in capacitance measurement.

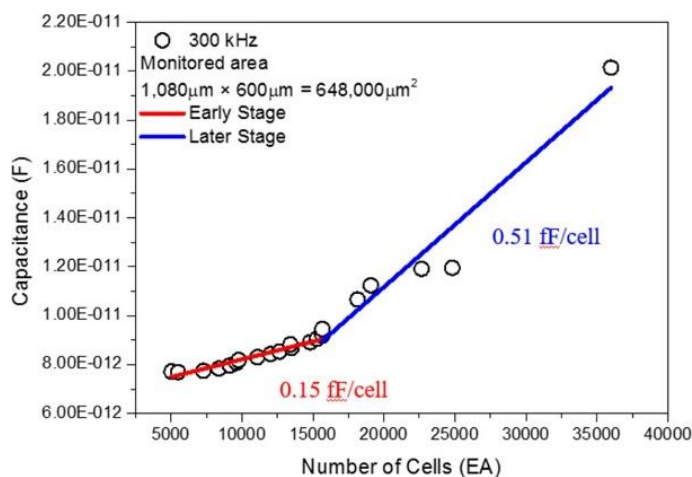
Keywords: Impedance biosensor, Capacitance measurement, Single cell capacitance

FIG. 1. Graph for comparison with the number of cells and capacitance measured on 300 kHz.

EE-I06 (Invited)**Development of a 3D bio-printing system for blood vessel growing from the multilineage-differentiating stress-enduring (MUSE) spheroids**

Nguyen Ngoc Dinh*, Luu Manh Quynh, Hoang Thi My Nhung

Faculty of Physics, VNU-HUS, Hanoi, Vietnam

* Corresponding author's e-mail: nguyennngocdinh@gmail.com

Tissue autologous reconstruction has promised to pave a revolutionary pathway for transplant surgery to avoid biological rejections. To this, 3D bio-printing is a reasonable technique involving the rearrangement of cell patterns in a limited space using printing technology, in which the so called suitable “bio-inks” are developed for target tissues. In this study, 500 μ m diameter multilineage-differentiating stress-enduring (MUSE) spheroids were grown from three types of cells-human dermal fibroblast cells (hDFCs), human aortic smooth muscle cells (hASMCs) and human umbilical cord vascular endothelial cells (hUVECs) and were used as ink for blood vessel development. The MUSE cells were rearranged into a cylinder formation using Kenzan method by a house-developed 3D bio-printing system. After 3 days growth, a 2 – 5 mm diameter 7 mm long blood vessels were observed. Biochemical measurement showed that the as-prepared vessels were suitable for further transplant applications.

Keywords: autologous reconstruction, 3D bio-printing, MUSE spheroids

Session: Multiferroics and magnetic materials (MM)**MM-I01 - MM-I11****MM-I01 (Invited)****PbCuTe₂O₆ – a quantum spin liquid candidate showing ferroelectric order close to a quantum critical point**

M. Lang^{1,*}, Ch. Thurn¹, P. Eibisch¹, A. Ata¹, M. Winkler², P. Lunkenheimer², I. Kézsmárki², U. Tutsch¹, Y. Saito¹, S. Hartmann¹, J. Zimmermann¹, A. R. N. Hanna^{3,4}, A. T. M. N. Islam⁴, S. Chillal⁴, B. Lake^{3,4}, B. Wolf¹

¹ Phys. Institut, Goethe-Universität Frankfurt(M), 60438 Frankfurt, Max-von-Laue-Str.1, Germany

² Experimentalphysik V, Zentrum für Elektronische Korrelationen und Magnetismus, Universität Augsburg, Universitätsstr. 1, 86159 Augsburg, Germany

³ Inst. für Festkörperforschung, Techn. Universität Berlin, Hardenbergstr. 36, 10623 Berlin, Germany

⁴ Helmholtz-Zentrum Berlin für Materialien und Energie, Hahn-Meitner Platz 1, 14109 Berlin, Germany

* Corresponding author's e-mail: michael.lang@physik.uni-frankfurt.de

PbCuTe₂O₆ has been considered a candidate material for a 3D frustrated quantum spin liquid featuring a highly-connected hyperkagome lattice [1-3]. According to previous magnetic studies, mainly on pressed-powder samples, the system lacks long-range magnetic order down to 0.02 K, and shows diffuse continua in the magnetic spectrum [3] consistent with fractional spinon excitations. There has been an issue relating to the appearance of small anomalies in the powder samples around 1 K of unknown origin [1–3] and signs of a phase transition around this temperature in first-generation single crystals. In this talk, we present results of a comprehensive study of thermodynamic, magnetic and dielectric properties on single crystalline and pressed-powder samples of PbCuTe₂O₆. The low-temperature properties of the powder samples are found to be consistent with the proposed quantum liquid state. Most remarkably, however, an even more exotic behavior is revealed for the single crystals [4], yielding a ferroelectric transition around $T_{\text{FE}} \approx 1$ K [5], accompanied by strong lattice distortions, and a modified magnetic response – still consistent with a quantum spin liquid – but with clear indications for quantum critical behavior [5]. By the application of magnetic fields $B \leq 15$ T, a rich phase diagram is revealed with indications for two field-induced quantum critical points at $B_{\text{c1}} \sim 8$ T and $B_{\text{c2}} \sim 11$ T.

Keywords: quantum spin liquid, ferroelectricity, quantum criticality

References

- [1] B. Koteswararao et al., Phys. Rev. B 90, 035141 (2014).
- [2] P. Khuntia et al., Phys. Rev. Lett. 116, 107203 (2016).
- [3] S. Chilla et al., Nat. Commun. 11, 2348 (2020).
- [4] A. R. N. Hanna et al., Phys. Rev. Mater. 5, 113401 (2021).
- [5] Ch. Thurn et al., npj – Quantum Materials 6, 95 (2021).

MM-I02 (Invited)**Application of magnetic field for selective reaction in magnetic alloys**Yoshifuru Mitsui^{1,*} and Keiichi Koyama¹¹ Graduate School of Science and Engineering, Kagoshima University, Kagoshima 890-0065 Japan

* Corresponding author's e-mail: mitsui@sci.kagoshima-u.ac.jp

Phase equilibrium and transformation of magnetic alloys can be controlled by magnetic field [1] because of the gain of Zeeman energy to the ferromagnetic phases. We have investigated that magnetic field also influenced the solid-solid [2], solid-liquid [3, 4], and gas-solid reaction [5]. For example, solid-phase reactive sintering of ferromagnetic MnBi from non-ferromagnetic Mn and Bi particles was enhanced by magnetic field and obtained MnBi phase was uniaxially-oriented [2]. Above in-magnetic-field synthesis indicated the possibility of selective reaction of the ferromagnetic phase from non-ferromagnetic precursor or raw materials. In diffusion couples, the reacted phases with various magnetic state exhibited. Therefore, it is expected that the in-magnetic-field reaction using diffusion couples show the unique phase growth. Recently, we investigated the effects of magnetic field on the solid-liquid reactions of diffusion couples between magnetic metal and low melting-point metal. In this study, in-magnetic-field reactions of ferromagnetic Fe-Ga [3], and non-ferromagnetic Mn-Ga [4] were investigated.

In Fe-Ga diffusion couple, Fe₃Ga, the eutectic regions of Fe₃Ga and Fe₆Ga₅, Fe₆Ga₅, Fe₃Ga₄ and FeGa₃ phase were observed at Fe/Ga boundary. The growth rate of reacted phase was suppressed by magnetic field at both ferromagnetic and paramagnetic state of α -Fe. It was found that magnetic-field-induced reduction of the growth rate was due to the pre-exponential factor of the diffusion coefficient, and the activation energy did not change. On the other hand, in Mn-Ga diffusion couple, many phases with various magnetic state exhibited at Mn/Ga boundary as reacted phase. Mn-rich phases were ferrimagnetic or ferromagnetic, and Ga-rich phases were non-ferromagnetic. The phase growth of Ga-rich phases was faster than that of Mn-rich phases in a zero field. Meanwhile, the growth rate for Mn-rich phase did not change in 5 T, but the growth rate for Ga-rich phase reduced. Therefore, it is indicated that magnetic field promotes the selective growth of ferromagnetic/ferrimagnetic phase.

Keywords: ferromagnetic alloys, high magnetic field, reaction**References**

- [1] J. -K. Choi, et al., *Scr. Mater.* 43 (2000) 221
- [2] Y Mitsui, et al., *J. Alloy. Compd.* 615 (2014) 131
- [3] Y. Mitsui, et al., *ISIJ Int.* 60 (2020) 807
- [4] Y. Watanabe, et al., *J. Alloy. Compd.* 887 (2021) 161310
- [5] M. Onoue, et al., *J. Alloy. Compd.* 835 (2020) 155193

MM-I03 (Invited)**Crystal structures and electronic properties of vanadium oxides**Hajime Yamamoto ^{1,*}¹ Institute of Multidisciplinary Research for Advanced Materials, Tohoku University, Sendai 980-8577, Japan

* Corresponding author's e-mail: hajime.yamamoto.a2@tohoku.ac.jp

Vanadium shows valence states ranging from 2+ to 5+. The charge, orbital, and spin degrees of freedom of vanadium ions lead to a variety of physical properties and functions. In this study, we especially focus on perovskite-type and ilmenite-type oxides containing tetravalent vanadium ions. Tetravalent vanadium ion has only one t_{2g} electron, which causes the Jahn-Teller effect and the formation of molecular orbitals between adjacent vanadium ions. By utilizing these effects, we found novel properties and functions, such as colossal negative thermal expansion in electron-doped PbVO_3 [1,2], and cation dimerization in the ilmenite-type vanadium oxides $M\text{VO}_3$ (M = divalent metal ions) [3-5], as shown in FIG 1.

Keywords: Strongly correlated electron systems, High-pressure synthesis, Oxides, Magnetism, Structure transition

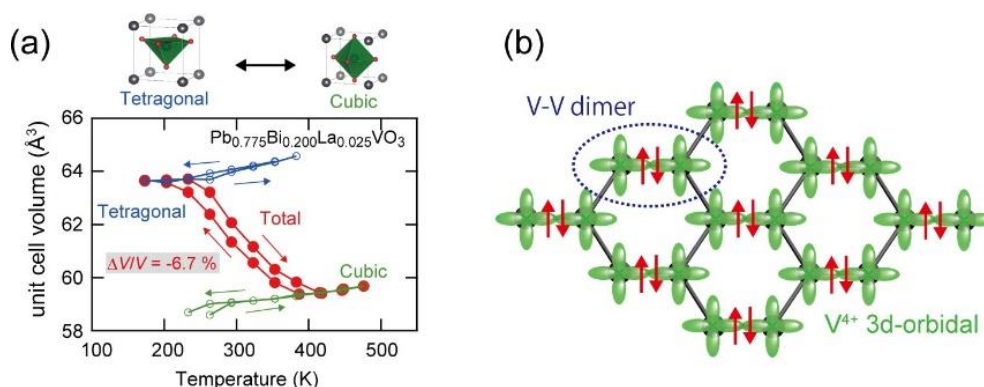


FIG. 1. (a) Colossal negative thermal expansion in electron-doped (perovskite-type) PbVO_3 . (b) Schematic of cation dimerization in ilmenite-type MgVO_3 .

References

- [1] H. Yamamoto et al., Angew. Chem. 57 (2018) 8170.
- [2] H. Yamamoto et al., Inorganic Chemistry 58, (2019) 2755.
- [3] H. Yamamoto et al., J. Am. Chem. Soc. 144 (2022) 1082.
- [4] S. Kamiyama, H. Yamamoto et al., Inorganic Chemistry 61 (2022) 7841.
- [5] H. Yamamoto et al., Appl. Phys. Lett. 120 (2022) 7841.

MM-I04 (Invited)**Anomalous transport properties in a Weyl metal**

Jeehoon Kim*

Department of Physics, Pohang University of Science and Technology, Pohang 37673, Republic of Korea

* Corresponding author's e-mail: jeehoon@moeemotion.com

Weyl metal has shown fascinating transport phenomena such as negative magneto resistant, anomalous Hall effect, and nonohmic conductance, which results from chiral anomaly. As a topological semimetal it naturally has both surface and bulk topological transport channel via Fermi arc and 1D channel between two Weyl cones. Chiral-anomaly transport channel naturally gives rise to a variety of anomalous transport properties. In this talk, we discuss anomalous electronic transport in BiSb alloys with inclusion of Weyl states.

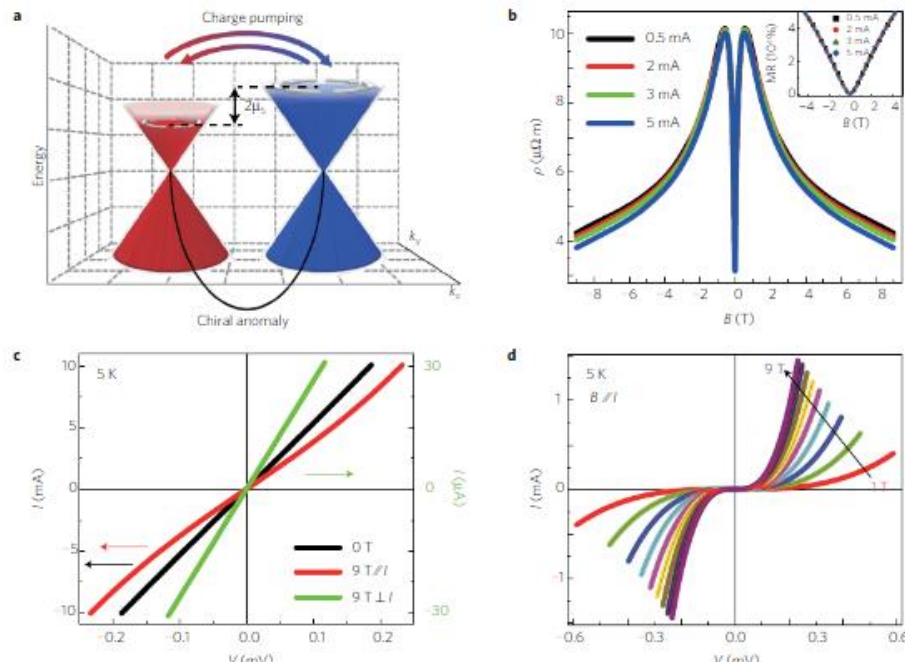


Figure 1. Nonlinear conductivity in a Weyl metal.

References

- [1] D. W. Shin, et al, Nature Materials 16,1096 (2017)

MM-I05 (Invited)**Tuning the ground state of strongly correlated $\text{EuPd}_2(\text{Si}_{1-x}\text{Ge}_x)_2$ using He-Gas pressure**

Bernd Wolf*, Felix Spathelf, Jan Zimmermann, Theresa Lundbeck, Marius Peters, Kristin Kliemt, Cornelius Krellner, Michael Lang

Physikalisches Institut, Goethe University, 60438 Frankfurt/Main, Germany

* Corresponding author's e-mail: wolf@physik.uni-frankfurt.de

The strongly correlated intermetallic compound EuPd_2Si_2 is one of the rare examples where a strong valence-change crossover is observed as a function of temperature. The valence change from $\text{Eu}^{(2+\delta)+}$ to $\text{Eu}^{(3-\delta')}$ which occurs in a small temperature range is accompanied by pronounced lattice effects together with significant changes in the magnetic properties [1]. According to spectroscopic and thermodynamic measurements, this material is located on the high-pressure side (crossover range) of the second-order critical endpoint (CEP). This end point terminates the first-order valence transition line in the generalized p - T phase diagram of Eu-based intermetallics [2]. At the CEP novel collective phenomena which originate from a particularly strong coupling between electronic-, magnetic- and lattice degrees of freedom can be expected [3]. The aim of our study is to identify a suitable chemical modification of EuPd_2Si_2 , corresponding to a negative chemical pressure, so that the CEP can be accessed via fine pressure tuning by using He-gas technique.

We present magnetic susceptibility measurements and thermal expansion data taken on high-quality single crystals of $\text{EuPd}_2(\text{Si}_{1-x}\text{Ge}_x)_2$ for nominal Ge-concentrations $0 \leq x_{\text{nom}} \leq 0.2$ in the temperature range $2 \text{ K} \leq T \leq 300 \text{ K}$. The experiments have been performed using He-gas pressure up to 0.5 GPa. For $x = 0$ at ambient pressure we observe a pronounced valence crossover centered around $T_V \sim 160 \text{ K}$ leading to a non-magnetic ground state. This valence-change crossover is characterized by an extraordinarily strong pressure dependence of $dT_V/dp \approx (80 \pm 10) \text{ K/GPa}$. As expected, T_V shifts to lower temperatures with increasing Ge-concentration, reaching $T_V \sim 90 \text{ K}$ for $x_{\text{nom}} = 0.1$, while still showing a non-magnetic ground state. In contrast, for the system with $x_{\text{nom}} = 0.2$ we observe a magnetic ground state with long-range antiferromagnetic order setting in below $T_N = 47.5 \text{ K}$. The important finding is that the application of weak pressure as low as 0.2 GPa the long-range magnetic order can be suppressed giving way to a non-magnetic ground state with pronounced valence fluctuations. We therefore consider this compound a promising target material for studying pressure-induced strong-coupling effects.

Keywords: strongly correlated materials, valence transition, He-gas pressure

References

- [1] B. Batlogg et al., in Valence Instabilities, ed. P. Wachter and H. Boppart, North-Holland Publishing Company, 229, (1982).
- [2] Y. Onuki et al., Philosophical Magazine 97, 3399 (2017).
- [3] E. Gati et al., Science Advances 2, e1601646 (2016).

MM-I06 (Invited)**Soft magnetic Fe(Co)-based high Bs nanocrystalline alloys for applications at elevated temperatures**Ivan Škorvák^{1,*}, Branislav Kunca¹, Jozef Marcin¹, Peter Švec²¹ Institute of Experimental Physics, Slovak Academy of Sciences, 040 01 Košice, Slovakia² Institute of Physics, Slovak Academy of Sciences, 842 28 Bratislava, Slovakia

* Corresponding author's e-mail: skorvi@saske.sk

The continuing interest in Fe(Co)-based nanocrystalline alloys is motivated mainly due to the combination of high saturation magnetic flux density with good magnetic softness and their capability to operate at elevated temperatures. A further improvement of magnetic performance in these alloys is possible by using a careful compositional tuning as well as by employing special processing techniques resulting in optimal phase content and reduced grain sizes. Special attention of our work is focused on rapid annealing technique that utilizes a compression of samples between pair of pre-heated Cu blocks [1]. Here, very high heating rates and short processing times result in a formation of markedly smaller nanocrystalline grains as compared to conventional furnace annealing. Selected results showing the impact of rapid annealing on the soft magnetic properties will be presented for high Bs Fe-(Co)-B-(Cu) and Fe-Sn-B alloys with a reduced metalloid content. A part of our research interest is devoted also to the application of external magnetic field during the conventional furnace annealing in order to improve their soft magnetic characteristics. It is shown that the specimens of Fe-Co-B-(Cu) amorphous and nanocrystalline alloys annealed in conventional furnace without a presence of external magnetic field exhibit an unwanted increase of coercivity. In addition, the corresponding hysteresis loops show a presence of steps due to the depinning of domain walls from the positions stabilized during annealing. After heat treatment in longitudinal or transverse magnetic field one can obtain smooth hysteresis loops with markedly reduced coercivity. We show that similar effects can be achieved also by employing of rapid annealing techniques. Examples of our work on testing the magnetic behavior of these alloys at elevated temperatures [2] will be briefly presented and discussed.

Keywords: nanocrystalline alloys, heat treatment, microstructure, magnetic properties**Acknowledgement:** This work was supported by the projects APVV-19-0369 and VEGA2/0171/19**References**

[1] K. Suzuki et al., Appl. Phys. Lett. 110 (2017) 012407

[2] B. Kunca et al., J. Alloys Compd. 911 (2022) 165033

MM-I07 (Invited)

X-ray spectro- and microscopic-techniques on novel materials

Way-Faung Pong*

Department of Physics, Tamkang University, New Taipei City, Taiwan

* Corresponding author's e-mail: wfpong@mail.tku.edu.tw

The presentation will focus on the use of synchrotron radiation-based spectroscopic and microscopic techniques for probing the electronic and atomic structures of novel and low dimensional materials. Elucidating electronic structures during an electrochemical reaction of energy materials, such as batteries and electrochemical materials, is essential to understanding better the energy conversion mechanism. Unlike other techniques, *in-situ* X-ray absorption spectroscopy (XAS) directly provides information on electronic structures, which is critical for tracking the charge states of active elements during a chemical reaction. The studies primarily have been involved with using XAS, X-ray emission spectroscopy (XES)/resonance inelastic X-ray scattering (RIXS) at Taiwan Photon Source (TPS)/Taiwan Light Source (TLS) and other synchrotron-related facilities. This presentation will report the current achievements and perspectives of XAS, XES/RIXS and Scanning Transmission X-ray Microscopy (STXM) techniques on relevant materials. Emerging characterization tool developed at TPS 45A and 27A beamlines will be also presented.

Keywords: XAS, XES/RIXS and STXM

MM-I08 (Invited)**Substrate polarity, phase stability, electronic structure and magnetic properties of multiferroic YMnO₃ thin films**Tahta Amrillah¹, My Ngoc Duong² and Jenh-Yih Juang^{3, *}¹ Department of Nanotechnology, Faculty of Advanced Technology and Multidiscipline, Universitas Airlangga, Indonesia² Department of Electrophysics, National Yang Ming Chiao Tung University, Taiwan³ Department of Electrophysics, National Yang Ming Chiao Tung University, Taiwan

* Corresponding author's email: jyjuang@nycu.edu.tw

In this study, we explored the effects of surface polarity and orientation of substrates on the phase stabilisation of multiferroic hexagonal YMnO₃ (YMO) thin films. It is found that the configuration of the initial atomic layers during the growth of YMO thin films plays a key role in minimising the misfit strain and, hence, stabilising the resultant phases. Remarkably, it is also observed that the polarity of the terminating substrate surface is playing an equally important role in determining the eventual microstructure, electronic structure and magnetic properties of the YMO films. We suggest that the extent of charge accumulation induced by the substrate surface polarity may have resulted in significant effect on the film/substrate interfacial intermixing, which, in turn, alters the crystalline structure and, hence, physical properties of the films. Results obtained from YMO films grown on MgO(100) and MgO(111) substrates will be presented and discussed. It is believed that the present results represent an alternative possibility of manipulating the magnetic properties of YMO films via interfacial engineering, which might be beneficial for various next-generation oxide electronics.

Keywords: Surface Polarity of Substrate, Phase stabilisation, Multiferroic manganites thin films, Electronic Structure, Magnetic properties

MM-I09 (Invited)**Point contact Andreev reflection spectroscopy on topological Kondo insulator SmB₆**

Masanobu Shiga^{1,*}, Takurou Harada¹, Tsubasa Teramoto¹, Takuya Takahashi¹, Fumitoshi Iga², and Tatsuya Kawae¹

¹ Department of Applied Quantum Physics, Kyushu University, Fukuoka 819-0395, Japan

² Institute of Quantum Beam Science, Graduate school of Science and Engineering, Ibaraki University, Mito 310-8512, Japan

* Corresponding author's e-mail: shiga.masanobu.881@m.kyushu-u.ac.jp

SmB₆ is famous for Kondo insulator (TI). In KI, the electrical resistivity increases rapidly below the Kondo temperature due to the formation of hybridization gap near the Fermi energy, which originates from the hybridization between the conduction electrons and *f* electrons (*c-f* hybridization). Meanwhile, the electrical resistivity of SmB₆ saturates below $T \sim 5$ K despite the full development of the hybridization gap, which has been interpreted as the existence of the in-gap state inside the hybridization gap [1]. On the other hand, recently, a new scenario is proposed by Dzero *et al.*, which pointed out that SmB₆ is classified as a topological Kondo insulator (TKI) [2]. If the SmB₆ is a TKI, the metallic state exists on a surface of SmB₆. So far, to explore the surface metallic state on SmB₆, many experiments have been conducted [3]. However, the origin of the metallic behavior at low temperatures is still controversial. In the present study, we performed point contact Andreev reflection spectroscopy (PCARS) measurements to examine the metallic surface state of SmB₆.

Figure 1 shows the PCARS spectrum of SmB₆ using a Nb probe tip at $T = 4.5$ K, where the temperature is lower than the superconducting transition temperature T_c of Nb. A narrow dip structure is observed at around zero bias, which is overlapped by a broad asymmetric dip-shaped background. Importantly, the narrow dip structure disappears above the T_c of Nb, indicating that the narrow dip comes from the Andreev reflection at SmB₆/Nb interface. These demonstrate the existence of the surface metallic state on SmB₆. From the fitting of spectra by the theoretical model, the spin polarization of the surface state is estimated to be $P \sim 0.5$, strongly suggesting that a high spin polarized metallic state exists on the surface although SmB₆ is a paramagnetic insulator. Our findings support that SmB₆ is a topological Kondo insulator.

Keywords: topological Kondo insulator, SmB₆, point contact Andreev reflection

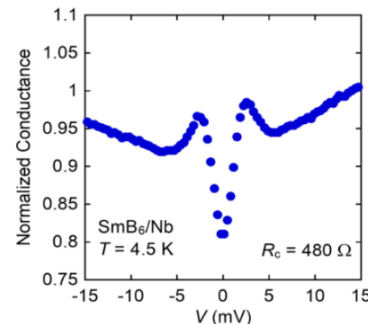


FIG. 1. dI/dV spectra of SmB₆/Nb interface at $T = 4.5$ K.

References

- [1] N. E. Sluchanko, et al., Phys. Rev. B 61, 9906 (2000).
- [2] M. Dzero, *et al.*, Phys. Rev. Lett. 104, 106408 (2010).
- [3] N. Xu et al., Nat. Commun. 5, 4566 (2014).

MM-I10 (Invited)**Searching for the origin of magnetic inhomogeneity of FeRh film**

Sehwan Song¹, Jiwoong Kim¹, Chang-woo Cho¹, Jisung Lee^{1,2}, Dooyong Lee¹, Doukyun Kim¹, Hyegyung Kim^{1,3}, Haeyong Kang¹, Chul-Hong Park⁴, Jun Kue Park⁵, Jae Hyuck Jang², Noboru Miyata⁶, Neeraj Kumar⁷, Yeong-Ah Soh⁷, Chanyoung Hwang⁸, Brian J. Kirby⁹, Sungkyun Park^{1,*}

¹ Department of Physics, Pusan National University, Busan 46241, Korea

² Korea Basic Science Institute, Daejeon 34133, Korea

³ Core Research Facilities, Pusan National University Busan 46241, Korea

⁴ Department of Physics Education, Pusan National University, Busan 46241, Korea

⁵ Multi-Purpose Accelerator Complex, Korea Atomic Energy Research Institute, Gyeongju 38180, Korea

⁶ Neutron Science and Technology Center, Compressive Research Organization for Science and Society, 162-1 Shirakata, Tokai, Naka, Ibaraki 319-1106, Japan

⁷ Paul Scherrer Institute, 5232 Villigen, Switzerland

⁸ Quantum Spin Team, Korea Research Institute of Standards & Science, Daejeon 34113, Korea

⁹ NIST Center for Neutron Research, National Institute Standard & Technology, Gaithersburg, MD 20878, USA

* Corresponding author's email: psk@pusan.ac.kr

Antiferromagnetic (AFM) FeRh exhibits magnetic phase transition from AFM to ferromagnetic (FM) system around room temperature. Therefore, utilizing the phase transition characteristics in modern spintronic applications get more attention due to advantageous AFM characteristics. In order to adapt device architecture, the interface characteristics of FeRh film are essential. Previously, it has been known that the pristine FeRh films exhibit residual ferromagnetism in the AFM state (i.e., below transition temperature). Therefore, it is disadvantageous to obtain magnetically clean interfaces owing to the formation of residual ferromagnetism at the interfaces. In this presentation, we examined the temperature- and depth-dependent magnetic properties of DC sputtered FeRh films to enhance our understanding of the residual ferromagnetism in the AFM state. As a result, we found the presence of non-uniform magnetic properties at the interfaces. Furthermore, we showed the different origins of residual ferromagnetism at the top and bottom interfaces.

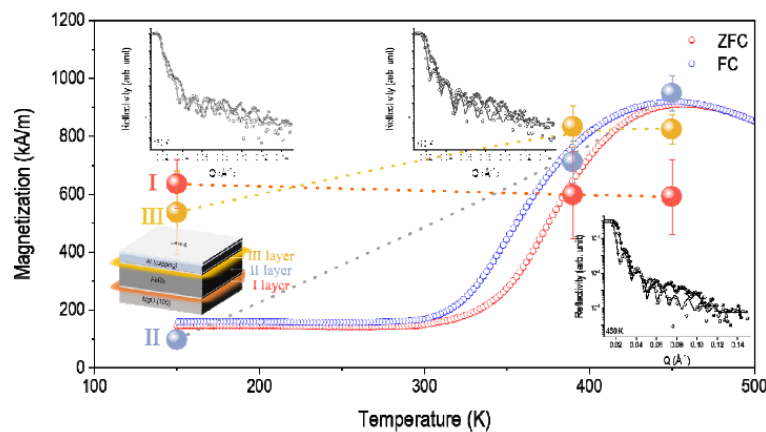


FIG. 1. Temperature- and depth-dependent magnetic characteristics of FeRh film.

Acknowledgement: This study was supported in part by NRF-2018R1D1A1B07045663, NRF-2020K1A3A7A09077715, NRF-2021M3H4A6A02045432, NRF- 2022M3H4A1A04071154, and No. 2021R1A6C101A429.

MM-I11 (Invited)**Magnetic skyrmion for the Brownian computing**

Y. Suzuki^{1, 2, *}, S. Miki¹, R. Ishikawa³, M. Goto^{1, 2}, H. Mori¹, K. Hashimoto¹, E. Tamura¹, H. Nomura^{1, 2} and K. Emoto¹

¹ Graduate school of engineering science, Osaka University, Osaka 560-8531, Japan

² Spintronics Research Network Division, Institute for Open and Transdisciplinary Research Initiatives, Osaka University, Yamadaoka 2-1, Suita, Osaka, 565-0871, Japan

³ ULVAC-Osaka University Joint Research Laboratory for Future Technology, Osaka University, 2-1, Yamadaoka, Suita, Osaka 560-0871, Japan

* Corresponding author's e-mail: suzuki.yoshishige.es@osaka-u.ac.jp

Magnetic Skyrmion is a particle-like magnetic excitation in ferromagnetic material. The magnetic Skyrmion shows Brownian motion [1, 2] as if it is a micro- or nano-size particle sintered in a liquid. The skyrmion system can be an ideal platform for designing stochastic computer [1] and/or Brownian computer [3].

To create the Skyrmions, Ta/Co-Fe-B/Ta sandwiched films [4] possessing perpendicular magnetic anisotropy and the interfacial-Dzyaloshinskii-Moriya interaction (i-DMI) were fabricated. Changing the upper and lower Ta film thicknesses independently, the ratio of the i-DMI energy to the magnetic anisotropy energy was adjusted. In addition, by eliminating the annealing process, the generation of grain boundaries was suppressed. The annealing free process enhanced the diffusion coefficient of skyrmions by a factor of more than 10 compared to the previous study [1] and comparable to the recent observations [4, 5]. The Skyrmions are adjusted to have a diameter of about 1 μm to allow the observation by an optical microscope with polarization analysis (MOKE microscope).

In this talk, film preparation and microfabrication of skyrmion channels and boxes [6] by means of SiO₂ add layer deposition [4] and ion implantation [7] will be introduced. In the end, the perspective on the implementation of the Brownian computer will be discussed.

Keywords: Skyrmion, Brownian computer, Spintronics, Diffusion, Artificial intelligence

Acknowledgments: This work was supported by the ULVAC, JSPS Grant-in-Aid for Scientific Research (S) Grant Number JP20H05666, Japan, CREST (Non-classical Spin project, JPMJCR20C1) of the Japan Science and Technology Agency, and Center for Spintronics Research Network (CSRN), Graduate School of Engineering Science, Osaka University.

References

- [1] J. Zazvorka et al., Nat. Nanotech. 14, 658 (2019).
- [2] S. Miki et al., J. Phys. Soc. Jpn. 90, 083601 (2021).
- [3] F. Peper et al., ACM J. Emerg. Technol. Comput. Syst, 9, 1, Article 3 (2013).
- [4] Y. Jibiki et al., Appl. Phys. Lett. 117, 082402 (2020).
- [5] L. Zhao et al., Phys. Rev. Lett. 125, 027206 (2020).
- [6] R. Ishikawa et al., Appl. Phys. Lett. 119, 072402 (2021).
- [7] S. Miki et al., submitted for publication.

Session: Photonics and Hybrid Materials**PH-I01 - PH-I06****PH-I01 (Invited)****Local environment of emission center ions in phosphor materials**Tomoyuki Yamamoto^{1,*}¹ Waseda University, Shinjuku, Tokyo, 169-8555, Japan

* Corresponding author's e-mail: tymmt@waseda.jp

Recently importance of the phosphor materials is raising in many fields, since the applications of the phosphor materials are not only for our ambient lightings but also for agriculture and generations of electricity together with solar cells. Most of the phosphor materials are synthesized with doping techniques, i.e., incorporation of dilute ions as emission center. For instance, rare-earth ions such as Pr and Eu ions are often doped in wide-gap host materials such as oxides and fluorides, which act as an emission center for the efficient phosphors. It is well known that photon emission intensity of the phosphor materials are strongly related to the local environment of emission center ions.

In this presentation, local environment analysis of Mn ions in red phosphors both with experimental and theoretical methods will be introduced. For the former experimental analysis, X-ray absorption near edge structure (XANES) and electron spin resonance (ESR) analysis for Mn ions are shown, while for the latter theoretical one the first principles calculations within a framework of the density functional theory (DFT) level are shown. In some cases, co-doping can enhance the emission intensity of the phosphors. To reveal the reason why such enhancement occurs due to co-dopings, combined analysis of the above experimental and theoretical calculations were carried out for $\text{CaAl}_{12}\text{O}_{19}:\text{Mn}$ co-doped with divalent ions, such as Mg^{2+} , Zn^{2+} , Cd^{2+} and Sr^{2+} [1], which suggested co-doped ions contribute to the change in local environment of Mn ions.

References

[1] U. Zafari et al., Opt. Mater. X, submitted.

PH-I02 (Invited)**Luminescence and non-linear optical properties at mid-infrared spectral range**

Michał Piasecki¹, G.L. Myronchuk², Andrzej Suchocki³, Anatoli Popov⁴, Mikhail G. Brik^{1,5,6,7}, I.E. Barchiy⁸, O.Y. Khyzhun⁹

¹ Department of Theoretical Physics, J. Długosz University, Armii Krajowej 13/15, 42-200 Częstochowa, Poland,

² Lesya Ukrainka Eastern European National University, 9 Potapova Str., UA-43021 Lutsk, Ukraine

³ Institute of Physics, Polish Academy of Sciences, Warszawa, Poland,

⁴ Institute of Solid-State Physics, University of Latvia, Riga LV 1063, Latvia

⁵ Institute of Physics, University of Tartu, W. Ostwald Str. 1, Tartu 50411, Estonia,

⁶ College of Sciences & CQUPT-BUL Innovation Institute, Chongqing University of Posts and Telecommunications, Chongqing 400065, People's Republic of China,

⁷ Academy of Romanian Scientists, Ilfov Street, no 3, 050044 Bucharest, Romania,

⁸ Inorganic Chemistry Department, Uzhhorod National University, UA-88000, Uzhhorod, Ukraine

⁹ Frantsevych Institute for Problems of Materials Science, NAS of Ukraine, 03142 Kyiv, Ukraine

* Corresponding author's e-mail: m.piasecki@ujd.edu.pl

The Mid-red (MIR) spectral range shown great important for both fundamental and possible applications such as optical communications, gasses pollutants detection, trace chemical analysis as well as the next generation imaging devices for remote sensing and medical contrast agents due their fundamental absorption features in the wavelength regions from 1,5 μm to 15 μm . Therefore, strong emitting sources in MIR spectral range will be extremely useful in the construction of lidar allowing remote detection of gases (including hazardous gases), which is important for health and environmental protection, chemical rescue, the mining industry or military applications. Currently, the most effective ways of obtaining radiation in MIR are luminescence phenomena or radian form CO₂ lasers by utilise a non-linear-optical effects (SHG, THG).

From the other hand, the range of high spectral transparency for chalcogenide or halide crystals, glasses or ceramics (from about 400-700 nm to several dozen micrometres) is unique and do not available for oxygen containing materials. In addition, these materials with low energy of the phonon system are predestined at the matrices for embedding active elements (RE or 3d elements) for long-wave luminescence or construction lasers operating in the mid-infrared range along with explanation limitations regarding embedding of rare earth ions in chalcogenide/halide structures, which is not an easy experimental undertaking.

Next, we focus on the influence of the structural properties (composition, complexity and defects, presenting in real materials) on the stability, luminescence optical and nonlinear-optical efficiency for the group of binary, ternary and quaternary halide and chalcogenide crystals, that have found practical applications in IR optoelectronics. Especially above-mentioned defects shown the significant impact on nonlinear-optical and luminescence properties.

Keywords: Mid-Red, luminescence, non-linear optics, halides, chalcogenides

PH-I03 (Invited)**Magnetoplasmonic core-shell nanowires: synthesis and self-assembly for structural colors and chiral metasurfaces**

Huu-Quang Nguyen, My-Chi Thi Nguyen, Jaebeom Lee*

Department of Chemistry, Chungnam National University, Daejeon, 34134, Republic of Korea

* Corresponding author's e-mail: nanoleelab@cnu.ac.kr

A facile one-pot solvothermal synthesis method was developed for growing an anisotropic hybrid nanostructure composed of magnetic oxide nanoparticles coated on plasmonic gold nanowires (Au@Fe_xO_y MagPlas NWs). The effects of reaction temperature, time, reducing agent and precursor as well as post-synthesis treatment were optimized to produce highly uniform NWs in the aspect ratio of 25 ~ 82. The synthesized structures inherited the magnetic properties from the iron oxide layer and anisotropic localized surface plasmon resonance (LSPR) of the gold nanowires, which are potentially useful for a wide range of optical and sensing applications. Especially, by exploiting the interaction of NWs with an external magnetic field, MagPlas NWs were aligned into 2D photonic surfaces with high periodicity, which can generate distinctive structural colors that are uniquely iridescent and polarization-sensitive. Furthermore, we demonstrated the fabrication of a bioinspired Bouligand-type chiral cholesteric metasurface, by stacking the 2D aligned microchains continuously with a rotating pitch angle. This film displays remarkable sensing capability with circular dichroism spectroscopy, which could detect the change of surface alignments upon the addition of analyte molecules. These intriguing properties of MagPlas anisotropic NWs and their self-assemblies could be consequently valuable for developing photonic, catalysts, and sensing applications.

Keywords: magnetoplasmonic, nanosynthesis, nanowires, chiral, structural color

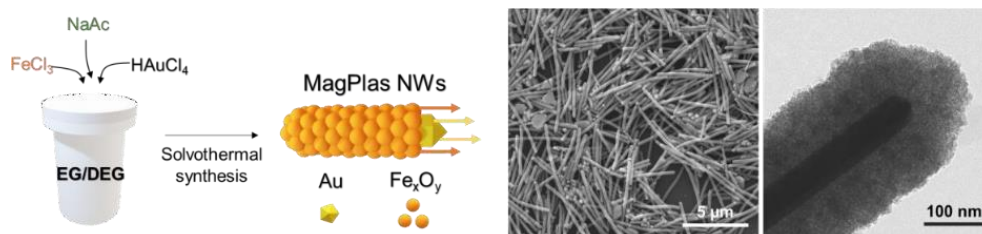


FIG. 1. Schematics of the synthesis process and electron microscopic images of the synthesized MagPlas NWs

References

- [1] Nguyen, H-Q., et al. (2022) ACS Nano, 16(4), 5795–5806
- [2] Tran, VT., et al. (2018). Anal. Chem., 90(1), 225–239.

PH-I04 (Invited)**High-performance colorful semitransparent organic solar cells with etalon electrodes**

Jin Young Kim*

School of Energy and Chemical Engineering, UNIST, Ulsan 44919, Republic of Korea

* Corresponding author's e-mail: jykim@unist.ac.kr

Semitransparent organic solar cells (STOSCs) are a technology that combines the benefits of visible light transparency and light-to-electrical energy conversion. One of the greatest opportunities for STOSCs is their integration into windows and skylights in energy-sustainable buildings. For this application, the aesthetic aspects of solar cells maybe as important as their electrical performance. Here, our strategy enables to achieve high-quality and colorful STOSCs using Fabry-Pérot etalon-type electrodes. These electrodes are composed of an antimony oxide (Sb₂O₃) cavity layer and two thin Ag mirrors. These dichroic tri-layer structures perform two functions as top conducting electrodes and colorfilters. These dual-function electrodes were applied to photovoltaic devices and displayed vivid colors, natural transparency, and good performance as compared to devices that use conventional metal electrodes. Furthermore, to achieve saturated colors and low photocurrent losses, active layer materials were selected such that their transmittance peaks matched the transmittance maxima of the electrodes. These strategies for colorful STOSCs result in power conversion efficiencies (PCEs) of up to 13.3% and maximum transmittances (T_{MAX}) of 24.6% in blue devices, PCEs of up to 9.71% and T_{MAX} of 35.4% in green devices, and PCEs of up to 7.63% and T_{MAX} of 34.7% in red devices.

Keywords: organic solar cells, colourful, semitransparent, antimony oxide, Fabry-Pérot etalon

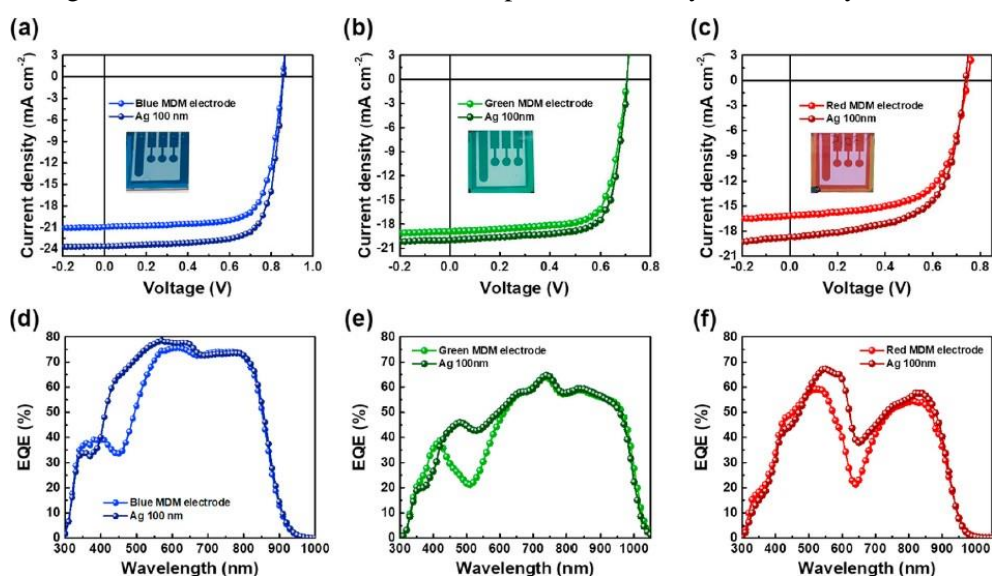


FIG. J-V curves and EQE spectra of the control (Ag 100 nm) and semitransparent (blue, green, red MDM electrodes) devices based on (a, d) PM6:Y6 as blue active materials, (b, e) PTB7-Th:CO₈DFIC:PC₇₁BM as green active materials, (c, f) J52:IEICO-4F:NIDCS-HO as red active materials, respectively, under AM1.5G (100 mW cm⁻²) illumination.

Reference

[1] H. R. Yeom et al., Nano Energy 77 (2020) 105146.

PH-I05 (Invited)**Probing the exciton wavefunction in low-dimensional materials by photoemission momentum microscopy**G. S. Matthijs Jansen^{1, *}¹ I. Physical Institute, University of Göttingen, Göttingen, Germany

* Corresponding author's e-mail: gsmjansen@uni-goettingen.de

The strong and long-lived excitonic response of low-dimensional semiconductors such as two-dimensional transition metal dichalcogenides (TMDs) and zero-dimensional organic semiconductors provides an outstanding opportunity for innovation, with applications ranging from organic solar cells to new logic devices beyond current electronics. Efficient application of these materials, however, depends on an accurate understanding of the opto-electronic response, ultimately characterized by a complete knowledge of the out-of-equilibrium wavefunction that arises upon optical excitation. Such knowledge, which is extremely difficult to achieve using experimental and theoretical methods alike, has now come within our grasp through the development of multi-dimensional time- and angle-resolved photoelectron spectroscopy devices [1]. In particular, this has enabled 1) a fully time-, 2D momentum-, energy-resolved characterization of the out-of-equilibrium electronic structure and 2) the application of photoemission orbital tomography to acquire direct access to the real-space properties of the electronic wavefunction in thin organic molecular layers [2]. As demonstrated recently [3], this does provide a unique access to the real-space excited-state wavefunction under optical excitation. Here, I will demonstrate how time-resolved momentum microscopy allows us to trace the formation of interlayer excitons in a twisted TMD heterostructure through space and time [4], and secondly enables the characterization of out-of-equilibrium excitonic wavefunctions in a crystalline buckminsterfullerene (C₆₀) multilayer.

Keywords: Excitons, ARPES, photo-emission orbital tomography, pump-probe

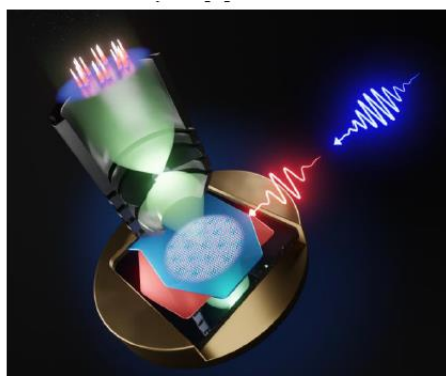


FIG. 1. Photoemission momentum microscopy enables to probe the full energy- and 2D momentum-resolved electronic structure with femtosecond time resolution and provides unprecedented information on dynamics in micro-scale TMD heterostructures, organized organic thin films and many other low-dimensional systems.

References

- [1] M. Keunecke et al., Rev. Sci. Instr. 91 063905 (2020). [2] G. S. M. Jansen et al., NJP, 22 6, 063012 (2020)
 [3] R. Wallauer et al. Science 371 6533, 1056-1059 (2021)
 [4] D. Schmitt et al., Nature 608 7923, 499-503 (2022).

PH-I06 (Invited) Cancel**Metamaterials: plasmonic properties, ultrafast dynamics, heat transfer, and tuneability**

Nguyen Thanh Tung*

Institute of Materials Science, Vietnam Academy of Science and Technology, Hanoi 11307, Vietnam

* Corresponding author's email: tungnt@ims.vast.ac.vn

In macroscopic physics, many properties of bulk materials are usually independent of the sample size. Metamaterials that are made up by periodic subwavelength pieces of matter, however, reveals a not only different but also fascinating picture: their properties are not derived from the constituent materials, but from their newly designed structures [1]. The motivation behind metamaterial research in our group arises, on one hand, from fundamental interest in various aspects of physical properties from the nano-scale to the solid-state limit, and on the other hand, from the desire of using smarter structures for novel technological applications. In this talk, we present our results on plasmonic properties, ultrafast dynamics, heat transfer, and tuneability of metamaterials (see Fig. 1) operating at various frequency regimes (GHz, THz, and optics) [2, 3]. The recent implementation of metamaterials for energy harvesting and advanced sensing applications is also discussed [4].

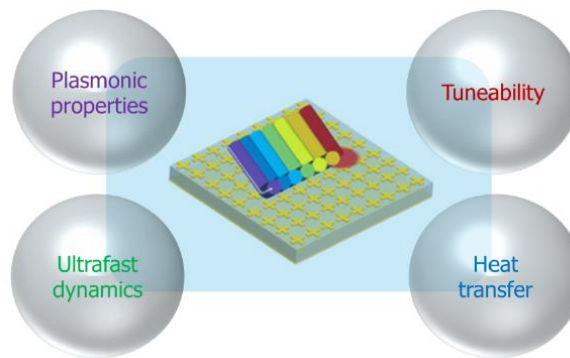


FIG. 1. The motivation behind metamaterial research arises from fundamental interest in various aspects of physical properties, for example, plasmonic properties, ultrafast dynamics, heat transfer, and tuneability.

Keywords: metamaterials, sensing, plasmonics, ultrafast dynamics, tuneability

Reference

- [1] M. Wegener, Science 342 (2013) 939.
- [2] D.T. Viet et al., Appl. Phys. Express 8 (2015) 032001.
- [3] M. Bejide et al., Opt. Express 29 (2020) 170.
- [4] U.T.D. Thuy et al., APL Mater. 7 (2019) 071102.

Session: Spintronic materials and devices**SD-I01 - SD-I12****SD-I01 (Invited)****Observation of flat band in millimeter-scale magic-angle twisted bilayer graphene**

Wataru Norimatsu*

Department of Materials Science and Engineering, Nagoya University, Aichi, 464-8603, Japan

* Corresponding author's e-mail: norimatsu.wataru@material.nagoya-u.ac.jp

Twisted bilayer graphene (TBG) has attracting great interest as a method to introduce a novel degree of freedom in the electronic states in graphene. Particularly, the magic-angle (1.1°) TBG exhibited superconductivity, induced by the flat band [1]. In order to expand the field of “twistronics”, the large-area TBG formation and the control of the flat band energy are required. In this study, we obtained the 5 x 5 mm² TBG sample, and observed the electronic structure, including the flat band. We obtained two samples of epitaxial monolayer graphene (EMLG) by thermal decomposition of SiC. We exfoliated one graphene from the SiC substrate, and transferred it onto other EMLG/SiC with a twist angle [2]. Angle-resolved photoemission spectroscopy (ARPES) was carried out to reveal the electronic structure of the TBG samples.

Figure 1 is the ARPES results of a TBG sample [3]. In this TBG sample, EMLG of 5 x 5 mm² size was transferred with a target twist angle of 1.1°, and its optical micrograph is shown in the inset. The ARPES image in (a) includes two or more bands as shown by blue and red arrows. One of the striking features of the ARPES image is the high density of states at -0.22 and -0.51 eV. In addition to the states at -0.22 and -0.51 eV, another band at -0.37 eV was observed in between them, as shown by dotted lines in the figure. These features can be readily explained by the calculated spectral function shown in Fig. 1(c) and (d), which clearly shows the flat band at -0.37 eV.

Keywords: graphene, twisted bilayer graphene, magic-angle, flat band, ARPES

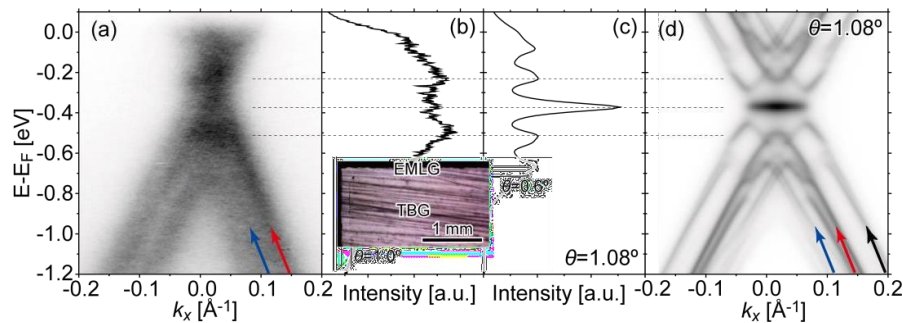


FIG. 1. (a) ARPES image of the TBG sample. (b) Intensity profile along $k_x = 0.016 \text{ \AA}^{-1}$ line in (a). (c)(d) Spectral function of 1.08° TBG. (c) Intensity profile along $k_x = 0.016 \text{ \AA}^{-1}$ line in (d).

References

- [1] Y. Cao, et al., Nature 556, 43 (2018).
- [2] J. Kim, et al., Science 342, 833 (2013).
- [3] K. Sato, et al., Commun. Mater. 2, 117 (2021).

SD-I02 (Invited)**Towards magnetic skyrmionics**Chanyong Hwang^{1,*}¹ Quantum Technology Institute, Korea Research Institute of Standards and Science, Daejeon, 34113, Korea

* Corresponding author's e-mail: chanyong.hwang@gmail.com

Magnetic skyrmion has drawn lots of attention due to its topological characteristics and its use as an information carrier. Over the last decades, the formation of the magnetic skyrmion was quite limited to few cases, where kinds of perturbative methods have been applied. Since this formation process is not quite systematic, the sample is quite limited. We have found the systematic way to form, delete and move the magnetic skyrmion in all kinds of magnetic films with perpendicular magnetic anisotropy. With this general recipe for skyrmion formation, we can drive lots of devices which can be used in spintronics. Skyrmion racetrack memory, magnetic skyrmion transistor, also neuromorphic device with magnetic skyrmion will be presented.

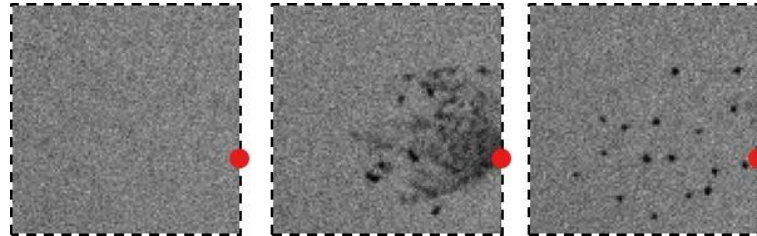
Keywords: magnetic skyrmion, PMA, skyrmionics, spintronic device

FIG. 1. Formation of Magnetic Skyrmion using vertical current pulse.

References

- [1] K.-W. Moon et al., NPG Asia Materials 13, 20 (2021)
- [2] S. Yang et al., Adv. Mater. 33, 2104406(2021)

SD-I03 (Invited)**Neuromorphic devices based on electrochemical metallization and charge trapping**

Bae Ho Park*

Department of Physics, Konkuk University, Seoul 05029, Korea

* Corresponding author's e-mail: baehpark@konkuk.ac.kr

Neuromorphic systems have attracted much attention because they can provide suitable solutions for problems emerging in ‘big data’ era. Up to now, neuromorphic systems emulating the functions of human brain have been implemented in a variety of applications but have revealed limitations due to a large number of devices and high energy consumption. Therefore, it is required to develop neuromorphic systems based on neuromorphic devices which emulate the hardware of human biological systems, such as synapses and neurons.

In this talk, I will introduce recent research activities of my laboratory to implement neuromorphic devices based on inorganic nano materials. By combining cation migration and ferroelectric polarization reversal, we implemented an energy efficient and selectively activated synaptic device [1]. It was found that electrochemical metallization devices with a ferroelectric electrolyte could implement both neuron and synaptic devices depending on the active electrode material. Progressive and stable synaptic plasticity with femtojoule energy consumption could be achieved by the interface engineering of a metal/ferroelectric/semiconductor [2]. Multi-stable resistive states and synaptic behaviors were observed in a capacitor structure with an emerging two-dimensional insulator, CrPS4 [3]. It was demonstrated that vertical Ag/CrPS4/Au capacitors could be promising inorganic devices compatible with next-generation, flexible neuromorphic technology [4]. Furthermore, a vertical two-terminal Pt/bi-layer $\text{Sr}_{1.8}\text{Ag}_{0.2}\text{Nb}_3\text{O}_{10}$ nanosheet/Nb:SrTiO₃ device could emulate heterosynaptic plasticity by controlling the number of electron trap sites through A-site deficiency control of the nanosheet.

Keywords: neuromorphic, synaptic device, neuron device, ferroelectric, heterosynaptic plasticity

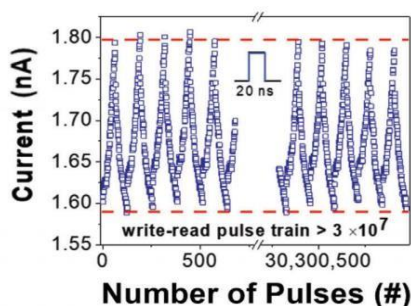


FIG. 1. Demonstration of stable synaptic weight update for $\text{i/Pb}(\text{Zr}_{0.52}\text{Ti}_{0.48})\text{O}_3/0.5 \text{ wt.}\% \text{ Nb-doped SrTiO}_3$ with ultralow energy consumption below 9 fJ during over 3×10^7 pulses.

References

- [1] C. Yoon & B. H. Park et al. Nano Letters 17, 1949 (2017).
- [2] S. Kim & B. H. Park et al. Advanced Science 2201502 (2022).
- [3] M. J. Lee & B. H. Park et al. NPG Asia Materials 10:23 (2018).
- [4] M. J. Lee & B. H. Park et al. NPG Asia Materials 12:82 (2020).

SD-I04 (Invited)**Superconducting diode effect in Rashba superlattice**

Hideki Narita¹, Ryo Kawarazaki¹, Yuta Miyasaka¹, Yuhei Ikeda², Ryusuke Hisatomi¹, Akito Daido², Yoichi Shiota¹, Takahiro Moriyama¹, Youichi Yanase^{2,3}, Alexey V. Ognev⁵, Alexander S. Samardak⁵, and Teruo Ono^{1,4,5,*}

¹ Institute for Chemical Research, Kyoto University, Gokasho, Uji, Kyoto, 611-0011, Japan

² Department of Physics, Graduate School of Science, Kyoto University, Kitashirakawa, Sakyo, Kyoto 606-8502, Japan

³ Institute for Molecular Science, Okazaki, 444-8585, Japan

⁴ Center for Spintronics Research Network, Institute for Chemical Research, Kyoto University, Gokasho, Uji, Kyoto, 611-0011, Japan

⁵ Laboratory of Spin-Orbitronics, Institute of High Technologies and Advanced Materials, Far Eastern Federal University, Vladivostok 690922, Russia

* Corresponding author's e-mail: ono@scl.kyoto-u.ac.jp

The diode effect is fundamental to electronic devices and is widely used in rectifiers and AC-DC converters. However, conventional diodes have an energy loss due to finite resistance. We found the superconducting diode effect (SDE) in Nb/V/Ta superlattices with a polar structure, which is the ultimate diode effect exhibiting a superconducting state in one direction and a normal state in the other [1-3]. SDE can be considered as the nonreciprocity of the critical current for the metal-superconductor transition. We also found the reverse effect, i.e., the nonreciprocal critical magnetic field under the application of the supercurrent [4]. We also found that the polarity of the superconducting diode shows a sign reversal as a magnetic field is increased, which can be considered as the crossover and phase transitions of the finite-momentum pairing states predicted theoretically [5]. SDE in Nb/V/Ta superlattices needs an application of an external magnetic field to break the time reversal symmetry, which is a disadvantage in applications. We recently succeeded in demonstrating SDE in a zero-field by introducing ferromagnetic layers in superlattices. The polarity of the SDE is controlled by the magnetization direction of the ferromagnetic layer, leading to development of novel non-volatile memories and logic circuits with ultralow power consumption.

Acknowledgement: This work was partly supported by JSPS KAKENHI Grant Numbers (18H04225, 18H01178, 18H05227, 20H05665, 20H05159, 21K18145), the Cooperative Research Project Program of the Research Institute of Electrical Communication, Tohoku University, the Collaborative Research Program of the Institute for Chemical Research, Kyoto University, and the Russian Ministry of Science and Higher Education under Megagrant No. 075-15-2021-607.

References

- [1] F. Ando et al., J. Magn. Soc. Japan 43, 17 (2019).
- [2] F. Ando et al., Nature 584, 373 (2020).
- [3] F. Ando et al., Jpn. J. Appl. Phys. 60, 060902 (2021).
- [4] Y. Miyasaka et al., Appl. Phys. Express 14, 073003 (2021).
- [5] A. Daido et al., Phys. Rev. Lett. 128, 037001 (2022).

SD-I05 (Invited)**Enhanced anomalous Nernst effect in metallic superlattices**Takeshi Seki^{1,*}¹ Institute for Materials Research, Tohoku University, Sendai, 980-8577, Japan

* Corresponding author's e-mail: takeshi.seki@tohoku.ac.jp

Spin caloritronics, the field studying the interconversion between charge current (J_c) and heat current (J_q) mediated by spin current (J_s) and/or magnetization (M), has attracted much attention not only for academic interests but also for practical applications. The newly discovered spin caloritronic phenomena have stimulated the renewed interest in the thermoelectric phenomena in ferromagnets. One of the thermoelectric phenomena in ferromagnets is the anomalous Nernst effect (ANE), in which J_c appears in the cross-product direction of M and a temperature gradient (∇T). Although ANE has been known for a long time, the microscopic physical picture for ANE has not fully been understood. In addition to the fundamental point of view, this magneto-thermoelectric effect is possibly beneficial for thermoelectric conversion applications. The key for the ANE-based thermoelectric conversion is to find a material with a large anomalous Nernst coefficient (S^{ANE}).

We previously reported the enhancement of ANE in the Fe-based metallic multilayers [1], implying that the low dimensionality of layer and/or the existence of interface plays a role for the increase in ANE. This means that metallic multilayers or superlattices with a number of interfaces are promising for achieving large ANE.

In this talk, we introduce our recent studies on the ANE using the Ni / Pt metallic superlattices [1] and the Co₂MnGa / AlN multilayers [2]. For the former, the perpendicularly magnetized Ni/Pt (001) epitaxial superlattices were fabricated directly on a non-conductive SrTiO₃ substrate [3], and the Ni layer thickness dependence of ANE was investigated for [Ni (t nm) / Pt (1.0 nm)] _{$\times N$} . We found that the values of S^{ANE} for the Ni/Pt superlattices are one order of magnitude larger than that for the bulk Ni. The enhanced ANE is attributable to the large transverse thermoelectric conductivity.

For the latter, the polycrystalline Co₂MnGa / AlN multilayer films were deposited on an amorphous substrate, which shows $S^{\text{ANE}} = 4.9 \mu\text{V K}^{-1}$. This large S^{ANE} is comparable to the values reported for the single crystal Co₂MnGa bulks. The detailed structural analysis and the transport measurement suggest that the effect of interfacial strain on the Seebeck coefficient plays an important role for enhancing the ANE. Since the AlN layer is available on any substrate materials, even on a flexible polyimide substrate, large ANE is successfully achieved for the Co₂MnGa / AlN stack.

Keywords: Metallic Superlattice, Anomalous Nernst Effect, Ordered Alloy, Flexible Substrate

References

- [1] T. Seki, Y. Sakuraba, K. Masuda, A. Miura, M. Tsujikawa, K. Uchida, T. Kubota, Y. Miura, M. Shirai, and K. Takanashi, Phys. Rev. B 103, L020402-1-7 (2021).
- [2] J. Wang, Y.-C. Lau, W. Zhou, T. Seki, Y. Sakuraba, T. Kubota, K. Ito, and K. Takanashi, Adv. Electron. Mater., 2101380-1-8 (2022).
- [3] T. Seki, M. Tsujikawa, K. Ito, K. Uchida, H. Kurebayashi, M. Shirai, and K. Takanashi, Phys. Rev. Mater. 4, 064413-1-9 (2020).

SD-I06 (Invited)**Extended X-ray absorption spectroscopy and Debye–Waller factor under pressure**Ho Khac Hieu^{1, 2, *}, Hai Hoang^{1, 2}, Pham Thi Minh Hanh³, and Tran Thi Hai⁴¹ Institute of Research and Development, Duy Tan University, Da Nang 55000, Vietnam² Faculty of Natural Sciences, Duy Tan University, 03 Quang Trung, Hai Chau, Da Nang 550000, Vietnam³ Hanoi Pedagogical University No2, Nguyen Van Linh, Vinh Phuc 15900, Vietnam⁴ Hong Duc University, 565 Quang Trung, Dong Ve, Thanh Hoa 441430, Vietnam

* Corresponding author's e-mail: hieuhk@duytan.edu.vn

The pressure effects on extended X-ray absorption spectroscopy (EXAFS) and the atomic mean-square relative displacement characterizing the Debye–Waller factor have been investigated based on the Debye model [1]. The analytical expressions of the Debye frequency and EXAFS Debye–Waller factor have been derived as functions of crystal volume compressibility. Based on the well-established equation-of-state including the contributions of the anharmonic and electronic thermal pressures [2], numerical calculations have been performed for iron up to a pressure of 220 GPa and compared with experimental data when possible. These results show that the Debye frequency increases rapidly with compression, and beyond 150 GPa it behaves as a linear function of pressure [3]. Meanwhile the mean-square relative displacement curve drops robustly with pressure, especially at pressures smaller than 100 GPa. This phenomenon causes the enhancement of EXAFS signals at high pressure. Reversely, the increasing of temperature will reduce the amplitude of EXAFS spectra.

Keywords: High pressure, Melting curves, Vanadium, Niobium, Statistical moment method**References**

- [1] N.V. Hung, et al., *Physica B* 405(2010), 2519–2525.
- [2] P. Dewaele et al., *Phys. Rev. Lett.* 97 (2006), 215504.
- [3] H.K. Hieu et al., *J. Synchrotron Rad.* 27(2020), 1372–1375.

SD-I07 (Invited)**Material properties and growth mechanism of β -Ga₂O₃ epilayers grown on sapphire by metal organic chemical vapor deposition**

Ray-Hua Horng^{1, 2, *}, Apoorva Sood¹, Fu-Gow Tarntair¹, Dong-Sing Wu³, Singh Jitendra Pratap⁴

¹ Institute of Electronics, National Yang Ming Chiao Tung University, Hsinchu 30010, Taiwan

² Center for Emergent Functional Matter Science, National Yang Ming Chiao Tung University, Hsinchu 30010, Taiwan

³ Department of Applied Materials and Optoelectronic Engineering, National Chi Nan University, Nantou 54561, Taiwan

⁴ Physics Department, Indian Institute of Technology Delhi, New Delhi 110016, India

* Corresponding author's e-mail: rayhua@nycu.edu.tw

In this study, the monoclinic gallium oxide (β -Ga₂O₃) epilayer was successfully grown on c-plane (0001) sapphire substrate by metalorganic chemical vapor deposition (MOCVD) at different process parameters (growth time, TEGa flow rate and temperature). The surface properties of β -Ga₂O₃ thin film were observed using scanning electron microscopy, atomic force microscope, and X-ray diffraction. The experimental results found that the β -Ga₂O₃ epilayer possess superior crystalline quality that includes (-201), (-402), and (-603) three main crystalline orientations. In addition, by varying the growth time and TEGa flow rate increases, the crystallization characteristics and full width at half maximum of β -Ga₂O₃ film can be effectively improved. The thickness and surface roughness of β -Ga₂O₃ film increase with growth time and TEGa flow rate. However, as the growth temperature increases above 825°C, the thickness of β -Ga₂O₃ film decrease clearly. Furthermore, it can be found that the growth rate decreased as the growth time increasing. Due to the lattice mismatch between the β -Ga₂O₃ and sapphire, the growth mechanism of 3D growth at first, then lateral growth and 2D growth after the thick epilayer being grown was proposed. Furthermore, the β -Ga₂O₃ films are insulating and exhibit high resistance, with a value range of $10^{12} \sim 10^{13} \Omega$ approximately.

Keywords: gallium oxide, metal organic chemical vapor deposition, crystalline, roughness, growth mechanism

SD-I08 (Invited)**Fabrication of quantum devices by fine sputtering using a focused ion beam with nitrogen gas field ion source**

Masashi Akabori *

Center for Nano Materials and Technology, Japan Advanced Institute of Science and Technology, Asahidai 1-1, Nomi, Ishikawa, 923-1292, Japan

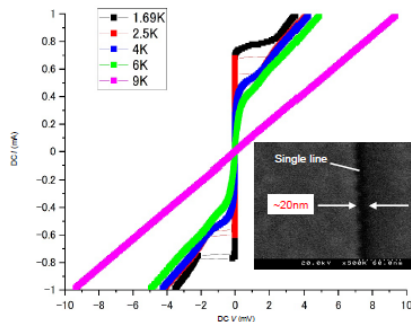
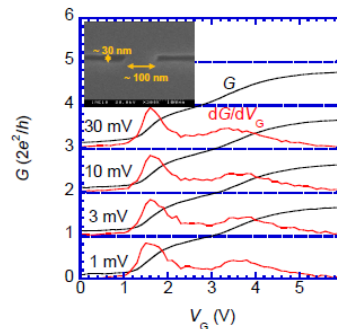
* Corresponding author's e-mail: akabori@jaist.ac.jp

In fabrication of various quantum devices, nanometer-order fine patterning is usually required. To this end, electron beam lithography (EBL) is frequently and widely used. In this study, instead of EBL, we focused on a focused ion beam with nitrogen gasfield ion source (N₂-GFIS-FIB), which has a capability of direct etching by fine sputtering at 10-nm-level or more less [1]. Using this, we fabricated two different types of quantum devices, such as Josephson junction (JJ) devices based on Nb thin film [2] and quantum point contact (QPC) devices based on InGaAs heterostructures [3].

To fabricate JJ devices, we simply performed single line etching of Nb on a semi-insulating GaAs substrate. Figure 1 shows temperature dependence of DC I - V characteristics of a JJ device with inset of a scanning electron microscope (SEM) image. By single line etching of 20-nm-width, a typical JJ behavior can be confirmed.

To fabricate QPC devices, we formed QPC by the direct etching followed by insulator gate stack using atomic layer deposition of Al₂O₃, and evaporation and lift-off of Ti/Au. Figure 2 shows Conductance characteristics of a QPC device with inset of a SEM image. Even though the QPC was depleted at 0 V of gate voltage, conductance was increased and seemed step-like structure with applying positive gate voltage.

Keywords: Gas Field Ion Source (GFIS), Josephson Junction (JJ), Quantum PointContact (QPC)

FIG. 1. I - V and SEM image of a JJ device.FIG. 2. G - V and SEM image of a QPC device.**References**

- [1] F. Aramaki et al., Proc. SPIE 8441 (2012) 84410D.
- [2] S. Sudo et al., Jpn. J. Appl. Phys. 61 (2022) SB1016.
- [3] M. Akabori et. al., Jpn. J. Appl. Phys. 53 (2014) 18002.

SD-I09 (Invited)**Study of nano-scale heat transports using magneto-thermoelectric effects**

Takashi Kimura*

Department of Physics, Kyushu University, Japan

* Corresponding author's email: t-kimu@phys.kyushu-u.ac.jp

Recent development of nano-fabrication techniques enables to realize functional electronic devices with the lateral dimension down to nano-meter scale. In the operation of such nano sized devices, understanding and controlling the heat transfer is an important issue because a small cross section produces a significant Joule heating effect. Since the characteristic lengths such as the mean free path and phase coherent length are comparable to the device dimension, the heat transport in nanostructured systems may be different from the bulk state and its combination. On the other hand, In the field of spintronics, in addition to the intriguing spin-dependent transports, various conversion phenomena between spin and heat have been reported recently, and a new research field has been emerged named as spincaloritronics. Therefore, it is essential to deepen understanding the heat transfer in nanospintronic devices for manipulating the heat as well as for developing spincaloritronics. In this presentation, we introduce heat-transport phenomena in various ferromagnetic/nonmagnetic metal hybrid structures by using unique magneto-thermoelectric effects.

First, the spatial temperature distribution in a laterally configured nanostructure based on GMR nanowire has been investigated [1]. A large thermal spin valve effect enables us to distinguish the flowing direction of the heat in the GMR nanowire. We find that the heat flow from the substrate is significant. Second, a temperature distribution in a ferromagnetic nanowire has been investigated by using various magneto-thermoelectric effects [2]. The combination between the anisotropic magneto-Seebeck effect and anomalous Nernst effect enables us to understand a three-dimension temperature gradient in a ferromagnetic nanowire precisely. We find that the transverse heat flow is a significant contribution on the field dependence of the Seebeck voltage. Finally, temperature dependence of the thermal spin valve effect and anisotropic magneto-Seebeck effect have been investigated. We find that the signs of the voltage changes were reversed at specific temperatures. Possible mechanism has been discussed in order to explain the unique signatures.

Thus, by the optimization of the device structures, enhanced thermal spin valve version of the GMR effect, anisotropic magneto-Seebeck effect and anomalous Nernst effect have been obtained. Multiple ways in which heat interacts with spin and the interplay of such effects enable us to evaluate the heat distribution. These demonstration paves the way for the precise analysis of the heat flow in nano-structured electronic devices.

References

- [1] Md. Kamruzzaman, et al. Appl. Phys. Express. 14, 073004(2021).
- [2] Md. Kamruzzaman, et al. Phys. Status Solidi RRL, 2100608(2022).

SD-I10 (Invited)**Sub-second and ppm-level optical sensing of hydrogen using templated control of nano-hydride geometry and magnetic composition**Tho Duc Nguyen^{1, *}¹ Department of Physics and Astronomy, University of Georgia, Athens, Georgia 30602, USA

* Corresponding author's e-mail: ngtho@uga.edu

The use of hydrogen (H₂) fuel as a clean and renewable alternative is one of the most practical solutions for the already serious fossil-fuel shortages, global climate change, and air pollution. However, significant challenges remain with respect to the safe deployment of H₂ fuel sources due to its relatively low ignition energy in a broad flammability range, which is a serious barrier preventing its widespread adoption. Unfortunately, a suite of flammability mitigating technologies, particularly robust sensors for H₂ leak detection and concentration monitoring has not been achieved. To this end, we have developed a class of lightweight optical H₂ sensors based on a metasurface of Pd nano-patchy particle arrays¹, which fulfills the increasing requirements of a safe H₂ fuel sensing system with no risk of sparking. The structure of the optical sensor is readily nano-engineered to yield extraordinarily rapid response to H₂ gas (<3 s at 1 mbar H₂) with a high degree of accuracy (<5%). By incorporating 20% Ag, Au or Co, the sensing performances of the Pd-alloy sensor are significantly enhanced, especially for the magnetic hydride Pd₈₀Co₂₀ sensor whose optical response time at 1 mbar of H₂ is just ~0.85 s, while preserving the excellent accuracy (<2.5%), limit of detection (2.5 ppm), and robustness against aging, temperature, and interfering gases. The superior performance of our sensor places it among the fastest and most sensitive optical H₂ sensors.

References

[1] Hoang Mai Luong, Minh Thien Pham, Tyler Guin, Richa Pokharel Madhogaria, Manh-Huong Phan, George Keefe Larsen & Tho Duc Nguyen, "Sub-second and ppm-level optical sensing of hydrogen using templated control of nano-hydride geometry and composition", Nature Communications volume 12, Article number: 2414 (2021).

SD-I11 (Invited)**Detection of weak, low-frequency magnetic field using single nanoscale MgO magnetic tunnel junctions**

T.N. Anh Nguyen^{1, 2, *}, Q. Ngan Pham¹, V. Thanh Chu^{1, 3}, K. Tung Do¹, T. Huong Nguyen¹, H. Nam Pham¹, Minori Goto^{4, 5}, Miyoshi Fukumoto⁴, Hiroyuki Tomita⁴, Tatsuki Watanabe⁴, Hitoshi Kubota⁶, Akio Fukushima⁶, Kei Yakushiji⁶ and Yoshishige Suzuki^{4, 5, 6}

¹ Institute of Materials Science (IMS), Vietnam Academy of Science and Technology, 18 Hoang Quoc Viet, Cau Giay, Hanoi 11355, Vietnam

² Graduate University of Science and Technology (GUST), Vietnam Academy of Science and Technology, 18 Hoang Quoc Viet, Cau Giay, Hanoi 11355, Vietnam

³ International Training Institute for Materials Science, Hanoi University of Science & Technology (HUST), 1 Dai Co Viet, Hai Ba Trung, Ha Noi 10000, Vietnam

⁴ Graduate School of Engineering Science, Osaka University, Toyonaka, Osaka 560-8531, Japan

⁵ Center for Spintronics Research Network (CSRN), Osaka University, Toyonaka, Osaka 560-8531, Japan

⁶ National Institute of Advanced Industrial Science and Technology (AIST), Research Center for Emerging Computing Technologies, Tsukuba, Ibaraki 305-8568, Japan

* Corresponding author's e-mail: ngocanhnt.vn@gmail.com

Magnetic tunnel junctions (MTJ) have been widely studied as ultra-sensitive magnetic sensors, due to their high TMR, high sensitivity, excellent scalability and low power consumption [1-3]. In this study, the magnetotransports and noise properties of the 300 nm diameter MTJ at room temperature were investigated. Their sensitivity of more than 100 % in a few Oe at RT. The hard axis bias magnetic field and bias voltage dependence of noise properties both showed that MTJs exhibit relatively low noise spectral density of about which depend inversely on frequency (f) at low frequencies. The noise-based measurement of the developed MTJs is able to detect the presence of a nanotesla AC magnetic field ($H_{AC}=6.7$ nT) in the wide range of frequency ($f=100$ -20000 Hz). A noise measurement provides an approach to detect nanotesla-level, low-frequency alternating magnetic fields with a large signal response and contrast-to-noise, presenting an important step in sensing biological fields.

Keywords: Magnetoresistive sensor; tunnel magnetoresistance sensor; magnetic tunnel junctions (MTJ); 1/f magnetic noise

Acknowledgments

This work was financially supported by Vietnamese Ministry of Science and Technology (MOST) with grant number NDT.88.JP/20. Part of this work was supported by JSPS Grant-in-Aid for Scientific Research (S) Grant Number JP20H05666, Japan and CREST (Non-classical Spin project, JPMJCR20C1) of the Japan Science and Technology Agency.

References

- [1] P.P. Freitas et al., Lab Chip 12 (2012) 546–557.
- [2] M. Pannetier-Lecoœur et al., Appl. Phys. Lett. 98 (2011) 153705.
- [3] Kanno et al., Scientific Reports, 12(1) (2022) 6106-6106.

SD-I12 (Invited)

Neutron diffraction study of state-of-the-art 2D materials

Toan Dang^{1, 2, *}

¹ Institute of Research and Development, Duy Tan University, 550000 Da Nang, Vietnam

² Faculty of Natural Sciences, Duy Tan University, 550000 Da Nang, Vietnam

* Corresponding author's e-mail: dangngoctoan1@duytan.edu.vn

The 2D van der Waals materials with honeycomb magnetic lattice exhibit a large variety of novel physical phenomena due to the interplay of long-range magnetic order and spin fluctuations and they have great potential for technological applications as graphene-like magnetic systems. Recent studies of the model 2D van der Waals compound FePS₃ have revealed structural phase transitions, spin crossover, and emerging superconductivity under high pressure. However, the high-pressure response of magnetic properties of this system remains poorly explored. Here, using the neutron diffraction method, we have observed the emergence of novel magnetic states in FePS₃ under high pressure accompanied by structural transitions. The spin configurations and the formation mechanisms of these phases have been revealed.

Keywords: neutron diffraction, high-pressure, 2D materials, phase transition

Session: Theory and computation

TC-I01 - TC-I10

TC-I01 (Invited)**Thermodynamic properties of the Shastry-Sutherland model for $\text{SrCu}_2(\text{BO}_3)_2$**

Andreas Honecker*

Laboratoire de Physique Théorique et Modélisation, CNRS UMR 8089, CY Cergy Paris Université, 95302 Cergy-Pontoise, France

* Corresponding author's e-mail: andreas.honecker@cyu.fr

Reliable computation of the low-temperature thermodynamic properties of highly frustrated quantum magnets is important for experiments, but also a considerable challenge since, e.g., conventional Quantum-Monte-Carlo (QMC) simulations suffer from a severe minus sign problem. $\text{SrCu}_2(\text{BO}_3)_2$ is famous for its rich physical properties and as a realization of the two-dimensional spin-1/2 Shastry-Sutherland model. In this model, an orthogonal arrangement of dimers gives rise both to geometric frustration and an exact dimer ground state. Beyond the dimer phase at small inter-dimer coupling, the ground-state phase diagram contains two further phases: an antiferromagnetic one at large interdimer couplings and an intermediate plaquette phase.

We use this example to illustrate recent progress in numerical methods. AQMC method in the dimer basis reduces the minus sign problem sufficiently to be able to obtain accurate results for the specific heat C and the magnetic susceptibility χ in a large part of the dimer phase [1, 2]. However, the low-temperature behavior in the parameter regime relevant to $\text{SrCu}_2(\text{BO}_3)_2$ remains out of reach of the QMC simulations. Consequently, we also resort to other methods, in particular a finite-temperature version of the infinite Projected Entangled Pair States (iPEPS) [3].

Application of pressure to $\text{SrCu}_2(\text{BO}_3)_2$ allows to tune the ratio of the coupling constants across the phase transition between the dimer and plaquette phases [4]. High-precision specific-heat measurements demonstrate that the pressure-temperature phase diagram has a first-order transition line that separates phases with different local magnetic energy densities, and that terminates at an Ising critical point. These results are in agreement with results of the numerical methods and reminiscent of the phase diagram of water.

Keywords: Frustrated magnetism, quantum spins models, Quantum Monte Carlo

References

- [1] S. Wessel, I. Niesen, J. Stapmanns, B. Normand, F. Mila, P. Corboz, A. Honecker, Thermodynamic Properties of the Shastry-Sutherland Model from Quantum Monte Carlo Simulations, *Phys. Rev. B* 98 (2018) 174432.
- [2] A. Honecker, L. Weber, P. Corboz, F. Mila, S. Wessel, Quantum Monte Carlo Simulations of Highly Frustrated Magnets in a Cluster Basis: The Two-Dimensional Shastry-Sutherland Model, *J. Phys.: Conf. Ser.* 2207 (2022) 012032.
- [3] A. Wietek, P. Corboz, S. Wessel, B. Normand, F. Mila, A. Honecker, Thermodynamic Properties of the Shastry-Sutherland Model Throughout the Dimer-Product Phase, *Phys. Rev. Research* 1 (2019) 033038.
- [4] J. Larrea Jiménez, S.P.G. Crone, E. Fogh, M.E. Zayed, R. Lortz, E. Pomjakushina, K. Conder, A.M. Läuchli, L. Weber, S. Wessel, A. Honecker, B. Normand, Ch. Rüegg, P. Corboz, H.M. Rønnow, F. Mila, A Quantum Magnetic Analogue to the Critical Point of Water, *Nature* 592 (2021) 370–375.

TC-I02 (Invited)**The activation energy of glass transition**Koun Shirai^{1, 2, *}¹ VNU Vietnam Japan University, Hanoi, Luu Huu Phuoc Road, My Dinh 1 Ward, Nam Tu Liem District, Hanoi, Vietnam² SANKEN, Osaka University, 8-1 Mihogaoka, Ibaraki, Osaka 567-0047, Japan

* Corresponding author's email: shirai.k@vju.ac.vn

The Arrhenius analysis is a universal tool for studying transitions of the states of materials, owing to the fact that a large number of the transitions have the thermally activated type. The obtained activation energies are well interpreted by the energy barrier separating the terminal states of a transition. Unfortunately, this standard analysis cannot be applied to the glass transition. The temperature (T) dependence of the viscosity at the glass transition often exhibits non-Arrhenius behavior, whereas the so-called strong glasses obey the Arrhenius law. The class of glasses which do not obey the Arrhenius law is called fragile glass. A simple interpretation is that the energy barrier in fragile glass has T dependence. This interpretation seems likely but yet other interpretations are discussed. In either case, the difficulty is its unusually large value of the activation energy Q_a . The value is of the order of 1 eV (sometimes near 10 eV) even for molecular glasses whose melting temperature is less than room temperature. For molecular glasses, Q_a value is even larger than the cohesive energy, which is almost impossible on the physics ground. The glass researchers have been plagued with this problem for a century.

Recently, this problem has been solved by the author [1]. The energy barrier for atom rearrangements significantly changes in the transition range with width ΔT_g . This change in the energy barrier alters the manner in which the apparent activation energy constitutes the Arrhenius form. Analysis of available experimental data shows that the real value of energy barrier is significantly smaller than the apparent activation energy. The overestimation of the apparent activation energy depends on the ratio $T_g/\Delta T_g$, which is larger for fragile glasses than for strong glasses. Importantly, the linear term in the temperature dependence of the energy barrier does not appear in Arrhenius plots. This explains why the T dependence of viscosity for strong glasses obeys well the Arrhenius law, despite that the T dependence of energy barrier is equally expected for every glass. The mechanism of this overestimation was also supported by the specific-heat jump of the glass transition [2].

References

- [1] K. Shirai, J. Phys. Commun. 5, 095013 (2021).
- [2] K. Shirai, K. Watanabe, and H. Momida, J. Phys.: Condens. Matters 34, 375902 (2022).

TC-I03 (Invited)**Selective control of propagation-conduction of two different quantum waves by lattice imperfections: electrons and phonons**Masato Yoshiya^{1,2,*}, Tomofumi Hara¹, Wataru Sekimoto¹, Ryohei Nishioka¹, Susumu Fujii^{1,2}¹ Division of Materials and Manufacturing Science, Graduate School of Engineering, Osaka University, Suita, Osaka 565-0871, Japan² Nanostructures Research Laboratory, Japan Fine Ceramics Center, Nagoya, Aichi 456-8587, Japan

* Corresponding author's e-mail: yoshiya@mat.eng.osaka-u.ac.jp

Demands to materials to meet with demands from our societies for our bright future are kept increasingly severe than ever. While conventional theories for materials properties guide us to improve each of materials properties, materials are now required to simultaneously acquire multiple properties, which often go beyond correlated or trade-off relationships among multiple materials properties. Simultaneously to enhance electronic conduction and to suppress thermal conduction by phonons for thermoelectric energy conversion from waste-heat to electricity is just one of many examples being tackled with today and coming years, from liquid-crystal display, Li-ion battery, to advanced turbines for power stations and jet-engines, to name a few.

While machine learning now enable us to explore a room further to find new materials or compounds having new properties whether efficiently or by brute-force, we need to be reminded that there is another room just in front of us: Lattice Imperfections, including point defects including vacancies or dopants, line defects including dislocations, planar defects including interfaces and grain boundaries, all of which significantly modify materials properties, or in other words, materials properties that we know of are due to the lattice imperfections, except in textbooks.

In this presentation, it will be discussed how dislocations, known to dominate plastic deformation or hardness of materials, would selectively modify electronic and thermal conduction in model materials beyond conventional theories.

Keywords: electronic conduction; thermal conduction; ab initio calculations; molecular dynamics; lattice defects

References

- [1] K. Matsunaga, M. Yoshiya, N. Shibata, H. Ohta, T. Mizoguchi, "Ceramic Science of Crystal Defect Cores", *J. Ceram. Soc. Jpn.*, 130 [8] (2022) 648-667.
- [2] W. Sekimoto, S. Fujii, M. Yoshiya, "Direct numerical analyses of nanoscale thermal transport near MgO edge dislocations", *Scr. Mater.*, 202 (2021) 113991.
- [3] T. Yokoi and M. Yoshiya "Atomistic simulations of grain boundary transformation under high pressures in MgO", *Physica B: Condensed Matter*, 532 (2018) 2-8.
- [4] S. Fujii, T. Yokoi, M. Yoshiya, "Atomistic Mechanisms of Thermal Transport across Symmetric Tilt Grain Boundaries in MgO", *Acta Mater.*, 171 (2019) 154-162.
- [5] S. Fujii, T. Yokoi, C. A. J. Fisher, H. Moriwake, M. Yoshiya, "Quantitative prediction of grain boundary thermal conductivities from local atomic environments", *Nature Commun.*, 11 (2020) 1854.

TC-I04 (Invited)**Computational approaches to study heavy element materials**

Manh-Thuong Nguyen*

Pacific Northwest National Laboratory, Richland, WA 99352, United States

* Corresponding author's email: manhthuong.nguyen@pnnl.gov

Heavy elements (lanthanides and actinides), exhibiting interesting chemical and physical properties, are widely used in technological applications. However, due to the complexity of f electrons, *first principles*-based modeling of heavy element materials is largely impacted by time and length scales that need to be accessed. In this talk, I will briefly summarize our recent contributions in the study of these elements: (i) the development of pseudopotentials and basis sets [1, 2] that allow for large scale *ab initio* molecular dynamics (AIMD) simulations; and (ii) an adaptive-learning algorithm [3] that enables the location of multiple low-energy minima in high-dimensional spaces. I will then present applications of these tools to investigate molecular complexes of lanthanides in gas and condensed phases [4, 5]. Finally, I will discuss the use of AIMD and data science in understanding actinide molten salt systems [6, 7].

Keywords: Heavy element materials, *ab initio* molecular dynamics, data science**References**

- [1] J.B. Lu, D.C. Cantu, M.-T. Nguyen, J. Li, V.A. Glezakou, R. Rousseau, J. Chem. Theory Comput. 15 (2019) 5987.
- [2] J.-B. Lu, D.C. Cantu, C.-Q. Xu, M.-T. Nguyen, H.-S. Hu, V.-A. Glezakou, R. Rousseau, J. Li, J. Chem Theory Comput 17 (2021) 3360.
- [3] J. Zhang, V.-A. Glezakou, R. Rousseau, M.-T. Nguyen, J. Chem Theory Comput 16 (2020) 3947.
- [4] R.C. Shiery, J.L. Fulton, M. Balasubramanian, M.-T. Nguyen, J.-B. Lu, J. Li, R. Rousseau, V.-A. Glezakou, D.C. Cantu, Inorganic Chemistry 60 (2021) 3117.
- [5] M.-T. Nguyen, J. Zhang, D.C. Cantu, R. Rousseau, V.-A. Glezakou, Rare Earth Elements and Actinides: Progress in Computational Science Applications, ACS Publications, 2021, p. 219-245.
- [6] M.-T. Nguyen, R. Rousseau, P.D. Paviet, V.-A. Glezakou, ACS Applied Materials & Interfaces 13 (2021) 53398.
- [7] M.-T. Nguyen, B.A. Helfrecht, R. Rousseau, V.-A. Glezakou, Journal of Molecular Liquids 365 (2022) 120115.

TC-I05 (Invited)**Artificial-neural-network descriptor and interatomic potential for molecular simulations of lattice defects**T. Yokoi^{1,*}, Y. Oshima¹, K. Matsunaga^{1,2}¹ Department of Materials Physics, Nagoya, 464-8601, Japan² Nanostructures Research Laboratory, Japan Fine Ceramics Center, Nagoya, 456-8587, Japan

* Corresponding author's e-mail: yokoi@mp.pse.nagoya-u.ac.jp

In crystalline materials, lattice defects are inevitably introduced due to thermodynamic stability and material fabrication process, having large impacts on material properties. To accurately predict atomic configurations and physical properties of lattice defects with practical computational cost, artificial-neural-network (ANN) interatomic potentials have been employed extensively. However, if an ANN potential learns various atomic environments of lattice defects at once, error with respect to training data becomes large, which leads to severely limited ability to predict lattice defect properties. Consequently, the construction of general-purpose ANN potentials for lattice defects is not yet achieved. To tackle this issue, this work proposed new ANN descriptors and interatomic potentials and compared their error with that of a conventional ANN potential.

For an ANN descriptor, two separate ANNs were used to describe two- and three-body interactions, as shown in Fig. 1. Their outputs were fed to the input nodes of a next ANN. In this architecture, conventional symmetry functions are replaced with the ANN descriptor. Training these three ANNs, the optimal functions of atomic descriptors and interatomic potentials were obtained without manually choosing analytic functions. To generate training and test datasets, DFT calculations were performed using the projector augmented wave method implemented in the VASP code. Here Si was chosen as a model system.

It is found that the ANN-descriptor potential exhibits sufficiently small errors with respect to training datasets, even when the datasets contain various lattice defects including point defects, surfaces and grain boundaries. The mean absolute error (MAE) is calculated to be 0.97 and 2.2 meV/atom for the present ANN potential and a conventional ANN potential, respectively. Our ANN potential is thus expected to exhibit higher predictive ability to lattice defects properties. The trained three-body ANN descriptor is found to involve complicated functional forms (Fig. 2), which cannot be constructed using a single trigonometric function. This may be a reason that our ANN potential shows the lower MAE than that of a conventional ANN potential.

Keywords: Interatomic potential, Machine learning, First-principles calculation

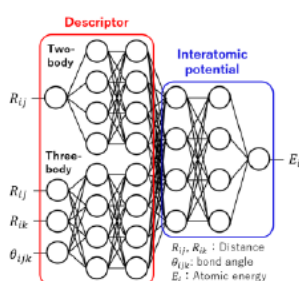


FIG. 1. ANN descriptor and interatomic potential.

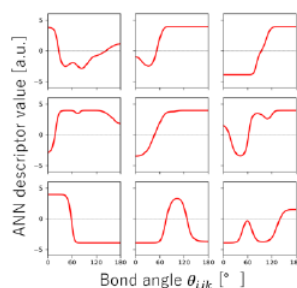


FIG. 2. Trained three-body ANN descriptors

Acknowledgement: This work was supported by JST-CREST (JPMJCR17J1) and JSPS (JP21K14405).

TC-I06 (Invited)**Accelerating materials discovery using universal neural network potential and ab-initio calculations**

Tien Quang Nguyen^{1, *}, Yusuke Nanba¹, Michihisa Koyama¹, Mary Clare Escaño², Masahiko Tani²

¹ Research Initiative for Supra-Materials, Shinshu Univ., Nagano 380-8553, Japan

² Research Center for Development of Far-infrared Region, Univ. of Fukui, Fukui 910-8507, Japan

* Corresponding author's e-mail: quang@shinshu-u.ac.jp

The discovery of novel materials with good performance for specific applications has been a hot topic in the field of materials science. In this talk, two cases of materials discovery approaches and results in the fields of Li-ion batteries and terahertz (THz) devices will be presented. In the first case, traditionally, materials discovery often consumes a vast amount of time and resources in experiments and computational simulation due to the limitations of experimental conditions or theoretical foundations. Thus, it is crucial to approach this task in a new way. One is the use of neural network potentials, which model the interactions of atoms by mimicking the neural networks in the human brain. In this work, by using the recently developed universal neural network potential, PFP (Preferred Potential) [1], simulations of the delithiation process in Li-ion battery cathode materials will be demonstrated. Also, in combination with Wang-Landau sampling [2], a screening scheme for exploring cathode materials will be introduced. In this scheme, the total energy is calculated quickly and accurately using the PFP, while the thermodynamic properties of the searched compound are determined by using Wang-Landau sampling. For the second case, first-principles methods based on spin density functional theory and *ab-initio* multichannel Landauer formalism for spin-transport will be introduced. These were applied to calculate the spin-dependent interface resistance in the Fe/Pt bilayer used as a spintronic THz emitter [3, 4]. In this research, we found that spin-up interface resistance is lower than that of spin-down, in agreement with previous interface reflectivity studies. The above-mentioned theoretical methods can also be used to predict interface resistances, which are more directly and experimentally measurable than reflectivity and thus spin-injection efficiency of other candidate metal bilayer systems for the accelerated search for efficient spintronic THz emitters.

Keywords: Li-ion Battery, Terahertz Device, Neural Network Potential, Wang-Landau Sampling, Ab-initio Calculation

References

- [1] S. Takamoto et al., Nat. Commun. 13 (2022) 2991.
- [2] F. Wang and D. Landau, Phys. Rev. Lett. 86 (2001) 2050.
- [3] V. K. Mag-usara et al., iScience 25 (2022) 104615.
- [4] M. C. Escaño et al., IEEE “47th International Conference on Infrared, Millimeter, and Terahertz Waves (IRMMW-THz)”, Delft, Netherlands 2022.

TC-I07 (Invited)**Exploration for non-perovskite proton-conducting oxides using high-throughput computation and machine learning**S. Fujii^{1, 2, *}, Y. Shimizu^{3, 4, 5}, J. Hyodo^{3, 5}, A. Kuwabara², Y. Yamazaki^{3, 4, 5}¹ Division of Materials and Manufacturing Science, Osaka University, Osaka 565-0871, Japan² Nanostructures Research Laboratory, Japan Fine Ceramics Center, Nagoya 456-8587, Japan³ INAMORI Frontier Research Center, Kyushu University, Fukuoka 819-0395, Japan⁴ Department of Materials, Kyushu University, Fukuoka, 819-0395, Japan⁵ Kyushu University Platform of Inter-/Transdisciplinary Energy Research (Q-PIT), Kyushu University, Fukuoka, 819-0395, Japan

* Corresponding author's e-mail: susumu.fujii@mat.eng.osaka-u.ac.jp

Proton-conducting oxides have attracted attention as electrolytes for solid oxide fuel cells (SOFCs). Perovskite has been considered as the most promising candidates for the electrolytes, and highly conductive Sc-doped BaZrO₃, for example, have been developed recently [1]. On the other hand, there are limited reports on proton-conducting oxides with non-perovskite structures [2]. This is due to the complex nature of proton-conducting oxides, which requires a suitable acceptor dopant to create oxygen vacancies, ease of hydration, crystal structure where protons easily migrate, chemical stability, and so on. It is challenging to find one that meets these requirements simultaneously among the vast number of host compound and dopant combinations.

Here, we developed a scheme of high-throughput *ab initio* computational screening for exploring proton-conducting oxides [3]. This scheme includes multiple stages of bandgap, hydration, proton migration pathways, thermodynamic stability, and solubility of dopants. The screening results show that, although there are many compounds that hydrate once oxide-ion vacancies are formed, very few of them form proton conduction pathways and have dopants that are easily soluble. Based on this computational screening, we successfully synthesized a new proton-conducting non-perovskite oxide for the first trial in experimental synthesis.

Big data obtained by this screening, which includes both non-perovskite and perovskite oxides, is essential for general understanding of the inherent nature of proton-conducting oxides. For this perspective, prediction models for hydration energies and solution energies of dopants were also developed using machine learning. The interpretation of these models clearly highlights the physicochemical properties necessary for proton conduction. In this presentation, the details of the computational methodology, the characteristics of the discovered compounds, the approach of machine learning, and the understanding gained will be discussed.

Keywords: proton-conducting oxides; high-throughput calculations; machine learning

Acknowledgements: This work was supported by the Japan Science and Technology Agency CREST, Grant Number JPMJCR18J3.

References

- [1] J. Hyodo, K. Okuyama, Y. Yamazaki et al., *Adv. Energy Mater.*, 10 (2020) 2000213.
- [2] S. Fop, *J. Mater. Chem. A*, 9 (2021) 18836.
- [3] S. Fujii, Y. Shimizu, J. Hyodo, A. Kuwabara, Y. Yamazaki, in preparation.

TC-I08 (Invited)**Computational materials design of high-entropy alloys based on FPKKR-CPA calculation and machine learning techniques**

Kazunori Sato^{1, 2, 3, *}, Genta Hayashi¹, Kazuma Ogushi¹, Shuichi Okabe¹, Katsuhiro Suzuki¹, Tomoyuki Teraï¹, Hitoshi Fujii⁴, and Masako Ogura⁵

¹ Graduate School of Engineering, Osaka University, Osaka, 565-0871, Japan

² CSRN, Graduate School of Engineering Science, Osaka University, Osaka, 560-0043, Japan

³ Spintronics Research Network Division, OTRI, Osaka University, Osaka, 565-0871, Japan

⁴ Laboratory of Advanced Science and Technology for Industry, University of Hyogo, Hyogo 678-1205, Japan

⁵ Department of Chemistry, University of Munich, D-81377 Munich, Germany

* Corresponding author's e-mail: ksato@mat.eng.osaka-u.ac.jp

High-entropy alloys (HEAs) are composed of more than 5 different elements with nearly equal atomic concentration, and are attractive materials due to their possibility to realize various functionality depending on the choice of the kinds of elements. However, a number of combinations is too large, so exhaustive materials search by experiments is impractical. Recently, first-principles calculations are combined with machine learning techniques to obtain prediction models for physical properties of interest and applied to design new HEAs [1]. In this paper, as one of such attempts, we demonstrate that the combination of the full potential Korringa-Kohn-Rostoker coherent potential approximation (FPKKR-CPA) [2] and the linearly independent descriptor generation (LIDG) method [3] works reasonably and effectively for the prediction of elastic and magnetic properties of HEAs.

Firstly, we try to construct a prediction model of elastic constants of HEAs. Total energy calculations are performed within the framework of the DFT by systematically applying deformations. By using the FPKKR-CPA method one can calculate configuration average of the electronic structure of disordered HEAs without using a large super-cell. The elastic constants are calculated for randomly sampled BCC equi-atomic quinary HEAs composed from 25 transition metals. Then linear regression is performed on calculated elastic constants. The descriptors of the regression are generated by the LIDG method from arithmetic means and standard deviations of 3 independent elastic constants, lattice constant, group and period of elements, atomic number and electron density parameter r_s of components of HEA. By optimizing the combination of descriptors by the genetic algorithm, we can achieve comparable accuracy to the model generated by the neural network. Based on the model, we discuss chemical trend of elastic constants. Similar procedure can be utilized to construct a linear model for predicting magnetic properties of HEAs.

Next, we assess the stability of HEAs. For this purpose, we calculate not only the heat of formation of HEAs but also effective pair interactions (EPIs) between constituent atoms by the generalized perturbation method [4]. We perform Monte Carlo simulations with using the calculated EPIs and simulate temperature dependence of the short-range order in HEAs. This method might help to pick up a candidate HEA from a view point of synthesizability.

Keywords: first-principles calculations, machine learning, high entropy alloy

References

- [1] Y. Ikeda et al., *Materials Characterization*, 147 (2019) 464.
- [2] M. Ogura and H. Akai, *J. Phys.: Condens. Matter* 17 (2005) 5741.
- [3] Y. Kanda, H. Fujii and T. Oguchi, *Sci. Technol. Adv. Mat.* 20 (2019) 1178.
- [4] F. Ducastelle and F. Gautier, *J. Phys. F: Met. Phys.*, 6 (1976) 2039.

TC-I09 (Invited)

Accelerating materials science with artificial intelligence

Huan Tran*

School of Materials Science and Engineering, Georgia Institute of Technology, United States

* Corresponding author's email: huan.tran@mse.gatech.edu / huantd@gmail.com

Computational materials science has been driven by traditional physics-based approaches, in which physics and chemistry concepts are employed to understand materials (generally solids) from their atomic-scale information. Challenges of such approaches, which range from the technical side, e.g., enormous computational facility and time are required for a meaningful simulation, to a more fundamental level, e.g., how to describe a material and its properties by a model, are never trivial. During the last decade, artificial intelligence (AI) is joining the mainstream of materials research, creating a subfield named materials informatics. In this research area, AI-based approaches are used to complement and significantly accelerate the traditional computational and experimental approaches in understanding, optimizing, discovering, and designing new functional materials, especially those with targeted properties. In this talk, I will outline the fundamental and technical aspects of the AI-based approaches and illustrate them by some of my works in materials informatics. Then, I will offer my outlook on remaining challenges that need to be surmounted for widespread adoption of AI-based approaches in materials science and engineering.

Keywords: Materials science, Materials informatics, Materials discovery & design, Artificial intelligence, Machine learning

TC-I10 (Invited)**Material intelligence: in-materio reservoir computing devices composed by random network of nanoparticles**Hirofumi Tanaka^{1, 2, *}¹ Research Center for Neuromorphic AI Hardware, Kyushu institute of Technology (Kyutech), 2-4 Hibikino, Wakamatsu, Kitakyushu, 8080196, Japan² Graduate School of Life Science and Systems Engineering, Kyutech, Japan.

* Corresponding author's e-mail: taanaka@brain.kyutech.ac.jp

The superior computational capabilities of software-based deep learning have been widely recognized, and the practical application of artificial intelligence is rapidly expanding. Meanwhile, attempts to replace artificial intelligence (AI) algorithms with hardware have also begun. We have shown that the properties of materials can be treated as physical phenomena and are conducting research to realize a new form of AI hardware. I will share our recent outputs at the presentation.

In recent years, there is a growing interest in hardware technologies that physically implement artificial neural networks (ANNs), neuromorphic or brainmorphic information processing systems, and the applications (AI systems hereafter), as well as new materials and devices. A critical difference between the presently required device functionality and that in conventional computational systems is the use of chemical dynamics. By cleverly using nanomaterials' nonlinearity and network structure, devices that spontaneously generate pulses, noise, and other physical phenomena are expected to be realized to utilize for the AI hardware. These devices will enable drastically lower power consumption and higher integration of AI systems. In the learning process of ANNs, it is necessary to constantly change and store the weights of the weighted sum (sum-of-products) part. We have been working on materials that can complement CMOS for AI systems by using molecules and nanocarbon materials, and further, we are trying to apply them to autonomous AI robots. This paper introduces these nanomaterials and networks' formation as AI devices [1], the key points of the devices' functionalization, application to robots, and other recent research results [2-7].

Keywords: Neuromorphic Hardware, Physical Reservoir Computing, Random Network, Chemical Dynamics, Robot Operating System

Acknowledgment: HT would like to thank to Prof. J. Gimzewski of UCLA for fruitful discussion on reservoir device measurement. He also would like to thank to financial support from CREST, Japan Science and Technology Agency and Kakenhi, Japan Society for the Promotion of Science (JSPS) and Core-to-Core program, JSPS.

References

- [1] H. Tanaka et al., Adv. Mater. 18, 1411 (2006).
- [2] H. Tanaka et al., Nat. Commun. 9, 2693 (2018). Selected as the most read 50 articles published in 2018 (Physics).
- [3] T. Kotooka, H. Tanaka et al., Research Square, DOI:10.21203/rs.3.rs-322405/v1.
- [4] Hadiyawardman, H. Tanaka et al., Jpn. J. Appl. Phys. 60, SCCF02 (2021).
- [5] Recently, Kyutech team won the RoboCup and other world series five times by TOYOTA HSR. The same robot was used for the demonstration.
- [6] Y. Usami, H. Tanaka et al., Adv. Mater., 33, 2102688 (2021).
- [7] D. Banerjee, H. Tanaka et al., Adv. Intel. Syst., 4, 2100145 (2022). Appeared in inner cover.

Session: Materials for energy and environment (EE)

EE-O01 - EE-O05

EE-O01 (Oral)

Review of Langmuir-Blodgett films of octadecylamine: fabrication, properties, and application

Thi Thao Vu ^{1*}, Xuan Tung Nguyen¹, Dinh Tu Bui¹, Thi Huong Giang Do¹, Phuong Hoai Nam Nguyen¹, Duc Cuong Nguyen¹, Tuan Canh Nguyen¹, Ngoc An Nguyen¹

¹ University of Engineering and Technology, Vietnam National University Hanoi, Hanoi, Vietnam

* Corresponding author's e-mail: vtthao@vnu.edu.vn

Nowadays, the fabrication of hydrophobic and self-cleaning nanoscale coatings is increasing. In that trend, scientists have been interested in amine octadecylamine (ODA) - a surfactant that can create stable floating films with the desired nanostructure by the Langmuir-Blodgett method. However, to fabricate and apply ODA-based film as a different functional material, it is necessary to control the factors affecting the process of film formation and deposition. In this review paper, we discuss the influence of film forming parameters on their properties and applicability, specifically: i) Spreading solution (solvent, concentration, composition), ii) Film compression velocity, iii) Subphase (pH, solvents, presence of other compounds), iv) Film deposition methods, v) Initial surface coverage degree, vi) substrate (material and surface structure); vii) Research and application of ODA films in coating technology.

Keywords: Langmuir-Blodgett, octadecylamine, Langmuir-Schaefer, coating material

EE-O02 (Oral)**Lanthanide-based magnetoplasmonic probes for highly sensitive aqueous copper(II) sensing**

My-Chi Thi Nguyen, Huu-Quang Nguyen, Jaebeom Lee*

Department of Chemistry, Chungnam National University, Daejeon, 34134, Republic of Korea

* Corresponding author's e-mail: nanoleelab@cnu.ac.kr

Lanthanide complexes are widely applied in imaging and sensing owing to their unique intra-configurational 4f-4f transitions. In this work, a europium (Eu) complex Eu(dbm)₃phen (dbm: dibenzoylmethane, phen: 1,10-phenanthroline) was efficiently doped into magnetoplasmonic (MagPlas) Ag@Fe₃O₄ NPs, forming a multifunctional photoluminescence NPs with intense red-emission and good response to magnetic field. The as-synthesized MagPlas NPs greatly enhanced photoluminescence intensity and quantum yield compared to the ones without the plasmonic Ag core. Furthermore, an addition of aqueous copper(II) dramatically diminished the photoluminescence emission of the Eu-doped MagPlas NPs. This quenching effect is the result of energy transfer into non-radiative emission between the doped fluorophores and copper(II). The decrease in photoluminescence intensities showed a good log-linearity in the range of 0.005-0.1 µg/mL. Therefore, Eu-doped MagPlas NPs are potential probes for sensitive detection and quantification of Cu²⁺ in aqueous samples.

Keywords: Lanthanides, magnetoplasmonic, copper(II), sensing**References**

- [1] Li, X., et al. (2019) Appl Nanosci, 9(8), 1833-1844
- [2] Liu, J., et al. (2014) Nanoscale, 6(19), 11473-11478.

EE-O03 (Oral)**Fast synthesis of ZnO/Ag heterostructure nanoparticles for enhanced photocatalytic**

Cong Doanh Sai¹, Van-Phu Vu², Viet Tuyen Nguyen¹, Nguyen Hai Pham¹, An Bang Ngac^{1*}

¹ Faculty of Physics, VNU Hanoi University of Science, 334 Nguyen Trai, Thanh Xuan, Hanoi

² School of Semiconductor and Chemical Engineering, Jeonbuk National University, Jeonju, Korea

* Corresponding author's e-mail: ngacnabang@hus.edu.vn

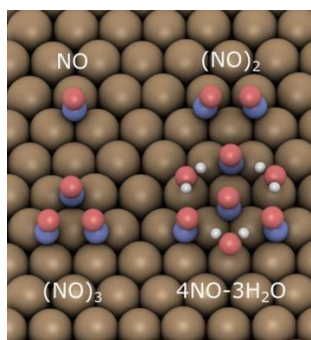
ZnO/Ag heterostructure nanoparticles were successfully synthesized by solution method. The crystal structure and optical properties of the samples were studied by X-ray diffraction (XRD), ultraviolet-visible absorption spectroscopy (UV-Vis), and photoluminescence (PL) equipment, respectively. Morphologies of ZnO/Ag heterostructure nanoparticles composed of ZnO nanoparticles with 30 nm diameter and silver nanoparticles decorated on surface ZnO nanoparticles were examined by scanning electron microscope (SEM). Photocatalytic of ZnO/Ag heterostructure nanoparticles was evaluated by analyzing the degradation of methylene blue under UV irradiation at room temperature. The degradation of methylene blue depends on the density of Ag nanoparticles decorated on the surface of ZnO nanoparticles. The maximum methylene blue degradation efficiency of the prepared ZnO/Ag nanoparticles is up to 99% after 60 minutes of the UV treatment.

Keywords: ZnO/Ag heterostructure; Photocatalytic; nanoparticles.

EE-O04 (Oral)**Van der Waals density functional study of NO-H₂O coadsorption on Cu(111)**Thanh N. Pham^{1*}, Y. Hamamoto^{1,2}, K. Inagaki^{1,2}, I. Hamada^{1,2}, and Y. Morikawa^{1,2,3}¹ Department of Precision Engineering, Osaka University, 2-1 Yamada-oka, Suita, Osaka 565-0871, Japan² Elements Strategy Initiative for Catalysts and Batteries (ESICB), Kyoto University, 1-30 Goryo-Ohara, Nishikyo-ku, Kyoto 615-8245, Japan³ Research Center for Precision Engineering, Graduate School of Engineering, Osaka University, 2-1 Yamada-oka, Suita, Osaka 565-0871, Japan

* Corresponding author's e-mail: thanh@cp.prec.eng.osaka-u.ac.jp

Elucidating the interaction between adsorbed nitric oxide (NO) and water (H₂O) on metal surfaces is of paramount importance to uncover mechanistic details of their competitive coadsorption behavior and to guide the design of new NO_x purification catalysts under wet condition.¹ Herein, we studied coadsorption and complex formation of NO and H₂O on Cu(111) using the nonlocal van der Waals density functional method.² The energetics, adsorption geometries, and vibrational properties of several $n\text{NO}-m\text{H}_2\text{O}$ complexes ($n = 1-4$, $m = 1-3$) on Cu(111) are reported, and the relative stabilities of those complexes are compared with their respective NO and H₂O clusters on Cu(111). We find that the mixed $n\text{NO}-m\text{H}_2\text{O}$ complexes on Cu(111) are more stable than separated NO and H₂O clusters due to the attractive NO-H₂O and NO-NO interactions on the surface. The attractive NO-H₂O interaction originates mainly from the hydrogen bonding between H₂O and the negatively charged NO upon adsorption. Moreover, hydrogen bonding also induces an additional back donation process from Cu(111), further strengthening the NO-H₂O coadsorption. In addition to hydrogen bonding, the NO-NO interaction originating from $2\sigma^*\sigma$ orbital hybridization further stabilizes the formation of the $4\text{NO}-3\text{H}_2\text{O}$ complex, which is observed in the experiment.³ Even though the hydrogen bonding strength in $n\text{NO}-m\text{H}_2\text{O}$ complexes is slightly weaker than the one in H₂O clusters, due to the saturation of hydrogen bonding and the NO-NO interaction, NO and H₂O tends to form the NO-H₂O complex on Cu(111), in agreement with experiment. Our findings shed light on the role of intermolecular interactions between NO and H₂O in the formation of the NO complex, which is important for understanding the reaction of NO in three-way catalysts.

Keywords: NO_x catalysts, NO, H₂O, coadsorption.FIG. 1. Stable NO clusters and a NO-H₂O complex on Cu(111).**References**

- [1] T. Hirakawa *et al.* ACS Appl. Nano Mater. **4**, 10613 (2021)
- [2] T. N. Pham *et al.* Phys Rev. Mater. **6**, 077801 (2022).
- [3] [2] T. N. Pham *et al.* J. Phys. Chem. C **122**, 8894 (2018).

EE-O05 (Oral)**Development of high-efficient multi-layer microwave absorbers using Co-doped BaMnFe₁₁O₁₉ nanoparticles**Ngo Tran^{1,2,*}, Ruey-Bin Yang³, Bo Wha Lee⁴¹ Institute of Research and Development, Duy Tan University, Da Nang, 550000, Viet Nam² Faculty of Natural Sciences, Duy Tan University, Da Nang, 550000, Viet Nam ³ Department of Aerospace and System Engineering, Feng Chia University, Tai Chung 407, Taiwan⁴ Department of Physics and Oxide Research Center, Hankuk University of Foreign Studies, Yongin 17035, South Korea

* Corresponding author's e-mail: tranngo@duytan.edu.vn

Co-doped BaMnFe₁₁O₁₉ (BaMn_{1-x}Co_xFe₁₁O₁₉, $x = 0, 0.4$, and 0.95) samples were successfully prepared using co-precipitation method. XRD patterns and RS spectra confirmed M-type hexaferrite phase formation and its purity. Electromagnetic (EM) properties of the epoxied samples were modified by doping. Microwave absorption properties of epoxied samples were calculated from EM data using transmission line theory, which showed an enhancement performance for the increase of Co doping concentration. The undoped sample (BaMnFe₁₁O₁₉, named Co-0) showed a minimum reflection loss (RL) of -23.08 dB at a frequency (f) of 18 GHz for a thickness (t) of 2.25 mm. When the doping concentration increased to 0.4 (BaMn_{0.6}Co_{0.4}Fe₁₁O₁₉, named Co-4), the minimum RL achieved a value of -42.91 dB at $f = 18$ GHz with $t = 6$ mm. With higher doping concentration of $x = 0.95$ (BaMn_{0.05}Co_{0.95}Fe₁₁O₁₉, named Co-9.5), the minimum RL value bound back to the value of -37.18 dB at 10.32 GHz for a $t = 7.25$ mm. The RL values of $x = 0.4$ and 0.95 epoxied samples reached the values corresponding to $\sim 99.99\%$ of the incident microwave being absorbed. However, the t values to achieve those RL values were pretty thick. In order to enhance the microwave absorption properties with the thinner thickness of these materials, the tri-layer absorbers made from as-prepared samples were simulated for total thicknesses of $4, 5$, and 6 mm. Based on the difference in layer stacking, there were six cases for each total thickness. In the case of a total thickness of 4 mm, no enhancement could be observed for tri-layer absorbers compared to single-layer ones. When the total thickness was 5 mm, the microwave absorption performance of tri-layer absorbers was significantly improved compared to single-layer ones for all six cases. In detail, the third to sixth cases slightly improved compared to single layers (the best value of RL of single layer absorbers was -18.84 dB, which was observed for Co-9.5). Notably, the first and second cases of tri-layer absorbers stacking Co-9.5/Co-4/Co-0 and Co-95/Co-0/Co-4 with thicknesses of $3/1/1$ (mm) achieved the minimum RL of -34.85 and -36.58 dB, which is similar to the best values of single-layer ones but much thinner. In the case of tri-layer absorbers with a total thickness of 6 mm, the RL values of tri-layer absorbers could not be better than the best value of single-layer ones (achieved for $x = 0.4$ sample). However, the 6 -mm-total tri-layer absorbers could reduce the absorption frequency to lower ranges, which could benefit more practical applications.

Keywords: M-type hexaferrite; Microwave absorption properties; Reflection loss; Single-layer absorber; Multi-layer absorber

Session: Multiferroics and magnetic materials (MM)

MM-O01 - MM-O07

MM-O01 (Oral)

An emergent quasi-2D metallic state derived from the Mott insulator framework

Jiunn-Yuan Lin*

Institute of Physics, National Yang Ming Chiao Tung University, Hsinchu 30010, Taiwan

* Corresponding author's e-mail: ago@nycu.edu.tw

Recent quasi-2D systems with judicious exploitation of the atomic monolayer or few-layer architecture exhibit unprecedented physical properties that challenge the conventional wisdom on condensed matter. Here we show that infinite layer SrCuO₂ (SCO), a topical cuprate Mott insulator, can manifest an unexpected metallic state in the quasi-2D limit when SCO is grown on TiO₂-terminated SrTiO₃ (STO) substrate. The sheet resistance does not conform to Landau's Fermi liquid paradigm. Hard X-ray core-level photoemission spectra demonstrated a definite Fermi level of the hole doped metal, and the soft X-ray absorption spectroscopy revealed features analogous to those of a doped Mott insulator. The key element of hole doping is not at the interfaces between SCO and STO, and likely comes from emergent transient layers between the chain-type and planar-type structures within the SCO sector as implied by an energy scan of X-ray Laue nano-diffraction. The present work emphasizes on the discovery of a new metallic state, and invites further exploration to elucidate the mysterious origin of this finding.

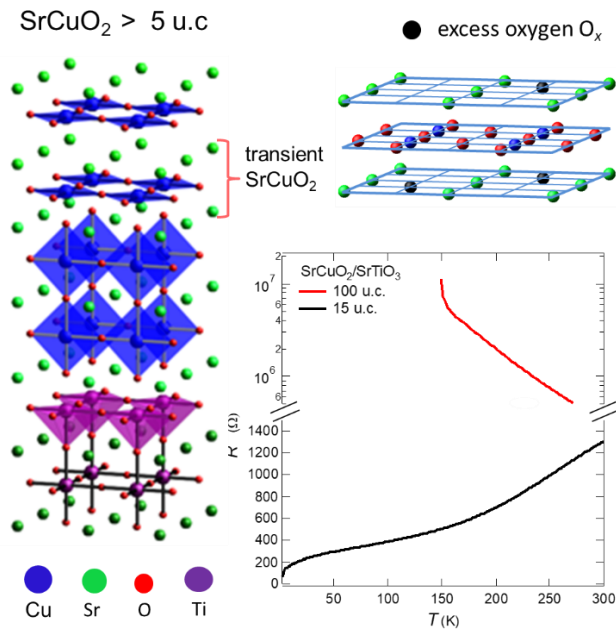


FIG. 1. The ultrathin SrCuO₂ films on SrTiO₃ become metallic.

Acknowledgments

This work was supported by MOST of Taiwan.

MM-O02 (Oral)**Deriving maximally orthogonalized supercells with given size**Yoyo Hinuma^{1,*}¹ Department of Energy and Environment, National Institute of Advanced Industrial Science and Technology, Ikeda, Osaka, Japan 563-0026

* Corresponding author's e-mail: y.hinuma@aist.go.jp

Supercells with desirable size and reasonable geometry, such as basis vectors with similar length and are close to orthogonal, are useful for defect calculations and dilute alloy calculations. However, finding supercells with given size and reasonable geometry is a non-trivial task because standard lattice reduction algorithms cannot be directly applied. I developed a computational algorithm, applicable to any crystal, that finds supercells with a certain size N with maximally and almost maximally orthogonalized basis vectors¹⁾. The list of transformation matrices converting a primitive cell to supercells with maximally and almost maximally orthogonalized basis vectors could be very long; there are 4,408,368 maximally orthogonal $N=387$ supercells of an ideal hcp lattice. One such supercell that is almost cubic is given in Fig. 1. The number of maximally orthogonalized supercells scale as roughly $O(N^2)$ at least in bcc, fcc, and sc lattices. The computational cost could be reduced to approximately $O(N^2)$ by carefully choosing basis vector lengths as $a \leq b \leq c$ and mathematically deriving upper limits to the lengths of a and b .

Using almost maximally orthogonalized basis vectors allows conversion of basis vectors in similar crystals with very different crystallographic conventional basis vectors, such as NASICON-type structure $\text{Ag}_3\text{Sc}_2(\text{PO}_4)_3$. The algorithm is also useful in converting different basis vector choices in energy application-related materials, LiCoO_2 , and Li_2MnO_3 .

Keywords: Supercell, maximally orthogonalized, basis vectors, algorithm

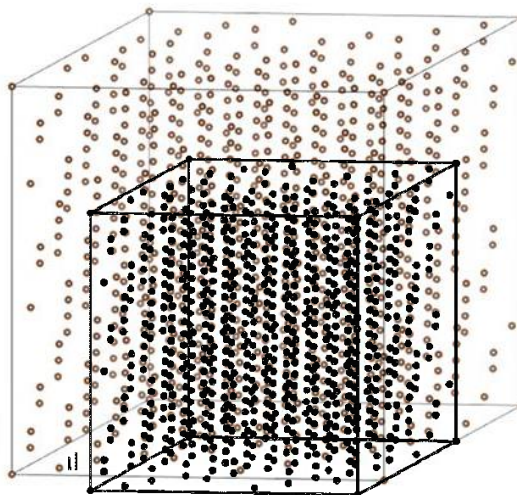


FIG. 1. 387-supercell of an ideal hcp lattice that is almost cubic.

References

- [1] Y. Hinuma, Sci. Technol. Adv. Mater. Meth. 2 (2022) 267.

MM-O03 (Oral)**Bayesian optimization design of high entropy oxide for oxygen evolution catalysis**

Yuichi Okazaki¹, Yushi Fujita¹, Hidenobu Murata¹, Naoki Masuyama², Yusuke Nojima², Hidekazu Ikeno¹, Ikuya Yamada¹, and Shunsuke Yagi³

¹ Graduate School of Engineering, Osaka Metropolitan University, Sakai, Osaka 599-8531, Japan

² Graduate School of Informatics, Osaka Metropolitan University, Sakai, Osaka 599-8531, Japan

³ Institute of Industrial Science, The University of Tokyo, Tokyo 153-8505, Japan

* Corresponding author's e-mail: ikuya_yamada@omu.ac.jp

High entropy oxides (HEOs), containing five or more kinds of mixed metals, have been investigated as highly active oxygen evolution reaction (OER) catalysts [1]. Recently, it was reported that the Co-enriched perovskite oxide of $\text{LaCr}_{1/6}\text{Mn}_{1/6}\text{Fe}_{1/6}\text{Co}_{1/3}\text{Ni}_{1/6}\text{O}_3$ ($\text{M}_{1/6}\text{Co}_{1/3}$) exhibited a higher activity than that with equimolar 3d transition metals ($\text{LaCr}_{1/5}\text{Mn}_{1/5}\text{Fe}_{1/5}\text{Co}_{1/5}\text{Ni}_{1/5}\text{O}_3$: $\text{M}_{1/5}$) [2]. This enhancement indicates that the chemical compositions of HEOs play a crucial role in OER catalytic activities, whereas the vast composition space of HEOs prevents the optimization by experiments. In this study, we performed Bayesian optimizations to achieve the highly active catalysts in the $\text{La}(\text{Cr}, \text{Mn}, \text{Fe}, \text{Co}, \text{Ni})\text{O}_3$ HEOs. We conducted three cycles of experiments (synthesis, phase identifications, and electrochemical characterization) via Bayesian optimization using the initial composition–activity dataset of references and HEOs with random compositions (R-HEOs). The data of HEOs with the compositions determined by Bayesian optimizations (BO-HEOs) were added to the dataset in the respective cycles. All the R- and BO-HEOs crystallized in orthorhombic and rhombohedral perovskite-type structures. OER catalytic activities (AOER) in 0.1M KOH solution were evaluated using the rotating disk electrode system described in the reference [3]. The average AOER of BO-HEOs [$0.14(6) \text{ mA cm}^{-2}$ in BO_{ave}] was larger than that of R-HEOs [$0.04(2) \text{ mA cm}^{-2}$ in R_{ave}], as displayed in Fig. 1. The AOER of BO-HEOs were larger than or comparable to that of $\text{M}_{1/5}$ with a high probability, differing from lower activities in most of R-HEOs. Consequently, we propose that the Bayesian optimization is a useful way to adjust the chemical compositions for highly active HEO in the limited number of trials.

Keywords: oxygen evolution reaction catalyst, Bayesian optimization, high-entropy oxide

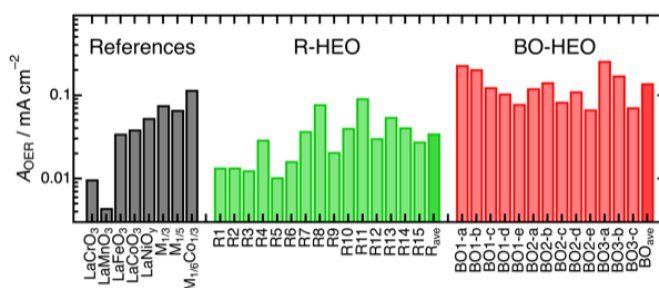


FIG. 1 OER activities (AOER) for references (black), R-HEOs (green), and BO-HEOs (red), together with their average values of R_{ave} and BO_{ave} .

References

- [1] X. Yang et al., Int. J. Hydrogen Energy 68 (2022) 721.
- [2] T. Nguyen et al., Adv. Funct. Mater. 31 (2021) 2101632.
- [3] Y. Okazaki et al., Nat. Commun. under review.

MM-O04 (Oral)**Magnetocaloric effect from first-principles calculations and Monte Carlo simulations**Hung Ba Tran^{1,2*}, Yu-ichiro Matsushita^{1,2,3}¹ Institute of Innovative Research, Tokyo Institute of Technology, Tokyo, 152-8550, Japan² Quemix Inc., Taiyo life Nihombashi Building, Tokyo, 103-0027, Japan³ Quantum Material and Applications Research Center, National Institutes for Quantum Science and Technology, Tokyo, 152-8552, Japan

* Corresponding author's e-mail: tran.h.ag@m.titech.ac.jp

Sustainable energy, which utilizes clean and affordable energy, becomes essential to sustainable development goals (SDGs). One of the most energy consumption parts for many developed and developing countries is cooling and heating energy due to global warming and climate change. Traditional cooling and heating method is harmful to the environment due to the use of greenhouse gas, which will be banned in Europe and other countries shortly. The magnetocaloric effect, as the intrinsic property of magnetic material, is a promising candidate for future cooling devices. This work studies the magnetocaloric effect of several well-known materials by combining first-principles calculations and Monte Carlo simulations [1,3]. All parameters for the simulations, such as isotropic exchange coupling constant (J_{ij}), Dzyaloshinskii-Moriya interactions (D_{ij}), and magnetocrystalline anisotropy energy (MAE), are estimated from first-principles calculations based on density functional theory. Temperature-dependent of magnetocrystalline anisotropy energy is quantitatively reproduced by considering the magnetization-magnetic field (M - H) integration in Monte Carlo simulations. In addition, the isothermal magnetic entropy change is calculated by the Maxwell relation, which is discussed and compared with experimental works in detail.

Keywords: Isothermal magnetic entropy change, Density functional theory, Monte Carlo simulations.**References:**

- [1] H. B. Tran and Y. Matsushita, arXiv.2207.10408
- [2] H. B. Tran, H. Momida, Y. Matsushita, K. Sato, Y. Makino, K. Shirai and T. Oguchi, Phys. Rev. B 105 (2022) 134402.
- [3] H. B. Tran, H. Momida, Y. Matsushita, K. Shirai and T. Oguchi, Acta Mater. 231 (2022) 117851.

MM-O05 (Oral)**Synthesis of bifunctional magnetic-plasmonic Fe₃O₄@SiO₂-Au nanoparticles by an ultrasound assisted chemical method**

Phi Thi Huong^{1,2,*}, Bui Duc Tri³, Nguyen Thi Thanh Van⁴, Tran Thi Hong⁵, Luu Manh Quynh¹, Nguyen Hoang Luong^{2,3}, Nguyen Hoang Nam^{2,3,*}

¹ Faculty of Physics, VNU University of Science, Hanoi, Viet Nam

² Nano and Energy Center, VNU University of Science, Hanoi, Viet Nam

³ Master Program in Nanotechnology, VNU Vietnam Japan University, Hanoi, Viet Nam

⁴ Vietnam Academy of Cryptography Techniques, Hanoi, Viet Nam

⁵ Faculty of Environmental Sciences, VNU University of Science, Hanoi, Viet Nam

* Corresponding author's e-mail: phithihuong@hus.edu.vn, namnh@hus.edu.vn

Bifunctional magnetic-plasmonic nanoparticles Fe₃O₄@SiO₂-Au (FSAs) were successfully synthesized by an ultrasound assisted chemical method. Gold ions were absorbed on the surface of 3-aminopropyltriethoxysilane (APTES)-functionalized silica-coated magnetic nanoparticles and then reduced by sodium borohydride (NaBH₄) under the influence of a 200 W ultrasonic wave for 45 min. The composed FSAs exhibit superparamagnetism with high saturation magnetization and simultaneously absorb visible blue light with the surface plasmon resonant (SPR) peak at around 545 nm. When the amount of precursor gold ions increased from 16 μmol to 40 μmol, the relative the atomic ratio of gold/iron increasing from 0.84 to 3.35, likewise the peak absorption positions increased from 540 nm to 550 nm regarding to the increase of the Au crystal size. The controllable magnetic and absorption properties of the particles make the particles become a reasonable for wide range of bio-application, such as MIR imaging, magnetophoretically-enhanced photothermal therapy, etc.

Keywords: Bifunctional nanoparticles, magnetic-plasmonic, ultrasound assisted chemical method.

MM-O06 (Oral)**Thermal evaporation synthesis and some properties of WO₃/ITO electrochromic thin films**

Nguyen Duy Thien¹, Nguyen Quang Hoa¹, Vuong Van Hiep¹, Le Van Vu¹, Hoang Nam Nhat², Nguyen Ngoc Dinh^{1*}

¹ Faculty of Physics, University of Science, Vietnam National University, Hanoi, 334 Nguyen Trai, Thanh Xuan, Hanoi, Vietnam

² Faculty of Engineering and Nanotechnology, VNU-University of Engineering and Technology, 144 Xuan Thuy, Cau Giay, Ha Noi, Vietnam

* Corresponding author's e-mail: nguyennngocdinh@hus.edu.vn

This paper reports the results of thermal evaporation synthesis and properties of WO₃/ITO electrochromic thin films. The influence of annealing temperature on the crystal structure and Raman scattering spectrum of WO₃/ITO thin films were investigated in detail by X-ray diffraction (XRD) and Raman scattering spectroscopy. The results shown that thin films annealed at 400 °C and 500 °C have crystallized in triclinic, film is quite smooth, with surface roughness of only 4 nm. The electrochromic characteristics investigation of WO₃/ITO thin films shown that them have a high transmittance of about 92 % in the visible wavelength region from 400 to 900 nm, good substrate adhesion. The transmittance of WO₃ thin film was reduced to around 2% in visible region when increasing the coloration time from 0 s to 90 s at applied voltage of 0.7 V. The transmittance of the film was recovered to 85 % by using an applied voltage of 0.7 in time of 150 s. The change in the optical bandgap of WO₃/ITO thin films in the coloration process were observed.

Keywords: Electrochromic, electrochemical, WO₃, thin film, thermal evaporation.

MM-O07 (Oral)**Fabrication of RuO₂ thin film for spin orbit torque – induced magnetization switching**

Nguyen Thi Van Anh^{1,2,*}, Vu Duong³

¹ Center for Science and Innovation Spintronics (Core Research Cluster), Tohoku University, Japan

² Center for Innovative Integrated Electronic Systems, Tohoku University, Japan

³ Institute of Physics, Vietnam Academy of Science and Technology, Hanoi, Vietnam

* Corresponding author's e-mail: nguyen.thi.van.anh.e7@tohoku.ac.jp

Transition metal oxide RuO₂ is widely used in electrochemical reactions, as well as in electrical applications thanks to its peculiar properties such as low resistivity, chemical stability, and so on [1]. Especially, some recent studies have reported the high-temperature antiferromagnetic properties, the Dirac nodal semimetal, or the spin-split effect in RuO₂ film [2], making it attractive for spintronic device applications. We recently reported spin-orbit torque-induced magnetization switching in a RuO₂-based stacking structure [3]. However, a detailed investigation of the crystallinity is lacking. Herein, we report the fabrication of RuO₂ films and analyze their crystallinity and their Raman spectroscopy in detail.

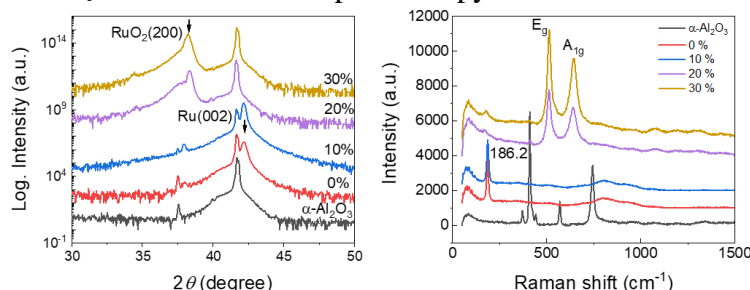


Fig. 1: (a) XRD 2θ - θ patterns and (b) Raman spectra of Ru-O films prepared at different ratio of Oxygen gas.

RuO₂ thin film was fabricated on an α -Al₂O₃ (0001) substrate by reactive sputtering at 300°C with a mixture of O₂ gas and Ar gas at different ratios of O₂ gas (PO_2). Figure 1 (a) shows the X-ray diffraction (XRD) patterns of Ru-(O) films at different PO_2 . As $PO_2 \leq 10\%$, only Ru(002) peak was observed. As $PO_2 \geq 20\%$, only RuO₂(200) peak was observed, indicating the formation of the (100)-oriented RuO₂ film. Figure 1 (b) shows the Raman spectra of Ru-O films at different PO_2 . Only one peak at 186.2 cm⁻¹ was observed for films prepared at $PO_2 \leq 10\%$, which can be attributed to the Ru-Ru stretching vibration in a Ru film [4]. At $PO_2 \geq 20\%$, two phonon modes in RuO₂ were observed at 513.2 cm⁻¹ (E_g) and 644.8 cm⁻¹ (A_{1g}) [5]. Using the RuO₂ film prepared at $PO_2 = 30\%$, we observed the spin-orbit torque-induced magnetization switching in a RuO₂/Co-Fe-B bilayer. More details will be discussed in the presentation.

Keywords: Transition metal oxide, Rutile, spin-orbit torque, RuO₂.

References

- [1] H. Over, Chem. Rev. 112 (2012) 3356.
- [2] Bose et al., Nat.Elec. **5**, 267 (2022).
- [3] T. V. A. Nguyen et al, 2022 Autumn JSAP Meeting, 22p-B201-10.
- [4] O. Tonomura et al, J. Electrochemical Soc., 159 (2012) G1.
- [5] Y. S. Huang et al, Solid state commun. 43 (1982) 921.

Session: Photonics and Hybrid Materials (PH)

PH-O01 - PH-O05

PH-O01 (Oral)**Boosting surface enhanced Raman scattering from ZnO/Au nanorods by UV excitation**Thi Ha Tran¹, Van Tan Tran², Nguyen Hai Pham², An Bang Ngac², Viet Tuyen Nguyen^{2*}¹ Hanoi University of Mining and Geology, Duc Thang, Tu Liem, Hanoi² Faculty of Physics, VNU-University of Science, Thanh Xuan, Hanoi, Vietnam,

* Corresponding author's e-mail: nguyenviettuyen@hus.edu.vn

Surface-enhanced Raman spectroscopy (SERS) has attracted much interest from scientists and engineers because of its potential applications in detection of environmental pollutants, explosives and biomolecules at trace levels. Recently, Photo Induced Enhanced Raman scattering (PIERS) has been reported as a novel technique to further intensify SERS signal under excitation by suitable light prior to or during Raman measurement. In this research, ZnO nanorods were first prepared by galvanic assisted hydrothermal method. Sputtering technique was then applied to fabricate ZnO/Au nanorods. The study showed that Raman signal can be boosted up to 30 times by in situ UV-excitation compared with traditional SERS measurement. This approach provides a robust, fast technique for detection of substances at low concentration.

Keywords: ZnO/Au nanorod; hydrothermal; galvanic; SERS; UV excitation.**References**

- [1] M. Zhang, et al., ACS Sensors. 4 (2019) 1670.
- [2] Brognara et al., Small 18 (2022) 2201088.
- [3] J. Zhao et al., Nanoscale. 13 (2021) 8707.
- [4] T. Man et al., Biosens. Bioelectron. 147 (2020) 1.
- [5] S. Ben-Jaber et al., Nat. Commun. 7 (2016) 1.

PH-O02 (Oral)**Preparation of nanoparticulate WO₃/MoO₃ films for making electrochromic devices**

Chia-Chun Wei, Tung-Han Wu, Wen-Bin Jian*

Department of Electrophysics, National Yang Ming Chiao Tung University, 1001 University Road, Hsinchu 30010, Taiwan

* Corresponding author's e-mail: wbjian@nycu.edu.tw

Sustainable and green technologies of electro-exploding wire and spray coating were employed for the deposition of nanoparticulate WO₃/MoO₃ films. The WO₃ and MoO₃ nanoparticles were characterized by TEM and AFM and the spray-coated nanoparticulate films were inspected using XRD and Raman spectroscopy. The films were immersed in electrolyte in a potentiostat for current-voltage measurements to obtain the diffusion coefficients, stored charge densities, transmittance, and electrochromic switching time. Finally, optical performances of electrochromic devices (ECDs) based on nanoparticulate WO₃/MoO₃ films were measured. Our results presented an enhancement of violet and ultraviolet switching after introduction of MoO₃ into WO₃ films.

Keywords: Electrochromic Devices, Tungsten Trioxides, Molybdenum Trioxides, Nanoparticle Composites

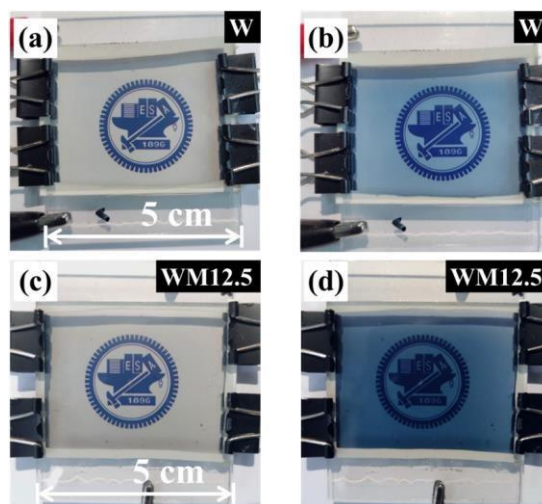


FIG. 1. (a) and (b) are photographs of colored and bleached state of ECD based on nanoparticulate WO₃ films that are driven at -3.3 V and 2 V, respectively, for 20 s. (c) and (d) are photographs of colored and bleached state of ECD based on nanoparticulate (WO₃)_{0.875}(MoO₃)_{0.125} films.

Reference

[1] C. M. Chang, Y. C. Chiang, M. H. Cheng, S. H. Lin, W. B. Jian, J. T. Chen, Y. J. Cheng, Y. R. Ma, K. Tsukagoshi, Sol. Energy Mater. Sol. Cells 223, 110960 (2021).

PH-O03 (Oral)**Studying defects in TMD materials and devices by STM**

Chun-Liang Lin*

Department of Electrophysics, National Yang Ming Chiao Tung University, Hsinchu, Taiwan

* Corresponding author's e-mail: clin@nycu.edu.tw

Transition metal dichalcogenide (TMD) materials with ultrathin thickness provide a promising solution to scale down current semiconductor devices. Many studies have demonstrated that molybdenum disulfide (MoS₂) is able to fabricate field-effect transistors (FETs). However, the carrier mobility in MoS₂ FET is usually lower than the theoretical prediction. Although this poor performance can be attributed to the defects, it still lacks a quantitative analysis clarifying the correlation between carrier mobility and defect density. By using scanning tunneling microscopy (STM), we directly counted the defects in MoS₂ FETs with different carrier mobility. It's found that vacancies and impurities equally contribute to carrier mobility and the total defect density induces a power-law decreasing tendency to the carrier mobility of MoS₂ FET. Therefore, it urgently requires a method to eliminate defects in TMD materials. Here, a counterintuitive approach to eliminating surface defects on TMD materials is found. It's a two-step process including Ar ion bombardment and subsequent annealing. By using STM, it's proved that the defects on the *in-situ* cleaved TMDs surfaces were decreased by more than 99% after ion bombardment and subsequent annealing.

Keywords: transition metal dichalcogenide (TMD), scanning tunneling microscopy (STM), defects, carrier mobility

PH-O04 (Oral)**Abnormal spectral shift of surface plasmon resonance**

Heongkyu Ju^{1,*}, Saikiran Kosame¹, Than Thi Nguyen¹, and Jun-Ho Lee²

¹ Department of Physics, Gachon University, Seongnam-si, 13120, Republic of Korea

² Laser& Opto-electronics Team, Korea Electronics Technology Institute (KETI), Seongnam-si, 13509, Republic of Korea

* Corresponding author's e-mail: batu@gachon.ac.kr

We experimentally demonstrated the spectral blue shift of surface plasmon resonance due to coupling of plasmons with photo-induced excited emitters. Such spectral blue shifts that are in contrast to red shifts widely witnessed in surface plasmon spectroscopy [1-2], could be demonstrated in either linear or nonlinear regime of light matter interactions.

First, the linear interaction for such abnormal spectral shift took place by plasmons-excited quantum dots coupling in a plasmonic nanofilm coated optical fibers [3-5]. Experimental observations were interpreted using the theoretical modelling with the Kramers-Kronig (KK) relation at the visible wavelength of light. The blue shift observed could be interpreted as resulting from excited quantum dots coupling with plasmons whereby the KK relation could predict the negative local refractive index near plasmons [6-7]. Second, the abnormal blue shift of plasmon resonance was also obtained in a nonlinear interaction of light where indigo carmine (an organic dye) acted as a nonlinear medium that simultaneously coupled with plasmons. The third-order optical nonlinearity for the self-defocusing negative refractive index induced by indigo carmine at plasmon resonant wavelengths accounted for such spectral blue shift. We provided discussion on the experimental results with theoretical interpretations using energy structures of indigo carmine for applications possibly found in optical limiting technologies.

Keywords: plasmon resonance, spectral blue shift, quantum dot, nonlinearity, negative refractive index

References

- [1] S. Hayashi et al., *Physics D: Applied Physics* 45 (2012), 433001.
- [2] J. S. Seok et al., *Micromachines* 11 (2020), 895.
- [3] V. T. Tran et al., *J. Mater. Chem. A* 6 (2018), 23894.
- [4] J. Kim et al., *Micromachines* 9 (2018), 506.
- [5] J. Kim, et al., *J. Electron. Mater.* 45 (2016), 2354.
- [6] T. T. Nguyen et al., *Nanomaterials* 12 (2022), 2076.
- [7] H. Ju, *Nanomaterials* 11 (2021), 3063

PH-O05 (Oral)**Electronics and optoelectronics of atomically thin semiconductors**

Der-Hsien Lien*

Institute of Electronics, National Yang Ming Chiao Tung University, Hsinchu, Taiwan

* Corresponding author's e-mail: dhlien@nycu.edu.tw

Ultrathin semiconductors, such as 2D transition-metal dichalcogenide (TMDC) and < 2 nm-thick oxide semiconductors (OS), have drawn significant attention in the past decade due to their promising device performance and profound physics. 2D TMDC provides an ideal platform to investigate the photophysics of excitons and their complexes. Such 2D excitonic systems are promising for optoelectronic applications. The monolayer of 2D TMDC shows near-unity photoluminescence (PL) quantum yields (QYs), a key metric dictating the maximum efficiency as using the material for light-emitting diodes, lasers, and solar cells applications. I will discuss the recombination mechanisms of excitons in monolayers and show that the non-radiative recombination pathways can be fully suppressed by electrostatic gating, despite the presence of native defects. This result reveals that room-temperature excitons are robust and bright regardless of monolayer quality, indicating the potential of achieving highly efficient excitonic devices. Ultrathin OS is regarded as potential channels materials for FETs as they exhibit high carrier mobilities and high on/off ratio. I will show the degree of freedom to engineering transport characteristics of the OS transistors. I will show that precise control over V_T assists in realizing complex integrated systems that requires extensive manipulation of operating conditions.

Keywords: 2D semiconductors, transition metal dichalcogenide (TMD), exciton physics, oxide semiconductors, transistors.

Session: Spintronic materials and devices (SD)**SD-O01 -SD-O07****SD-O01 (Oral)****Solid-liquid structure of Cu₂S: Theoretical acanthite-like model for electronic and transport properties investigations**

Ho Ngoc Nam^{1,2*}, Katsuhiro Suzuki², Akira Masago³, Tien Quang Nguyen², Hikari Shinya^{3,4,5}, Tetsuya Fukushima^{3,6,7}, and Kazunori Sato^{2,3}

¹ Department of Precision Science and Technology, GSE-Osaka University, Osaka 565-0871, Japan

² Division of Materials and Manufacturing Science, GSE-Osaka University, Osaka 565-0871, Japan

³ Center for Spintronics Research Network, GSES-Osaka University, Osaka 560-8531, Japan

⁴ Research Institute of Electrical Communication, Tohoku University, Miyagi 980-8577, Japan

⁵ Center for Spintronics Research Network, Tohoku University, Sendai, Miyagi 980-8577, Japan

⁶ Institute of Solid State Physics, The University of Tokyo, Chiba 277-8581, Japan

⁷ Institute for AI and Beyond, The University of Tokyo, Bunkyo-ku, Tokyo 113-8656, Japan

* Corresponding author's e-mail: honam@mat.eng.osaka-u.ac.jp

Ideas of compact, wearable, and environmentally friendly personal electronic devices that are capable of self-charging using human body temperature have become more feasible in recent years. However, the development of this technology strongly depends on thermoelectric (TE) material that must have ductility and high TE performance at low temperatures [1]. Recently, experimental work uncovered the extraordinary ductility of the inorganic semiconductor Ag₂S [2], potentially paving the way for developing flexible TE devices. In this work, the electronic and transport properties of Cu₂S, a promising candidate for flexible TE application are theoretically elucidated by using first-principles calculations combined with the Boltzmann transport equation [3]. The interesting properties of Cu₂S are mainly driven by the liquid-like behavior of the Cu atoms, which is also a barrier that confuses us in determining their atomic positions and electronic properties. Using a theoretical model driven from a similar low-temperature phase of Ag₂S called the acanthite-like phase, we confirm the appearance of electronic structure with the indirect bandgap of 0.9-0.95 eV as observed in the experiment [4]. In addition, the use of the electron-phonon scattering approximation allows us to estimate the electron energy relaxation time, thereby reproducing the reasonable results of transport property compared to experimental observation. Therefore, demonstrates that the acanthite-like model is ideally suitable and can be used for TE material design related to the low-temperature phase of Cu₂S.

Keywords: electronic structures, transport properties, electron-phonon coupling, flexible thermoelectrics.

References

- [1] H. N. Nam, K. Suzuki, A. Masago, T. Q. Nguyen, H. Shinya, T. Fukushima, and K.Sato, Appl. Phys. Lett. 120, 143903 (2022).
- [2] X. Shi, H. Chen, F. Hao, R. Liu, T. Wang, P. Qiu, U. Burkhardt, Y. Grin, and L. Chen, Nat. Mater. 17, 421 (2018).
- [3] H. N. Nam, K. Suzuki, T. Q. Nguyen, A. Masago, H. Shinya, T. Fukushima, and K.Sato, Phys. Rev. B 105, 075205 (2022).
- [4] L. D. Partain, P. S. McLeod, J. A. Duisman, T. M. Peterson, D. E. Sawyer, and C. S. Dean, J. Appl. Phys. 54, 6708 (1983).

SD-O02 (Oral)**Graphene supported liquid crystal phase retarders on rigid glass and flexible polydimethylsiloxane substrates**Stefan Petrov¹, Vera Marinova^{1,2} and Shiuan Huei Lin^{1*}¹ Department of Electrophysics, National Yang Ming Chiao Tung University, Hsinchu 30010, Taiwan² Institute of Optical Materials and Technologies, Bulgarian Academy of Sciences, Sofia 1113, Bulgaria

* Corresponding author's e-mail: lin@nycu.edu.tw

To implement unique functionality of graphene into Liquid Crystal (LC) enable devices for practical applications, the key challenge is still encountered to have a large scale (inches-by-inches) high-quality graphene offering low sheet resistance and high optical transmittance as well as high precise alignment of LC molecules on the top of the graphene surface. In this paper, we demonstrate functionality of multilayer graphene, grown by atmospheric pressure CVD method, to support large surface area (inch-scale) tunable LC phase retarders on rigid glass and flexible polydimethylsiloxane (PDMS) substrates. We first focused on important steps during fabrication process of LC structures based on a detailed investigation of interfacial interaction between graphene/LC molecules by considering graphene's surface free energy as well as proper selection of polyamide (PI) as a polar layer for a non-contact planar alignment of LC molecules. A non-contact planar alignment of LC molecules instead of mechanical rubbing technique enables prevention of graphene de-attachment from the target substrate. Moreover, multilayer graphene shows excellent wettability when contacting with the polyamide. Measured electro-optical characteristics, such as voltage-dependent transmittance, response time and electrically tunable phase modulation of fabricated LC phase retarders reveal completely equivalent performance of LC retarders using conventional ITO contacts. Besides excellent phase modulation repeatability over the large scale area of the retrofitted LC structure, we demonstrate an electrically tunable LC phase retarder supported by graphene on PDMS that exhibits great potential for future ITO-free LC photonic devices and bio-oriented technologies. We also expect these demonstrations are relevant to use in high-end optoelectronics and would provide a significant step in fabricating tunable graphene-based LC components for flexible and stretchable optoelectronics.

Keywords: multilayer graphene, ITO-free liquid crystal photonic device, flexible photonic device.**References**

- [1] S. Petrov et al., Appl. Surface Sci. 566 (2021) article id. 150646, 1-8.
- [2] V. Marinova et al., Mater. Proc., 4(1) (2020) 65.

SD-O03 (Oral)**Advantages, challenges and opportunities of x-ray absorption spectroscopy for advanced investigation of energy materials**Chung-Li Dong^{1,*}¹ Department of Physics, Tamkang University, Tamsui 25137, Taiwan

* Corresponding author's e-mail: cldong@mail.tku.edu.tw

The materials scientists are devoted to searching for sustainable and clean energy in response to the global surge in demand for energy. It has never been easy to be green without developing advanced renewable energy materials. We have to approach the zero-emission future from different angles. The universal emphasis on energy is to develop advanced functional materials for more efficient energy conversion, storage, and conservation. The concepts to improve the energy conversion, storage or conservation efficiency of current energy materials are simple and clear, but are always much technically challenging. Most of the physical and chemical properties of a material is closely related to its unique atomic and electronic structures. Hence, without knowing the fundamental atomic and electronic structures, and particularly how they response in its working condition, it is difficult to better engineer the materials in an efficient way for a practical use with a greater performance. Synchrotron x-ray spectroscopies, including x-ray absorption and x-ray emission spectroscopies are powerful tools to study the local unoccupied and occupied electronic states. Moreover, utilization of the in situ technique that gives us the opportunity to track the modulations of atomic and electronic structures of the energy material at work. The emerging x-ray spectro-microscopic approach, scanning transmission x-ray microscopy providing the spatially resolved x-ray spectroscopy, is also gearing up for energy science. This presentation will report the significances of using x-ray spectroscopies for atomic and electronic structure characterizations of several important energy material systems, such as artificial photosynthesis materials, advanced nanocatalysts, and smart materials. Emerging characterization tool, recent progress of in situ technique development, a number of recent studies and Tamkang University (TKU) end-stations recently constructed at the Taiwan Photon Source (TPS) 45A & 27A beamlines for energy science will also be presented.

Keywords: X-ray absorption spectroscopy, energy materials, atomic and electronic structures, in situ x-ray absorption spectroscopy

SD-O04 (Oral)**Fabricate electrospun nanofiber for rechargeable batteries**

Nguyen Tuan Canh^{1,*}, Nguyen Phuong Hoai Nam¹, Nguyen Duc Cuong¹, Vu Thi Thao¹, Bui Dinh Tu¹

¹ Faculty of Engineering Physics and Nanotechnology, VNU-UET, Hanoi, Vietnam

* Corresponding author's e-mail: canhnt@vnu.edu.vn

Nanofibers produced by sol-gel electrospinning show an interlaced and highly porous structure with a large surface-to-volume ratio. Such property makes the nanofibers useful in several applications such as healthcare, food packaging, biotechnology, environmental engineering, defense & security, rechargeable, and energy storage. In this study, an Electrospinning system fabricated polyvinyl alcohol (PVA) nanofibers as a mock-up separator in the lithium metal battery. By varying the PVA: DI water ratio by mass, nanofibers were obtained by manipulating various parameters of electrospinning: applied voltage, flow speed, working distance, and spinning time. The ratio of PVA in DI water was found to affect the electrospinnability, fiber morphology, and diameter of fibers. The highly-porous nanofibrous structure was observed by a scanning electron microscope (SEM), and the physical properties were analyzed including porosity, toughness, and heat resistance.

Keywords: Electrospinning, nanofiber, PVA, separator

SD-O05 (Oral)**Is it possible to electropolish tungsten carbides?**

Minh Nhat Dang¹, Surinder Singh¹, Thomas G. Pattison¹, Hoang Le², Rosalie Hocking¹, Scott A. Wade¹, Guy Stephens³, Angelo Papageorgiou³, Hong Tuan Nguyen⁴, James Wang^{1,*}

¹ Australian Research Council (ARC) Industrial Transformation Training Centre in Surface Engineering for Advanced Materials (SEAM), School of Engineering, Swinburne University of Technology, Hawthorn VIC 3122, Australia

² The Electron Microscopy And Materials Analysis Research Group, School of Computing and Engineering, University of Huddersfield, Queensgate, Huddersfield HD1 3DH, United Kingdom

³ Sutton Tools, 378 Settlement Rd, Thomastown VIC 3074, Australia

⁴ Centre for Advanced Materials Technology Development, Centre for High Technology Development, Vietnam Academy of Science and Technology (VAST), 18 Hoang Quoc Viet, Hanoi 100000, Vietnam

* Corresponding author's e-mails: nhatminh@swin.edu.au & jawang@swin.edu.au

Tungsten carbide (WC) based alloys are widely used in cutting tools due to their superior tensile strength, compression strength stiffness, and wear resistance, compared to other carbide based alloys. The addition of cobalt as a primary binder improves the overall strength of the material. For cutting tools not only are the substrate properties important, but the geometry, cutting edge profile, and surface finish are also critical to the performance and working life of the tool. A high quality surface finish and cutting edge preparation can improve the service life of the cutting tools. Chemical methods of surface treatment can offer an even surface finish to geometrically complex substrates such as drill bits which are challenging to finish evenly using physical techniques. Compared to etching and electrical discharge machining, electropolishing offers tailorability over the surface finishing process, resulting in a high degree of control over material removal. This process can produce surfaces with very low surface roughness ($S_a > 100$ nm), maintaining edge geometries of the tool. This talk will discuss the potential for electropolishing to provide a high quality finish to WC substrates, and in particular the challenges to be considered when applying chemical polishing techniques to WC-Co surfaces

Keywords: electropolishing, cutting tools, tungsten carbide, cobalt leaching, edge preparation

SD-O06 (Oral)**Tandem cyclooxidative reaction of anthranilamide and alcohols over Fe(III)-based MOFs: effect of structure on catalytic efficiency**Tan Le Hoang Doan^{1*}¹ Center for Innovative Materials and Architectures, Vietnam National University Ho Chi Minh City

* Corresponding author's email: dlhtan@inomar.edu.vn

Metal-organic frameworks (MOFs), porous crystalline materials, have emerged as promising heterogeneous catalysts in organic transformations. In this research, triangular Fe(III) cluster-based MOFs were highly efficient heterogeneous catalysts for the solvent-free one-pot reaction of 2-aminobenzamide and alcohols to synthesize quinazolin-4-ones under microwave irradiation. The catalytic properties of the Fe-MOFs ranging from microporous to mesoporous structures with the various geometrical pore structures were investigated. Owning the opening accessible spaces for reactants and high density of active sites, MOF-907, built from trimmer Fe clusters and a mixture of two linkers, was more effective than other Fe(III)-MOFs. The catalyst can be used in a broad substrate scope and recycled several times without losing its structure and activity.

Keywords: Metal-organic frameworks, Heterogeneous catalyst, Solvent-free, Microwave irradiation

SD-O07 (Oral)**Nanowire single crystal grain field effect transistors and their applications**Thi Thuy Nguyen^{1,2}, Tatsuaki Hirata¹, and Shin-Ichiro Kuroki¹¹Research Institute for Nanodevices, Hiroshima University, Hiroshima 739-8527, Japan.²Faculty of Physics, Hanoi National University of Education, Ha Noi, Vietnam.

* Corresponding author's email: nguyenthuy@hnue.edu.vn

Single crystal grain (s-G) field effect transistors (FETs) have been the key target for their large electronic applications such as monolithic three-dimensional integrated circuits (3DICs), and glass sheet computers. Highly (110)-(111)-(211) and (100) biaxial-oriented poly-Si thin films have been realized by multiline beam continuous-wave laser lateral crystallization (MLB-CLC) with very long crystal grains.[1, 2] By aligning TFTs' channels to elongate the longitudinal crystal grains, s-G FETs were fabricated at a low temperature process of below 550°C with nanowire Si channels. Figure 1 shows the ID and μ_{eff} versus V_G curves at $V_D = 0.5$ V of a nanowire s-G FET of 220 nm width. It indicates that this transistor had an ultrahigh performance with an electron field effect mobility of 1360 cm²/Vs, an ON/OFF ratio of 10⁷-10⁸, subthreshold slope (S) of 0.17 V/dec, a threshold voltage (V_{th}) of -0.5 V. This performance enhancement was brought about by the uniaxial tensile strain in the poly-Si thin film.

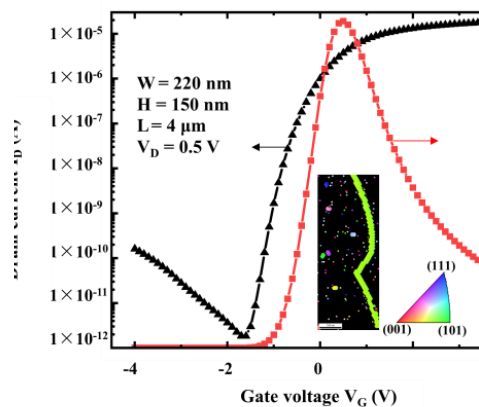


FIG. 1. ID and μ_{eff} versus V_G curves of a nanowire s-G FET.

Acknowledgments

Part of this research was supported by National Foundation for Science & Technology Development, Vietnam (NAFOSTED) (grant no. 103.02-2019.36)

References

- [1] S.-I. Kuroki, Y. Kawasaki, S. Fujii, K. Kotani, and T. Itob, J. Electrochem. Soc., vol.158, no. 9, p. H924, 2011.
- [2] T. T. Nguyen et al., Jpn. J. Appl. Phys., vol. 59, p. 115504, 2020.

Session: Theory and computation (TC)

TC-O01 - TC-O02

TC-O01 (Oral)

The first-principles analysis of multiplet excitations using QSGW

Katsuhiko Suzuki^{1,*}, Takao Kotani^{2,3}, Kazunori Sato^{1,2,4}

¹ Graduate School of Engineering, Osaka University, Osaka 565-0871, Japan

² CSRN-Osaka, Osaka University, Osaka 560-8531, Japan

³ Department of Applied Mathematics and Physics, Tottori University, Tottori, 680-8552, Japan

⁴ Spintronics Research Network Division, OTRI, Osaka University, Osaka, 565-0871, Japan

* Corresponding author's e-mail: k-suzuki@mat.eng.osaka-u.ac.jp

The photoluminescence of rare-earth atoms is one of the important phenomena in strongly correlated electron systems. In these phenomena, the multiplet transitions of $4f$ orbitals are important. However, it is difficult for analyzing from the first-principles calculation. Traditionally, the model-Hamiltonian methods based on the atomic multiplet theory have been developed to explain the photoluminescence spectra of rare-earth atoms. These theories have empirical parameters to reproduce experiments. Therefore, the application of computational material design is difficult. On the other hand, the first-principles calculation can be applied for hypothetical structure, but we cannot discuss multiplet excitations directly. In this study, we try to obtain excitation of the f -orbitals system from the first-principles calculation. Generally, it is known that DFT calculation with LDA/GGA functional underestimates electron correlations. Thus, we use quasi-particle self-consistent GW (QSGW) approximation [1] to consider more accurate correlations. After that, we estimate the parameters of the model Hamiltonian so that the band structure from QSGW reproduces the local atom model Hamiltonian applied mean-field approximation [2]. Figure 1 shows the QSGW band structure of free Eu ion and onsite energy of model Hamiltonian. It shows that the mean-field model Hamiltonian reproduces QSGW results. We discuss the trend of parameters and multiplet excitations for trivalent free rare-earth ions, and the difference in parameters of Eu ion in each material.

Keywords: rare-earth ion, multiplet excitation, first-principles calculation, QSGW

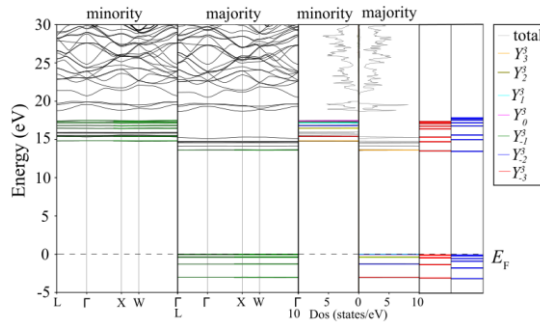


FIG. 1. (left and middle) Band structure and density of states from QSGW of free Eu ion. (right) comparison of QSGW Hamiltonian (red) and mean-field Hamiltonian (blue).

References

- [1] T. Kotani, and M. van Schilfgaarde: Phys. Rev. B 76 (2007) 165106.
- [2] K. Suzuki *et al.*, arXiv: 2206.10862

TC-O02 (Oral)**Carrier-trapping induced transformation of dislocation core structures in Zn compounds**Sena Hoshino^{1*}, Yu Oshima¹, Tatsuya Yokoi¹, Atsutomo Nakamura², Katsuyuki Matsunaga^{1,3}¹ Department of Materials Physics, Nagoya University, Aichi, 464-8603, Japan² Department of Mechanical Science and Bioengineering, Osaka University, Osaka, 560-0043, Japan³ Nanostructures Research Laboratory, Japan Fine Ceramics Center, Aichi, 456-8587, Japan

* Corresponding author's e-mail: hoshino.sena.i9@s.mail.nagoya-u.ac.jp

Zn compound semiconductors exhibit increased deformation stress when irradiated with light [1], which is well known as the photoplastic effect (PPE). Recently, our theoretical calculations on ZnS demonstrated that Shockley partial dislocations form new like-atom bonds at the cores by trapping excess carriers [2]. Such additional bonds must be broken for dislocations to move, which is thus expected to decrease dislocation mobility. Since excess carriers are introduced by light irradiation, carrier-induced transformation of dislocation cores may be closely related to the PPE. However, it is not clear whether such phenomenon originating from dislocation cores is general in other Zn compounds. This work thus aimed to determine dislocation core structures and their energetics with and without excess carriers in ZnS, ZnSe and ZnTe.

Density-functional theory (DFT) calculations were performed using the projected augmented wave method implemented in the VASP core. The three Zn compounds examined have the zincblende structure, which typically has the easiest slip plane with {111} polar planes. In this case, two types of Shockley partial dislocation cores can be considered depending on a character of an inserted extra half plane: the Zn core and the anion core, which were modeled. Excess electrons and holes were then introduced into supercells containing the partial dislocations by changing the number of electrons.

Fig. 1 (a) shows the most stable structure for the Te core in ZnTe without excess carriers. In this case, undercoordinated Te atoms remain along the dislocation line. By contrast, the Te core transforms to a “reconstructed” structure having new Te-Te bonds in the presence of excess holes (Fig. 1(b)). The similar core transformations were also observed at the S core in ZnS [2] and Se core in ZnSe. Dislocation formation energies indicated that in the presence of excess carriers, the reconstructed dislocation cores are energetically more favorable than the unreconstructed ones, with energy differences of 0.74, 0.59 and 0.35 eV/nm in the S core, Se core and Te core, respectively. These values can be considered as the required energy to break the like-atom bonds. It is thus expected that PPE becomes more pronounced in the order of ZnS, ZnSe and ZnTe.

Keywords: Dislocation, Carrier trapping, DFT calculation, Compound semiconductor

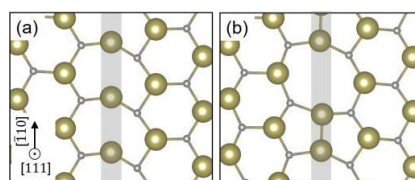


FIG. 1. Dislocation core structures for the Te core in ZnTe. Silver and golden balls indicate Zn and Te atoms, respectively. Gray lines show the dislocation lines.

References

- [1] C. N. Ahlquist et al., J. Phys. Chem, Solids. 33 (1972) 337-342.
- [2] K. Matsunaga et al., Acta. Mater. 195 (2020) 645-653.

Session: Materials for energy and environment (EE)

EE-P01 - EE-P30

EE-P01 (Poster)**Progressive and stable synaptic plasticity with attojoule energy consumption by the interface engineering of a metal/ferroelectric**Sohwi Kim^{1*}, Chansoo Yoon¹, Bae Ho Park¹, Hyung Kook Kim²¹ Division of Quantum Phases & Devices, Department of Physics, Konkuk University, Seoul, Korea² Department of Nano Energy Engineering, Pusan National University (PNU), Busan, Korea

*Corresponding author's e-mail: baehpark@konkuk.ac.kr

In the era of “big data”, the cognitive system of the human brain is being mimicked through hardware implementation of highly accurate neuromorphic computing by progressive weight update in synaptic electronics. Low-energy synaptic operation requires both low reading current and short operation time to be applicable to large-scale neuromorphic computing systems. In this study, we implement an energy-efficient synaptic device comprising a Ni/Pb(Zr_{0.52}Ti_{0.48})O₃ (PZT)/0.5 wt% Nb-doped SrTiO₃ (Nb:STO) heterojunction with a low reading current of 10 nA and short operation time of 20–100 ns. Ultralow attojoule operation up to 5.5 aJ at a synaptic event, which is significantly lower than the energy required for synaptic events in the human brain (10 fJ), is achieved by adjusting the Schottky barrier between the top electrode and ferroelectric film. Moreover, progressive domain switching in ferroelectric PZT successfully induces both low nonlinearity/asymmetry and good stability of the weight update. The synaptic device developed here can facilitate the development of large-scale neuromorphic arrays for artificial neural networks with low energy consumption and high accuracy.

Keywords: Energy efficiency, Low reading current, Short operation time, Linearity, Symmetry, Variability, Neuromorphic computing

References

- [1] Kim, S., Yoon, C., Oh, G., Lee, Y. W., Shin, M., Kee, E. H., ... & Kim, Y. H. “Progressive and Stable Synaptic Plasticity with Femtojoule Energy Consumption by the Interface Engineering of a Metal/Ferroelectric/Semiconductor”, *Advanced Science*, 2201502, 2022.

EE-P02 (Poster)**Silver nanoparticles synthesis using chromolaena odorata (L.) Extract in thermosensitive polymer solutions and evaluation of wound healing capability**

Anh-Quan Hoang^{1,2}, Thi-Phuong Le¹, Le-Hang Dang¹, Duy-Khanh Pham¹, Ngoc-Quyen Tran^{1,2}, Thi-Lieu Nguyen^{2,4}, Anh-Kiet Le⁵, Ngoc-Anh Nguyen⁵, Phuong-Tung Nguyen^{1,3*}

¹ Institute of Applied Materials Science - Vietnam Academy of Science and Technology, 01B TL29 Street, Thanh Loc Ward, 12 Dist., Ho Chi Minh city;

² Graduate University of Science and Technology - Vietnam Academy of Science and Technology, 18 Hoang Quoc Viet Street, Cau Giay Dist., Ha Noi;

³ CIRTech Institute - Ho Chi Minh City University of Technology, 475A Dien Bien Phu Street, Binh Thanh Dist., Ho Chi Minh city;

⁴ Industrial University of Hochiminh City, 12 Nguyen Van Bao, W. 4, Dist., Go Vap, Ho Chi Minh city;

⁵ International University, Vietnam National University, Ho Chi Minh City, Quarter 6, Linh Trung Ward, Thu Duc Dist., Ho Chi Minh city.

* Corresponding author's e-mail: phuongtungng@gmail.com

Trauma wound is an inevitable health issue in life. Many researchers have endeavored to develop multifunctional materials to enhance wound healing after injury. *Chromolaena odorata* (L.), a plant with fresh leaves and decoction, is widely used in Vietnam and tropical countries to treat soft tissue wounds, burns, skin infections, and periodontal diseases. Silver nanoparticles (AgNPs) (which were synthesized in the herbal extract solution) and Pluronic polymer (which plays roles in enhancing healing and protecting the colloidal nanosilver and active components from medicinal plant extracts) were used to create a thermosensitive polymeric nanocomposite solution that can form a multifunctional hydrogel film on the wound surface. Phytochemical analysis was performed to determine the total phenolic, flavonoid contents, and the iron reduction capacity of the CO extract responsible for reducing and capping the biosynthesized CO-AgNPs by using the Folin–Ciocalteu method, the aluminum chloride colorimetric method, and the Oyaizu method, respectively. Antimicrobial and antioxidant activities of the SR extract and CO-AgNPs were tested using the Kirby-Bauer and DPPH methods. The synthesized products were characterized using different techniques, such as UV–visible spectroscopy, dynamic light scattering (DLS), Fourier transform infrared (FTIR) spectroscopy, X-ray diffraction (XRD), and transmission electron microscopy (TEM). The results proved that both ultrasound-supported ethanol CO extract and CO-AgNPs have high efficiency in antimicrobial and antioxidant activities, but CO-AgNPs show superiority. Furthermore, the multifunctional hydrogel system was evaluated, and the results show that the products have high efficiency in antibacterial activities and anti-inflammatory regulation.

Keywords: Antibacterial activity, thermosensitive hydrogel, *Chromolaena odorata*, silver nanoparticles, wound healing.

EE-P03 (Poster)**Construction of highly condensed Cu₂O/CuO composites on Cu sheet and its photocatalytic in photodegradation of hazardous colouring agent rose bengal**

Cong Doanh Sai¹, Van Thanh Pham¹, Thi Ngoc Anh Tran¹, Thi Thuong Huyen Tran^{2*}, Thi BichNgoc Vu³, Thi Huong Hue Hoang³, Anh Son Pham³, Thi Minh Thuy Nguyen⁴, Thi Thu Hoai Duong⁴, Thi Thanh Van Nguyen⁵, Huy Hoang Do^{3*}

¹ Faculty of Physics, VNU - Hanoi University of Science, Vietnam National University, 334 Nguyen Trai, ThanhXuan, Hanoi, Viet Nam

² Institute of Materials Science, Vietnam Academy of Science and Technology, 18 Hoang Quoc Viet, Cau Giay, Hanoi, Viet Nam

³ Faculty of Chemistry, VNU - Hanoi University of Science, Vietnam National University, 19 Le Thanh Tong, HoanKiem, Hanoi, Viet Nam

⁴ Thai Nguyen University of Education, 20 Luong Ngoc Quyen, Quang Trung, Thai Nguyen, Viet Nam

⁵ Vietnam Academy of Cryptography Techniques, 141 Chien Thang, Tan Trieu, Thanh Tri, Hanoi, Vietnam

* Corresponding author's email: dohuyhoang@hus.edu.vn

Binary copper oxides with different copper ion oxidation states including cuprous Cu₂O and cupric CuO have already been successfully synthesized by the simple and highly repeatable grow-up technique from the modified copper Cu sheet. By controlling the annealing time and temperature, the copper oxide (CuO, Cu₂O) composites were hierarchically formed on Cu surface. All obtained samples were characterized using X-ray diffraction (XRD) spectroscopy and scanning electron microscopy (SEM). The results showed that the modified Cu sheets after annealing in air yielded the mixture of CuO and Cu₂O phases. The obtained Cu₂O/CuO composites have been used as active photocatalysts to decolourize the 10 ppm dyes rose bengal solution with the degradation efficiency of 73% over a period of 3 h under UV-A irradiation after three uses. These results make them attractive as reusable photocatalytic materials in form of flat sheet. The other testing conditions as pH values and oxidant agent (H₂O₂) was carried out. It was observed that the photodegradation achieved up to 96% with the presence of H₂O₂.

Key words: CuO, Cu₂O, film-based photocatalyst, reusability, stability, photodegradation.

EE-P04 (Poster)**Chemical expansivity and oxygen transport in oxide perovskite ceramics**Tran Cong Than^{1,*}, Mark De Guire¹¹ Case School of Engineering–Case Western Reserve University, Cleveland, OH 44106, US

* Corresponding author's e-mail: tct19@case.edu

Oxygen transport membranes are necessary to create portable gas reformers. A dense oxide layer with mixed electronic and ionic conductivity (MEIC) performs efficiently for selective diffusion of oxygen but they are mechanically unstable due to their chemical expansion under oxygen partial pressure gradients in working conditions. Various designs to circumvent this instability were proposed but they may affect functionality. As a measure of the membrane's functionality, oxygen flux needs to be measured for comparison, but direct measurement methods require complex equipment.

R code was used to calculate a membrane's oxygen diffusivity from measurements of its chemical expansion. Oxygen diffusivity measures how fast oxygen moves inside the material under a gradient in oxygen potential, related to oxygen flux. By measuring the membrane's expansion and contraction due to step changes in oxygen partial pressure, the oxygen diffusivity can be approximated. It is noticed that the accuracy of this approach is sensitive to the precision of the chemical expansion measurements.

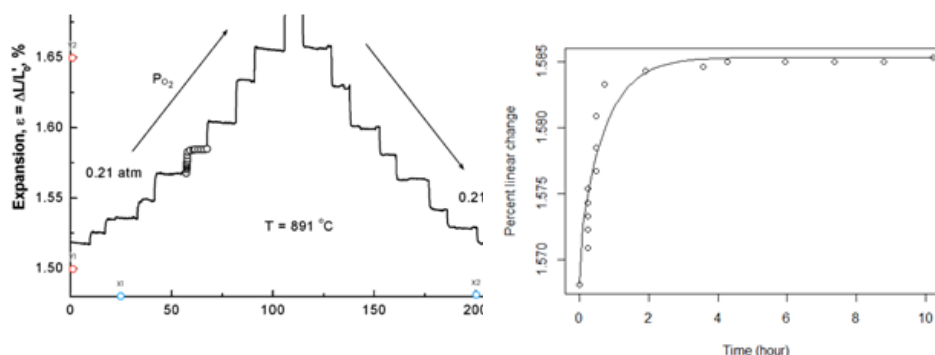


FIG. 1. Digitalized data of sample expansion when exposed to partial pressure changes of oxygen (left) and the resulting curve when fitted in R [1].

References

- [1] X. Chen, J. Yu, and S. B. Adler, Chem. Mater. 17 (2000) 4537–4546.

EE-P05 (Poster)**Zr and Hf-based metal-organic frameworks used as efficient heterogeneous catalysts for the synthesis of heterocyclic compounds**

Linh Ho Thuy Nguyen^{1, 2*}, Trang Thi Thu Nguyen^{1, 2}, Minh Huy Dinh Dang^{1, 2}, Phuong Hoang Tran^{2, 3}, Tan Le Hoang Doan^{1, 2}

¹ Center for Innovative Materials and Architectures

² Viet Nam National University-Ho Chi Minh City, Ho Chi Minh

³ Department of Organic Chemistry, Faculty of Chemistry, University of Science, Vietnam National University-Ho Chi Minh City

* Corresponding author's email: nhtlinh@inomar.edu.vn

Zirconium- and Hafnium-based metal-organic frameworks (Zr- and Hf-MOFs), which are constructed by a diversity of coordinated clusters, were shown to be highly effective heterogeneous catalysts for many reactions. Herein, we demonstrate strategies for designing, functionalizing, tailoring, and synthesizing defective 12-connected and 6-connected Zr- and Hf-MOFs used as reusable catalysts. These synthesized materials were fully characterized by several techniques, including powder X-ray diffraction, N₂ sorption isotherms, acid-base titration, and thermal gravimetric analysis to determine their features regarding structural defect, porosity, acidity, and stability. In the catalytic studies, the combination of Brønsted and Lewis acidic of these MOFs was efficiently applied for synthesizing heterocyclic bioactive compounds such as benzoxazole, benzimidazole, benzothiazole, and quinazolinone. MOFs with Zr₆ or Hf₆ nodes could identify a significantly enhanced yield in Brønsted acid catalyzed reactions by using the wide opening spaces structures and inherent high density of active sites. The catalysts can be used for a broad substrate scope and recycled several times without a significant loss in their activity.

Keywords: Zr-MOF, Bronsted acid MOF, Heterocyclic reaction, Benzoxazole derivatives, Quinazolinone

EE-P06 (Poster)**Modeling inductance of a coil dipping in solution**

Nam-Nhat Hoang^{1*}, Dinh-Tu Bui¹, Van-Hiep Vuong², The-Long Phan^{1,3}, Hong-Phuc Pham¹, Vinh-Tan Do¹, Dang-Co Nguyen¹

¹ Faculty of Engineering Physics and Nanotechnology, VNU-University of Engineering and Technology, 144Xuan Thuy, Cau Giay, Ha Noi, Viet Nam

² Faculty of Physics, VNU-University of Sciences, 334 Nguyen Trai, Thanh Xuan, Ha Noi, Viet Nam

³ Department of Physics, Hankuk University of Foreign Studies, Yongin 17035, South Korea

* Corresponding author's e-mail: nhathn@vnu.edu.vn

Self-inductance of a coil depends on dipping environment. The measured values vary slightly for vacuum, air and pure water [1-4] in large ranges of both temperature and applied frequency. However, for particular cases of solutions of salts such as NaCl, FeCl₃ etc., the measured inductance depends significantly on both temperature and frequency. In this article we show that the dependance of a coil's inductance on frequency and temperature when dipping in a salt solution may be derived from the mobility and relaxation time of ions at given concentration. The fit to measured data is demonstrated for the NaCl and FeCl₃ solutions of concentrations from 0.1 to 1.0 mol/l. The results show that for each given kind of ion at given concentration there is a specific frequency where the inductance is zeroed, and another one where it is maximum. This enable sensing separability of ion and its concentration in liquid water due to measurement of coil's self-inductance.

Keywords: Inductance, Coil, Ion, Solution, Soil, Magnetic Response

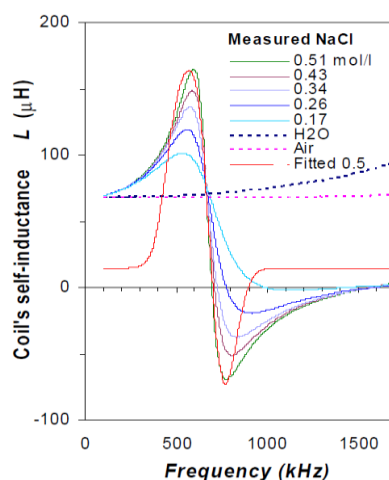


FIG. 1. Measured and fitted data for NaCl solution at various concentrations.

References

- [1] F. Gutierrez-Mejia, J.C.Ruiz-Suarez, J. Mag. Magn. Mater. 324 (2012) 1129 1132.
- [2] E. P. Day, J. Chem. Phys. 72 (1980) 4434.
- [3] V. Rana, P. Kumar, S. Banerjee, A. Biswas, J. Earth Syst. Sci. 130 (2021) 140.
- [4] R. Cini and M. Torrini, J. Chem. Phys. 49 (1968) 2826.

EE-P07 (Poster)**The Langmuir-Blodgett and Langmuir-Schaefer film of stearic acid: preparation and characterization**

Thi Thao Vu^{1*}, Tien Loi Do¹, Tri Duc Luong², Duc Cuong Nguyen¹, Van-Huong Tran³, Mai Ha Hoang⁴, Hoang Trang Nguyen⁵

¹ University of Engineering and Technology, Vietnam National University, Hanoi, Vietnam

² Foreign Language Specialized School, University of Languages & International Studies

³ School of Mechanical Engineering, Hanoi University of Science and Technology, Hanoi, Vietnam

⁴ Institute of Chemistry, Vietnam Academy of Science and Technology, Hanoi, Vietnam

⁵ University of Education, Vietnam National University Hanoi, Hanoi, Vietnam

* Corresponding author's e-mail: vtthao@vnu.edu.vn

Stearic acid (SA) is one of the most common long-chain saturated fatty acids and is a surfactant capable of forming stable floating films with different nanostructures by the Langmuir-Blodgett (LB) technique. These floating layers could be transferred to different substrates to obtain solid films by LB or Langmuir-Schaefer (LS) deposition method. Films of SA are used independently and in conjunction with other substances (e.g. chitosan, poly(p-phenylene vinylene) (PPV), metallic ions, other fatty acids, proteins, vitamins, and so on) to synthesize new materials for a wide range of applications. These applications include but are not limited to electronics, chemical and biological sensors, and filters. This paper systematically reviews LB and LS films of stearic acid especially experimental parameters in prior studies as well as advancements in the application of stearic acid-based films.

Keywords: Stearic acid, Langmuir-Blodgett, Langmuir-Schaefer, thin film

EE-P08 (Poster)**Preparation, photocatalytic degradation of pollutants and self-cleaning performance of TiO₂ based-nanomaterials (TiO₂, TiO₂-ZnO, TiO₂-Au)**

Thi Thuong Huyen Tran^{1*}, Thi Kim Chi Tran¹, Thi Dieu Thuy Ung¹, Thi Quynh Xuan Le¹,
Nhat Linh Nguyen¹, Thi Minh Thuy Nguyen², Thi Thu Hien Pham², Truong Son Nguyen³,
Hoang Tung Do³, Thi Huong Hue Hoang⁴, Huy Hoang Do^{4*}

¹ Institute of Materials Science, Vietnam Academy of Science and Technology, 18 Hoang Quoc Viet, Cau Giay, Hanoi, Viet Nam

² Thai Nguyen University of Education, 20 Luong Ngoc Quyen, Quang Trung, Thai Nguyen, Viet Nam

³ Institute of Physics, Vietnam Academy of Science and Technology, Vietnam, 18 Hoang Quoc Viet Street, Cau Giay District, Hanoi 10000, Vietnam

⁴ Faculty of Chemistry, VNU - Hanoi University of Science, Vietnam National University, 19 Le Thanh Tong, Hoan Kiem, Hanoi, Viet Nam

* Corresponding author's email: dohuyhoang@hus.edu.vn

Titanium dioxide (TiO₂), a non-toxic semiconductor, has garnered extensive interest due to their excellent photocatalytic, self-cleaning and antibacterial properties. Its wide bandgap with rutile phase (3.0 eV), anatase and brookite phases (3.2 eV) restricts the visible light photocatalytic applications. An effective approach to address this limitation is decorating the TiO₂ surface by plasmonic Au nanoparticles or engineering the heterostructure with ZnO metal-oxide leading to the multi-function photocatalyst. Herein, we have successfully prepared some TiO₂ based-nanomaterials (TiO₂, TiO₂-ZnO, TiO₂-Au) and investigated their photocatalytic activity and photocatalytic self-cleaning behavior. All obtained photocatalysts were prepared by chemical route (sol-gel and hydrothermal methods) and plasma jet technology. Characterization was analyzed by X-ray diffraction (XRD), Raman spectroscopy, scanning electron microscopy (SEM) technique. Ultra-hydrophilicity was assessed by measuring the contact angle. Photocatalytic properties were evaluated through the photodegradation of methylene blue (MB) and rhodamine 101 (RB) under the both simulated visible light and direct sunlight. The TiO₂-ZnO and TiO₂-Au photocatalysts are active under this condition while the pure TiO₂ in form of anatase, brookite and the anatase/brookite mixture exhibit high activity under the ultraviolet (UV) light.

Keywords: TiO₂, ZnO, Au, Photocatalytic, Self-cleaning, Hydrothermal, Plasma jet

EE-P09 (Poster)**Application of SiO₂ nano-spheres embedded in polypropylene matrix for the analytical blood filtering processes**

Ha Thi Phuong Thao^{1,2}, Cao Phuong An³, Nguyen Quang Minh³, Hoang Van Huy², Luu ManhQuynh^{2,*}

¹ Faculty of Biology, VNU-HUS, Hanoi, Vietnam

² Center for Materials Science, Faculty of Physics, VNU-HUS, Hanoi, Vietnam

³ The Olympia School

* Corresponding author's e-mail: luumanhquynh@hus.edu.vn

The human body responses to diseases or illnesses with significant, such as body-temperature elevation, oxidant-release and blood chemical level changing. As consequence, blood chemistry tests are of common processes, those are frequently performed to detect and identify a wide variety of medical conditions. In some chemistry tests, large-size blood components – usually blood cells themselves, aggregated cholesterol, lipids - might originate the positive or negative bias, which falsifies the investigation results. To minimize these interferences, this study introduced an advanced structural blood-filter using SiO₂ nanospheres embedded in a polypropylene matrix, which has the filtering pore-sizes 40 nm-smaller. The as-prepared nano blood filters were applied for calcium ion and organic filtering and let ~97% small size chemicals – calcium ions, Rohdamine B - transfer, and are suitable for blood chemistry test sampling.

Keywords: blood chemistry test, blood sampling, nano blood filter, SiO₂ nanospheres

EE-P10 (Poster)**Effects of surfactants on dispersion of expanded graphite in polyurethane foam**

Son Thanh Bach¹*, Huong Thi Thu Le¹, Thuy Thi Phan¹

¹ Institute of Physics, Vietnam Academy of Science & Technology, Vietnam

* Corresponding author's e-mail: stbach91@gmail.com

Using surfactants is a common strategy to exfoliate stacks of graphene sheets from graphite and enhance its processability. Two commercially available surfactants, Tween 80 and Triton X-100, are used to modify expanded graphite (EG) which serves as filler for polyurethane foam (PUF). Effects of the two surfactants on dispersion of EG within the polymer matrix are testified through scanning-electron microscopy (SEM) and thermal conductivity measurements of the EG/PUF composite samples. Modification of EG with Triton-X / Tween 80 results in more uniform dispersion of the filler material inside the polyurethane matrix and increases the thermal conductivity of EG/PUF composite from 0.057 to 0.074 / 0.080 (W.m⁻¹.K⁻¹), respectively.

Keywords: expanded graphite, polyurethane foam, surfactants

EE-P11 (Poster)

Study and characterization of betulin encapsulated by liquid compounds to improve its solubility in water

Le Thi Thu Huong^{*}, Nguyen Thi Mai Huong, Phan Thi Thuy, Nguyen Thanh Binh, Nguyen Trong Tinh

Institute of Physics, Vietnam Academy of Science & Technology, Hanoi, Vietnam.

^{*} Corresponding author's e-mail: thuhuong@iop.vast.vn

Betulin is a natural compound, extracted from the bark of the birch trees, known and used for a long time because of its anti-viral, anti-cancer, antioxidant properties etc. However, like many naturally occurring bioactive compounds, it has poor solubility, which greatly limits its pharmacologically promoting effects. Many studies on betulin have been conducted, but mainly on its acid and other derivatives. In this paper, the research direction was preparation of betulin in liquid phase in order to enhance the solubility in water. The particle sizes of obtained samples were less than 100 nm and their solutions were optically clear, and they could be stable for 24 hours. In addition, the results of SEM, UV-VIS, FTIR measurements of betulin powder and liquid formulation were also reported.

Keywords: Betulin, antioxidant, biological activities.

EE-P12 (Poster)

Coupling amorphous Ni hydroxide nanoparticles with single-atom Rh on Cu nanowire arrays for highly efficient alkaline seawater electrolysis

Ngoc Quang Tran^{1,2*}

¹ Center for Innovative Materials and Architectures, Ho Chi Minh City 700000, Viet Nam

² Vietnam National University, Ho Chi Minh City 700000, Viet Nam

* Corresponding author's e-mail: tnquang@inomar.edu.vn

Exploring efficient catalysts for alkaline seawater electrolysis is highly desired yet challenging. Herein, coupling single-atom rhodium with amorphous nickel hydroxide nanoparticles on copper nanowire arrays is designed as a new active catalyst for the highly efficient alkaline seawater electrolysis. We found that an amorphous Ni(OH)₂ nanoparticle is an effective catalyst to accelerate the water dissociation step. In contrast, the single-atom rhodium is an active site for adsorbed hydrogen recombination to generate H₂. The NiRh-Cu NA/CF catalyst shows superior electrocatalytic activity toward HER, surpassing a benchmark Pt@C. In detail, the NiRh-Cu NA/CF catalyst exhibits HER overpotentials as low as 12 and 21 mV with a current density of 10 mA cm⁻² in fresh water and seawater, respectively. At high current density, the NiRh-Cu NA/CF catalyst also exhibits an outstanding performance, where 300 mA cm⁻² can be obtained at an overpotential of 155 mV and shows a slight fluctuation in the current density

Keywords: Single-atom catalyst, Seawater electrolysis, cation exchange, nanowire array.

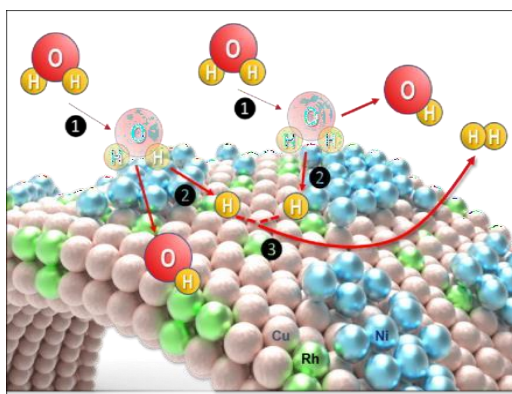


FIG. 1. Proposed mechanism to explain the enhanced HER activity of NiRh-Cu NA/CF catalyst.

References

- [1] N.Q. Tran et al., J. Phys. Chem. Lett. **2022**, 13, 8192-9199.

EE-P13 (Poster)**Pre-irradiation-induced grafting acrylamide onto polyvinylpyrrolidone matrix and evaluating combined copolymers with graphene oxide for high-temperature offshore oilfield application**

Lieu Nguyen Thi^{1,2*}, Anh-Quan Hoang², Anh-Tuyen Luu³, Van-Toan Le⁴, Duy-Khanh Pham², Phuong-Tung Nguyen^{5*}

¹ Industrial University of Ho Chi Minh City, Ho Chi Minh City, 700000, Vietnam

² Institute of Applied Materials Science, VAST, Ho Chi Minh City, 700000, Vietnam

³ Center for Nuclear Technologies, Ho Chi Minh City, 700000, Vietnam

⁴ Dalat Nuclear Research Institute, Dalat City, 670000, Vietnam

⁵ CIRTech Institute, HUTECH University, Ho Chi Minh City, 700000, Viet Nam

* Corresponding author's e-mail: lieubk49@gmail.com; np.tung@hutech.edu.vn

Crude oil will still be the primary source of energy for the economy, and an irreplaceable input material of the chemical industry, especially organic chemistry. Therefore, efficient exploitation of oil and gas is always the most critical task of the oil and gas industry, especially when, with the depletion of many large oil fields in the world, explore and exploit oil fields as far from the shore with greater depth and higher temperature (HT). Polymer solutions are widely used in oil and gas exploration and production. To meet the requirements of working effectively in the harsh conditions in offshore oilfields, thermal resistance and salt-stable in seawater with high hardness polymer solutions are required. In the present research, the irradiation-induced grafting of acrylamide (AM) onto polyvinylpyrrolidone (PVP) matrix with a number-average molecular weight (Mn) of 30000 by gamma pre-irradiation technique. Effects of the total dose, monomer concentration, reaction time, and temperature on the grafting percentage are studied in detail. It is shown that the optimum conditions for grafting are: the AM concentration of 20%, the reaction time of 7.5 h, and a total dose of 5 kGy. Then the conjugation of synthesized P(AM-NPV) copolymers on the thermostable GO nanosheets was performed to get GO-P(AM-PVP) nanocomposites. The structure of graft-polymers and GO-P(AM-PVP) nanocomposite was analyzed by Fourier transform infrared spectroscopy (FTIR), and Raman spectral analysis. The scanning electron microscopy (SEM) analyses and elemental mapping were performed to observe the composites morphology and atoms distribution of copolymers on the GO surface, respectively. The molecular weight of the polymer was determined by the Agilent Technologies Infinity gel permeation. Besides, thermal stability was analyzed using a thermogravimetric analysis (TGA). The advantages of P(AM-PVP) copolymer and GO-copolymer nanofluids in high viscosity, solubility in seawater, and stability at high White-Tiger Oligocene reservoir temperatures (> 128 °C and 135 °C) were confirmed by bottle tests at 128 °C and 135 °C in 31 days. These features render them suitable for EOR and other applications in HT offshore reservoirs.

Keywords: Pre-irradiation-induced grafting polymerization, nanofluid, high-temperature offshore reservoir, GO-polymer nanocomposite.

References

- [1] A. Bcdef et al., Phys. Rev. Lett. 100 (2000) 10001.
- [2] Z. Yxwv et al., Science 2 (1900) 1234.

EE-P14 (Poster)**Synthesis of cobalt sulfide nanopowders for non-enzyme urea sensors**

Nguyen Dang Phu^{1,*}, Luc Huy Hoang², Tran Nhu Chi¹, Nguyen Kieu Chang², Bui Thanh Tung¹

¹ Faculty of Electronics and Telecommunications, VNU – University of Engineering and Technology

² Faculty of Physics, Hanoi National University of Education, 136 Xuan Thuy, Cau Giay, Hanoi, Vietnam

* Corresponding author's e-mail: phund@vnu.edu.vn

Cobalt sulfide nanopowders were successfully synthesized by microwave assisted method. The structure, morphology, Raman scattering and electrochemical properties were investigated. The results show that the cobalt sulfide had morphology of nanoprim with mesoporous structure. The cobalt sulfide were applied in detection of urea. The sensing performance for urea was determined by changing the oxidation potential peak of 120 mV. The cobalt sulfide had a linear range from 1 mM to 8 mM corresponding to the urea concentration in blood. The sensitivity of proposed sensor was quite good ($7.5 \mu\text{A mM}^{-1}\text{cm}^{-2}$) compared to results from previous publications. The results presented here demonstrate the potential of the application for urea detection.

Keywords: Cobalt sulfide, electrochemical sensor, microwave assisted method, determination of urea

EE-P15 (Poster)

Evaluation of antioxidant capacity by in vitro methods for some biologically-active natural compounds

Nguyen Trong Tinh*, Nguyen Thi Mai Huong, Le Thi Thu Huong, Phan Thi Thuy, Le Thi Huong, Bach Thanh Son, Nguyen Thanh Binh.

Institute of Physics, Vietnam Academy of Science & Technology, Hanoi, Vietnam.

* Corresponding author's e-mail: nttinh@iapsi.vast.vn

Natural compounds with antioxidant property have amazing potential in the pharmaceutical industry. This field attracts a lot of research groups to focus on discovering, examining their biological properties and putting them into applications. Therefore, it is important to quantify the antioxidant capacity of such compounds as a way of pre-sorting before drug development. In this paper, different in vitro assays including DPPH, ABTS and CUPRAC are used to determine and evaluate the antioxidant capacity of several natural compounds such as curcumin, taxifolin, melanin...etc.

Keywords: in vitro, DPPH, ABTS, biological activities.

EE-P16 (Poster)**Nanostructured stable floating layers and Langmuir-Schaefer films of 5,10,15,20-tetraphenylporphine**

Thi Thao Vu^{1,*}, Larissa. A. Maiorova², Thi Thu Thuy Bui¹, Duc Thang Nguyen¹, Dao The Nam³, Mai Ha Hoang⁴, Oskar I. Koifman², Kien Cuong Dao⁵

¹ University of Engineering and Technology, Vietnam National University, Hanoi, Vietnam

² Institute of Macrocyclic Compounds, Ivanovo State University of Chemistry and Technology, Ivanovo, Russian Federation

³ Institute of chemistry and material, Academy of Military Science and Technology, Hanoi, Vietnam

⁴ Institute of Chemistry, Vietnam Academy of Science and Technology, Hanoi, Vietnam

⁵ Vietnam-Russia Tropical Centre

* Corresponding author's e-mail: vtthao@vnu.edu.vn

Porphyrins are macroheterocyclic organic compounds that are of particular interest to researchers around the world because of their wide application potential in many fields such as sensor fabrication, electrochemical catalysis, photodynamic therapy (PDT), antibacterial materials, energy conversion materials... Not only that, porphyrins are applied not only in solution form but also in thin films. Porphyrins are surfactants that can easily form stable monolayers and multilayers by the Langmuir–Blodgett method. In this study, we investigated the conditions affecting the LB film formation of 5,10,15,20-tetraphenylporphine (H₂TPP) such as concentration, initial surface coverage degree, compression speed, and other factors. The obtained films were investigated for their optical properties, film structure morphology, wettability, and film durability under UV irradiation. Thereby identifying the passport of (H₂TPP) film fabrication and orientation of their application in the fields of electrochemical catalysts, antibacterial, and sensors.

Keywords: porphyrin, Langmuir-Blodgett, Langmuir-Schaefer, floating layers

Acknowledgement. This work in the part of the films formation and study was supported by the grant of the RSF (20-12-00175), ISUCT, and Ministry of Science and Higher Education of the Russian Federation (FZZW-2020-0008) in the part of synthesis of the compound.

References:

- [1] L.A. Maiorova, *D.Sc. Diss.* Russia. 2012, 382 p.
- [2] L.A. Valkova, C. Betrencourt, A. Hochapfel et al. *Mol. Cryst. Liq. Cryst.* 996, 287, 269-273.
- [3] L.A. Valkova, A.S. Gilbin, O.I. Koifman, V.V. Erokhin. *JPP.* 2011, 15 (9-10), 1044-1051.
- [4] L.A. Valkova, A.S. Glibin, O.I. Koifman. *Macrocyclics.* 2011, 43), 222-226.

EE-P17 (Poster)**Sensitive detection of rhodamine B (RhB) in condiments using surface-enhanced Raman scattering (SERS) silver particles as substrate**

Nguyen Tran Truc Phuong^{1,2}, Do Thao Anh^{1,2}, Hanh Kieu Thi Ta^{1,2}, Ngoc Xuan Dat Mai^{2,3}, Ta Ngoc Bach⁴, Bach Thang Phan^{2,3}, Nhu Hoa Thi Tran^{1,2*}

¹ Faculty of Materials Science and Technology, University of Science, Ho Chi Minh City, Vietnam

² Vietnam National University, Ho Chi Minh City, Viet Nam

³ Center for Innovative Materials and Architectures (INOMAR), Ho Chi Minh City, Viet Nam

⁴ Institute of Materials Science, Vietnam Academy of Science and Technology, Ha Noi, Viet Nam

* Corresponding author's e-mail: ttnhoa@hcmus.edu.vn

The design of efficient substrates for surface-enhanced Raman spectroscopy (SERS) for large-scale fabrication at low cost is an important issue in chemical analysis. In this research, a facile large-scale preparation of SERS substrates for the determination of Rhodamine B (RhB) at the excitation wavelength of 532 nm based on silver nanoparticles (Ag NPs) has been developed. The morphology, structure, and properties of as-prepared AgNPs are characterized using ultraviolet-visible (UV-Vis) spectroscopy, field emission scanning electron microscopy (FE-SEM), and X-ray diffraction (XRD), respectively. It was found that different morphologies of the roughened Ag nanoparticles could be obtained under controlled conditions. The fabricated SERS sensor showed high sensitivity and good signal reproducibility. These Ag NPs show a broad range of tunable SERS enhancement factors ranging from 102 to 108 using rhodamine B as a probe molecule with the minimum detection limit of RhB was 10⁻¹⁰ M. The method showed that the proposed method was sensitive, convenient, low-cost, large-scale production of SERS substrates and feasible for the determination of RhB in condiments.

Keywords: SERS substrates, Rhodamine B, enhancement factor, condiments, silver particles

EE-P18 (Poster)**Effect of glycerol, gelatin and stearic acid on physical and mechanical properties of native cassava starch thin film**

Thi Thao Vu^{1*}, Thi Hoa Hoang¹, Van Dong Nguyen¹, Ha Duc Chu¹, Ngoc An Nguyen¹, The Nam Dao², Tuan Anh Le³, Viet Thanh Tung Bui¹

¹ University of Engineering and Technology, Vietnam National University Hanoi, Hanoi, Vietnam

² Institute of Chemistry and Material, Academy of Military Science and Technology, Hanoi, Vietnam

³ University of Science, Vietnam National University Hanoi, Hanoi, Vietnam

* Corresponding author's e-mail: vtthao@vnu.edu.vn

Single-use plastic waste, with the decomposition time up to thousands of years, is a critical issue of modern consumerism. The development and production of eco-friendly biofilms could be a long-term and more sustainable solution to this problem. In this research, we study the formation of a bio-degradable, thin film from cassava starch, an abundantly available material in tropical countries. By adjusting the starch film casting conditions, such as the proportion of glycerol, gelatin, stearic acid, casting mass, temperature and film incubation time, starch films with different thicknesses, water absorption, and moisture content can be obtained. The morphological properties of the investigated films were observed by using a scanning electron microscope. The dependence on the fabrication conditions of tensile strength, solubility in water, thermal stability, hydrophobicity, and time of film degradation of the different starch films was investigated. Our findings could support the development of cassava starch-based biofilms for use in packaging and protection technology.

Keywords: cassava, starch film, glycerol, gelatin, stearic acid.

EE-P19 (Poster)**Size sorting and hydrophilic functionalization of fly ash from a thermal power plant toward to latent fingerprint development**

Luu Manh Quynh^{1*}, Nguyen Thi Thu Ha¹, Hoang Van Huy¹, Pham Nguyen Hai¹ and Nguyen Hoang Nam²

¹ Faculty of Physics, VNU-HUS, Hanoi, Vietnam

² Nano and Energy Center, VNU-HUS, Hanoi, Vietnam

* Corresponding author's e-mail: luumanhquynh@hus.edu.vn

Fly ash is formed during the coal- fired combustion followed by the heat generation for industrial activities, such as thermal power plants, cast-iron manufactures or cement production. This residual by-product is considered as solid waste, which might cause air pollution and water contamination. To minimize the harmful effect of fly ash to the environment, collecting methods and application procedure have been introduced in recent decades. In this study, fly ash dust from Thuy Nguyen thermal power plant is collected, size classified to 5 μm smaller in average and then surface- functionalized with amine functional groups targeting to the latent fingerprint developing application. It was experienced that there are more than 20 % of fly ash from Thuy Nguyen thermal power plant was collected and conformed to the requirements for fingerprint developing powder, which dedicate a valuable use of this solid waste.

Keywords: Fly ash, thermal power plant, latent fingerprint development

EE-P20 (Poster)**Active colloidal photonic arrays of Ag@Fe₃O₄ nanoparticles as colorimetric sensing platforms for on-site environmental and food safety monitoring**

Van Tan Tran^{1*}, Jeonghyo Kim², Van-Tuan Hoang¹, Van-Duong Dao¹, Anh-Tuan Le¹, Jaebeom Lee²

¹ Phenikaa University

² Chungnam National University

* Corresponding email: tan.tranvan@phenikaa-uni.edu.vn

With rapid developments in industry and agriculture, as well as the high-consumption lifestyle, human beings are facing a massive environmental crisis. Besides, food-borne diseases, food contaminations are attracting a lot of attention due to repeated episodes of adulterated and unsafe food practices. The existence of very small amounts of toxic pollutants, such as heavy metal ions, organic compounds, bacteria, etc. can induce ecological risk and irreversible damage to people. Therefore, fast, real-time, visual, sensitive, and selective determination of toxic pollutants is significant. Although spectroscopic techniques have been widely used for the determination of various analytes with high sensitivity and selectivity, they are expensive, time-consuming, and required trained operators. Colorimetric method as an alternative has attracted tremendous attention recently due to its easy fabrication, quick detection, high sensitivity, and naked-eye sensing. Here, we aim at fabrication and investigation of a novel colorimetric sensing platform of active colloidal photonic arrays for rapid, visual, low-cost, and sensitive detection of a wide spectrum of organic molecules and inorganic ions. A novel magnetic-assisted assembly is introduced to fabricate active colloidal photonic arrays on various substrates. The use of Ag@Fe₃O₄ nanoparticles not only produces enhanced color saturation and sensitivity but also can offer an approach to magnetically purify/enrich samples.

Keywords: structural color, photonics, colorimetric sensor, on-site monitoring, Ag@Fe₃O₄

EE-P21 (Poster)

Preparation and characteristics of SnO₂ nanomaterials by Joule heating effect

Thi Huyen Trang Bui¹, Thanh Binh Nguyen¹, Minh Phuong Le¹, Van Thanh Pham¹, Thi Ha Tran², Van Tan Tran¹, Viet Tuyen Nguyen^{1*}

¹ Faculty of Physics, VNU-University of Science, Thanh Xuan, Hanoi, Vietnam,

² Hanoi University of Mining and Geology, Duc Thang, Tu Liem, Hanoi

* Corresponding author's e-mail: nguyenviettuyen@hus.edu.vn

SnO₂ nanostructures have been prepared using the thermal oxidation reaction with the Sn metal by a self resistive heating effect. The morphology and microstructure of the prepared SnO₂ nanoproducts are characterized by means of scanning electron microscopy (SEM), X-ray diffraction and Raman spectrum. In addition, the possible growth mechanism of the SnO₂ nanoproducts is also discussed.

Keywords: SnO₂ nanowires; Joule heating; current; thermal oxidation.

EE-P22 (Poster)**Cu-doped effect on structural and optical properties of ZnO nanoparticles towards the application of maize growth**

Dang Thi My Nga¹, La Thi Ngoc Mai¹, Nguyen Van Loi², Nguyen Duy Phuong², Bui Nguyen Quoc Trinh^{1,3,*}

¹ Faculty of Advanced Technologies and Engineering, Vietnam Japan University, Vietnam National University, Hanoi, Luu Huu Phuoc, Nam Tu Liem, Hanoi, Vietnam

² Faculty of Basic Science, Vietnam Academy of Cryptography Techniques, 141 Chien Thang, Thanh Tri, Hanoi, Vietnam

³ Key Laboratory for Micro-Nano Technology, University of Engineering and Technology, Vietnam National University, Hanoi, 144 Xuan Thuy, Cau Giay, Hanoi, Vietnam

* Corresponding author's e-mail: trnhbnq@vnu.edu.vn

Agricultural application-oriented Cu-doped ZnO nanoparticles were synthesized by co-precipitation method. Effect of Cu doping ratio on the structural, morphological, and optical characteristics of the nanoparticles was systematically examined with respect to pure and 1-5 % wt. doping concentrations. X-ray diffraction showed that the nanoparticles had a wurtzite crystal structure of pure ZnO, but the CuO phase appeared interspersed with the ZnO phase when changing the Cu concentration. Scanning electron microscopy micrographs revealed that the nanoparticles were granular with a relatively uniform size, of which the typical sizes were in range of 40 nm to 130 nm, once the concentration of Cu varied. The X-ray spectrum of energy-dispersive energy confirmed a uniformity of Cu element distribution. The ultra-violet emission peak of 380 nm appeared for the pure ZnO, and reduced to 374 nm for the Cu-containing nanoparticles. As a result, the Cu-doped ZnO nanoparticles utilized as nano-fertilizers brought a new impact into the growth of maize at the concentration of 100 ppm.

Keywords: CuO, ZnO, nanoparticle, co-precipitation, maize

EE-P23 (Poster)

Preparation and characteristics of CuO nanowires by Joule heating effect

Minh Phuong Le¹, Van Thanh Pham¹, Thi Ha Tran², Van Tan Tran¹, Viet Tuyen Nguyen^{1,*}

¹ Faculty of Physics, VNU-University of Science, Thanh Xuan, Hanoi, Vietnam,

² Hanoi University of Mining and Geology, Duc Thang, Tu Liem, Hanoi

* Corresponding author's e-mail: nguyenviettuyen@hus.edu.vn

Nanomaterials have been well known for their enhanced properties compared with their bulk counterparts. Among widely studied nanomaterials, copper oxide (CuO) nanowires has attracted much interest thanks to its diversity applications in various fields. In this research, CuO nanowires were prepared by thermal oxidation via a self heating process. The effect of heating current, annealing time on morphology and structures of the products were investigated. The study contributes a novel method for fast and convenient synthesis of CuO nanowires, which can be easily scale up for mass production.

Keywords: CuO nanowires; Joule heating; current; thermal oxidation.

EE-P24 (Poster)**Corrosion evaluation of carbonate apatite-coated pure magnesium by electrochemical measurement**Kazuma Midorikawa^{1,2}, Sachiko Hiromoto^{1,2*}, Tomoyuki Yamamoto¹¹ National Institute for Materials Science, Ibaraki, 305-0047, Japan² Faculty of Science and Engineering, Waseda University, Tokyo, 169-8555, Japan

* Corresponding author's e-mail: HIROMOTO.Sachiko@nims.go.jp

In temporary-use implant materials such as fracture fixation materials and sutures, it is ideal that they are absorbed in their body after healing of the affected area. Mg is one of the candidates for bone substitution due to its high specific strength, similar Young's modulus to that of bone, and low toxicity [1]. However, as a corrosion resistance of Mg is low, improvement of corrosion resistance of Mg has been investigated by coating with carbonate apatite (CAp), which is a hydroxyapatite (HAp) with partial replacement of phosphate ions by carbonate ions [2]. CAp is resorbed by osteoclasts, and the carbonate ions in CAp are responsible for the resorption of CAp by osteoclasts [3]. This suggests that the resorption by osteoclasts can be adjusted by changing the content of carbonate ions in the CAp coating. Therefore, it has been tried to develop a CAp coating that can adjust bone resorption by osteoclasts by changing the carbonate content in the CAp coating and moderately inhibits Mg corrosion depending on the affected area. In this study, HAp and CAp with various carbonate contents were coated on pure Mg disks and their anodic and cathodic polarization tests and impedance tests were carried out in 0.9 % NaCl (37°C) to evaluate the corrosion properties of the coated Mg. Curve fitting for the impedance spectra was performed by an equivalent circuit including the film resistance and the charge transfer resistance at the bottom of the film defects. It was revealed that the polarization resistance per film thickness increased with increasing carbonate content (FIG. 1).

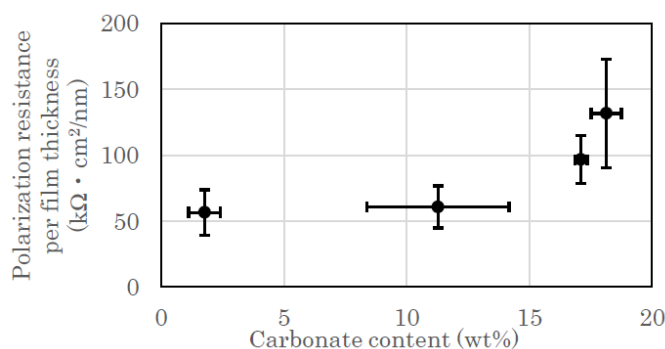
Keywords: HAp, CAp, Mg, Impedance, Polarization

FIG. 1. Relationship between carbonate content in CAp and polarization resistance per film thickness.

References

- [1] M. Tomozawa, S. Hiromoto, *Acta Mater.* 59, 355-363 (2011).
- [2] S. Hiromoto, et al., *Sci. Tech. Adv. Mater.* 21, 346-358 (2020).
- [3] K. Ishikawa, *Ceram Soc Jpn.* 127, 595-601 (2019).

EE-P25

SVM based-metal ion detection and identification in contaminated water sources

Trung Thanh Le^{*}, Viet Dung Nguyen, Thi Thuy Quynh Tran, Dang Co Nguyen, Dinh Tu Bui, Linh Trung Nguyen, Nam Nhat Hoang

VNU University of Engineering and Technology

^{*} Corresponding author's e-mail: thanhletrung@vnu.edu.vn

We consider the problem of heavy metal ion detection and identification in natural water sources. Fast and accurate detection of those ions plays an important role for early treatment to protect human life and safeguard the environment. To this end, we present an experiment setup to study the characteristics of metal ions such as inductance, impedance, and phase. Then, we propose an efficient classification method based support vector machine (SVM) that exploits such characteristics as input signals. Moreover, we also propose a novel set of features based on waveform of inductance and impedance. Performance of the proposed method is validated with experiments on synthetic data.

Keywords: SVM, metal ion, detection, identification

EE-P26 (Poster)**Biodegradable periodic mesoporous phenylene and tetrasulfide-based organosilica nanoparticles for controlled release of chemotherapeutic drug**

Ngoc Xuan Dat Mai^{1,2*}, Thang Bach Phan^{1,2}, Tan Le Hoang Doan^{1,2}

¹ Center for Innovative Materials and Architectures, Ho Chi Minh City, Viet Nam

² Vietnam National University-Ho Chi Minh City, Ho Chi Minh City, Viet Nam

* Corresponding author's e-mail: mnxdat@inomar.edu.vn

Biodegradable periodic mesoporous organosilica (BPMO) is a class of promising nanocarriers for anticancer drug delivery due to their superior biodegradability and high drug loading capacity. In our research, we synthesized a phenylene-containing tetrasulfide-based BPMO, named P4S. Incorporating aromatic phenylene groups into the framework creates a strong interaction between nanoparticles (NPs) with aromatic rings in the cordycepin molecules. This results in a low-release profile under various conditions. In addition, the replacement of this linker slowed the degradation of nanoparticles. The biodegradability of P4S is also demonstrated in a reducing environment and the 100 nm spherical nanoparticles completely decomposed within 14 days. The porous structure of P4S has a high loading of hydrophilic cordycepin (approximately 731.52 mg.g⁻¹) with a slow releasing speed. The release rates of P4S NPs are significantly lower than other materials, such as liposomes, gelatin nanoparticles, and photo-crosslinked hyaluronic acid methacrylate hydrogels, in the same solution. This specific release behavior could guarantee therapeutic drug effects with minimum side effects and optimized drug dosages. Most importantly, according to the in vitro cytotoxicity study, cordycepin-loaded P4S NPs could retain toxicity against liver cancer cells (HepG2) while suppressing the cytotoxicity against normal cells (BAEC).

Keywords: phenylene silica, biodegradable, cordycepin, controlled release, drug delivery

EE-P27**Thin films of triphenylcorrole: fabrication methods, properties, and their potential applications in the fields of sensing and catalysis**

Thi Thao Vu^{1*}, Larissa. A. Maiorova², Dmitrii B. Berezin², Minh Hieu Ho¹, The Nam Dao³, Mai Ha Hoang⁴, Duc Cuong Nguyen¹, Nadezhda M. Berezina²

¹ University of Engineering and Technology, Vietnam National University, Hanoi, Vietnam

² Institute of Macrocyclic Compounds, Ivanovo State University of Chemistry and Technology, Ivanovo, Russian Federation

³ Institute of Chemistry and Material, Academy of Military Science and Technology, Hanoi, Vietnam

⁴ Institute of Chemistry, Vietnam Academy of Science and Technology, Hanoi, Vietnam

* Corresponding author's e-mail: vtthao@vnu.edu.vn

Corroles have been listed as redox non-innocent ligands in many metal complexes. Corroles were used as the key components in catalysis, sensing of gaseous molecules, and medically oriented research. In this study, the conditions to fabricate different desired thin films of 5,10,15-triphenylcorrole were investigated by various methods. The obtained thin films were analyzed for their spectral properties, film morphology, contact angle, and electrocatalytic ability. Some potential applications are introduced for future development of sensing, electrochemical catalysis, and photocatalyst.

Keywords: corrole, Langmuir-Blodgett, Langmuir-Schaefer, thin film, spin-coating, self-assembly

Acknowledgement. This work in the part of films formation and study was supported by the grant of the RSF (20-12-00175), ISUCT, and Ministry of Science and Higher Education of the Russian Federation (FZZW-2020-0008) in the part of synthesis of the compound.

References

- [1] I. Aviv, Z. Gross, Chem. Commun. (2007) 1987.
- [2] C. D. Natale, C. P. Gros, R. Paolesse (2022) 1277.
- [3] V. T. Thao, L. A. Maiorova, D.B. Berezin et al. Macrocyclic Compounds (2016) 73.
- [4] L. A. Maiorova, T. V. Thao, O. A. Gromova, et al. BioNanoScience (2018) 81.
- [5] V. T. Thao, N. V. Kharitonova, L. A. Maiorova, et al. (2018) 286.

EE-P28**Evaluation of stability and *in vitro* anticancer activity of dihydroquercetin nanoemulsion**

Nguyen Thi Mai Huong, Nguyen Thanh Binh*, Le Thi Thu Huong, Phan Thi Thuy, Bach Thanh Son, Phan Xuan Thien, Le Thi Huong and Nguyen Trong Tinh.

Institute of Physics, Vietnam Academy of Science and Technology, 18 Hoang Quoc Viet Str., Cau Giay, Hanoi, Vietnam

* Corresponding author's e-mail: binhvlud@iop.vast.vn

Dihydroquercetin (DHQ), also known as taxifolin, is a flavonoid and commonly found in many plants. Dihydroquercetin has been documented to have powerful antioxidant activity and many beneficial properties for human health, especially its ability to inhibit certain types of cancer cells. However, its low solubility and bioavailability are major obstacles to biomedical applications. Moreover, DHQ is chemically unstable and quickly degrades when exposed to alkaline conditions. In the present study, a DHQ nanoemulsion formulation was prepared by Self Nano-Emulsifying Drug Delivery System (SNEDDS) technique to overcome these disadvantages. The obtained nanoemulsion system was also evaluated for its microscopic properties, stability, and *in vitro* cytotoxic activity against some cancer cells using tetrazolium dyes (MTS assay). Measurement results showed that the DHQ nanoemulsion was successfully synthesized with typical mean droplet sizes from 9 to 11 nm, and revealed excellent stability over time. Dihydroquercetin in a nanoemulsion was more stable than its unencapsulated form. *In vitro* experiments on cytotoxic activities against A549, Hela, and HepG2 cancer cell lines indicated that the prepared DHQ nanoemulsion effectively inhibited the growth of all these cell lines with IC₅₀ values (μg/mL) of 8.0, 20.4, and 29.5 respectively. The results of this study provide useful information on the potential use of DHQ nanoemulsion as a promising agent in cancer treatment and the development of a drug for human use.

Keywords: dihydroquercetin, nanoemulsion, anticancer, *in vitro*, enhanced solubility

EE-P29**A novel water-ethanol based modified inverse emulsion method for nanoparticles silica-coating in Si QDs/SiO₂ and NiFe₂O₄/SiO₂ core-shell submicron spheres synthesis.**

Luu Manh Quynh^{1,*}, Hoang Van Huy¹, Nguyen Quoc Khanh¹, Phi Thi Huong², Nguyen Hoang Nam²

¹ Center for Materials Science, Faculty of Physics, VNU-HUS, Hanoi, Vietnam

² Nano and Energy Center, VNU-HUS, Hanoi, Vietnam

* Corresponding author's e-mail: luumanhquynh@hus.edu.vn

An immiscible hydrophilic-surface nanoparticles-containing water-soluble emulsion was created in ethanol by adding trisodium citrate (TSC) – a water-soluble ethanol-insoluble reagent – as surface activator. The formation of as-named water-ethanol based inverse emulsion was measured via light-reflection under an UV-vis spectroscope, followed by the estimation of the TSC critical micelle concentration. Under that concentration of TSC, the high pH of the hydrophilic media in the micelles generated a suitable condition for (3-aminopropyl)thiethoxysilane to react with the water and created silica spheres, those covered the nanoparticles inside. By this method, the narrow size-distribution Si QDs/SiO₂ and NiFe₂O₄/SiO₂ core-shell submicron spheres were synthesized, which were promising for multipurpose applications, such as biological labeling, bio-separation.

Keywords: inverse emulsion, silica-coating, core/shell particles, sub-micron spheres

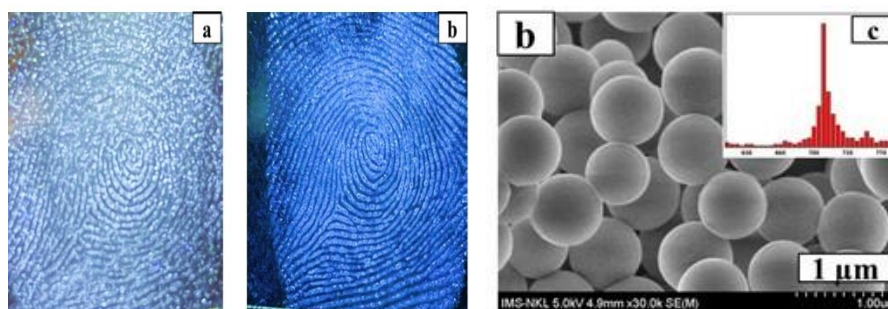


FIG. 1. SEM image of Si QDs/SiO₂ core/shell microspheres and their application in fluorescent latent fingerprint development.

EE-P30**Arrays of Nd₂Fe₁₄B clusters in PDMS background used to levitate human cells**

Viet Cuong Le^{*}, Huy Tiep Nguyen, Dinh Tu Bui

Faculty of Engineering Physics and Nanotechnology, VNU-University of Engineering and Technology, Hanoi, Vietnam

^{*} Corresponding email: cuonglv@vnu.edu.vn

Sorting and trapping cells play an important role in fundamental cellular and biology researches. That enables the study of single-cell behaviors, which are different in comparison with a cluster of cells. Contactless handling techniques using different optical, mechanical, or magnetic phenomena have been studied for single-cell trapping. Among them, the diamagnetic force created by magnetic structures on cells is significant and stable both in time and in space. In this work, arrays of hard magnetic clusters in the PDMS background (hereafter called magnetic structure) were successfully fabricated using the magnetic imprinting method. The magnetic structure shows a proper magnetic property and the possibility to sort and trap T47D single cells via the diamagnetic levitation phenomenon at defined positions, which are both experimentally observed and theoretically calculated. The obtained results show the promise of developing a simple way to separate directly living cells.

Keywords: Magnetic structures, diamagnetic properties, single-cell trapping

Session: Multiferroics and magnetic materials (MM)**MM-P01 - MM-P30****MM-P01 (Poster)****In-magnetic-field annealing effects on the phase growth of Mn-Bi-Sn ternary System**Kota Nakamoto^{1,*}, Yoshifuru Mitsui¹, Ryota Kobayashi¹, Kohki Takahashi², Keiichi Koyama¹¹ Graduate School of Science and Engineering, Kagoshima University, 890-0065, Kagoshima, Japan² Institute for Materials Research, Tohoku University, 980-8577, Miyagi, Japan

* Corresponding author's email: k1797895@kadai.jp

Effect of magnetic field on the crystal growth and phase transformation have been studied for magnetic materials [1]. Since ferromagnetic (FM) phase is stabilized by magnetic energy, its reaction and phase equilibrium can be controlled by magnetic fields. In particular, reaction from non-FM to FM phase is enhanced by magnetic field [2].

In the reaction of multi-elements system such as ternary or quaternary system, many equilibrium phases exist. If a magnetic field is applied during the synthesis reaction of the multi-elements system, selective reaction to FM phase and control of the reaction route can be expected. In this study, the in-magnetic-field reaction for Mn-Bi-Sn ternary system was performed for investigating the magnetic-field-induced phase growth from non-FM elements to the magnetic phases such as MnBi, Mn₃Sn₂, Mn₃Sn and MnSn₂.

The pellet-shaped samples were prepared from powder Mn (3N), Bi (4N) and Sn (4N). In-magnetic-field annealing was performed in a magnetic field of 5 T at 573 K.

Fig. 1 shows BSE images of the (a) 0 T-48 h and (b) 5 T-48 h samples. In both samples, MnSn₂, Mn₃Sn₂ and Mn₃Sn phases were observed in addition to the unreacted Mn and Bi. MnBi phase was not detected with or without magnetic field. The Mn-Sn compounds were found to be more stable than the FM MnBi even when 5 T field was applied. The phase fraction of FM Mn₃Sn₂ decreased with application of 5 T, and antiferromagnetic MnSn₂ became the main phase. As a result, it was found that Bi does not contribute to the reaction of Mn-Bi-Sn mixture, and the reaction rate of Mn-Sn is changed by magnetic field.

Keywords: Magnetic field, Zeeman energy, Ferromagnetic

References

- [1] S. Farjami, et al., Mater. Trans. 49 (2008) 1970.
- [2] Y. Mitsui, et al., J. Alloys Compd. 615 (2014) 131-134.

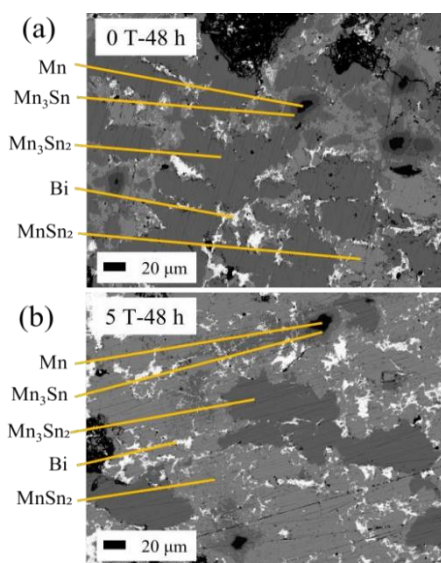


FIG. 1. The BSE images of Mn-Bi-Sn annealed at 573 K in (a) 0 T and (b) 5 T.

MM-P02 (Poster)**The crystal structure and magnetoelectronic properties in Mn-doped YCu₃Fe₄O₁₂**Yuta Kato¹, Manami Goto², Ikuya Yamada^{1,2,*}¹ Graduate School of Engineering, Osaka Prefecture University, Osaka 599-8531, Japan² Graduate School of Engineering, Osaka Metropolitan University, Osaka 599-8531, Japan

* Corresponding author's email: ikuya_yamada@omu.ac.jp

The quadruple perovskite oxides ACu₃Fe₄O₁₂ (A = Ca, Sr, La, Y) [1–4] (Fig. 1 left) undergo various electronic phase transitions because of the instability of the unusually high valence states of Fe, where the types of phase transitions are closely related to charge transfer/disproportionation. CaCu₃Fe₄O₁₂ exhibits charge disproportionation ($2\text{Fe}^{4+} \rightarrow \text{Fe}^{3+} + \text{Fe}^{5+}$) at 210 K, whereas the nominally isoelectronic SrCu₃Fe₄O₁₂ displays a negative thermal expansion in the temperature range of 200–270 K. LaCu₃Fe₄O₁₂ shows a discontinuous volume expansion at 360–400 K, which is derived from an intersite charge transfer between Cu and Fe ($3\text{Cu}^{2+} + 4\text{Fe}^{3.75+} \rightarrow 3\text{Cu}^{3+} + 4\text{Fe}^{3+}$). In contrast, YCu₃Fe₄O₁₂ undergoes a ferrimagnetic transition and metal-to-semiconductor transition at 250 K simultaneously with a charge disproportionation ($\text{Fe}^{3.75+} \rightarrow 5/8\text{Fe}^{3+} + 3/8\text{Fe}^{5+}$). In this study, we investigated the crystal structure and magnetoelectronic properties of Mn-doped YCu₃Fe₄O₁₂.

YCu₃Fe_{4-x}Mn_xO₁₂ ($x = 0-4$) samples were successfully synthesized at 12 GPa and 1273 K. The lattice constant a at room temperature monotonically decreased with increasing x . The Y–O and (Fe, Mn)–O bond lengths also monotonically decreased, while the Cu–O bond lengths monotonically increased. Figure 1 (right) displays the X-ray absorption spectra for the Cu K-edge of YCu₃Fe_{4-x}Mn_xO₁₂ at room temperature. The absorption edge shifted monotonically from the higher to lower energy side with increasing x , estimating the reduction in Cu valence from Cu^{~2.33+} ($x = 0$) to Cu^{~2+} ($x = 4$). In the presentation, the magnetoelectronic properties will be discussed.

Keywords: quadruple perovskite oxides, high-pressure synthesis, charge transfer

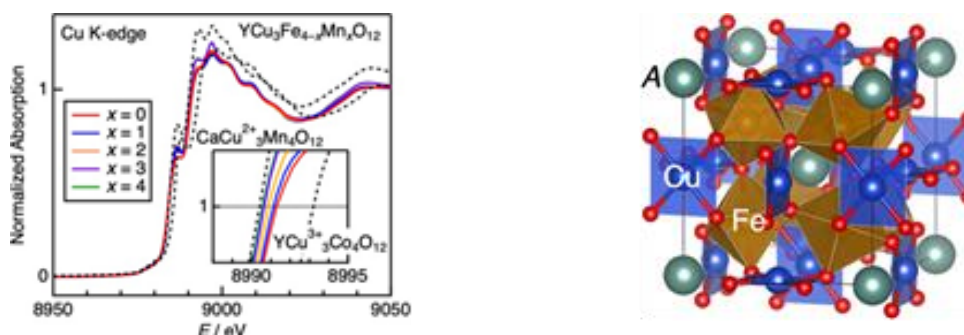


FIG. 1. (left) Crystal structure of quadruple perovskite oxide ACu₃Fe₄O₁₂ (right) X-ray absorption spectra of YCu₃Fe_{4-x}Mn_xO₁₂ at room temperature.

References

- [1] I. Yamada et al., *Angew. Chem. Int. Ed.*, 120 (2008) 7140.
- [2] I. Yamada et al., *Angew. Chem. Int. Ed.*, 50 (2011) 6579.
- [3] Y. W. Long et al., *Nature*, 458 (2009) 60.
- [4] H. Etani et al., *J. Am. Chem. Soc.*, 135 (2013) 6100.

MM-P03 (Poster)**Magnetic properties of Ni₂MnAl by prepared in high magnetic field**

Kota Ryota Kobayashi^{1, *}, Yoshifuru Mitsui¹, Rie Y. Umetsu², Kohki Takahashi², Keiichi Koyama¹

¹ Graduate School of Science and Engineering, Kagoshima University, 890-0065, Kagoshima, Japan

² Institute for Materials Research, Tohoku University, 980-8577, Sendai, Miyagi, Japan

* Corresponding author's email: k3579242@kadai.jp

L_{21} -Ni₂MnAl is a ferromagnetic Heusler alloy with magnetic moment of 4.02 $\mu\text{B}/\text{f.u.}$ and Curie temperature T_C of 361 K [1-2]. Ni₂MnAl shows order-disorder transformation between L_{21} phase and $B2$ phase at 774 K. Ordering from the $B2$ phase to the L_{21} phase takes a long annealing time of about one month at relatively lower temperatures below 774 K [2]. This means that a very long-term annealing at lower temperature is required to obtain highly ordered L_{21} -Ni₂MnAl, which has made the investigation of the ordering mechanism in Ni₂MnAl difficult.

Meanwhile, recently, we found that $B2$ - L_{21} ordering was accelerated by magnetic fields at 673 K [3]. It was pointed out that magnetic field influenced the reduction of critical radius of L_{21} phase in $B2$ -matrix, resulting in the enhancement of the ordering. In this study, in order to clarify the ordering mechanism of Ni₂MnAl in a magnetic field, annealing treatment was carried out at 623 K under magnetic fields.

$B2$ -Ni₂MnAl were prepared by reactive sintering at stoichiometric compositions. The samples were annealed at 1373 K for 48 hours and then quenched. The obtained samples were annealed at 623 K in magnetic fields of 0 T, 10 T, and 15 T.

Figure 1 shows the thermomagnetization (M - T) curves for the sample prepared at 673 K in 15 T for 72 h [3] and prepared at 623 K in 15 T for 48 h. A single peak due to the T_C of L_{21} phase was reported for the sample annealed at 673 K [3]. For the sample annealed at 673 K, two-peak separation was appeared at 318 K and 67 K, which were due to Néel temperature T_N of $B2$ -phase and T_C of L_{21} -phase, respectively. T_C of 623 K-annealed sample was slightly higher than that of 673 K-annealed sample. These results suggest that the order degree and T_C of L_{21} phase depend on the annealing temperature in a magnetic field. The growth of L_{21} phase in fields was explained by nucleation of L_{21} phase at certain order degree in $B2$ matrix.

Keywords: Heusler alloy, Order-disorder transformation, ferromagnetic material, Magnetic field

References

- [1] T. Busgen et al., Phys. Rev. B., 70 (2004) 01411.
- [2] M. Acet, et al., J. Appl. Phys., 92 (2002) 3867-3871.
- [3] R. Kobayashi, et al., J. Magn. Magn. Mater., 547 (2022) 168908

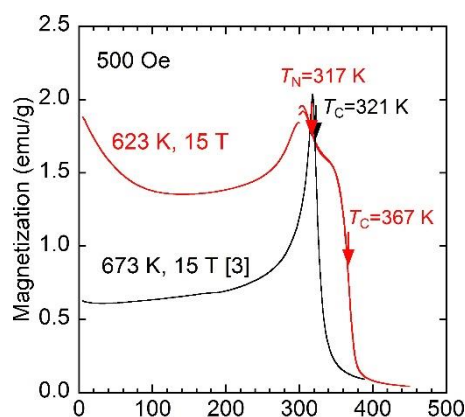


FIG. 1 The thermomagnetization curve for the sample prepared at 673 K in 15 T for 72 h [3] and prepared at 623 K at 15 T for 48 h.

MM-P04 (Poster)**Crystal structure and magnetic property of magnetoplumbite-structured BaFe_{12-x}Rh_xO₁₉**Ippo Aoki¹, Ikuya Yamada^{1,*}¹ Osaka Prefecture University, Sakai, Osaka 599-8531, Japan

* Corresponding author's email: ikuya_yamada@omu.ac.jp

Magnetoplumbite ferrites AFe₁₂O₁₉ (A = Ba, Sr, La) have been widely utilized as functional magnetic materials. Site-selective substitutions of Fe are desired to control the magnetic properties precisely [2], but it is generally difficult because of many crystallographic sites of 2a, 2b, 4f₁, 4f₂, and 12k of magnetoplumbite structure [Fig. 1(a)]. In this study, we attempted the site-selective substitution of Fe³⁺ by Rh³⁺ in BaFe₁₂O₁₉ by using high pressures up to 8.0 GPa and investigated the magnetic properties.

The BaFe_{12-x}Rh_xO₁₉ phases ($x = 1-6$) were isostructural to the magnetoplumbite. With increasing x from 1 to 6, the amounts of impurity phases of Fe₂O₃ and Rh increased, indicating that the solubility limit of Rh was less than 50% in the synthesis conditions of the present study. Rietveld refinement using the synchrotron X-ray powder diffraction data confirmed that the Fe ions at 2a, 4f₂, and 12k sites with octahedral coordination were preferentially substituted by Rh ions, whereas the other sites were not substituted by Rh ions. This is consistent with the fact that Rh³⁺ ions usually occupy the octahedral sites.

Fig. 1(b) shows the isothermal magnetization curves of BaFe_{12-x}Rh_xO₁₉ ($x = 0, 1, 2$) at 300 K. The saturation magnetization drastically decreased with increasing x . This behavior indicates that the Rh³⁺ ions in the low-spin configuration ($S = 0$) substituting for the Fe³⁺ ions ($S = 5/2$) at 2a and 12k sites preferentially decreased the population of the majority spins. This finding proposes that the site-selective substitutions drastically change the magnetic properties of magnetoplumbite ferrites.

Keywords: magnetism, high-pressure synthesis, site-selective substitution

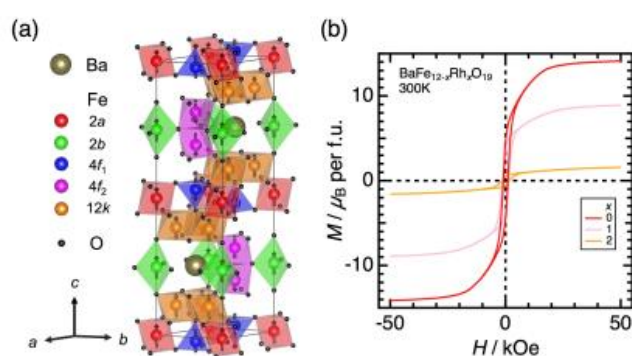


FIG. 1. (a) Schematic of crystal structure of BaFe₁₂O₁₉. The arrows represent the directions of the magnetic moments. (b) Isothermal magnetization curves of BaFe_{12-x}Rh_xO₁₉ ($x = 0, 1, 2$) at 300 K.

Reference

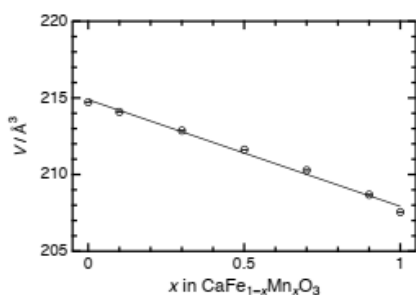
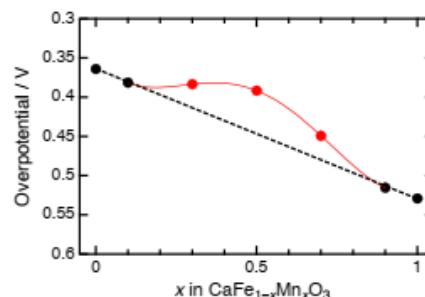
- [1] R. Pullar et al., Prog. Mater. Sci. 57 (2012) 1191.
 [2] T. Waki et al., doi: 10.2139/ssrn.4085484.

MM-P05 (Poster)**High-pressure synthesis and oxygen evolution reaction activity of Fe⁴⁺-Mn⁴⁺-mixed perovskite oxide CaFe_{1-x}Mn_xO₃**Asuka Ochi¹, Ikuya Yamada^{1,*}, Sogo Asakura¹, Hidekazu Ikeno¹, Shunsuke Yagi²¹ Graduate School of Engineering, Osaka Prefecture University, Osaka 599-8531, Japan² Institute of Industrial Science, The University of Tokyo, Tokyo 153-8505, Japan

* Corresponding author's email: ikuya_yamada@omu.ac.jp

Perovskite oxides are known as efficient catalysts for oxygen evolution reaction (OER). A tetravalent iron oxide, CaFeO₃, exhibits high catalytic activity because of the preferable electronic structure with small charge-transfer energy [1]; however, high-pressure synthesis is needed to stabilize the Fe⁴⁺ ions. The Fe⁴⁺-Co⁴⁺-mixed perovskite oxide, CaFe_{0.5}Co_{0.5}O₃, demonstrates higher catalytic activity than CaFeO₃ because of the synergistic effect between Fe⁴⁺ and Co⁴⁺ ions [2]. In this study, we performed high-pressure synthesis and characterization of CaFe_{1-x}Mn_xO₃ ($x = 0, 0.1, 0.3, 0.5, 0.7, 0.9$ and 1) to study the synergistic effects between Fe⁴⁺ and Co⁴⁺ ions on OER catalytic activity.

OER catalytic activities in 0.1 M KOH aqueous solution were evaluated using a rotating disk electrode system in the same manner as the previous study [2]. Synchrotron X-ray diffraction revealed that CaFe_{1-x}Mn_xO₃ at each studied composition crystallized in the orthorhombic perovskite structures. Lattice volume refined by the Rietveld method monotonically decreased with the increase in Mn amount (Fig. 1). As shown in Fig. 2, the OER overpotentials were compared with a linear interpolation of end points. The samples near the end points ($x = 0.1$ and 0.9) had the same overpotentials as the values derived from the linear interpolation, suggesting no synergistic effect. In contrast, substantial decreases in the overpotentials for $x = 0.3, 0.5$, and 0.7 were observed, suggesting the synergistic effect in the intermediate compositions (Fig. 2). We conclude that the synergistic effect is predominant in Fe⁴⁺-Mn⁴⁺-mixed oxides as well as the Fe⁴⁺-Co⁴⁺ system.

Keywords: Oxygen evolution reaction catalyst, Perovskite, high-pressure synthesisFIG.1 Refined lattice volume of CaFe_{1-x}Mn_xO₃FIG.2 OER overpotential of CaFe_{1-x}Mn_xO₃**References**

- [1] I. Yamada et al., J. Phys. Chem. C 49 (2018) 27885.
- [2] I. Yamada et al., Chem. Mater. 12 (2020) 3893.

MM-P06 (Poster)**Brownian motion of depinned skyrmion under applying in-plane alternating electric current**T. Watanabe^{1,*}, M. Goto^{1,2}, R. Ishikawa³, S. Miki¹, H. Nomura^{1,2}, and Y. Suzuki^{1,2}¹ Graduate School of Engineering Science, Osaka University, Toyonaka, Japan² Center for Spintronics Research Network (CSRN), Osaka University, Toyonaka, Japan³ ULVAC-Osaka University Joint Research Laboratory for Future Technology, Osaka University, Suita, Japan

* Corresponding author's email: watanabe-t@spin.mp.es.osaka-u.ac.jp

Magnetic skyrmions are topologically protected particle-like spin textures and have unique properties. One of the important properties is the Brownian motion at near room temperature [1-2]. In recent years, the application of skyrmions to novel computers such as Brownian / probabilistic computers is expected [3-4]. In order to apply skyrmions to these computers, deepening the understanding of skyrmion dynamics is essential. Various effects on skyrmion dynamics have been studied, such as increasing temperature [1], applying gate voltage [2], and magnetic field noise [5]. While direct-electric-current-driven skyrmion dynamics has been studied [6], skyrmion dynamics under alternating electric current (AC current) has not been studied. Therefore, in this study, we explore the effect of AC current on the skyrmion dynamics.

A skyrmion film consisting of Ta(5)|Co₁₆Fe₆₄B₂₀(1.2)|Ta(0.2)|MgO(1.5)|SiO₂(3.0) (described by nm) were deposited by magnetron sputtering. The motion of the skyrmions was observed by magneto-optical Kerr effect microscope, and the diffusion coefficient of skyrmions D were calculated from the trajectories of skyrmions. Fig. 1 is the diffusion coefficient as a function of frequency of 0.336 mA AC current. Fig. 1 shows that D_{xx} and D_{yy} have the almost same value at 100 Hz, and then 100 Hz AC current dependence of the diffusion coefficient (Fig. 2) was obtained. We found out that 100 Hz AC current can exponentially increase the diffusion coefficient of both axes. This result is attributed to the depinning of the skyrmions by applying the AC current. This research was supported by ULVAC, Inc., JST CREST Grant number JPMJCR20C1 Japan and JSPS Grant-in-Aid for Scientific Research (S) Grant Number JP20H05666.

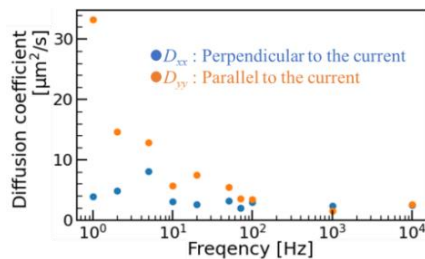
Keywords: Skyrmion, Brownian motion, Diffusion coefficient, Alternating electric current

FIG. 1 Diffusion coefficient as a function of frequency of AC current of 0.336 mA (Root mean squared value)

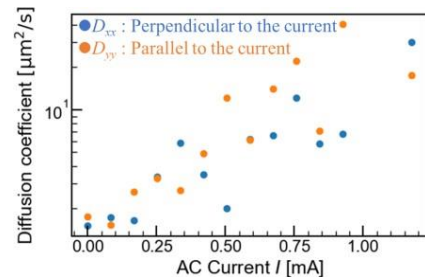


FIG. 2 100 Hz AC current (Root mean squared value) dependence of the diffusion coefficient

References

- [1] J. Zázvorka et al., Nat. Nanotechnol., 14, 658-661 (2019)
- [2] T. Nozaki et al., Appl. Phys. Lett., 114, 012402 (2019).
- [3] Y. Jibiki et al., Appl. Phys. Lett., 117, 082402 (2020).
- [4] R. Ishikawa et al., Appl. Phys. Lett., 119, 072402 (2021).
- [5] M. Goto et al., J. Magn. Magn. Mater., 536, 167974 (2021).
- [6] W. Jiang et. Al., Science, 349, 6245 (2015)

MM-P07 (Poster)

Crystal structure and thermochromism of a high-pressure phase of $\text{Yin}_{1-x}\text{MnxO}_3$

Masaya Oshita¹, Ikuya Yamada^{1,*}, Hidenobu Murata¹, Isaac Oda-Bayliss², Wang Wencong², Shunsuke Yagi²

¹ Graduate School of Engineering, Osaka Metropolitan University, Osaka 599-8531, Japan

² Institute of Industrial Science, The University of Tokyo, Tokyo 153-8505, Japan

* Corresponding author's email: ikuya_yamada@omu.ac.jp

A Mn-doped YinO_3 ($\text{Yin}_{1-x}\text{MnxO}_3$) exhibits a bright blue color [1]. $\text{Yin}_{1-x}\text{MnxO}_3$ crystallizes in a hexagonal structure with the space group $P6_3cm$, where InO_5 units form five-coordinated trigonal bipyramids (Fig. 1a). Light of ~ 2 eV is absorbed by the d-d transition of the doped Mn^{3+} , resulting in its blue color.

YinO_3 is reported to undergo a structural phase transition to an orthorhombic perovskite structure under high pressures of 12–15 GPa at room temperature (Fig. 1b) [2], whereas the detailed structure of the high-pressure (HP) phase is not experimentally clarified. Since the trigonal bipyramid units are lost in the HP phase, color fading is expected. Hence, the phase transition from the HP phase to the ambient-pressure (AP) phase may exhibit a significant change in color. In this study, we aim to clarify the crystal structure and the thermochromism of HP phases of $\text{Yin}_{1-x}\text{MnxO}_3$ ($x = 0, 0.1$).

Synchrotron X-ray powder diffraction patterns confirmed that the HP phases of $\text{Yin}_{1-x}\text{MnxO}_3$ ($x = 0, 0.1$) crystallized in the GdFeO_3 -type orthorhombic perovskite structures with the space group of $Pnma$ (Fig. 2a). The volume per formula unit in the HP phase of YinO_3 decreased by 8.15% from the AP phase. The HP phase of $x = 1$ displayed grayish-black due to the aforementioned lack of the trigonal bipyramidal structure, and annealing at 1200 °C in air resulted in the color change to bright blue (Fig. 2b). Thermogravimetry-differential thermal analysis supported the phase transition at 1100 °C. The blue-colored sample after the annealing was confirmed to be the AP phase by X-ray diffraction. The present study revealed that an irreversible thermochromism is realized in the HP-to-AP-phase transition of $\text{Yin}_{1-x}\text{MnxO}_3$.

Keywords: pigment, phase transition, thermochromic material, high-pressure synthesis

References

- [1] A. E. Smith et al., J. Am. Chem. Soc. 131 (2009) 17084.
- [2] A. Dwivedi et al., High Press. Res. 39 (2019) 17.

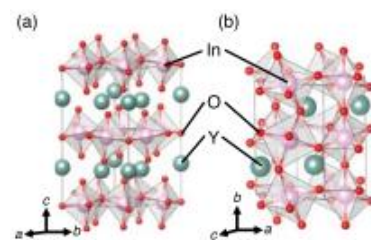


FIG. 1 Schematics of crystal structures of YInO_3 in (a) AP and (b) HP phases

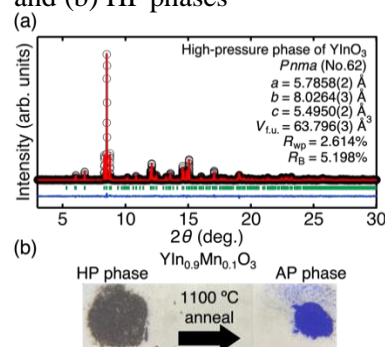


FIG. 2 (a) Synchrotron X-ray diffraction pattern and Rietveld refinement result for HP phase of YInO_3 . The wavelength is 0.41996+. (b) Color information from HP-to-AP phase of $\text{Yin}_{1-x}\text{MnxO}_3$

MM-P08 (Poster)

V-V dimerization and its effect on magnetism in ilmenite-type CoVO_3

S. Kamiyama¹, H. Yamamoto^{1,*}, T. Nakamura¹, H. Kimura¹, I. Yamada², Y. Okazaki³, M. Fukuda⁴, M. Azuma^{4,5}, T. Nishikubo^{4,5}

¹ Institute of Multidisciplinary Research for Advanced Materials, Tohoku University Sendai, 980-8577, Japan

² Dept. Materials Science, Osaka Metropolitan University, Osaka, 599-8531, Japan

³ Dept. Materials Science, Osaka Prefecture University, Osaka, 599-8531, Japan

⁴ MSL, Tokyo Institute of Technology, Yokohama, 226-8503, Japan

⁵ Kanagawa Institute of Industrial Science and Technology, Kanagawa, 243-0435, Japan

* Corresponding author's email: hajime.yamamoto.a2@tohoku.ac.jp

The magnetic properties of transition-metal oxides can be explained by the interactions between isolated ions. The formation of a molecular orbital due to a closer metal-metal distance alters the electronic properties. The magnetism of such a compound is not sufficient to consider only the interaction between isolated ions. One of the most famous examples is the Peierls transition in VO_2 . Formation of direct V-V bond results in an insulator (non-magnetic) to metal (paramagnetic) transition.

We have focused on ilmenite-type CoVO_3 . In this compound, the Co^{2+} and V^{4+} form honeycomb lattices, respectively, and are stacked alternately (Fig. 1). The V-V dimers are expected to be formed in the vanadium layers. In this study, we reveal the existence of V-V dimers by crystallographic studies and the magnetic properties of CoVO_3 [1].

CoVO_3 samples were synthesized at high-pressure and high-temperature conditions of 8 GPa and 1100°C. The crystal structure analysis revealed the existence of V-V dimers below 550 K. The divalent cobalt ion in CoVO_3 shows an $S = 3/2$ state, whereas a $J_{\text{eff}} = 1/2$ state was reported in ilmenite-type CoTiO_3 [2]. The reduction of structural symmetry by V-V dimerization could change the magnetic ground state.

Keywords: dimer, crystal structure transition, magnetism, transition metal oxides

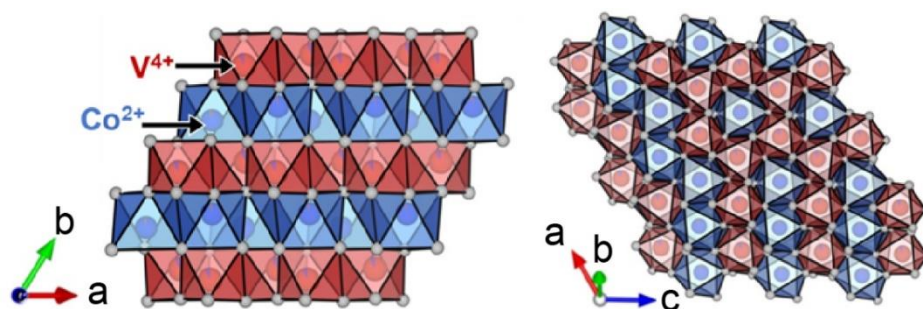


FIG. 1. Crystal structure of CoVO_3 at 300 K viewed along the c axis and b^* direction. The V-V dimers exist in V-honeycomb layer.

References

- [1] S. Kamiyama et al., Inorg. Chem. 71 (2022) 7841-7846.
- [2] M. Hoffmann, Phys. Rev. B, 104, 014429 (2021).

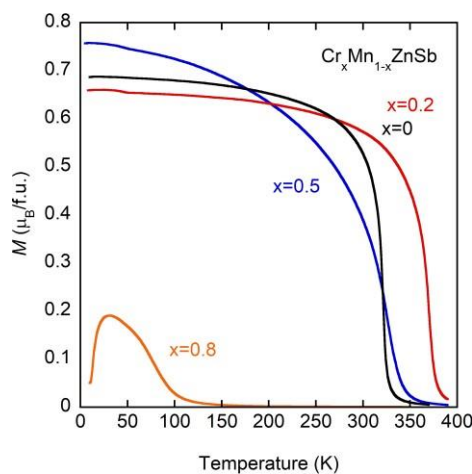
MM-P09 (Poster)**Magnetic and structural properties of $\text{Cr}_x\text{Mn}_{1-x}\text{ZnSb}$ with tetragonal Cu_2Sb -type structure**Moriharu Nagano^{1,*}, Yoshifuru Mitsui¹, Ryota Kobayashi¹, Rie Y. Umetsu², Keiichi Koyama¹¹ Graduate School of Science and Engineering, Kagoshima University, Kagoshima 890-0065, Japan² Institute for Materials Research, Tohoku University, Sendai 980-8577, Japan

* Corresponding author's email: k5628486@kadai.jp

Mn-based ternary ferromagnets with a tetragonal Cu_2Sb -type crystal structure (MnAlGe , MnGaGe , and MnZnSb) are paid attention because of the high uniaxial magnetocrystalline anisotropy [1]. It was reported that Cr-substitution for MnZnSb enhanced Curie temperature T_C [2]. On the other hand, when Mn was completely replaced by Cr, CrZnSb also crystallized with the tetragonal Cu_2Sb -type structure. However, CrZnSb had a quite small magnetic moment and did not show ferromagnetic properties. Therefore, in this study, for optimizing magnetic properties of $(\text{MnCr})\text{ZnSb}$, magnetic and structural properties of $\text{Cr}_x\text{Mn}_{1-x}\text{ZnSb}$ ($0 \leq x \leq 1$) were investigated.

$\text{Cr}_x\text{Mn}_{1-x}\text{ZnSb}$ ($0 \leq x \leq 1$) samples were prepared by reactive sintering. From X-ray diffraction experiments, all samples showed the tetragonal Cu_2Sb -type structure. Magnetization measurements were carried out by a SQUID magnetometer.

Figure 1 shows the thermomagnetization curves of $\text{Cr}_x\text{Mn}_{1-x}\text{ZnSb}$ at $x = 0, 0.2, 0.5$, and 0.8 . T_C increased with increasing x from 0 to 0.2, and rapidly decreased for $x > 0.2$. It was found that the maximum value of T_C was obtained at 371 K at $x = 0.2$, which was 15.6% higher than T_C of MnZnSb ($x = 0$).

Keywords: Ferromagnetic compounds, Magnetic propertiesFIG. 1. Thermomagnetization curves of $\text{Cr}_x\text{Mn}_{1-x}\text{ZnSb}$ at 0.1 T.**References**

- [1] S. Mori et al., Jpn. J. Appl. Phys. 32, 273 (1993)
- [2] P. A. E. Murgatroyd, et al., Adv. Funct. Mater. 31, 2100108 (2021)

MM-P10 (Poster)**Negative thermal expansion in Mn-doped $\text{CaCu}_3\text{Fe}_4\text{O}_{12}$** Manami Goto¹, Yuta Kato², Yuta Kizawa², Ikuya Yamada^{1, 2, *}¹Graduate School of Engineering, Osaka Metropolitan University, Osaka 599-8531, Japan²Graduate School of Engineering, Osaka Prefecture University, Osaka 599-8531, Japan

* Corresponding author's email: ikuya_yamada@omu.ac.jp

Quadruple perovskite oxides $\text{ACu}_3\text{Fe}_4\text{O}_{12}$ ($A = \text{Ca}, \text{Sr}, \text{Cd}$, rare-earth metals, Bi; see crystal structure in Fig. 1) exhibit various functional properties such as negative thermal expansion [1], thermal energy storage, and oxygen evolution reaction catalysis. $\text{CaCu}_3\text{Fe}_4\text{O}_{12}$, whose valence state at room temperature is represented as the ionic model of $\text{CaCu}^{\sim 2.4+}\text{Fe}^{\sim 3.7+}\text{O}$, undergoes a charge disproportionation transition below 210 K simultaneously with a Fe-to-Cu electron charge transfer ($3\text{Cu}^{\sim 2.4+} + 4\text{Fe}^{\sim 3.65+} \rightarrow 3\text{Cu}^{\sim 2.2+} + 4\text{Fe}^{\sim 3.8+}$) [2, 3], leading to the discontinuous lattice shrinkage. In the present study, we synthesized $\text{CaCu}_3\text{Fe}_{4-x}\text{Mn}_x\text{O}_{12}$ ($x = 0-4$) under high-pressure and high-temperature conditions of 12 GPa and 1273 K, and investigated the effect of Mn doping on the structures and electronic properties.

Synchrotron X-ray powder diffraction confirmed that $\text{CaCu}_3\text{Fe}_{4-x}\text{Mn}_x\text{O}_{12}$ at all the compositions crystallized in the cubic quadruple perovskite structures. The temperature dependence of the lattice constant is shown in Fig. 2. A negative thermal expansion (NTE) was observed in $x = 0.5$ at temperatures between 230 and 280 K, obtaining a large negative linear thermal expansion coefficient $\alpha_L = -2.28(8) \times 10^{-5} \text{ K}^{-1}$. The Cu–O bond lengths decreased on cooling in the NTE range, whereas the (Fe, Mn)–O bond lengths increased as observed in $\text{SrCu}_3\text{Fe}_4\text{O}_{12}$ [1]. The direction of the charge transfer between Cu and Fe in $\text{CaCu}_3\text{Fe}_4\text{O}_{12}$ is inverted by the Mn doping, as indicated by the Cu–O bond shrinkage and (Fe, Mn)–O bond elongation in the NTE temperature range on cooling.

Keywords: negative thermal expansion, quadruple perovskite oxides, high-pressure synthesis

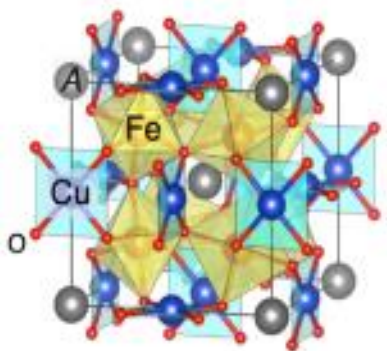


FIG. 1 (left) Schematic of crystal structure of quadruple perovskite $\text{ACu}_3\text{Fe}_4\text{O}_{12}$.

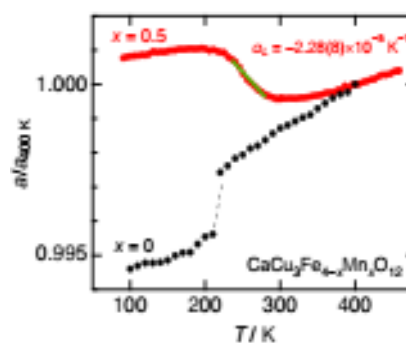


FIG. 2 (right) Temperature dependence of the normalized lattice constant for $\text{CaCu}_3\text{Fe}_{4-x}\text{Mn}_x\text{O}_{12}$ ($x = 0, 0.5$). The data for $x = 0$ were taken from the reference [3].

References

- [1] I. Yamada et al., *Angew. Chem. Int. Ed.* 50 (2011) 6579.
- [2] I. Yamada et al., *Angew. Chem. Int. Ed.* 120 (2008) 7140.
- [3] I. Yamada et al., *Inorg. Chem.* 55 (2016) 1715.

MM-P11 (Poster)**Stabilization of α -FAPbI₃ by addition of dopamine hydrochloride**

Ryohei Oonaga^{1,3}, Naoyuki Shibayama², Masashi Ikegami², Tsutomu Miyasaka², Yu Miyazawa³, Daisuke Kobayashi³, Kazuyuki Hirose^{1,3}, Tomoyuki Yamamoto^{1,*}

¹ Waseda University, Tokyo 169-8555, Japan

² Toin University of Yokohama, Kanagawa 225-8503, Japan

³ JAXA, Kanagawa 252-5210, Japan

* Corresponding author's email: tymmt@waseda.jp

Perovskite solar cells using organic-inorganic hybrid perovskite crystals ABX₃ (A: organic cation, B: inorganic cation, X: inorganic anion) as light absorbing materials were developed by Miyasaka et al. in 2009 [1]. MAPbI₃, where MA is a methylammonium ion, i.e., CH₃NH⁺, is widely studied at an early stage, but its volatility of the organic cation is an issue to overcome for the commercial application. Recently FAPbI₃, where FA is a formamidinium ion CH(NH₃)⁺ has been actively studied as an absorbent material to improve stability at high temperature. Although FAPbI₃ has improved thermal tolerance compared to MAPbI₃, non-active δ -FAPbI₃ appears as the stable phase at room temperature in air, rather than the photoactive phase, α -FAPbI₃, which is stable at high temperature. Therefore, maintaining α -FAPbI₃ at room temperature in air is a major challenge. It was reported that the introduction of dopamine hydrochloride (hereafter DA) as an additive to MAPbI₃ can improve energy conversion efficiency and isolation from the external environment [2]. In the present study, DA is introduced as an additive to FAPbI₃, and the effect of DA addition on the phase stability of FAPbI₃ at room temperature in air is evaluated using X-ray diffraction (XRD) measurements. Observed XRD patterns are shown in Fig. 1, which shows that pure FAPbI₃ (DA:0mM) undergoes a phase transition to δ -FAPbI₃ after one day from preparation, while the one with DA (20 mM) can maintain α -FAPbI₃ for about a month after preparation.

References

- [1] A. Kojima et al., J. Am. Chem. Soc., 2009, 131, 6050-6051.
- [2] J. Zhang et al., J. Energy Chem., 2021, 54, 291-300.

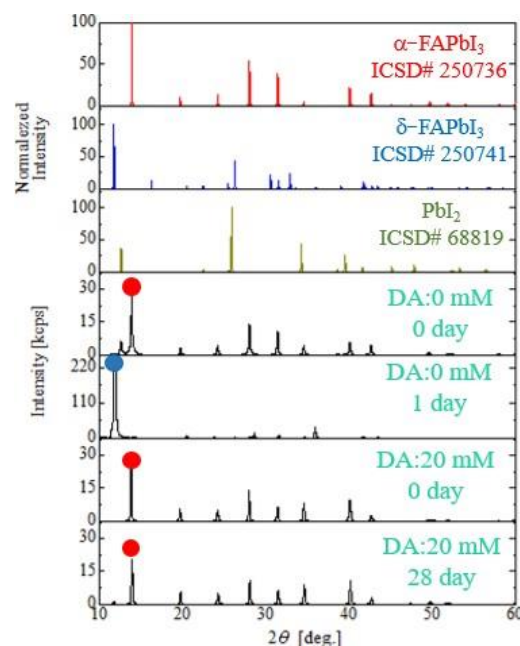


FIG. 1. XRD patterns of FAPbI₃.

MM-P12 (Poster)**Evaluation of structural stability of quadruple perovskites $\text{RMn}_3\text{Al}_4\text{O}_{12}$** **($R = \text{Ce, Pr, Eu, Dy, Y, Yb}$)**Yuta Kizawa¹, Ikuya Yamada^{1,2*}, Shogo Kawaguchi³¹ Graduate School of Engineering, Osaka Prefecture University, Sakai, Osaka, Japan² Graduate School of Engineering, Osaka Metropolitan University, Sakai, Osaka, Japan³ Japan Synchrotron Radiation Research Institute, Sayo-gun, Hyogo, Japan

* Corresponding author's email: ikuya_yamada@omu.ac.jp

Quadruple perovskite oxides (general formula: $\text{AA}'\text{B}_4\text{O}_{12}$) are one of the cation-ordered perovskites, in which the original A-sites are divided into icosahedral (A) and pseudosquare (A') coordinated sites. Unlike simple perovskite of ABO_3 , the three distinctive crystallographic sites of A-, A', and B-sites inhibit the rational evaluation of the structural stabilities solely from the tolerance factor. The global instability index [1], G , calculated by the bond valence sums can evaluate the structural stability, regardless of its structure type. In the previous study, G of $\text{RMn}_3\text{Al}_4\text{O}_{12}$ series ($R = \text{rare-earth metals}$) were predicted by using SPuDS software, obtaining relatively stable compounds with $G < 0.2$ v.u. ($R = \text{Dy, Y, Yb}$), although those with higher G ($R = \text{La}$) could not be synthesized [2]. In the present study, we investigated the structural stability of $\text{RMn}_3\text{Al}_4\text{O}_{12}$ ($R = \text{La, Ce, Pr, Eu, Dy, Y, Yb}$) using G obtained from the experiment.

$\text{RMn}_3\text{Al}_4\text{O}_{12}$ ($R = \text{Ce, Pr, Eu}$) were successfully obtained at high pressures up to 12 GPa. The powder X-ray diffraction (XRD) patterns were indexed with the cubic quadruple perovskite structure as well as the reported $\text{RMn}_3\text{Al}_4\text{O}_{12}$ ($R = \text{Dy, Y, Yb}$). The structure parameters were refined by Rietveld analysis of the synchrotron XRD data calculating the experimentally determined G (G_{exp}). The G_{exp} demonstrated a parabolic dependence on ionic radii of the R ion as well as $\text{RCu}_3\text{Fe}_4\text{O}_{12}$ series [3]. We found that the G_{exp} is related to the lower limit of the synthesis pressure (P_L), which was determined by synthesis experiments at various pressures from 3 to 12 GPa. Figure 1 depicts the results of synthesis as a function of G_{exp} for $\text{RMn}_3\text{Al}_4\text{O}_{12}$. The P_L increased almost linearly with G_{exp} , indicating that higher pressures are needed to stabilize the compounds with severe instability with larger G_{exp} . This finding provides a valuable guide to designing the optimum synthesis conditions.

Keywords: quadruple perovskite, structural stability, high pressure**References**

- [1] A. Salinas-Sanchez et al., J. Solid State Chem. 100 (1992) 201.
- [2] T. Saito et al., Bull. Chem. Soc. Jpn. 84 (2011) 802.
- [3] I. Yamada et al., Inorg. Chem. 52 (2013) 13751.

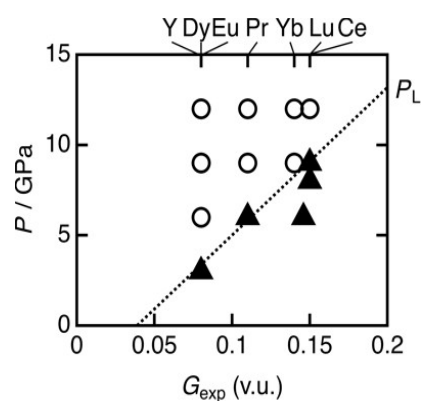


FIG. 1. The results of synthesis of $\text{RMn}_3\text{Al}_4\text{O}_{12}$. Open circles indicate that the quadruple perovskite phases were successfully obtained, whereas solid triangles denote that samples that the quadruple perovskite phases could not be obtained. The dashed line represents the lower limit of the synthesis pressure.

MM-P13 (Poster)**Magnetic and hyperfine properties of MnCoGe-MnFeGe system**Akari Onaka¹, Masahira Onoue², Reisho Onodera³, Yoshifuru Mistui^{1,*}, Keiichi Koyama^{1,2}¹ Graduate School of Science and Engineering, Kagoshima University, Kagoshima, 890-0065, Japan² Center for Advanced Science of Research and Promotion, Kagoshima University, Kagoshima, 890-0065, Japan³ Department of Industrial Engineering, National Institute of Technology, Ibaraki College, Ibaraki, 312-8508, Japan

* Corresponding author's email: mitsui@sci.kagoshima-u.ac.jp

MnCoGe-based compounds exhibit giant magnetocaloric effect due to first order magnetic phase transition accompanied by structural phase transition. $\text{Mn}_{1-x}\text{Fe}_x\text{CoGe}$ and $\text{MnCo}_{1-x}\text{Fe}_x\text{Ge}$ show magnetostructural phase transition around room temperature¹. However, magnetostructural transition is affected by both Fe content and the heat treatment condition greatly. Noguchi *et al* reported that the structural phase transition temperature changed at different heating temperature². In this study, to clarify the microscopic information of Fe substitution effect on MnCoGe, ^{57}Fe Mössbauer spectroscopy measurements, X-ray diffraction experiments, and magnetization measurements were performed for $\text{MnCo}_{1-x}\text{Fe}_x\text{Ge}$ ($0.2 \leq x \leq 1.0$).

The hyperfine property of Mn-site and Co-site was evaluated by ^{57}Fe Mössbauer spectroscopy at 15 K. Figure 1 shows the Fe content x dependence of isomer shift IS (a) and quadrupole splitting QS (b). Increase of x influences effectively for isomer shift of Mn-site rather than Co-site. Meanwhile, sign of QS at only Co-site changed. Therefore, it is suggested that Fe-substitution effectively changed electron distribution at Mn-site, and electric field gradient around Co-site.

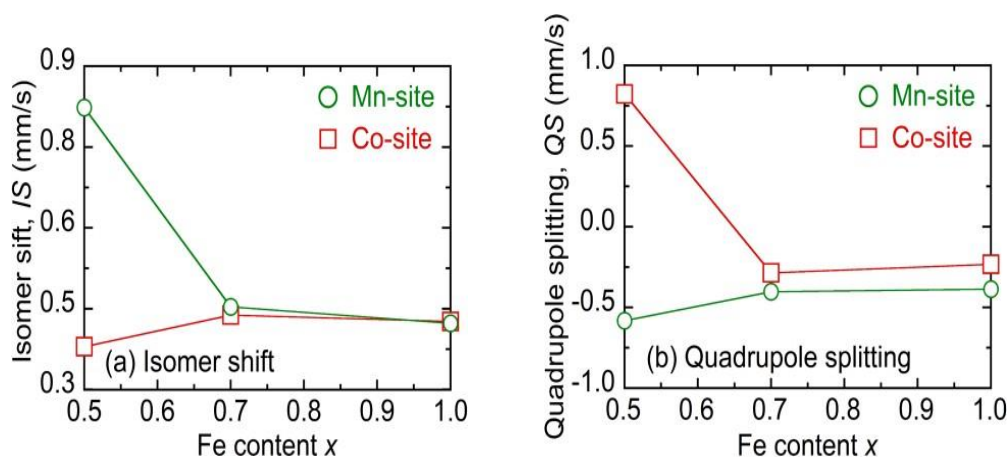
Keywords: Mössbauer spectroscopy, MnCoGe, magnetic measurement

FIG. 1. Fe content x dependence of isomer shift IS (a) and quadrupole splitting QS (b) of $\text{MnCo}_{1-x}\text{Fe}_x\text{Ge}$ ($0.5 \leq x \leq 1.0$).

References

- [1] G.J. Li et al., J. Magn. Magn. Mater. 332 (2013) 146-150.
- [2] K. Noguchi et al., J. Magn. Magn. Mater. 499 (2020) 166199.

MM-P14 (Poster)**Systematic QSGW analysis of excited states and model construction of 3d transition metal luminescent centers in α -Al₂O₃**Harutaka Saito^{1,*}, Katsuhiko Suzuki¹, Kazunori Sato^{1,2,3}, Takao Kotani^{2,4}¹ Graduate School of Engineering, Osaka University, Osaka, 565-0871, Japan² Center for Spintronics Research Network (CSRN), Graduate School of Engineering Science, Osaka University, Osaka, 560-0043, Japan³ Spintronics Research Network Division, OTRI, Osaka University, Osaka, 565-0871, Japan⁴ Department of Mechanical and Physical Engineering, Tottori University, Tottori, 680-8552, Japan

* Corresponding author's email: saito.harutaka@mat.eng.osaka-u.ac.jp

Transition metal (TM) luminescent centers have been played an essential role in light-emitting devices such as LEDs and laser devices. The partially occupied 3d orbitals of TM ions lead to exhibit many electron-configurations and transitions between these configurations (multiplets) observed in visible light region. In order to efficiently design new light-emitting materials, the multiplet energy levels should be predicted by first-principles calculations. However, first-principles calculations usually refer to the ground state properties. It is thus necessary to develop a first-principles method for excited state properties without semi-empirical parameters nor specific models.

To go beyond usual local density approximation in density functional theory, we employed quasiparticle self-consistent GW (QSGW) method implemented in ecalj package developed by Kotani *et al* [1]. Specifically, we used QSGW80 method to quantitatively reproduce band gap energy of various semiconductors [2]. The localized 3d electron in TM luminescent centers are described using local atomic model Hamiltonian consisted of crystal-field (CF) terms and effective Coulomb interaction terms. This model Hamiltonian can be described by CF parameters and Slater-Condon parameters. These parameters are determined so that eigenvalues of the model Hamiltonian with Hartree-Fock approximation reproduce the QSGW80 TM 3d band structure as exactly as possible. As a confirmation, we first estimated Slater-Condon parameters of free TM ions. We found that our method gave comparative values compared with experimental ones. Next, we focus on Cr³⁺ in α -Al₂O₃. Our method also gave reasonable values of parameters in comparison with experiment. Furthermore, we show the Tanabe-Sugano diagram in FIG. 1. This diagram shows CF dependence on multiplet energy levels. The multiplet structure obtained by QSGW80 qualitatively reproduces that of experimental analysis [3] in the low energy region (FIG. 1(b) and (c)). Finally, we obtained the chemical trend of TM ions in α -Al₂O₃. It shows that our method reproduces the trend of experimental works.

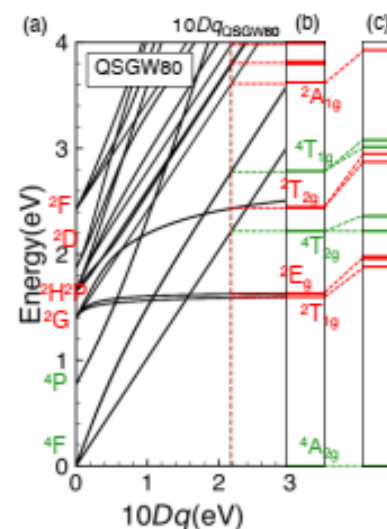


FIG. 1. (a) Tanabe-Sugano diagram, (b) multiplet structure by QSGW80, (c) multiplet structure by experimental analysis [3] of Cr³⁺ in α -Al₂O₃.

References

- [1] T. Kotani, and M. van Schilfgaarde, Phys. Rev. B 76 (2007) 156106.
- [2] D. Deguchi, et al., Jpn. J. Appl. Phys. 55 (2016) 051201.
- [3] M. O. J. Y. Hunault, et al., J. Phys. Chem. A 122 (2018) 4399.

MM-P15 (Poster)**Site selectivity of Cu or Fe in Cu-doped or Fe-doped MnCoGe**Taisei Takaoka^{1,*}, Yoshifuru Mitui¹, Keiichi Koyama¹, Shinpei Fujii¹¹ Graduate School of Science and Engineering, Kagoshima University, Kagoshima 890-0065, Japan

* Corresponding author's email: k5820144@kadai.jp

With decreasing temperature, MnCoGe alloys undergo a structural transition from Ni₂In-type hexagonal structure (“Hex”) to TiNiSi-type orthorhombic structure (“Orth”) at $T_{str} = 420$ K and a magnetic transition from paramagnetic state to ferromagnetic one at $T_C = 355$ K [1,2]. Partial substitution of Cu or Fe for Mn or Co in MnCoGe alloys brings about stabilization of “Hex” and results in a decrease in T_{str} [3-5].

Our results of DFT calculations for $(\text{Mn}_{1-x}\text{X}_x)\text{CoGe}$ and $\text{Mn}(\text{Co}_{1-x}\text{X}_x)\text{Ge}$ ($x = 0.125$) have shown that “Hex” is more stable for $(\text{Mn}_{1-x}\text{Cu}_x)\text{CoGe}$. This fact is not in agreement with experimental results [5]. In the case of $\text{Mn}(\text{Co}_{1-x}\text{Cu}_x)\text{Ge}$, we cannot determine whether “Hex” or “Orth” is more stable. In the case of Fe substitution, “Orth” becomes more stable in both cases, which is not consistent with the experimental result [3] (Fig. 1). In order to investigate the reason for this disagreement between experiment and theoretical results, we have performed DFT calculations for structures containing Cu or Fe at both Mn and Co sites.

Keywords: Cu-doped, Fe-doped, MnCoGe, Ni₂In-type, TiNiSi-type

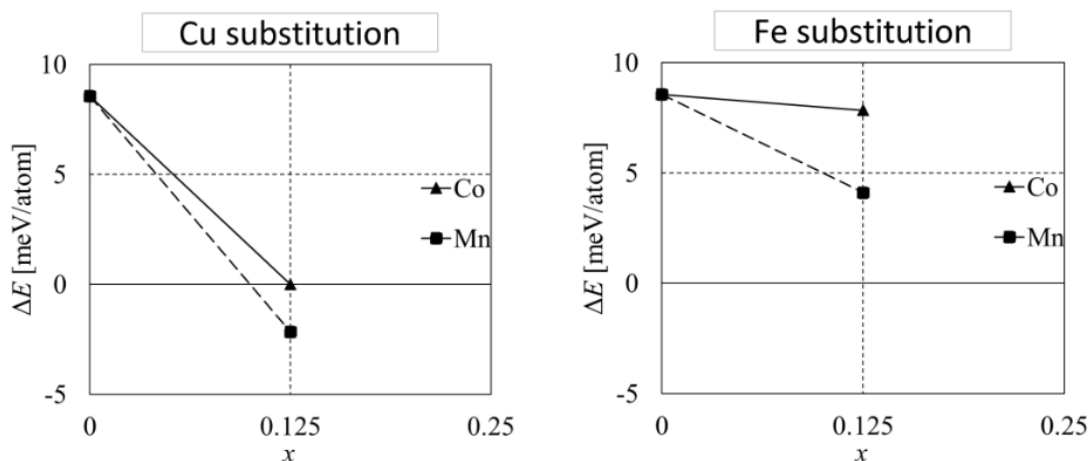


FIG. 1. Change of ΔE ($\Delta E = E_{\text{Hex}} - E_{\text{Orth}}$) with Cu or Fe substitution for Mn or Co site.

References

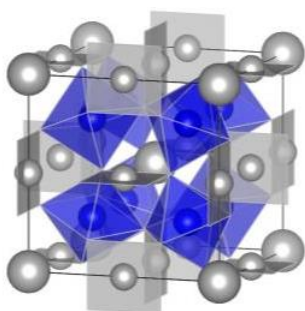
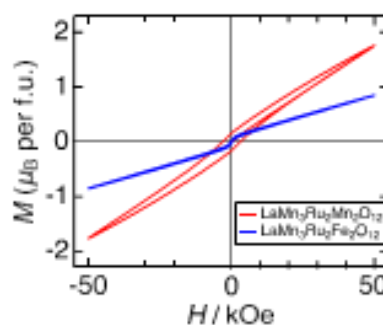
- [1] V. Johnson, Inorg. Chem. 14 (1975) 1117.
- [2] S. Niziol, et al., Solid State Commun. 39 (1981) 1081.
- [3] G. J. Li, et al., J. Magn. Magn. Mater. 332 (2013) 146.
- [4] K. Ozono, et al., Mater. Trans. 57 (2016) 316.
- [5] S. K. Pal, et al., J. Alloys Compd. 775 (2019) 22-29.

MM-P16 (Poster)**Structures and magnetic properties of novel quadruple perovskite oxides $\text{LaMn}_3\text{Ru}_2\text{Mn}_2\text{O}_{12}$ and $\text{LaMn}_3\text{Ru}_2\text{Fe}_2\text{O}_{12}$** Amane Morimura¹, Ikuya Yamada^{1,*}¹ Department of Materials Science, Graduate School of Engineering, Osaka Metropolitan University, 1-1 Gakuen-cho, Naka-ku, Sakai, Osaka 599-8531, Japan

* Corresponding author's email: ikuya_yamada@omu.ac.jp

A-site ordered quadruple perovskite oxides, $\text{AA}'_3\text{B}_4\text{O}_{12}$, exhibit various functional properties such as giant dielectric constants and room-temperature magnetoresistance, most of which are related to their structural feature with two distinct crystallographic sites of A' - and B -sites for transition metals (Fig. 1). Further cationic ordering at B -sites may be achieved in selected couples of B -site ions, as represented in the formula $\text{AA}'_3\text{B}_2\text{B}'_2\text{O}_{12}$, which leads to intriguing physical properties. $\text{LaMn}_3\text{Cr}_4\text{O}_{12}$ has A' -site Mn and B -site Cr ions coupled antiferromagnetically at each site,¹ whereas $\text{LaMn}_3\text{Ni}_2\text{Mn}_2\text{O}_{12}$ has antiferromagnetically ordered A' -site Mn ions and ferromagnetically ordered B -site Ni and Mn ions in an orthogonal spin order.² The $\text{LaMn}_3\text{B}_2\text{B}'_2\text{O}_{12}$ family is composed of only 3d metals, forming independent A' - and B -site magnetic sublattices. The effects of 4d or 5d metal ions on the magnetic properties in $\text{LaMn}_3\text{B}_2\text{B}'_2\text{O}_{12}$ have not been clarified yet. In this study, we aimed to elucidate the magnetic interactions of new 3d-4d hybridized quadruple perovskite oxides of $\text{LaMn}_3\text{Ru}_2\text{M}_2\text{O}_{12}$ ($M = \text{Mn}, \text{Fe}$), which are synthesized under high-pressure and high-temperature conditions.

The synchrotron X-ray diffraction patterns of $\text{LaMn}_3\text{Ru}_2\text{M}_2\text{O}_{12}$ ($M = \text{Mn}, \text{Fe}$) confirmed that the main phases were crystallized in a cubic quadruple perovskite structure without B -site ordering between Ru and M ions. X-ray absorption spectroscopy revealed that their valence states are interpreted as the ionic models of $\text{LaMn}_3^{3+}\text{Ru}_2^{3+}\text{M}_2^{3+}\text{O}_{12}$ ($M = \text{Mn}, \text{Fe}$). Both compounds exhibited no long-range magnetic ordering (Fig. 2). We conclude that the competition between ferromagnetic and antiferromagnetic interactions in B -site ions prevented the formation of long-range magnetic ordering of A' -site Mn ions which are originally independent in the distinct magnetic sublattices.

Keywords: Magnetism, Quadruple perovskite oxides, High-pressure synthesisFIG. 1 Schematic of crystal structure of $\text{AA}'_3\text{B}_4\text{O}_{12}$ -type quadruple perovskite oxidesFIG. 2 Isothermal magnetization curves for $\text{LaMn}_3\text{Ru}_2\text{M}_2\text{O}_{12}$ ($M = \text{Mn}, \text{Fe}$) at 5 K**References**

- [1] X. Wang et al., Phys. Rev. Lett. 115 (2015) 087601.
- [2] Y. Y. Yin et al., Chem. Mater. 28 (2016) 8988.

MM-P17 (Poster)**The epitaxially grown ferroelectric $\text{Hf}_{0.5}\text{Zr}_{0.5}\text{O}_2$ thin film using pulsed laser deposition method**Woohyeon Ryu¹, Chansoo Yoon¹, and Bae Ho Park^{1,*}¹ Division of Quantum Phases and Devices, Department of Physics, Konkuk University, Seoul 05029, Korea

*Corresponding author's e-mail: baehpakr@konkuk.ac.kr

The ferroelectric random access memory (FRAM), one of the nonvolatile memories, has powerful advantages like a fast access time and a low power consumption which allows the FRAM to be a promising technology in memory field. Most researches associated with the advance of the FRAM technology are focused on $\text{PbZr}_{0.52}\text{Ti}_{0.48}\text{O}_3$ (PZT) due to its large remnant polarization and low coercive voltage. However, scaling down a thickness of PZT under 50 nm cause significant leakage current in a FRAM device which is triggered by low bandgap and sidewall problem. HfO_2 -related materials are considered to be emerging ferroelectric materials for FRAM devices due to their excellent compatibility with CMOS process. In this study, pulsed laser deposition (PLD) method is used to deposit 10-nm-thick Zr-doped HfO_2 (HZO) films and $\text{La}_{0.67}\text{Sr}_{0.33}\text{MnO}_3$ (LSMO) bottom electrodes on the single crystalline SrTiO_3 (STO) substrates. The peaks from X-ray diffraction (XRD) demonstrate that the ferroelectric HZO film with orthorhombic phase is epitaxially grown on the STO substrate. The HZO thin film with very flat surface reveals large remnant polarization of up to $22 \mu\text{C}/\text{cm}^2$ measured by using positive-up negative-down (PUND) pulsed method. Therefore, ferroelectric properties of HZO thin film provide an opportunity to overcome the scaling down problems in the FRAM technology.

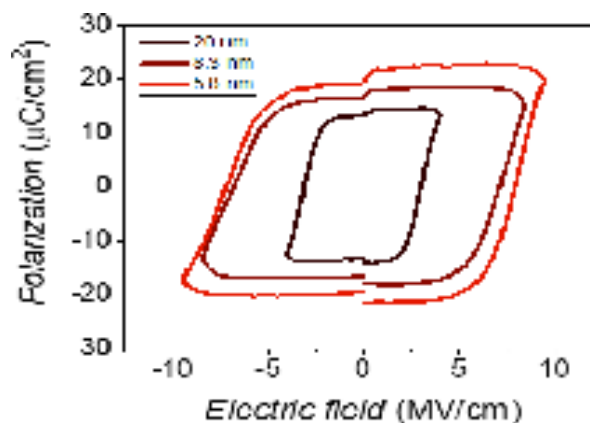
Keywords: PLD, ferroelectric, HZO, heterostructure

FIG. 1. P-E loop of HZO.

MM-P18 (Poster)**Effect of annealing on the exchange interaction between magnetic phases and the exchange bias effect in Co/CoO nanocomposite**

Nguyen Trung Hieu^{1, 2, *}, Vu Hong Ky³, Ta Ngoc Bach³, Do Khanh Tung³, Le Thi Hong Phong³, Do Hung Manh^{3, *}, Ivan Skorvanek⁴

¹ Institute of Theoretical and Applied Research, Duy Tan University, Hanoi, 100000, Viet Nam

² Faculty of Natural Sciences, Duy Tan University, Da Nang, 550000, Viet Nam

³ Institute of Materials Science, Vietnam Academy of Science and Technology, 18 Hoang Quoc Viet, Cau Giay, Hanoi, 100000, Viet Nam

⁴ Institute of Experimental Physics, Slovak Academy of Sciences, Watsonova 47, 040 01, Kosice, Slovakia

* Corresponding author's email: nguyentrunghieu23@duytan.edu.vn, manhdh@ims.vast.ac.vn

In this study, Co particles were synthesized by a polyol method and a post annealing in air was performed to prepare Co/CoO nanocomposite. The sample was characterized by scanning electron microscopy, X-ray diffraction, and magnetic property measurements. To determine the exchange bias field, the sample was cooled in a magnetic field of 50 kOe and measured hysteresis loops at 5 K. The effect of annealing on the exchange interaction between the Co ferromagnetic phase and CoO antiferromagnetic phase, which in turn affects the exchange bias effect in this material, was investigated. It showed that annealing enhanced the exchange interaction between two phases leading to an improvement of the exchange bias field (H_{eb}) in comparison to the non-annealed sample. A value of $H_{eb} = 155$ Oe was obtained with annealing at temperature of 300 °C in 90 minutes. The dependence of H_{eb} on the exchange interaction between phases is discussed.

Keywords: exchange interaction, exchange bias effect, Co/CoO nanocomposite, annealing

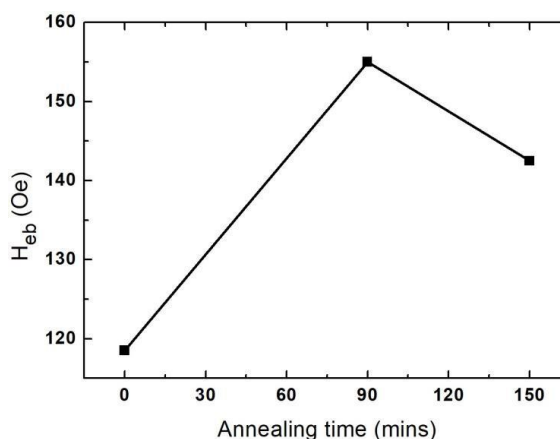


FIG. 1. The exchange bias field of samples annealed at 300 °C in different annealing time.

MM-P19 (Poster)**Thermodynamic properties of bilayer honeycomb spin lattice**Niem Tu Nguyen¹, Giang Huong Bach¹, Duy Huy Nguyen¹, Cong Thanh Bach^{1,*}¹ Faculty of Physics, VNU University of Science, Hanoi, Vietnam

* Corresponding author's email: congbt@hus.edu.vn

Magnetic order of the few layers honeycomb spin lattice films shows the thickness and field dependence. For example, the monolayer CrI₃ is ferromagnetic (FM) while the double layer one is antiferromagnetic (AF) as shown by the magneto-optical Kerr-effect measurement [1]. In this research, the thermodynamic properties of the honeycomb spin lattice consisting of two FM layers interacting by AF exchange interaction are investigated using the Heisenberg XZ-model in the longitudinal and transverse field [2], which is an extension of the previous transverse Ising model [3].

Expressions for the temperature and field dependent free energy, spin wave spectra (Magnon), magnetization are obtained and analyzed numerically. Some consequences like the magnetization process in the field perpendicular to the bilayer film plane is discussed and compared with experiment.

Keywords: thermodynamics, films, magnetization, magnon**References**

- [1] B. Huang et al., Nature 546 (2017) 271.
- [2] Niem T. Nguyen et al., Mater. Trans. 59 (2018) 1075.
- [3] Cong T. Bach et al., JMMM 483(2019) 136.

MM-P20 (Poster)**Design and experimental investigation of piezoelectric ceramic element PZT application for high-power ultrasonic welding transducer**

Tran Van Hiep^{1,*}, Nguyen Dang Co^{2,*}, Nguyen Huy Ngoc³, Nguyen Hai Binh³, Pham Thi Thanh³, Dang Duc Dung⁴, Nguyen Huy Dan³, Pham Duc Thang⁵, Vu Xuan Manh¹, Luong Trung Kien⁶, Bui Dinh Tu^{2,*}

¹ Center for Microelectronics and Information Technology, Institute of Technology Application, C6 Thanh Xuan Bac, Thanh Xuan, Hanoi, 100000, Viet Nam;

² Faculty of Engineering Physics and Nanotechnology, VNU-University of Engineering and Technology, 144 Xuan Thuy Road, Cau Giay District, Hanoi, 100000, Viet Nam;

³ Institute of Materials Science, Vietnam Academy of Science and Technology, 18 Hoang Quoc Viet, Cau Giay, Hanoi, 100000, Viet Nam;

⁴ School of Engineering Physics, Hanoi University of Science and Technology, 1 Dai Co Viet Road, Hanoi, 100000, Vietnam;

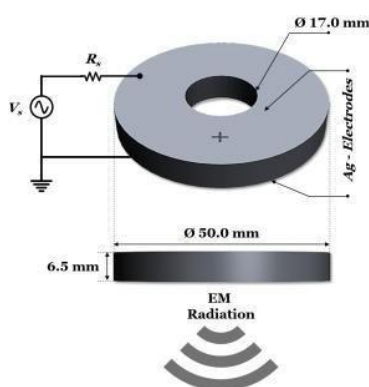
⁵ Phenikaa University Nano Institute, Phenikaa University, Nguyen Trac, Ha Dong, Hanoi, 100000, Vietnam;

⁶ School of Foreign Languages, Hanoi University of Science and Technology, 1 Dai Co Viet Road, Hanoi, 100000, Vietnam

* Corresponding author's email: hieptran95.yb@gmail.com; cond@vnu.edu.vn; buidinhthu@vnu.edu.vn

Currently, ultrasonic welding technology is developing rapidly and is widely applied in many fields: science and technology, agriculture, environment, medicine, industry, and especially applied in industrial transmission lines non-woven fabric industry. In the world, the application of piezoelectric ceramic materials in ultrasonic welding has many manufacturers and traders of piezoelectric ceramic elements, and many scientific works have published different types of piezoelectric ceramics depending on the purpose of the application. In this research, we have researched and fabricated piezoelectric ceramic materials described by the general formula PZT. The piezoelectric ceramics were fabricated by solid-state reaction technique, sintering was carried out for 2 hours at temperatures ranging from 1100°C to 1200°C. The existence of sintering temperatures on microstructures and hysteresis rings of ceramic systems has been investigated. The crystalline phase and microstructure of the sintered compositions were investigated in detail using X-ray diffraction (XRD) analysis and scanning electron microscopy (SEM). Dielectric properties, such as dielectric constant (ϵ_r) and dielectric loss ($\tan \delta$) have been measured. The room temperature hysteresis loops of all unpolarized sintered samples show similar behavior to the “hard” PZT ceramic. The phase transition temperature (T_c) and piezoelectric properties such as electromechanical coupling coefficient (K_p), quality factor (Q_m), and piezoelectric strain constant (d_{33}) have been studied and presented in detail.

Keywords: PZT, piezoelectric ceramic, ultrasonic welding transducer.



MM-P21 (Poster)**Study of metal-insulator transition in complex perovskite for sensing application**Thu Le Thi Anh^{1,*}, Dinh Nguyen Ngoc²¹ Viet Duc College of Medicine and Medical devices, 5 Trang Thi, Ha Noi, Viet Nam² Faculty of Physics, VNU University of science, 334 Nguyen Trai, Ha Noi, Viet Nam.

* Corresponding author's email: lethianhthu1982@gmail.com

Metal-insulator materials get great interest by its applicability in sensing application [1], [2]. Complex ferromagnetic-ferroelectric perovskites ([3],[4]) possess the multiferroic behavior and the metal-insulator transition (MIT), which can be adjusted for sensing application. In this report we study MIT behavior of $[\text{La}_{0.7}\text{Sr}_{0.3}\text{Mn}_{0.98}\text{Co}_{0.02}\text{O}_3]_{(1-x)}[(\text{La}_2\text{NiO}_4)_{0.9}(\text{BaTiO}_3)_{0.1}]_x$ or $(\text{LSMCO})_{1-x}(\text{LNBT})_x$ perovskite with $x = 0.0; 0.1; 0.2; 0.3; 0.4$. Samples are prepared by the ceramic technology method with high energy ball milling. LNBT is prepared firstly by solgel method and has core-shell structure. The thermomagnetic curves are measured by PPMS system. Ferroic behavior is clearly observed in $x=0.4$ sample. Temperature dependence of resistivity is recorded by four probe method and conducting mechanism is discussed using the two components: small Polaron and large Polaron concept. Potential for sensing application of MIT in some samples is pointed out.

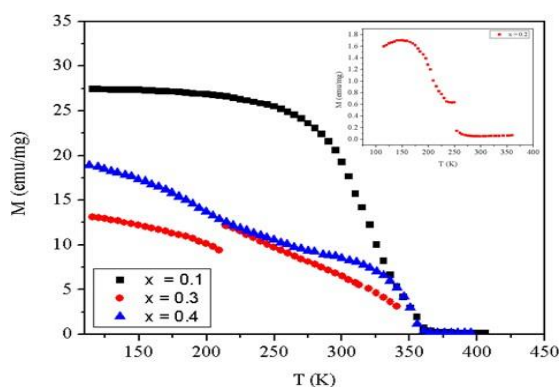
Keywords: Ferroic, small polaron, large polaron.

FIG. 1 Thermomagnetic curves of $(\text{LSMCO})_{(1-x)}\text{LNBT}_x$ with $x = 0.0, 0.1, 0.3, 0.4$. Inset shows the curve of $x = 0.2$ sample

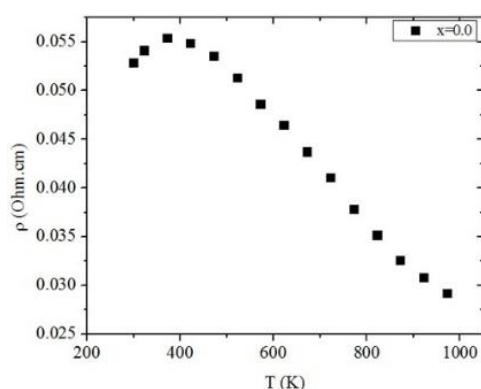


FIG. 2 The dependence of resistivity on temperature of $x = 0$ sample

References

- [1] M. Shellaial et. al., Chems. 8 (2020) 55.
- [2] Proposito et. al., Chems. 8 (2020) 26.
- [3] L.T.A. Thu et. al., Bull. Marter. Sci. 43 (2020) 10.
- [4] L.T.A. Thu et. al., Mater. Trans. 61 (2021) 1517.

MM-P22 (Poster)**Tuning independently the exchange bias and coercivity in top-pinned and bottom-pinned Co/Pd multilayers by FeMn film**

Van Cuong Giap¹, Khanh Tung Do², Thanh Huong Nguyen², Hong Ky Vu², Hung Manh Do², Dang Thanh Tran², Thi Ngoc Anh Nguyen^{2,3,*}

¹ Hung Yen University of Technology and Education, Hung Yen, Vietnam

² Institute of Materials Science, Vietnam Academy of Science and Technology, 18 Hoang Quoc Viet, Hanoi, Vietnam

³ Graduate University of Science and Technology, Vietnam Academy of Science and Technology, 18 Hoang Quoc Viet, Hanoi, Vietnam

* Corresponding author's email: ngocanhnt.vn@gmail.com

The interlayer coupling between a ferromagnet (FM) and an antiferromagnet (AFM) as well as the spin structure at such FM/AFM interface play an important role in magnetic properties, giving rise to various intriguing phenomena [1, 2] therefore being the key elements of novel spintronic systems. In this study we investigated perpendicular exchange bias (H_{EB}) and coercivity (HC) in Co/Pd multilayers (MLs) with an FeMn film at the bottom or on top. These MLs were fabricated by DC magnetron sputtering, the structural and the magnetic properties were characterized by X-ray diffraction (XRD) and Vibrating sample magnetometer (VSM). The results clearly show that magnetic properties (e.g. H_{EB} , HC) of the top- and bottom-pinned systems are remarkably different. The large perpendicular H_{EB} is observed for the top-pinned [Co/Pd]₅/Co/FeMn system but not for the bottom-pinned FeMn/[Co/Pd]₅ system. However, in terms of the HC, the HC of the bottom-pinned FeMn/[Co/Pd]₅ system is nearly two times higher than that of the top-pinned [Co/Pd]₅/Co/FeMn system which somehow is almost unchanged in comparison with the [Co/Pd]₅ system. Some physical models were used for visualization of the FM and AFM interaction as well as the spin configuration in these systems [3-6]. This approach opens up the way for tuning the magnetic coupling in top-pinned and bottom-pinned Co/Pd MLs by FeMn in order to tune their H_{EB} and HC independently.

Keywords: [Co/Pd]₅ multilayers, FM/AFM interaction, FM/AFM surface, perpendicular exchange bias, coercivity

Acknowledgement

This work was financially supported by Vietnam Academy of Science and Technology (VAST) under Project NCXS01.04/22-24.

References

- [1] P. Bruno, Phys. Rev. B 52, 411, 1995.
- [2] J. Nogues, I.K. Schuller, J. Magn. Magn. Mater. 192, 203-232, 1999
- [3] W. H. Meiklejohn and C. P. Bean, Phys. Rev. 102, 1413, 1956.
- [4] W. H. Meiklejohn, J. Appl. Phys. 33, 1328, 1962
- [5] L. Mobley et al., J. Phys.: Condens. Matter 16, 5897–5906, 2004
- [6] J.-Y. Chen et al., IEEE Trans. Magn. 46(6), 1401-1404, 2010

MM-P23 (Poster)**Correlation between structure and electromagnetic properties of some high permeability amorphous Fe and Co based alloys**

Nguyen Quang Hoa^{1,*}, Nguyen Ngoc Dinh¹, Vuong Van Hiep¹, Nguyen Duy Thien¹, Tran Vinh Thang¹, Le Van Vu¹, Tran Thi Ngoc Anh¹, Nguyen Trong Tinh², Nguyen Thi Mai Huong², Bach Thanh Son², Le Thi Thu Huong², Cong Thanh Bach¹

¹ Faculty of Physics, VNU University of Science, 334 Nguyen Trai, Thanh Xuan, Hanoi

² Institute of Physics, VAST, 18 Hoang Quoc Viet, Cau Giay, Hanoi

* Corresponding author's email: hoanq@hus.edu.vn

Several high permeability soft magnetic materials from the iron and cobalt based alloys $\text{Fe}_{73.5}\text{Si}_{13.5}(\text{BNbCu})_{13}$ [1], $\text{Co}_{65.5}\text{Fe}_{3.5}(\text{CrBSi})_{31}$ [2] systems have been produced by the rapid quenching method with the temperature cooling rate about 10^6 °C/s. X-ray analysis showed a complete amorphous structure of the as cast ribbons. The crystallization activation energy and crystallization process of the samples are determined using DSC 8231 equipment (FIG.1). DSC analysis results show that in the Iron based magnetic ribbons, α -Fe crystallization phase appears in the temperature range of 500-575°C. The α -Fe phase crystallization activation energy has been determined about 420 kJ/mol according to the Kissinger method. A significant reduction in the resistivity value ρ was observed due to crystallization upon thermal annealing, leading to the formation of a nanocrystal state in the alloys. The dynamical properties of the samples are also investigated. Magnetic permeability of the as-cast cobalt-based ribbon changes a little in the frequency range up to 100 kHz (FIG.2), while initial permeability reaches about 1.7×10^4 .

Keywords: amorphous ribbons, DSC, permeability

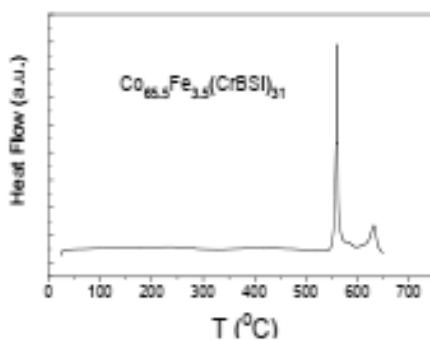


FIG. 1: DSC curve of the typical as-cast $\text{Co}_{65.5}\text{Fe}_{3.5}(\text{CrBSi})_{31}$ ribbons.

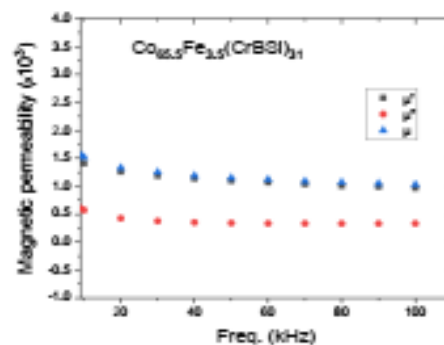


FIG. 2 Frequency dependence of the magnetic permeability of the typical as-cast $\text{Co}_{65.5}\text{Fe}_{3.5}(\text{CrBSi})_{31}$ ribbons.

References

- [1] N. Q. Hoa et al., Mater. Sci. Eng. A 449-451 (2007) 364-367.
- [2] A.V. Nosenko et al., Jour. Mag. Mag. Mater. 515 (2020) 167328.

MM-P24 (Poster)**Tunable electronic properties of novel 2D Janus MSiGeN₄ (M = Ti, Zr, Hf) monolayers by strain and external electric field**Vo T.T. Vi¹, Tran P.T. Linh², Cuong Q. Nguyen³, Nguyen N. Hieu^{3, *}¹ Faculty of Basic Sciences, University of Medicine and Pharmacy, Hue University, Hue 530000, Viet Nam² Faculty of Physics, Hanoi National University of Education, Ha Noi 100000, Viet Nam³ Institute of Research and Development, Duy Tan University, Da Nang 550000, Viet Nam

* Corresponding author's email: hieunn@duytan.edu.vn

Since the recent successful experimental synthesis of MoSi₂N₄ [1], the “MA₂Z₄ family” has been of particular interest to the scientists in the field of materials science due to its outstanding physical properties [2]. In addition, the vertical symmetry breaking in the two-dimensional (2D) layered nanostructures has given rise to many novel properties that do not exist in the symmetry materials [3–5]. Hence, we propose novel 2D Janus MSiGeN₄ monolayers (M = Ti, Zr, and Hf) and investigate their structural, elastic, and electronic properties using the first-principles calculations. The calculations of phonon spectra indicate that monolayers MSiGeN₄ are dynamically stable and can be experimentally synthesized. The obtained Young's modulus and Poisson's ratio of the Janus structures MSiGeN₄ are much larger than that of other binary 2D materials and meet the mechanical stability criteria suggested by Born and Huang. In the calculations using either PBE or HSE06 functionals, the Janus MSiGeN₄ structures exhibit indirect semiconductor characteristics with larger band gaps than that of similar septuple-atomic-layer materials, such as MoSiGeN₄ and WSiGeN₄. In addition, the influences of biaxial strain and external electric field on the electronic structure of MSiGeN₄ are investigated. It is found that the biaxial strain tunes the electronic characteristics more significantly than the external electric field. The obtained results could provide insights into novel Janus monolayers with potential applications in electronic devices.

Keywords: 2D Janus structures, Electronic properties, First-principles calculations**References**

- [1] Y-L. Hong *et al.*, Science 369 (2020) 670.
- [2] L. Wang *et al.*, Nat. Comm. 12 (2021) 2361.
- [3] N.N. Hieu *et al.*, Phys. Rev. B 105 (2022) 075402.
- [4] T.V. Vu *et al.*, Phys. Rev. B 104 (2021) 115410.
- [5] T.V. Vu *et al.*, Phys. Rev. B 103 (2021) 085422.

MM-P25 (Poster)**Critical exponents of $\text{La}_{2/3}\text{Ca}_{1/3}\text{MnO}_3$ nanoparticles**T. L. Phan^{1, *}, B. W. Lee¹, S. C. Yu², H. N. Nhat³, and N. T. Dang⁴¹ Department of Physics and Oxide Research Center, Hankuk University of Foreign Studies, Yongin 17035, South Korea² Department of Physics, Ulsan National Institute of Science and Technology, Ulsan 44919, South Korea³ Faculty of Engineering and Nanotechnology, VNU-University of Engineering and Technology, 144 Xuan Thuy, Cau Giay, Ha Noi, Vietnam⁴ Institute of Research and Development, Faculty of Environmental and Natural Sciences, Duy Tan University, Da Nang 550000, Vietnam

* Corresponding author's email: ptlong2512@yahoo.com

It is known that a $\text{La}_{2/3}\text{Ca}_{1/3}\text{MnO}_3$ (LCMO) perovskite-type compound shows the colossal magnetoresistive (MR) and magnetocaloric (MC) effects associated with a first-order phase transition. Upon fabricating nanostructures and doping a transition/rare-earth metal in it, one can remarkably improve the effects for application aspects [1,2]. Apart from the MR and MC related changes, it has also been observed the magnetic-order transformation from the first type to the second one. However, the variation tendency of critical exponents around the ferromagnetic-paramagnetic transition is less taken into account. This work presents a detailed study on the variation tendency in value of critical exponents (β and γ) of LCMO nanoparticles as changing the crystallite size t from 40 to ~ 100 nm. We have found LCMO showing a critical size (t_c) of the first-to-second-order transition with $t_c \approx 70$ nm, corresponding to tricritical-point exponents. Decreasing t smaller than t_c , we have found the value change of the exponent parameters towards the 3D-Heisenberg and mean-field models. This proves the establishment of long-range magnetic order as decreasing t . Analyses of X-ray absorption spectra and electron microscopy images have indicated local structural distortions and the presence of magnetic-dead layer. These are thought to be important factors that have directly influenced magnetic order of nanoparticles.

Keywords: Perovskite manganite; Nanoparticles; Critical behavior**References**

- [1] T. L. Phan et al., J. Magn. Magn. Mater. 441 (2017), 290.
- [2] T. L. Phan et al., IEEE Trans. Magn. 50 (2014), 2302604.
- [3] T. L. Phan et al., Current Appl. Phys. 42 (2022), 7.

MM-P26 (Poster)**Electric field control of magnetization in artificial microporous magnetic structure based multiferroics**

Vu Nguyen Thuc¹, Ho Anh Tam¹, Nguyen Van Tuan^{1,2}, Nguyen Thi Ngoc^{1,3}, Le Van Lich⁴, Van-Hai Dinh⁴, Pham Van Thuan¹, Nguyen Huu Duc¹, Do Thi Huong Giang^{1,*}

¹ VNU University of Engineering and Technology, Vietnam National University, Hanoi, Vietnam

² Department of Physics, Le Quy Don Technical University, Hanoi, Vietnam

³ University of Science and Technology of Hanoi, VAST, Hanoi, Vietnam

⁴ Hanoi University of Science and Technology, Hanoi, Vietnam

* Corresponding author's email: giangdth@vnu.edu.vn

Straintronics is currently a new bullet research area in solid state physics, at which strain-induced effects in solids are employed to establish next generation gadgets for information, energy transducer, and sensor. Achieving the comprehension of physical mechanisms is always desirable and in high demand for future straintronic devices and research standpoints. This letter will present an unconventional route to tune the magnetic anisotropy of the multiferroic systems of PZT/FeCSi by modulating the applying electric field. Thanks to extremely stress-sensitive characteristic of the microporous structure in FeCSi alloys, under the electric fields up to 20 kV/cm applied across the PZT substrate, the extrinsic magnetic properties purposely, i.e., magnetic susceptibility, magnetization, coercive force, and magnetic energy density can be easily tuned. The dependence of mentioned magnetic properties as a function of the electric field is then confirmed by phase-field simulation. Both experimental and phase-field simulated results shows the stress-activated domain process, where, the degree of electric field response strongly depends on the dimensions of microporous. This work will provide new pathways and additional degrees of freedom in understanding and tailoring the straintronics phenomena for future artificial straintronic devices.

Keywords: Straintronics, Magnetoelectric, Multiferroics, Microporous structure, Magnetic domain.

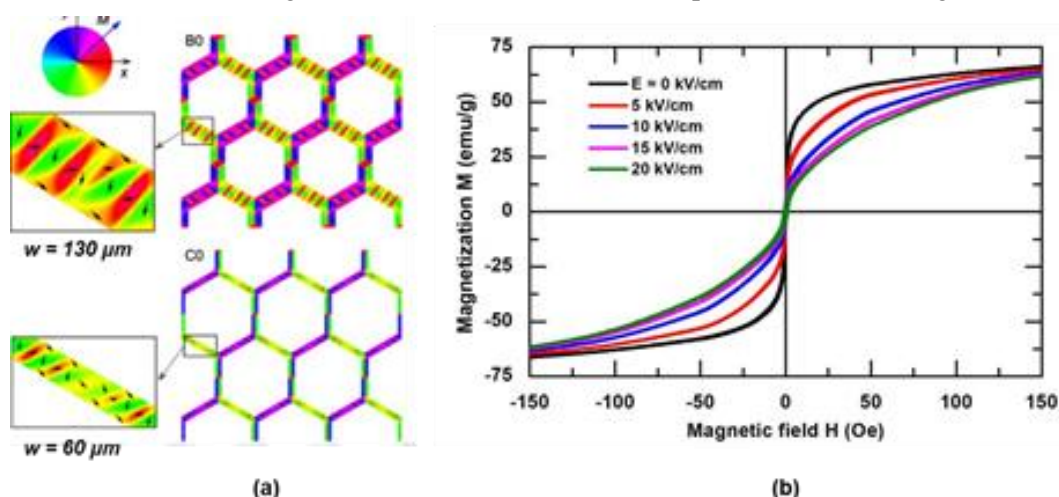


FIG. 1. Micromagnetic simulation of magnetic domain in FeCSi microporous structure (a) and magnetization loops measured at various applied electric fields (b).

MM-P27 (Poster)**Micro-patterned configuration controlling GMI effect in magnetic artificial system**

Ho Anh Tam¹, Nguyen Van Tuan^{1,2}, Nguyen Thi Ngoc^{1,3}, Le Van Lich⁴, Dinh Van Hai⁴, Manh-Huong Phan⁵, Cheol Gi Kim⁶, Vu Dinh Lam⁷, Nguyen Huu Duc¹, Do Thi Huong Giang^{1,*}

¹ VNU University of Engineering and Technology, Vietnam National University, Hanoi, Vietnam

² Le Quy Don Technical University, Hanoi, Vietnam

³ University of Science and Technology of Hanoi, VAST, Vietnam

⁴ Hanoi University of Science and Technology, Hanoi, Vietnam

⁵ University of South Florida, Tampa, Florida, USA

⁶ Daegu Gyeongbuk Institute of Science and Technology (DGIST), Daegu, Republic of Korea

⁷ Graduate University of Science and Technology, VAST, Vietnam

* Corresponding author's email: giangdth@vnu.edu.vn

Giant magnetoimpedance (GMI) effect has drawn intensively attention to the magnetic field sensing technology owing to outstanding sensitivity, resolution, and accuracy. Inspired by the artificial structure, the GMI effect in triangular spiral systems with various branch-widths (w) can be tuned and improved thanks to the shape anisotropy field optimization accompanied by the magnetic domain properties. The GMI effect is enhanced up to 250% under applied magnetic field of 100 Oe in the sensor with $w = 60\ \mu\text{m}$, much higher than that of 5% in $w = 250\ \mu\text{m}$ sensor. The magnetic characterizations demonstrate that the improvement of magnetic susceptibility at low field when the width is reduced is correlated to the shape anisotropy properties. The simulation shows that depending on the applied field directions, various closure magnetic domain configurations can be formed owing to the competition of anisotropy and Zeeman energies followed in the Stoner-Wohlfarth model. These results agree well with the augmentation of GMI effects assisted the transverse domain formations at critical dimension for micro-patterned magnetic system. These make the GMI spiral sensors a promising candidate for miniaturization of sensing magnetic applications.

Keywords: Magneto-impedance, magnetic sensor, micro-coils, magnetic domain

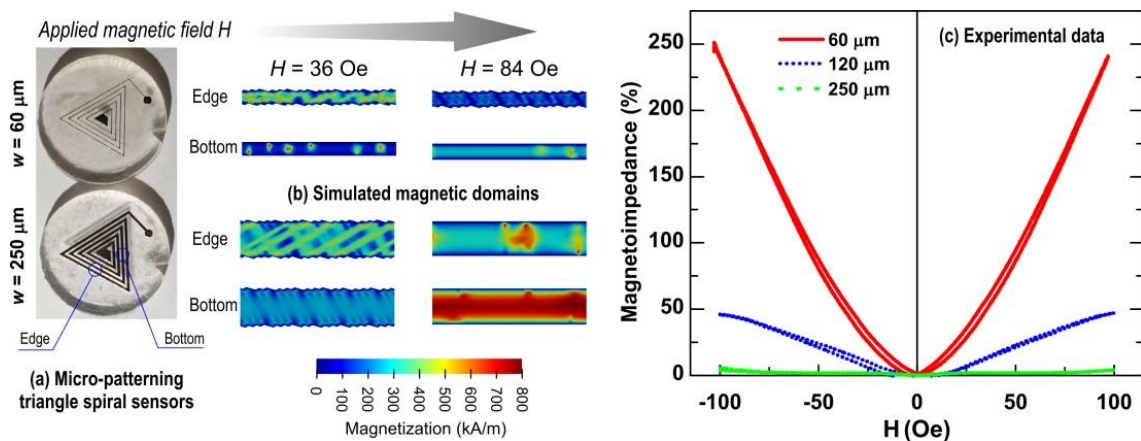


FIG. 1. Micro-patterned triangle spiral magnetic systems (a), micromagnetic simulation of domain formation (b), and characterised with giant magnetoimpedance effect.

MM-P28 (Poster)**Fundamentally different magnetoresistance mechanisms in related Co/Pd and Co/Pt multilayers for spintronic applications**

W.-B. Wu¹, T.N. Anh Nguyen^{2, *}, J. Kasiuk³, J. Przewoźnik⁴, Cz. Kapusta⁴, I. Svito³, K. Tung Do², T. Huong Nguyen², H. Manh Dinh⁵, J. Åkerman⁶

¹ College of Physical Science and Technology, Dalian University, Dalian, 116622, China

² Institute of Materials Science, Vietnam Academy of Science and Technology, Hanoi, Vietnam

³ Belarusian State University, Minsk, 220030, Belarus

⁴ AGH University of Science and Technology, Faculty of Physics and Applied Computer Science, Department of Solid State Physics, Krakow, 30-059, Poland

⁵ Physics Department, Hanoi National University of Education, 144 Xuan Thuy, Hanoi, Vietnam

⁶ Department of Physics, University of Gothenburg, Göteborg 41296, Sweden

* Corresponding author's email: ngocanhnt.vn@gmail.com

The mechanisms of electron and spin transport in *3d ferromagnet (FM)/5d(4d) heavy metal (HM)* multilayers (MLs) are of great interest for spintronics due to the high potential of such structures for magnetic recording [1]. Among them are Co/Pt and Co/Pd MLs with strong and tunable perpendicular magnetic anisotropy, which are widely studied for magnetic memory applications. Despite their high similarity, these MLs have been found to show completely different magnetoresistance (MR) mechanisms. The magnon MR, which dominates in the Co/Pd MLs [2], is almost completely suppressed in the Co/Pt-based structures. Inversely, strong anomalous and spin Hall effects determine the spin-dependent electron transport in the Co/Pt MLs, while they are definitely less significant for the MR of the Co/Pd MLs. Additional intriguing mechanisms appear only in the Pt-containing MLs, which are related to the enhanced contribution of the Lorentz-like MR mechanism at room temperature, as well as to the manifestation of anisotropic MR in a magnetic field rotating perpendicularly to the current. The origins of such differences between the MR mechanisms of the Co/Pt and Co/Pd MLs, which are supposed to lie in their interface structure, as well as in band structure of HM, have not yet been clearly elucidated. A comprehensive analysis of the MR and Hall voltage of both MLs in a wide range of temperatures $T = 3\text{--}300\text{ K}$, as well as the values and orientations of magnetic field $B = 0\text{--}9\text{ T}$, was carried out in correlation with the structural analysis to clarify the principles of the emerging mechanisms.

Keywords: multilayered films, perpendicular magnetic anisotropy, magnetoresistance, magnons, spin Hall effect

Acknowledgment

This work was financially supported by Vietnam Academy of Science and Technology under Project QTBY01.02/23-24 and Belarusian Republican Foundation for Fundamental Research (project no. F23V-003).

References

- [1] K. Garello et al., 2019 Symposium on VLSI Technology (2019) T194.
- [2] T.N. Anh Nguyen et al., Sci. Rep. 10 (2020) 10838.

MM-P29 (Poster)**Spin dynamics in ferromagnetic thin films**

Nguyen Le Thi¹, Junhyeok Bang¹, Seong-Cho Yu^{1, 2}, and Dong-Hyun Kim^{1, *}

¹ Department of Physics, Chungbuk National University, Cheongju 28644, Chungbuk, South Korea

² Department of Physics, UNIST, Ulsan 44919, South Korea

* Corresponding author's e-mail: donghyun@cbnu.ac.kr

Spin dynamics over wide timescales from ultraslow to ultrafast regions has attracted much attention due to possible application for ultrafast-operating and long-term stable spintronic devices. In this talk, several examples of spin dynamic phenomena will be introduced such as unusual minor hysteresis loop behaviors involved with domain wall creeping behavior and nonequilibrium spin dynamics on femtosecond timescale linked with mutual dynamics among spin, electron, and lattice in the ferromagnetic materials. THz emission behavior involved with ultrafast spin dynamics will be also covered.

Keywords: Magnetism, THz emission, Ultrafast spin dynamics

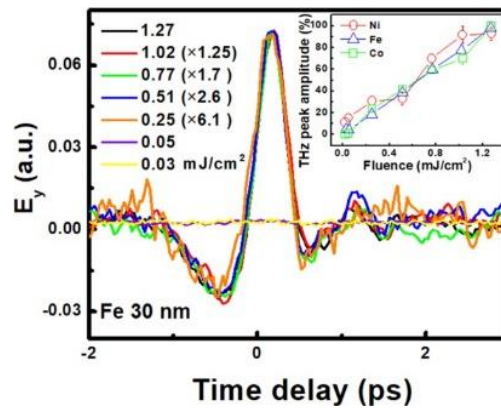


FIG. 1. THz emission profiles from Ni, Fe, and Co films with variation of pump fluences [1].

References

[1] H. Lin et al., Sci. Rep. 10, 15843 (2020).

MM-P30 (Poster)**Growth and multiferroics property of hybrid organic-inorganic perovskite single crystals**

Duc Hieu Nguyen[†], Phuc Dinh Dao[†], Thanh Tung Bui, Quang Thuan Nguyen, Long Bien Le, Duy Hiep Nguyen, The Thanh Luan Nguyen, Huy Tiep Nguyen*

Faculty of Engineering Physics and Nanotechnology, VNU-University of Engineering and Technology, Hanoi, Vietnam

[†]Contributed equally

* Corresponding author's e-mail: tiepnh@vnu.edu.vn

Recently, two-dimensional (2D) layered organic-inorganic perovskites have been a hot topic not only in photovoltaics but also in laser and photo-detection applications due to their remarkable electronic and optical properties. Structurally, these hybrids are suitable for studying piezoelectricity. However, the piezoelectric measurements of such hybrids have been limited by the internal stress in their substrate interface which leads to the suppression of their piezoelectric performance, and the absence of a fast method for making the single crystals of sufficient size and high quality. Here, we report a facile solvent method in growing the 2D layered (C₆H₅C₂H₄NH₃)₂NiCl₄ (or PENC) perovskite single crystals. The XRD patterns reveal their high crystalline quality with (n00) dominant plane (n = 2, 4, 6...). The ferroelectric property has been characterized by using Piezoelectric Force Microscopy (PFM). An effective piezoelectric coefficient of 80 pm V⁻¹ was generated. The ferromagnetic property has been confirmed by a Vibrating Sample Magnetometer (VSM). These results provide a new way to develop new multiferroics based on 2D layered hybrid perovskite single crystals.

Keywords: 2D hybrid organic-inorganic perovskite, single crystal, multiferroics

Session: Photonics and Hybrid Materials (PH)**PH-P01 - PH-P07****PH-P01 (Poster)****Influence of co-dopings of alkaline metal ions in Er-doped CaSnO₃ on its up-conversion emission intensity**Fuma Samejima¹, Naoki Ogi¹, Tomoyuki Yamamoto^{1,*}¹ Waseda University, Shinjuku, Tokyo, 169-8555, Japan

* Corresponding author's e-mail: tymmt@waseda.jp

Up-conversion phosphor, which can emit visible light excited by near infrared radiation, gains great attention, since it is expected to additionally use near infrared region for the generation of electricity by hybridizing with solar cells. It was reported that some types of rare-earth-doped oxides, such as Er/Yb-doped CaZrO₃ [1] and CaMoO₄ [2], show efficient up-conversion emission by 980 nm excitation and also that up-conversion emission intensity is enhanced by co-doping of alkaline metal ions [3]. However, the mechanism of the enhancement of the up-conversion emission intensity due to co-doping of alkaline metal ions has still remained unclear. In this study, Er-doped CaSnO₃ phosphors co-doped with alkaline ions, such as Li, Na, K, Rb and Cs, were synthesized with the conventional solid state reaction method and their crystal structures were characterized by the X-ray diffraction (XRD). The observed up-conversion emission spectra excited by 980 nm irradiation of Na co-doped CaSnO₃:Er are shown in Fig. 1 as an example of the current results. From these results, it is confirmed that up-conversion emission intensity is enhanced approx. 5 times by Na co-doping at maximum.

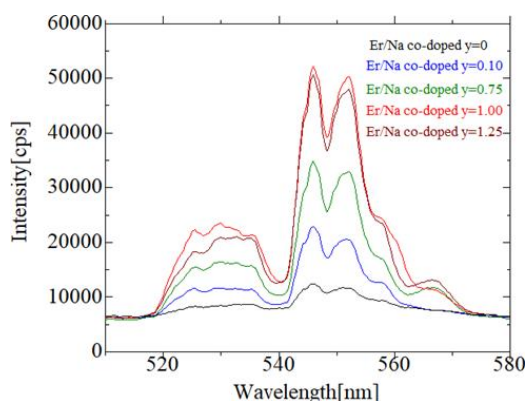


FIG.1. The up-conversion emission spectrum of Na co-doped CaSnO₃:Er ($x=0.01$ in $\text{Ca}_{1-x/2}\text{Sn}_{1-x/2}\text{Er}_x\text{O}_3$).

Keywords: up-conversion, CaSnO₃, Er, alkaline metal co-doping

References

- [1] R. Balda et al., J. Lumin. 129, 1422, 2009.
- [2] F. Huang et al., J. Alloys Compd. 639, 325, 2015.
- [3] A. Maurya et al., J. Alloys Compd. 786, 457-467, 2019.

PH-P02 (Poster)**Influence of oxygen ratio on growth and optical properties of ZnO thinfilm prepared by pulse electron deposition method**

Nguyen Duy Thien¹, Nguyen Van Viet¹, Le Van Vu¹, Nguyen Ngoc Dinh¹, Vuong Van Hiep¹, Bach Huong Giang¹, Pham Van Thanh¹, Hoang Nam Nhat², Nguyen Quang Hoa^{1,*}

¹ Faculty of Physics, University of Science, Vietnam National University, Hanoi, 334 Nguyen Trai, Thanh Xuan, Hanoi, Vietnam

² Faculty of Engineering and Nanotechnology, VNU-University of Engineering and Technology, 144 Xuan Thuy, Cau Giay, Ha Noi, Vietnam

* Corresponding author's e-mail: hoanq@hus.edu.vn

Zinc oxide (ZnO) nanocrystalline thin films have been synthesized by pulse electron deposition technique with difference of oxygen ratio. X-ray diffraction (XRD) studies confirm the presence of hexagonal wurtzite ZnO structure in synthesized films. The results show that the lattice constant slightly decreases and the crystal size increases with increasing oxygen concentration. The surface morphology of ZnO films were examined by scanning electron microscope (SEM). Ultraviolet-Visible (UV-Vis) spectroscopic analysis is carried out to calculate energy band gap of the ZnO films. The band gap decreases from 3.89 eV to 3.35 eV when increasing oxygen concentration from 0 to 100%.

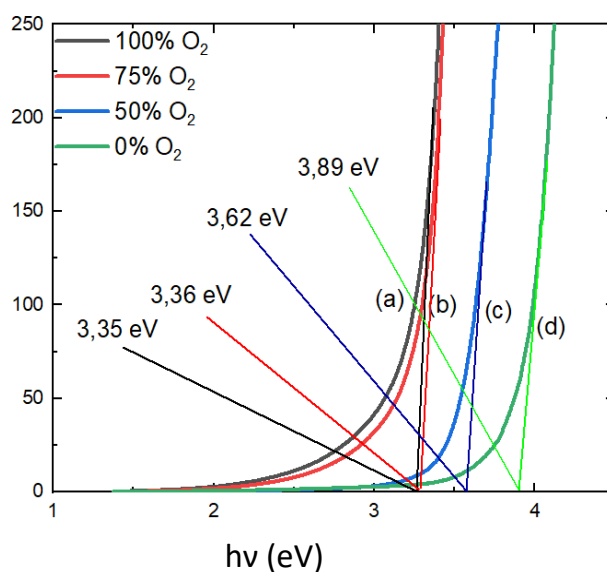


FIG. 1. $(\alpha hv)^2$ vs. photon energy ($h\nu$) of ZnO thin films deposited with different oxygen ratio.

Keywords: ZnO, nanocrystalline, UV-Vis, band gap

PH-P03 (Poster)**Enhancing the absorption figure of merit on solution-based CuO thin films by Ni doping**

La Thi Ngoc Mai¹, Nguyen Van Loi^{2, 4}, Do Hong Minh³, Nguyen Ngoc Dinh⁴, Bui Nguyen Quoc Trinh^{1, 5, *}

¹ Faculty of Advanced Technologies and Engineering, Vietnam Japan University, Vietnam National University, Hanoi, Luu Huu Phuoc, Nam Tu Liem, Hanoi, Vietnam

² Faculty of Basic Science, Vietnam Academy of Cryptography Techniques, 141 Chien Thang, Thanh Tri, Hanoi, Vietnam

³ Faculty of Physical and Chemical Engineering, Le Quy Don Technical University, Building S1, 236 Hoang Quoc Viet, Cau Giay, Hanoi, Vietnam

⁴ Faculty of Physics, University of Science, Vietnam National University, Hanoi, 334 Nguyen Trai, Thanh Xuan, Hanoi, Vietnam

⁵ Key Laboratory for Micro-Nano Technology, University of Engineering and Technology, Vietnam National University, Hanoi, 144 Xuan Thuy, Cau Giay, Hanoi, Vietnam

* Corresponding author's e-mail: trinhbnq@vnu.edu.vn

We evaluated an absorbance effectiveness on the solar spectrum using an absorption figure of merit (a-FOM) for the conducting thin films. In particular, Ni-doped and un-doped CuO thin films were deposited by a facile and sustainable solution-processed synthesis, whose Ni doping concentration was varied to be 0.2, 0.6, 1, 2, 3, 4 wt.%. We observed a change of smooth surface to an appearance of nanoparticles by Ni doping, which supported to form of a plasmonic mechanism for improving the light capture and retention. The absorption of long wavelengths was improved and extended to the near-infrared range. That is, the bandgap energy decreased from 2.10 to 1.88 eV with Ni doping. Also, we found that the absorption length decreased from 99.93 nm to 63.80 nm as the Ni doping increased. In addition, the CuO-based film with 4 wt.% Ni doping showed a maximal value of a-FOM as high as 30.88 $\Omega^{-1}\text{cm}^{-1}$. Corresponding author's to a resistance of 2.07 M Ω/sq and an absorption length of 63.80 nm. Our finding suggested that Ni-doped CuO thin films can be considered as an excellent selection of absorbent conductive oxide layers for application in optoelectronic devices and solar cell systems.

Keywords: CuO, Ni doping, oxide semiconductor, absorption length, absorption figure of merit

PH-P04 (Poster)**Chiropticality of magnetoplasmonic nanoparticle-doped titania hydrogels and aerogels**Huu-Quang Nguyen¹, Markus Niederberger² and Jaebeom Lee^{1,*}¹ Department of Chemistry, Chungnam National University, Daejeon, 34134, Republic of Korea² Department of Materials, ETH Zurich, Switzerland

* Corresponding author's e-mail: nanoleelab@cnu.ac.kr

Aerogel is a type of solid-phase material formed by the coordinated networking of organic or inorganic matters, which result in an open and highly porous structure. In this study, ultralight, magnetic translucent aerogel monoliths were fabricated from trizma-functionalized anatase (TiO₂) and magnetoplasmonic core/shell gold-magnetite composite nanowires (Au@Fe_xO_y MagPlas NWs). The resulting aerogel weigh only 0.13 grams per cubic centimeter and possess UV-visible broad absorption, which were modulated by the amount of doped MagPlas NWs. The combination between highly UV-absorbing TiO₂ anatase and magnetoplasmonic core-shell nanowires allows utilization of both UV- and visible spectrum range of light, which potentially enhances the light-harvesting efficiency and photocatalysis applications. Furthermore, the magnetic susceptibility of the gold-magnetite nanowires also allows unique arrangements in TiO₂ hydrogels, which opens up possibilities for self-assembly into unique linear and helical superstructures.



FIG. 1. Schematics of the solvent-triggered self-assembly process and images of the synthesized TiO₂ and TiO₂/MagPlas NWs.

Keywords: magnetoplasmonic, nanosynthesis, nanowires, chiral, structural color

References

- [1] Nguyen, H-Q., et al. (2022) ACS Nano, 16(4), 5795–5806.
- [2] Matter, F., et al. (2020). NanoToday, 30, 100827.

PH-P05 (Poster)**Effect piezo electric on surface enhanced Raman scattering from ZnO/Au nanorods**

Van Tan Tran¹, Thi Ha Tran^{1, 2}, Nguyen Hai Pham¹, An Bang Ngac¹, Viet Tuyen Nguyen^{1, *}

¹ Faculty of Physics, VNU-University of Science, Thanh Xuan, Hanoi, Vietnam,

² Hanoi University of Mining and Geology, Duc Thang, Tu Liem, Hanoi

* Corresponding author's e-mail: nguyenvietttuyen@hus.edu.vn

Surface-enhanced Raman spectroscopy (SERS) has emerged as a very potential tool for sensing toxicants at extremely low concentration. The sensitivity of the SERS substrates depends strongly on the design of noble metal nanostructures. However, optimization of morphology and size of noble metals can only offer a certain enhancement factor. Additional techniques for further boosting Raman signal were studied. In this research, ZnO/Au nanorods were synthesized by hydrothermal and sputtering techniques. The prepared materials can serve as good SERS substrates. Raman scattering can also be intensified efficiently by taking advantages of piezzo electricity of the ZnO/Au material.

Keywords: ZnO/Au nanorod; hydrothermal; galvanic; SERS; piezoelectric

References

- [1] Bharati MSS, et al.. Opto-Electronic Adv. 4(11) (2021) 1.
- [2] Yang D et al., Anal Chem. 90(24) (2018) 14269–78.

PH-P06 (Poster)**Raman enhanced signal of rhodamine 6G molecules on SERS substrate in application of detecting chemical residues**

Nguyen Kien-Cuong*

Faculty of Engineering Physics and Nanotechnology, VNU-UET, Hanoi, Vietnam

* Corresponding author's email: cuongnk@vnu.edu.vn

A common Raman spectrometer has not usually detected chemical residues at a lower concentration than 10^{-4} M. However, it can detect them at a lower concentration than 10^{-4} M, even lower up to 10^{-9} M with the support of a surface-enhanced Raman scattering (SERS) surface. In this paper, a SERS surface was formed by 5nm-diameter gold nanoparticles (AuNPs) in colloidal solution, and then, randomly deposited on a glass surface to create a SERS/AuNP-layer of 25nm in thickness. A Rhodamine 6G (Rh6G) dye-molecule, deposited on the SERS surface, was used to detect the enhanced Raman amplitude. The Rh6G-solution was diluted at different concentrations, ranging from the concentration from 10^{-4} M to 10^{-9} M. With the same concentration of 10^{-4} M of the Rh6G dye, its typical Raman peaks, deposited on the AuNPs surface, can be clearly detected while these peaks of Rh6G on a flat gold surface could not be seen. Even if the Rh6G solution on the AuNP surface was diluted up to the concentration of 10^{-9} M its typical peaks can still be clearly detected. The significant enhancement of the surface Raman signals at the different concentrations of the Rh6G solution, deposited on the AuNP surface, is due to the roughness of the AuNP surface.

Keywords: Gold nanoparticles (AuNPs), surface-enhanced Raman scattering (SERS), Rhodamine 6G (Rh6G).

PH-P07 (Poster)**Influence of hydrothermal temperatures on characteristics of rare earth upconversion NaYF₄ (Yb, Tm) nanoparticles**Thi Ngoc Anh Mai^{1*}, Dinh Lam Nguyen¹¹ Faculty of Engineering Physics and Nanotechnology, VNU-UET, Hanoi, Vietnam

* Corresponding author's e-mail: anhmtan@vnu.edu.vn

In this report, rare-earth upconversion NaYF₄: Yb, Tm nanoparticles were fabricated by a simple, low-cost, and high-efficiency method called the hydrothermal method. The characteristics of all samples were investigated by SEM, XRD, FTIR, and PL spectroscopy. The particle size was uniformly around 20 nm in diameter and strongly depended on hydrothermal temperature. When hydrothermal temperatures were controlled from 100°C to 180°C, all samples were multi-phases (cubic and hexagonal). And the hexagonal phase prevailed with an increase in the hydrothermal temperature. Furthermore, under 980 nm CW laser excitation, all samples showed PL peaks at 450 nm, 475 nm, and 802 nm. Corresponding author's to $^1D_2 \rightarrow ^3F_4$, $^1G_4 \rightarrow ^3F_4$, and $^3H_4 \rightarrow ^3H_6$ transition, respectively. And the highest PL peak intensity can be obtained since the hydrothermal temperature is 180°C. The results indicated that emission characteristic of the material strongly depends on the phase that can be controlled by the hydrothermal temperature.

Keywords: rare-earth nanoparticles, upconversion nanoparticles, hydrothermal temperature, photoluminescence, NaYF₄: Yb, Tm

References

- [1] U. Kostiv et al., Scientific Reports 10, 20016 (2020)
- [2] Z. Liu et al, Adv. Healthcare Mater. 11, 2102042 (2022)
- [3] Y. Rong et al, Journal of Food Composition and Analysis 100, 103929 (2021)
- [4] X. Lin et al, ACS Appl. Nano Mater. 4, 8, 8231-8240 (2021)
- [5] J. Loo et al, Coordination Chemistry Reviews 400, 213042 (2019)

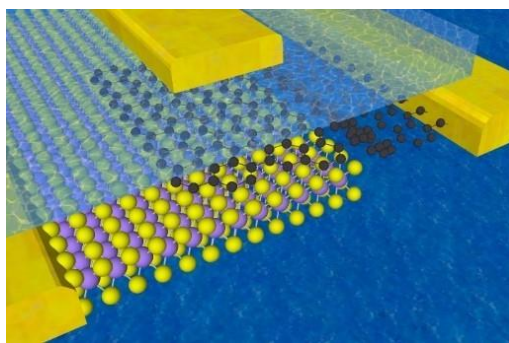
Session: Spintronic materials and Devices (SD)

SD-P01 - SD-P09

SD-P01 (Poster)**Gate-tunable photodetector and high-mobility ambipolar transistor**Gwangtaek Oh^{1*}, JeongEun Oh¹, SeoYul Lim¹, Bae Ho Park¹¹ Division of Quantum Phases & Devices, Department of Physics, Konkuk University, Seoul 05029, Republic of Korea

* Corresponding author's e-mail: baehpark@konkuk.ac.kr

High-quality channel layer is required for next-generation flexible electronic devices. Graphene is a good candidate due to its high carrier mobility and unique ambipolar transport characteristics but typically shows a low on/off ratio caused by gapless band structure. Here we propose a graphene/MoSe₂ channel layer with high-k ion-gel gate dielectric. The graphene/MoSe₂ device shows both high on/off ratio and carrier mobility. Most importantly, it reveals ambipolar behaviors which are controlled by external bias, although such ambipolarity has never been previously reported in graphene/semiconductor barristor structures. Therefore, our graphene/MoSe₂ barristor with ion-gel gate dielectric can offer various with high performances. Here we make a contact of graphene and MoSe₂. The graphene/ MoSe₂ barristor exhibits high on/off ratio of 104 and high mobility. The modulation of graphene's Fermi level (E_F) by applying gate voltage (V_g) is confirmed by the change in Schottky barrier height at the graphene/MoSe₂ junction. Such field effects including ambipolar behaviors are locally investigated by using scanning photocurrent microscopy (SPCM). We have shown that graphene/MoSe₂ barristor can be created to obtain highly efficient photocurrent generation and photodetection. Therefore, our graphene/MoSe₂ barristor with ion-gel gate dielectric can be a suitable candidate for a ambipolar transistor (with high mobility and on/off ratio) and gate tunable broad-area photodetector (with high EQE and responsivity)..

Keywords: Gate-tunable, photodetector, ambipolar transistor, high mobility, graphene,barristorFIG. 1. Graphene/MoSe₂ barristor characterization schematic diagram.**References**

- [1] Heejun Yang et al., Graphene Barristor, a Triode Device with a Gate-Controlled Schottky Barrier. Science 336 (2012) 1140-1143.
- [2] K. S. Novoselov et al., A roadmap for graphene, NATURE, 490 (2012) 192.

SD-P02 (Poster)**Neuromorphic devices based on the electrochemical metallization in the ferroelectric material**Chansoo Yoon¹, Bae Ho Park^{1, *}¹ Department of physics, Konkuk university, Seoul, Korea

* Corresponding author's e-mail: Baehpark@konkuk.ac.kr

The neuromorphic computing system aims to implement artificial neural networks (ANNs), which emulates biological neural networks composed of a large number of neurons massively interconnected by even larger number of synapses. Although several types of architectures have been used to demonstrate ANNs, artificial neurons and synapses have been separately developed by using a wide variety of materials and processes, leading to limited scalability, complex structures and processes, and high cost. If both artificial neurons and synapses can be simultaneously implemented by using electrochemical metallization (ECM) memristors with an identical electrolyte layer, they can become simplified fundamental building blocks in the design and fabrication of large-scale ANNs for future reconfigurable neuromorphic system. Here, we demonstrated the simultaneous implementation of artificial neurons and synapses in ECM memristors with an identical electrolyte layer, which are Ag, Cu, and Ni/PbZr_{0.52}Ti_{0.48}O₃(PZT)/La_{0.8}Sr_{0.2}MnO₃(LSMO) with an ultrathin ferroelectric PZT layer (~5nm). We introduced polarization bound charges of the ferroelectric layer for more controllable cation migration and set-process in an ECM memristor. The Ag/PZT/LSMO showed abrupt and volatile resistive switching caused by the high velocity of the cation migration and could emulate integration-and-fire with stochastic behavior and auto-recovery with low energy consumption. In contrast, the Ni/PZT/LSMO revealed gradual and non-volatile resistive switching due to the low velocity of the cation migration and could emulate synaptic plasticity with very low variability. Thus, our identical electrolyte-based system could provide an important step towards developing large-scale ANNs with high scalability, simple structure, and low cost.

Keywords: Electrochemical metallization, Ferroelectric, Synaptic device, Neuron device

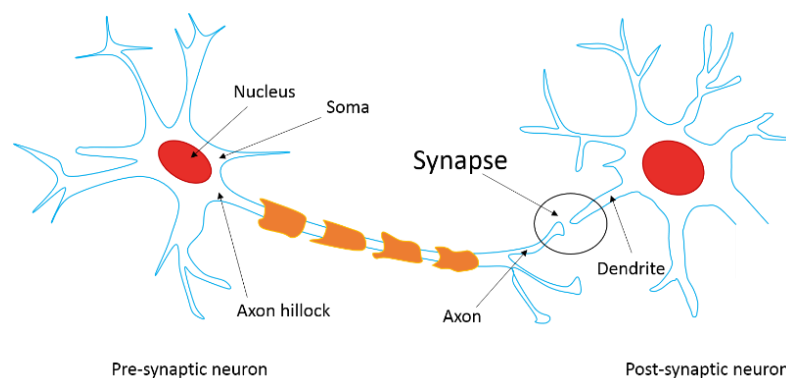


FIG. Schematic image of the biological neuron and synapse structure.

SD-P03 (Poster)**Thermoelectric properties of magnesium tin alloy thin films**

Anh Tuan Thanh Pham^{1, 2}, Hoa Thi Lai^{1, 3, *}, Vinh Cao Tran^{1, 2}, Thang Bach Phan^{1, 2, 3}

¹ Vietnam National University, Ho Chi Minh City, Vietnam

² Laboratory of Advanced Materials, University of Science, Ho Chi Minh City, Vietnam

³ Center for Innovative Materials and Architectures (INOMAR), Ho Chi Minh City, Vietnam

* Corresponding author's email: lthoa@inomar.edu.vn

In this work, magnesium tin (Mg-Sn) alloy thin films was synthesized in form of low-dimension structure by using magnetron co-sputtering in pure Ar plasma atmosphere. The formation of alloy Mg-Sn thin films was confirmed by X-ray diffraction. The thickness and morphology of the films were obtained from field-emission scanning electron microscopy. The thermoelectric properties of the films were investigated in the temperature range of 50 – 300°C. The results showed that the films had p-type semiconducting characterization, with some potential thermoelectric average values: electrical conductivity of 420 S/cm, Seebeck coefficient of 41.3 $\mu\text{V/K}$, and power factor of 72.4 $\mu\text{W/mK}^2$. Specifically, the alloy films had a high value of hole mobility of 51.1 cm^2/Vs Corresponding author's to a hole concentration of $2.4 \times 10^{19} \text{ cm}^{-3}$ measured at room temperature. These results are very potential for high-performance thermoelectric thin-film applications, especially in low-temperature range.

Keywords: Thermoelectrics, magnesium tin, magnetron co-sputtering, thin films

SD-P04 (Poster)**Fabrication of the ion-selective field-effect transistor array for determine the pH of solutions**

Tran Van Hiep¹, Nguyen Huy Khan¹, Vu Xuan Manh¹, Nguyen Huy Cong¹, Nguyen Thi Thuy², Bui Dinh Tu³, Nguyen Hai Binh^{4,*}

¹ Center for Microelectronic and Information Technology, National Center for Technological Progress, Hanoi, Vietnam

² Faculty of Electronics Technology, Electric Power University, Hanoi, Vietnam

³ Faculty of Engineering Physics and Nanotechnology, University of Engineering and Technology, Hanoi Vietnam National University, Hanoi, Vietnam

⁴ Institute of Materials Science, Vietnam Academy of Science and Technology, Hanoi, Vietnam

* Corresponding author's e-mails: binhnh@ims.vast.ac.vn

The research on fabrication of the Ion-Selective Field-effect transistor (ISFET) array by using microelectronic technology and apply for determine the pH of solutions was described on this paper. The ISFET array was designed and fabricated as below: the structure and mask of ISFET was designed by MEMSCapro software based on SCANA design rule; the shape of transistor was employed by UV-lithography technique, the electrodes and connect film was deposited by sputtering method, the gate electrode was fabricated by SiO₂-oxidation technique, the SOG/SOD method was used to dope the n⁺ region, the wire bonding and packaging technique was used on this project. The ISFET array was successfully developed with 8 transistor on chip, the width/length of gate electrode is 16 μ m/6 μ m and the thickness is 6nm. The characteristics of the transistor array was investigated by using Keithley 420SCS Instrument; the threshold voltage was -0.7V with I_{DSmax} = 1mA. The pH sensitive characteristic of the developed transistor was surveyed on range of 2-12 and the sensitivity of sensor was 16mV/pH with LOQ is lower than 0.05 pH, LOD = 0.01pH. The pH sensor was tested with the solutions of some lake in Hoa Binh province (such as: Hoa Binh hydropower reservoir, Chau – Da Bac Lake, Tinh-Da Bac Lake) with the high reliability and low RSD. The obtained results have opened up the possibility of developing compact - fast - real-time and reliable analytical systems to meet the needs of analysis in seafood production and environmental monitoring in Vietnam.

Keywords: Ion-selective field-effect transistor, pH, array sensor, Microelectronics technology

SD- P05 (Poster)**Design and fabrication of wireless contactless liquid level sensor based on LC passive circuit**

Pham Van Thanh^{1, *}, Do Trung Kien¹, Do Quang Loc¹, Sai Cong Doanh¹, Luong Thi Minh Thuy¹, Dang Thi Thanh Thuy¹

¹ Faculty of Physics, VNU-University of Science, Hanoi, Vietnam

* Corresponding author's e-mail: phamvanthanh@hus.edu.vn

In this research, a wireless contactless liquid level sensor has been designed and fabricated based on LC passive resonant circuit with low-cost and small size. The fabricated sensor includes of a contactless parallel electrode capacitor and a planar spiral inductor used as the reader coil. The principle of LC passive circuit is based on LC resonant circuit shown as in Fig.1a, in which the resonant frequency expressing as [1]:

$$f_{res} = \frac{1}{2\pi\sqrt{LC}}$$

where L and C are inductance and capacitance of LC passive circuit, respectively. In this sensor, capacitance C changes due to the vary of liquid level leading to a drift of the resonant frequency. This drift in resonance frequency can be estimated through analyzing the reflection coefficient S11 monitored by using reading coil connected to network analyzer system [2]. Fig.1b showed the reflection coefficient S11 when level of pure water changed from 0 to 175 mm. when the water level increased from 0 to 175 mm, the estimated resonant frequencies decreased from 39.8 down to 22.8 MHz. Based on two parallel capacitor model for this sensor, the linear dependence of $1/f_{res}^2$ vs. water level was investigated and shown as Fig.1c with a high correlation factor of $R^2=0.995$. The sensitivity of sensor was estimated to be $7.39 \times 10^{-6} \text{ MHz}^{-2}/\text{mm}$. Because of contactless, low-cost, small size and easy fabrication, this sensor is potential candidate for using in liquid level measurement of harsh environments such as oil liquid, toxic liquid, acid solution, etc..

Keywords: LC wireless passive, contactless liquid level measurement, wireless contactless sensor, LC passive resonant circuit

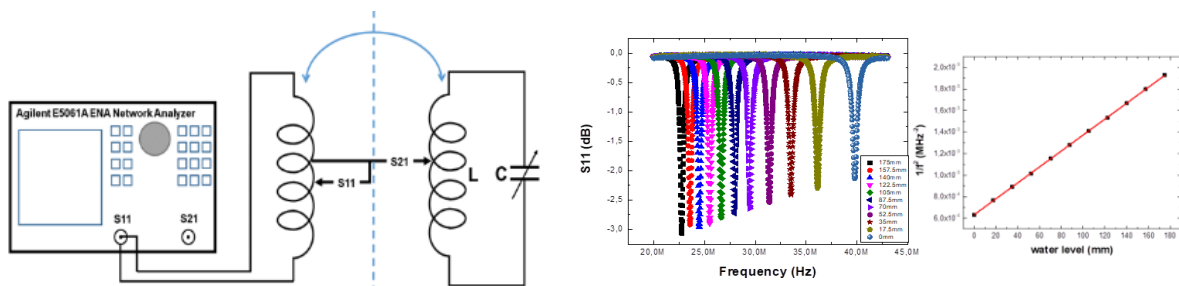


FIG. 1. (a) Principal sensor operation. (b). Reflection coefficient S11 vs. water level. (c) Linear dependence of $1/f_{res}^2$ vs. water level

References

- [1] Huang, Q. A., et al., Journal of Microelectromechanical Systems, 25(5), 822–841.
- [2] Do Quang, L., et al., IEEE Sensors Journal, 19(15), 6371 - 6380.

SD-P06 (Poster)

Plasma-assisted exfoliation of graphene from graphite: is graphene truly exfoliated?

Minh Nhat Dang^{1*}, Hong Phan Ngoc², Hong Tuan Nguyen², James Wang¹

¹ Australian Research Council (ARC) Industrial Transformation Training Centre in Surface Engineering for Advanced Materials (SEAM), School of Engineering, Swinburne University of Technology, Hawthorn VIC 3122, Australia

² Centre for Advanced Materials Technology Development, Centre for High Technology Development, Vietnam Academy of Science and Technology (VAST), 18 Hoang Quoc Viet, Hanoi 100000, Vietnam

*Corresponding author's e-mail: nhatminh@swin.edu.au

Graphene is an amazing material, exhibiting vast superior properties with numerous applications ranging from environmental treatment, concrete reinforcement, and energy. Among two approaches to graphene making: bottom-up from gaseous or liquid carbon-based precursors and top-down from graphitic sources, synthesising graphene directly from graphite remains the key method for industrial scale-up due to its availability, low cost, and large quantity of products per production. Chemical and mechanical exfoliation have dominated the graphite-to-graphene synthesis pie; however, irradiation exfoliation, particularly plasma-assisted electrochemical exfoliation, has been reported as a promising methodology for graphene synthesis in many recent works due to its novelty, ease of setup, and lack of toxic byproducts. Herein, in this talk, we will discuss how graphene is made from the so-called plasma-assisted "exfoliation" process, and the mechanism of exfoliation for arc discharge in both air and liquid media.

Keywords: graphene, plasma, electrochemical process, exfoliation, arc discharge.

SD-P07 (Poster)**Ultrafast and precessional magnetization dynamics in magnetic tunnel junctions (MTJ) for neuromorphic computing**

Tahereh Sadat Parvini^{1*}, Tim Boehnert^{2*}, Luana Benetti², Elvira Paz², Jakob Walowski¹, Ricardo Ferreira², Markus Muenzenberg¹

¹ Institute für Physik, Universität Greifswald, Greifswald, Germany

² INL, Avenida Mestre José Veiga, s/n, 4715-330 Braga, Portugal

* Corresponding author's e-mails: tahereh.parvini@uni-greifswald.de, tim.boehnert@inl.int

We develop new Magnetic Tunnel Junction (MTJ) layer-stacks with low energy requirements, thus, low critical current or in other words low oscillation threshold. The structures of the stacks are 5Ta/ 50CuN/ 5Ta/ 50CuN/ 5Ta/ 5Ru/ 6IrMn/ 2CoFe30/ 0.825Ru/ 2.6CoFe40B20/ MgO/ 2.0CoFe40B20/ 0.21Ta/ 6CoFeSiB/ 2Ta/ 4Ru (Si-MTJ) and 5Ta/ 50CuN/ 5Ta/ 50CuN/ 5Ta/ 5Ru/ 6IrMn/ 2CoFe30/ 0.825Ru/ 2.6CoFe40B20/ MgO/ 2.0CoFe40B20/ 0.21Ta/ 7NiFe/ 2Ta/ 4Ru (Py-MTJ), all thicknesses are in nm. The aim is to manipulate the oscillation via optical access, in our laboratory by using femtosecond laser

pulses on the route towards ultrafast spintronics. In our study, the oscillation frequency and effective damping parameters are investigated by using the time-resolved magneto-optical Kerr effect (TRMOKE) microscope as a function of the intensity and direction of the external magnetic field, the intensity of the pump, and cap layer thicknesses. We have shown that by changing the thickness of the capping layer Ta from 2-10nm and fixed Ru 4nm, there is no significant change in the oscillation frequency and effective damping constant. Our results show the temperature difference between cap layer and magnons in magnetic layers is the driving force for spin current generation by ultrafast demagnetization. This study paves the way for developing ultrafast spintronic devices for data storage and information processing. The research is part of the FET-open project SpinAge to develop neuromorphic chips. The final neuromorphic chip designed within the SpinAge consortium device will combine optical access, memristive parts and to spintronic oscillators in one neuron mimicking device. The work has received funding from the European Union's Horizon 20220 research and innovation program under grant agreement No. 899599 (project SpinAge).

Keywords: Magnetic Tunnel Junctions, TRMOKE, neuromorphic computing

References

- [1] G.-M. Choi, J. H. Oh, D.-K. Lee, S.-W. Lee, K. W. Kim, M. Lim, B.-C. Min, K.-J. Lee, and H.-W. Lee, Nat. Commun. 11, 1 (2020).
- [2] G.-M. Choi, B.-C. Min, K.-J. Lee, and D. G. Cahill, Nat. Commun. 5, 1 (2014).
- [3] C. Gonçalves, A. Silva, D. Navas, M. Miranda, F. Silva, H. Crespo, and D. Schmool, Sci. Rep. 6, 1 (2016).
- [4] B. Khodadadi, J. B. Mohammadi, J. M. Jones, A. Sri-vastava, C. Mewes, T. Mewes, and C. Kaiser, Phys. Rev. Appl. 8, 014024 (2017).
- [5] Y. Zhang, G. Wu, Z. Ji, X. Chen, Q. Jin, and Z. Zhang, Phys. Rev. Appl. 17, 034033 (2022).
- [6] W. Wang, P. Li, C. Cao, F. Liu, R. Tang, G. Chai, and C. Jiang, Appl. Phys. Lett. 113, 042401 (2018).

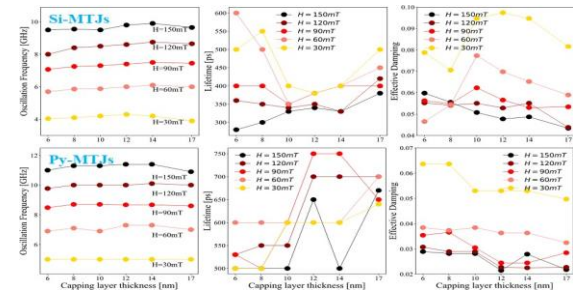


FIG. 1. The precession frequency, lifetime, and effective damping constant as a function of capping layer thickness and external magnetic field H .

SD-P08 (Poster)**Charge trapping memory device based on heterostructure of MoS₂ FET and CrPS₄**

Minjeong Shin¹, Mi Jung Lee¹, Chansoo Yoon¹, Tran Minh Duc¹, Je-Geun Park², Sungmin Lee², Bae Ho Park^{1,*}

¹ Dept. of Physics, Konkuk University, Seoul 05029, Korea

² Dept. of Physics and Astronomy, Seoul National University, Seoul 08826, Korea

* Corresponding author's e-mails: baehpark@gmail.com

Atomically thin two-dimensional (2D) materials have emerged as promising candidates for flexible and transparent electronic applications. Here, we introduce non-volatile charge trapping memory devices, based on the 2D heterostructure field-effect transistor consisting of a few-layer MoS₂ channel and CrPS₄ charge-trapping gate stack. Clockwise hysteresis behaviors in transfer curves measured at room temperature show a strong dependence on the thickness of CrPS₄, which are attributed to charge trapping at trap sites in the CrPS₄ layers [1]. Our heterostructure memory device with 75 nm thick CrPS₄ layer exhibits both large memory windows up to 99.7 V and high on/off current ratio (3×10^5) with good endurance during 625 cycles. Also, non-volatile memory property is obtained because of its excellent trapping ability of trap sites in the CrPS₄. Especially, the memory window size can be effectively tuned from 7.6 V to 99.7 V with high on/off current ratio by changing the sweep range of back gate voltage from 10 to 60 V at drain voltage, $V_D = 0.1$ V as shown in Fig. 1. Such high performances of the charge trapping memory device with a simple heterostructure provide a promising route towards next-generation memory devices utilizing 2D materials [2].

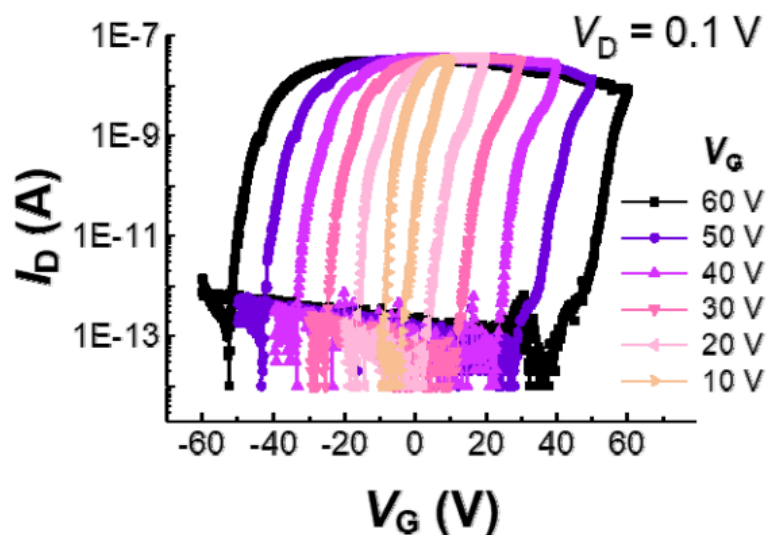


FIG. 1. Transfer characteristics of MoS₂ FET on bulk-like CrPS₄ with different sweeping range of V_G from 10 V to 60 V at $V_D = 0.1$ V

Keywords: Heterostructure, 2D materials, MoS₂, CrPS₄, TMDC, TMPS, FET, Memory

References

- [1] J. Lee and S. Pak et al, Nat. Commun. 8, 14734 (2017).
- [2] Q. Wang and Y. Wen et al, Sci. Adv. 4, eaap7916 (2018).

SD-P09 (Poster)**Development of the high sensitive measurement system to investigate the characteristics of magnetic fluids**Manh Xuan Vu^{1,2}, Tung Thanh Bui¹, Tu Dinh Bui¹, Binh Hai Nguyen³, Trinh Duc Chu^{1,*}¹University of Engineering and Technology, Hanoi Vietnam National University, Hanoi, Vietnam²Center for Microelectronic and Information Technology, National Center for Technological Progress, Hanoi, Vietnam³Institute of Materials Science, Vietnam Academy of Science and Technology, Hanoi, Vietnam

* Corresponding author's e-mails: trinhcd@vnu.edu.vn

In this paper, a very high magnetic field-sensitive measurement system based on a giant magnetometer resistance (GMR) sensor was developed to determine the relationship between the magnetization of superparamagnetic nanoparticles (SPMNP) in the liquid and the excitation magnetic field. The microfluidic device was integrated includes a microfluidic channel with a modified GMR sensor (bonded to a printed circuit board). It was placed in a highly uniform magnetic field that was generated by two Helmholtz coil pairs, which emit magnetic fields in perpendicular directions to magnetize the SPMNPs and define a linear working point for the GMR sensor. The system was used to determine the induced magnetic field of superparamagnetic nanoparticles (BSPMNPs) under the excitation magnetic field. The induced magnetic field, BSPMNPs, was used to calculate the magnetization of the SPMNPs, M , based on the construction of the measuring system and the excitation magnetic field. The proposed system was investigated using superparamagnetic- Fe_3O_4 fluids with diameter of 60 nm, saturation magnetization of 60 emu/g and a concentration of 4.64 mg/mL. A sine wave excitation magnetic field with a frequency of 25 Hz and a variable amplitude in the range of 0–25.7 G was used to magnetize SPMNPs. The results show the properties of SPMNPs were measured by the proposed measurement system and the vibrating sample magnetometer (VSM) system. This method allows to measure the magnetic properties of SPMNPs in liquid instead of measuring on dry samples like the two traditional methods, VSM and PPMS (physical property measurement system).

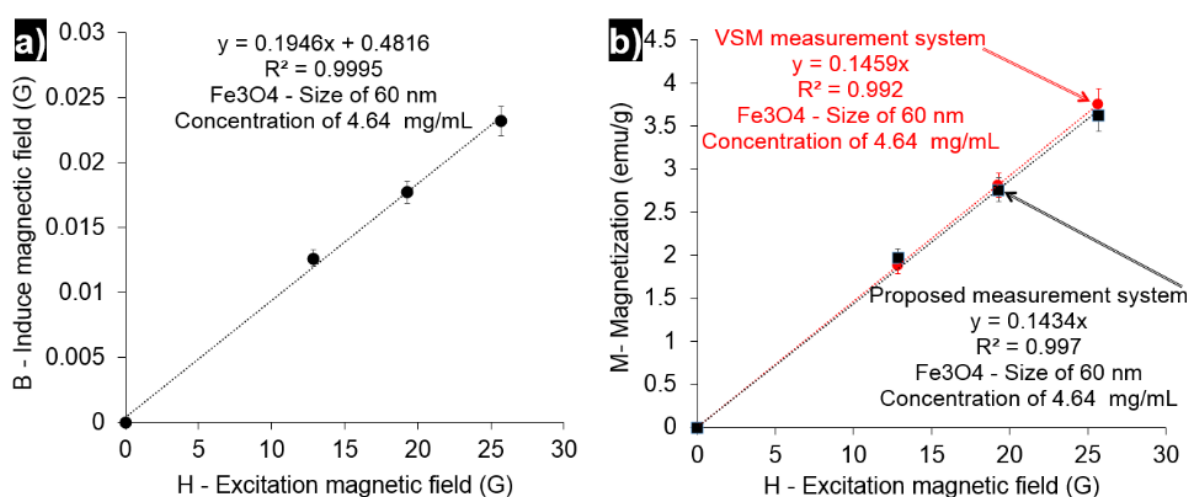


FIG. 1: a) The relationship between the induced magnetic field of SPMNPs in the liquid and the excitation magnetic field was measured by the proposed.

Keywords: GMR, microfluidics, Fe_3O_4 , magnetic fluids

Session: Theory and Computation (TC)

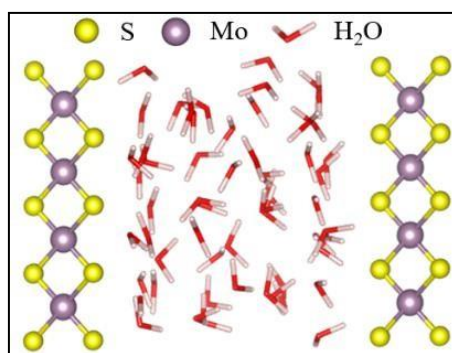
TC-P01 - TC-P07

TC-P01 (Poster)**Water molecular behavior at solid/liquid interfaces examined by abinitio molecular dynamics**Kaiyuan Yao^{1, *}, Susumu Fujii^{1, 2}, Masato Yoshiya^{1, 2}¹ Division of Materials and Manufacturing Science, Osaka University, Osaka, 565-0871, Japan² Japan Fine Ceramics Center, Nagoya, 456-8587, Japan

* Corresponding author's e-mail: Kaiyuan.Yao@mat.eng.osaka-u.ac.jp

Solid/liquid interfaces are ubiquitous in nature and the understanding of their atomic-level structure is crucial for elucidating the atomic mechanism behind reactions occurring on interfaces. Hydrogen evolution reaction (HER) is one of them, which is the dominating process of producing hydrogen upon using as clean energy. Furthermore, a preceding study has found the behavior of water molecules near the catalyst surface does influence the efficiency of HER^[1]. Thus, in this study, we used ab initio molecular dynamics (AIMD) simulation in order to figure out the behavior of water molecules and possible influence on the detailed mechanism behind the reaction. Here, we modelled three kinds of solid/liquid interfaces with different solid phases. The first two are pure metals: Pt and Au, which are well-known as highly efficient HER catalysts. The third one is MoS₂, a newly known low-cost promising candidate for HER catalyst^[2] with totally different interfacial features. Then, we carried out AIMD simulation to statistically analyses the behavior of water molecules on different interface models.

It turns out in all three models that the water density shows two peaks near the interface, which reveals the extraordinary molecular behavior. To investigate the details, we calculated (1) the angle between the O–H bond of water and the surface normal and (2) the angle between the water bisector and the surface normal of the interfacial water. Finally, the results show the distinct difference of molecular behavior between water on the metals and those on the MoS₂

Keywords: solid/liquid interface, AIMD simulation, MoS₂FIG. 1. MoS₂/water interface model.

Acknowledgments: This work was supported by JSPS Grant-in-Aid for Scientific Research on Innovative Areas ‘Crystal Defect Cores’ (JP19H05786, JP20H06195) and Scientific Research (20K05062).

References

- [1] Li, Chao-Yu, et al. Nature materials 18.7 (2019): 697-701.
- [2] Voiry, Damien, et al. Nano letters 13.12 (2013): 6222-6227.

TC-P02 (Poster)**Extraction of local structural information from x-ray absorption spectra: machine learning approaches**Megumi Higashi¹, Hidekazu Ikeno^{1,*}¹ Department of Materials Science, Osaka Metropolitan University, 599-8570, Japan

*Corresponding author's e-mail: h-ikeno@omu.ac.jp

X-ray absorption spectroscopy (XAS) is a useful technique for characterizing local atomic and electronic structures in materials. Theoretical fingerprint matching based on first-principles calculations is the most quantitative method for extracting local structures and local electronic states from XAS experimental spectra¹. Recently, machine learning approaches have been proposed to predict XAS from atomic structures to avoid the high computational cost of first-principles calculations. The results are being obtained in research on predicting XAS spectra from given information of atomic structures². Attempts have also been made to extract physical properties such as bond distances, ionic bonding properties, and radial distribution functions from XAS spectra. However, no machine learning model that predicts three-dimensional local atomic structure from XAS spectra.

In this work, we constructed machine learning models to predict structural descriptors that numerically represent the atomic structures in three dimensions. The neural network models that predict radial distribution functions (RDF) and orbital-field matrix (OFM)³, which is a descriptor that deals with the anisotropy of the local structure, the valence electron number of the ligand, and orbital information, were constructed. We used more than 120,000 O K-edge XAS spectra data from the Materials Project database as the training data set. We successfully constructed models that roughly predicted radial distribution functions with 80.4% of the test data. Furthermore, the model that predicted OFM also captured an overview of OFM in 83.0% of the test data. These results demonstrate that the atomic structural information can be directly extracted from XAS spectra by using neural network models.

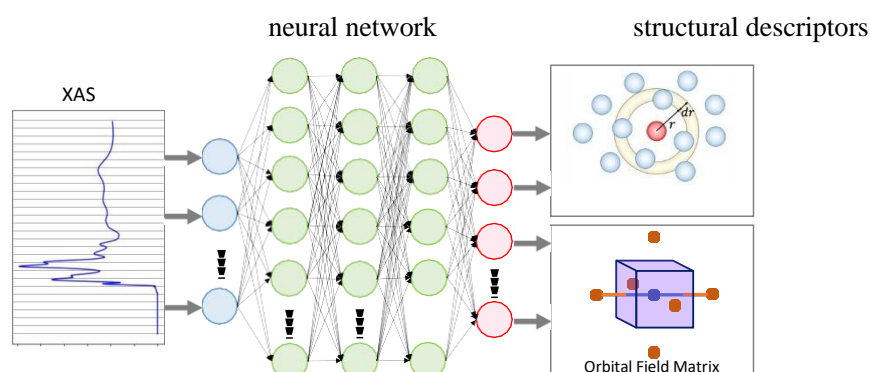


FIG. 1. Schematic representation of the neural network for predicting structural descriptors from XAS spectra.

References

- [1] H. Ikeno and T. Mizoguchi, *Micron* 66, 205 (2017).
- [2] S. Kiyohara, M. Tsubaki, T. Mizoguchi, *Npj Comput. Mater* 6, 1 (2020).
- [3] T. L. Pham, H. Kino, K. Terakura, et al., *Sci. Technol. Adv. Mater* 18, 756 (2017).

TC-P03 (Poster)**First-principles study on hydrogen adsorption and dissociation on Palladium clusters embedded in Zr-UiO-67 metal-organic frameworks**

Thong Nguyen-Minh Le^{1, *}, Trang Nguyen-Thuy², Tan Le Hoang Doan¹, Toan Nguyen The², Thang Phan Bach¹, Duc Nguyen-Manh³

¹ Center for Innovative Materials and Architectures, Vietnam National University Ho Chi Minh City, Ho Chi Minh City, Vietnam

² Key Laboratory for Multiscale Simulation of Complex Systems, University of Science, Vietnam National University – Hanoi, Hanoi, Vietnam

³ CCFE, United Kingdom Atomic Energy Authority, Abingdon, OX14 3DB, UK

* Corresponding author's e-mail: lnmthong@inomar.edu.vn

Hydrogen storage via hydrogen spillover effects is the key to enhancing storage capacity at room temperatures [1, 2]. Palladium clusters have been widely known for their efficiency to dissociate hydrogen molecules into hydrogen atoms for spillover activation [2]. Embedding palladium clusters on metal-organic frameworks (MOFs) is important in practical manipulations [3, 4]. In this work, we incorporate palladium clusters (Pd_n , $n=1-4$) into both the pristine and defective UiO-67 MOF structures to investigate the influence of the interaction between palladium clusters and host materials on hydrogen adsorption and dissociation. Results from density functional theory calculations (DFT) showed that the binding energies per palladium atom are higher in the pristine structure than that in defective ones because palladium clusters prefer chemical binding to the benzene linkers of the pristine instead of the metal nodes in the defect. The hydrogen adsorption energies on Pd_n embedded in pristine UiO-67 are increasing with the cluster sizes, in a range from 0.20 eV to 0.80 eV, while that trend is reversed for the adsorption on free Pd_n clusters and Pd_n embedded in defective UiO-67. It is predicted that the strong bindings of Pd_n with linkers in pristine UiO-67 suppress the electrostatic interaction of the clusters with hydrogen molecules. The dissociation of hydrogen molecules occurs easily without energy barriers on both free Pd_n clusters and Pd_n embedded in defective UiO-67, with $n=2$ and $n=3$, while it remains in molecular form for Pd_n in the pristine structures. The dissociation energy barriers for $n=4$ are comparable for all studied structures, i.e., in a range from 0.18 eV to 0.38 eV. The findings reveal that hydrogen adsorption energies on palladium clusters are notably affected by the incorporation of metal clusters on different host materials, but the dissociation energy barriers are less influenced.

Keywords: palladium clusters, metal-organic frameworks, hydrogen dissociation barriers, first-principles calculations

References

- [1] Li, Y. and R.T. Yang, J. Am. Chem. Soc., 2006. 128(3): p. 726-7.
- [2] Blanco-Rey, M., et al., J. Phys. Chem. C, 2016. 120(31): p. 17357-17364.
- [3] Lestari, W.W., et al., Mater. Res. Express, 2019. 6(8).
- [4] Li, Y. and R.T. Yang, J. Am. Chem. Soc., 2006. 128(25): p. 8136-7.

TC-P04 (Poster)**Novel few-layer nanosheets from layer structured gallium chalcogenides: structural, electronic and mechanical properties**Vu Ngoc Tuoc^{1, *}, Le Thi Hong Lien¹, Nguyen Ngoc Tuan¹ and Tran Doan Huan²¹ Institute of Engineering Physics, Hanoi University of Science and Technology, 1 Dai Co Viet Rd., Hanoi 10000, Vietnam² School of Materials Science and Engineering, Georgia Institute of Technology, 771 Ferst Dr. NW, Atlanta, Georgia 30332, USA

* Corresponding author's e-mail: tuoc.vungoc@hust.edu.vn

The low-dimensional gallium chalcogenide group semiconductors have recently emerged as interesting candidate materials for the tailoring of two dimensional (2D) layered structures due to their intriguing optical and electronic properties derived by the van der Waals bonding between layers. Herein, two novel series of few-layer nanosheets from gallium sulphur binary compound Ga₂S₃ and Ga₂S₅ are proposed. We have performed the first principle calculations on the structural, electronic and mechanical properties of suggested nanosheet series, to investigate the effects of structural modification and sheet thickness on their structural, electronic, and mechanical properties. Optimized geometries, formation energy, phonon spectra, electronic band structure, and elastic tensor calculation has ensured the energetically, dynamical and mechanical stability for the nanosheets. Furthermore, the theoretically found nanosheet series possess a direct band gap which are different from the well-known. GaS nanosheet series. These highly anisotropic semiconductor nanosheet series and their derivatives are expected to have broad applications in photocatalysis, and new generation nanoelectronic devices.

Keywords: Nanosheet, DFT, Gallium Chalcogen, structure prediction**References**

- [1] V.N. Tuoc, T.D. Huan, Lead-free hybrid organic-inorganic perovskites for solar cell applications, J. Chem. Phys. 152, 014104 (2020).
- [2] S. Yazdani, V.N. Tuoc, R. K. Sadabad, M. D. Morales-Acosta, Huan T.D., M. Zhou, Yufei Liu, J. He, R. D. Montaño, M. T. Pettes, Thermal transport in phase-stabilized lithium zirconate phosphates, Appl. Phys. Lett. 117, 011903 (2020) (2020)
- [3] V.N. Tuoc, N.T. Thao, L.T.H. Lien, P.T. Liem, Novel Chain and Ribbon ZnO Nanoporous Crystalline Phases in Cubic Lattice. Phys. Stat. Solidi B, 2100067 (2021).
- [4] P.T. Minh, E. Amerling, N.T. Anh, H.M. Luong, K. Hansen, L. Whitaker, T.D. Huan, P.T. Huy, Strong Rashba-Dresselhaus Effect in Non-chiral 2D Ruddlesden-Popper Perovskites, Adv. Optical Mater. 2021, 2101232.
- [5] V.N. Tuoc, Nga T. T. Nguyen, V. Sharma, and T.D. Huan, Probabilistic deep learning approach for targeted hybrid organic-inorganic perovskites, Physical Review Materials 5, 125402 (2021).

TC-P05 (Poster)

Magneto-optical absorption in a borophene monolayer with titled Dirac cones: effect of electron - optical phonon coupling

Bui Dinh Hoi*

Department of Physics and Center for Theoretical and Computational Physics, University of Education, Hue University, Vietnam

* Corresponding author's e-mail: buidinhhoi@hueuni.edu.vn

Two-dimensional (2D) Dirac materials have extraordinary properties and numerous potential applications. $8Pmmn$ -borophene is a 2D Dirac material with titled Dirac cones that promise many interesting optical transitions. In this work, we theoretically investigated the magneto-optical absorption properties in a monolayer $8Pmmn$ -borophene placed in a perpendicular static magnetic field and an electromagnetic wave. Utilizing the perturbation theory, the absorption coefficient (AC) was calculated considering the electron - optical phonon scattering. The resonant absorption peaks were observed in the absorption spectra. The dependence of the full width at half maximum of resonant peaks on the magnetic field and temperature was obtained. Effect of the titled Dirac cones was also considered by via the polarity of the AC versus valley indices. The obtained results are the basis for further studies on the applications of borophene to nano-optoelectronic devices and valleytronics.

Keywords: magneto-optical absorption; absorption coefficient; electron – phonon coupling; Dirac material; borophene

TC-P06 (Poster)**Controllable electronic properties and contact types of metal/semiconductor MoSH/MoSi₂N₄ heterostructure**Cuong Q. Nguyen^{1,2}, Le M. Duc³, Yee Sin Ang⁴, Nguyen V. Hieu⁵, Chuong V. Nguyen^{3,*},¹ Faculty of Physics, College of Education, Hue University, Hue 47000, Vietnam² Institute of Research and Development, Duy Tan University, Da Nang 550000, Vietnam³ Department of Materials Science and Engineering, Le Quy Don Technical University, Ha Noi 100000, Vietnam⁴ Science, Mathematics and Technology (SMT), Singapore University of Technology and Design (SUTD), Singapore 487372, Singapore⁵ Physics Department, The University of Danang - University of Science and Education, Da Nang 550000, Vietnam

* Corresponding author's e-mail: chuong.vnguyen@lqdtu.edu.vn

Following the successful synthesis of single-layer metallic Janus MoSH and semiconducting MoSi₂N₄, we investigate the electronic and interfacial features of metal/semiconductor MoSH/MoSi₂N₄ van der Waals (vdW) contact. We find that the metal/semiconductor MoSH/MoSi₂N₄ contact forms p-type Schottky contact (p-ShC type) with small Schottky barrier (SB), suggesting that Janus MoSH can be considered as an efficient metallic contact to MoSi₂N₄ semiconductor with high charge injection efficiency. The electronic structure and interfacial features of the MoSH/ MoSi₂N₄ vdW heterostructure are tunable under strain and electric fields, which give rise to the SB change and the conversion from p-ShC to n-ShC type and from ShC to Ohmic contact. These findings could provide a new pathway for the design of optoelectronic applications based on metal/semiconductor MoSH/MoSi₂N₄ vdW heterostructures [1].

Keywords: Electronic properties; First-principles calculations; van der Waals heterostructures; Contact types.

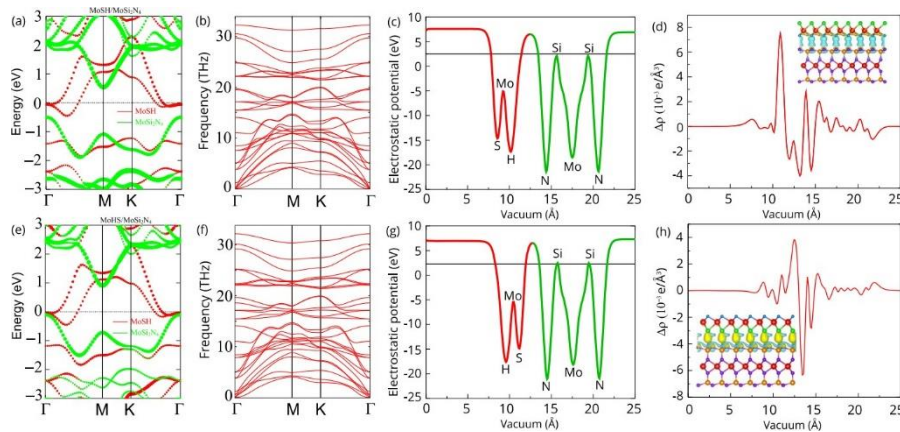


FIG. 1. (a and e) Orbital-projected band structures, (b and f) phonon dispersion curves, (c and g) plane-averaged electrostatic potentials, and (d and h) planar average charge density differences of MoSH/MoSi₂N₄ and MoHS/MoSi₂N₄ HTSs. The MoSH and MoSi₂N₄ layers are separated by red and green circles, respectively. The charge accumulation is depicted by yellow, and the charge depletion is illustrated by cyan.

References

[1] Chuong V. Nguyen et al., J. Phys. Chem. Lett. 13 (2022) 2576–2582

TC-P07 (Poster)**Quantum theory of the effect of increasing weak electromagnetic wave by a strong laser radiation in 2D Graphene**Tran Anh Tuan¹, Nguyen Dinh Nam^{1,*}, Nguyen Thi Thanh Nhan¹, Nguyen Quang Bau¹¹ Faculty of Physics, VNU-HUS, Hanoi, Vietnam

* Corresponding author's e-mail: nguyendinhnam@hus.edu.vn

Analytic expressions for the absorption coefficient (AC) of a weak electromagnetic wave (EMW) in 2D Graphene under influence of a strong laser radiation are calculated using the quantum kinetic equation for electrons in the case of electron-optical phonon scattering. The dependence of the AC on the intensity E_{01} and the frequency Ω_1 of a weak EMW, on the intensity E_{02} and the frequency Ω_2 of a strong laser radiation, on the temperature T of the system and on the parameters of 2D Graphene is obtained. The numerical results show that the AC of a weak (EMW) in 2D Graphene can have negative values. This demonstrates the possibility of increasing weak electromagnetic wave by a strong laser radiation in 2D Graphene. This is different from the similar problem in bulk semiconductors and from the case without strong laser radiation.

Keywords: absorption coefficient, electromagnetic wave, 2D Graphene, quantum kinetic equation

SPONSORS



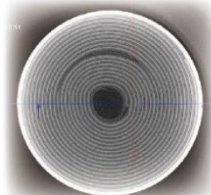
SGService has many years experience on X-ray analysis techniques by using synchrotron facility and in-house equipments. Contact with us now to know more!

In-house X-ray Computed Tomography (CT)

3D IC Chip



18650 Battery

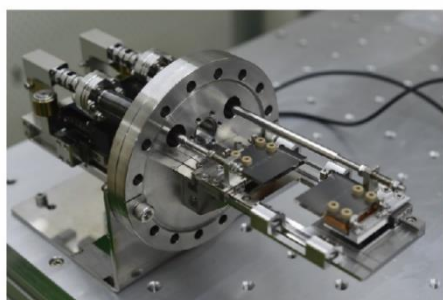


3 μ m Powder

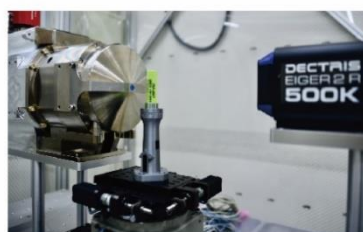


X-ray Components

X-ray Vacuum Slits



In-house X-ray CT

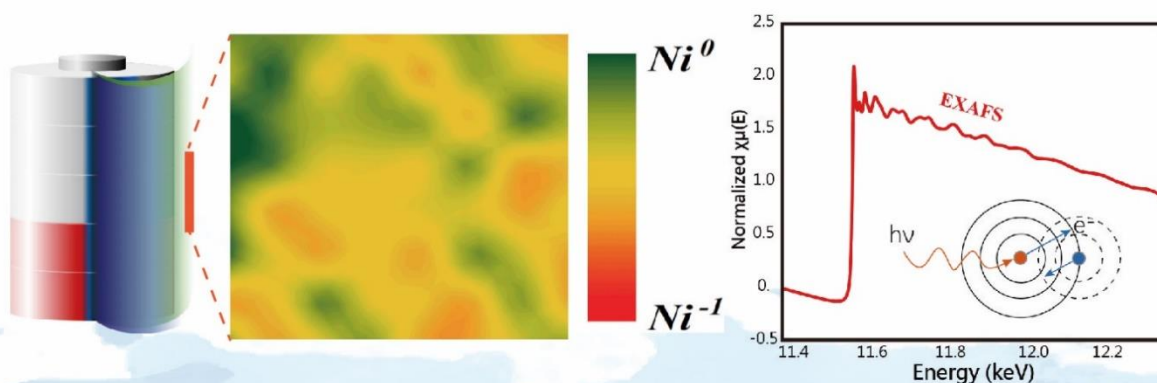


Our team has extensive experience in designing and manufacturing X-ray inspection equipment, including X-ray Computed Tomography (CT), Small-Angle X-ray Scattering (SAXS) for polymer applications, X-ray Laue Diffraction for metal materials defects and stress detection, Nano-beam X-ray Fluorescence (XRF) Imaging for micro-area element distribution, etc.





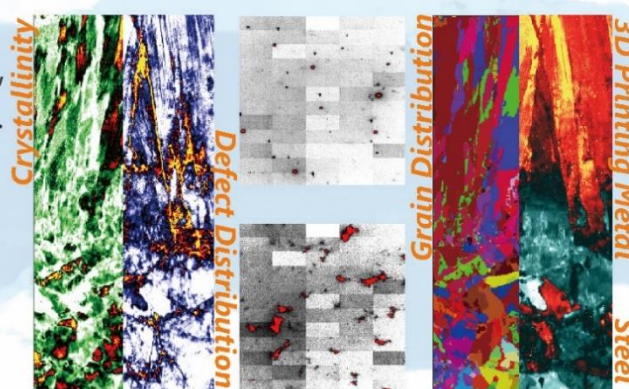
Nano-Beam X-Ray Absorption Mapping (2D n-XAS)



This technique provides images about the valence state distributions, coordination number, and bonding length of elements, which helps to develop and improve materials. As this method has very few restrictions on the sample type, it can be performed on solids, liquids, or even gaseous samples. Besides, in-situ experiment can also be conducted.

Nano-Beam X-Ray Nanodiffraction (2D n-XRD)

X-ray images provide real-space information. High-brightness synchrotron light sources provides high-quality imaging results. By using highly focusing X-ray beam down to 80 nm, it can be used to understand the internal crystal structure, chemical composition, and physical properties of materials.



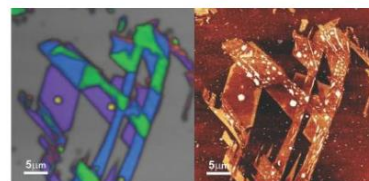
HORIBA



AFM - Raman
XploRA Nano

Key applications:

- 1D, 2D materials (Graphene, MoS2...)
- TERS Characterization of Nanoparticles
- Polymers, organic molecules
- Stress in semiconductors
- ...



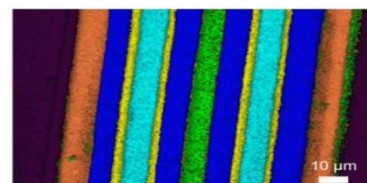
Raman-AFM co-localization image of graphene



Raman Microscope
Labram HR Evolution

Key applications:

- Routine analysis for Graphene and 2D materials, polymers and monomers, inorganics and metal oxides, ceramics, coatings and thin films, photovoltaics, catalysts
- Stress/strain measurement, alloy composition, chip structures, band gap analysis
-



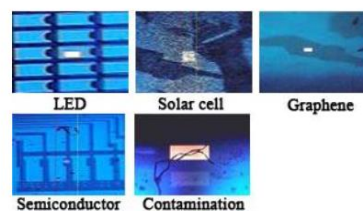
Multilayer film characterization by Raman mapping



Ellipsometry
UVISSEL Plus

Key applications:

- Thickness, optical constant
- Material/surface modification
- Roughness, porosity
- Gradient layer, interface
- Transmission, reactivity curve
- ...



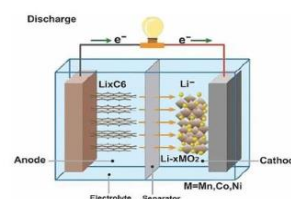
Real-time colour image of the sample and exact measurement spot



GD-OES
GD - Profiler 2

Key applications:

- Fast, simultaneous depth profile analysis of elements
- Corrosion study
- PVD coating process control
- Characterization of Electrodes of Li-ion Batteries
- ...



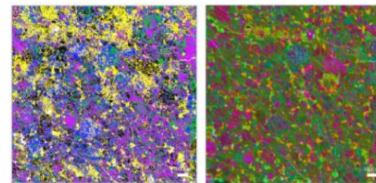
Electrode and Li-ion move reversely at charging



**X-Ray Analytical
Microscope
XGT-9000**

Key applications:

- Non-destructive failure analysis on electronic components
- QC, counterfeit products, presence of foreign materials
- Particle analysis of film and battery
- Fast thickness measurement of thin metal coatings
- QC of semiconductors which feature thin and narrow patterns
- ...



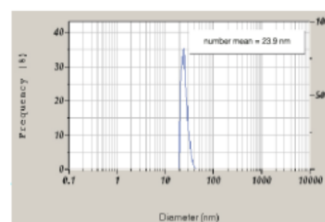
Maps of meteorite. (Left) Chemical Raman map. (Right) Elemental X-ray Fluorescence map



**Nano Particle Analyzer
nanoPartica SZ-100V2**

Key applications:

- Functional materials: metal nano, Colloidal Particles, catalyst, carbon nanotubes
- Polymers: Cellulose Nanofibers, Electrolytes, Adhesives
- Semiconductor: CMP Slurries
- Ceramics: Titanium Oxide, Silica, Aluminum Oxide
- Gel Materials: 3D Printer Materials, Medical Materials, Automobile Materials
- ...



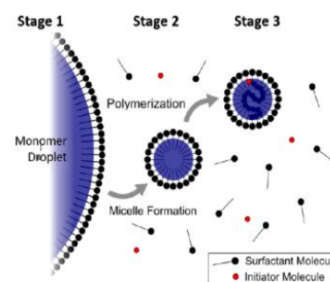
Colloidal copper particle size result



**Nano Particle Tracking
Analyzer
ViewSizer® 3000**

Key applications:

- Batteries
- Catalyst
- Nanoparticles
- Metal powder
- Polymer
- Semiconductor
-



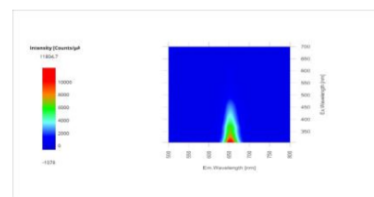
Schematic diagram showing the three stages of emulsion polymerization



**Fluorometer
Nanolog**

Key applications:

- Characterization of SWCNT
- Quantum Dot Absorbance, Photoluminescence Spectra and Lifetimes
- Measuring Silica Nanoparticles
- ...



A-TEEM™ for Qtracker® 655 quantum

HORIBA VIETNAM CO., LTD

Add: Lot 3-4, 16th Floor, Detech Tower II, 107 Nguyen Phong Sac Street,
Dich Vong Hau Ward, Cau Giay District, Hanoi, Vietnam

T: +84 24 3 7958 552 | F: +84 24 3 7958 553

W: <https://horiba.com.vn/> | E: info-sci.vn@horiba.com



About us

Metrohm Vietnam is a subsidiary of Metrohm Group, one of the world's most trusted manufacturers of high-precision instruments for chemical analysis. Metrohm is present in more than 80 countries with our own subsidiaries and exclusive distributors

OUR VALUES AND MISSION

Metrohm analysis instruments and methods allow our customers to work in a more accurate, reliable, environmentally compatible, and cost-effective way.

OUR MISSION

- Understanding our customers and their needs and delivering pioneering products and services for professional and sustainable solutions.
- Thinking globally, acting locally and focusing on intensive and innovative in-house development.
- Maintaining our financial independence.

OUR PRODUCTS – COMPREHENSIVE SOLUTIONS FOR CHEMICAL ANALYSIS

1. GLOBAL MARKET LEADER IN ANALYTICAL INSTRUMENTS FOR TITRATION ION CHROMATOGRAPHY (IC), PH AND CONDUCTIVITY MEASUREMENT, CVS, OXIDATION AND STABILITY TESTING

2. ONLINE PROCESS ANALYSIS: METROHM PROCESS ANALYTICS

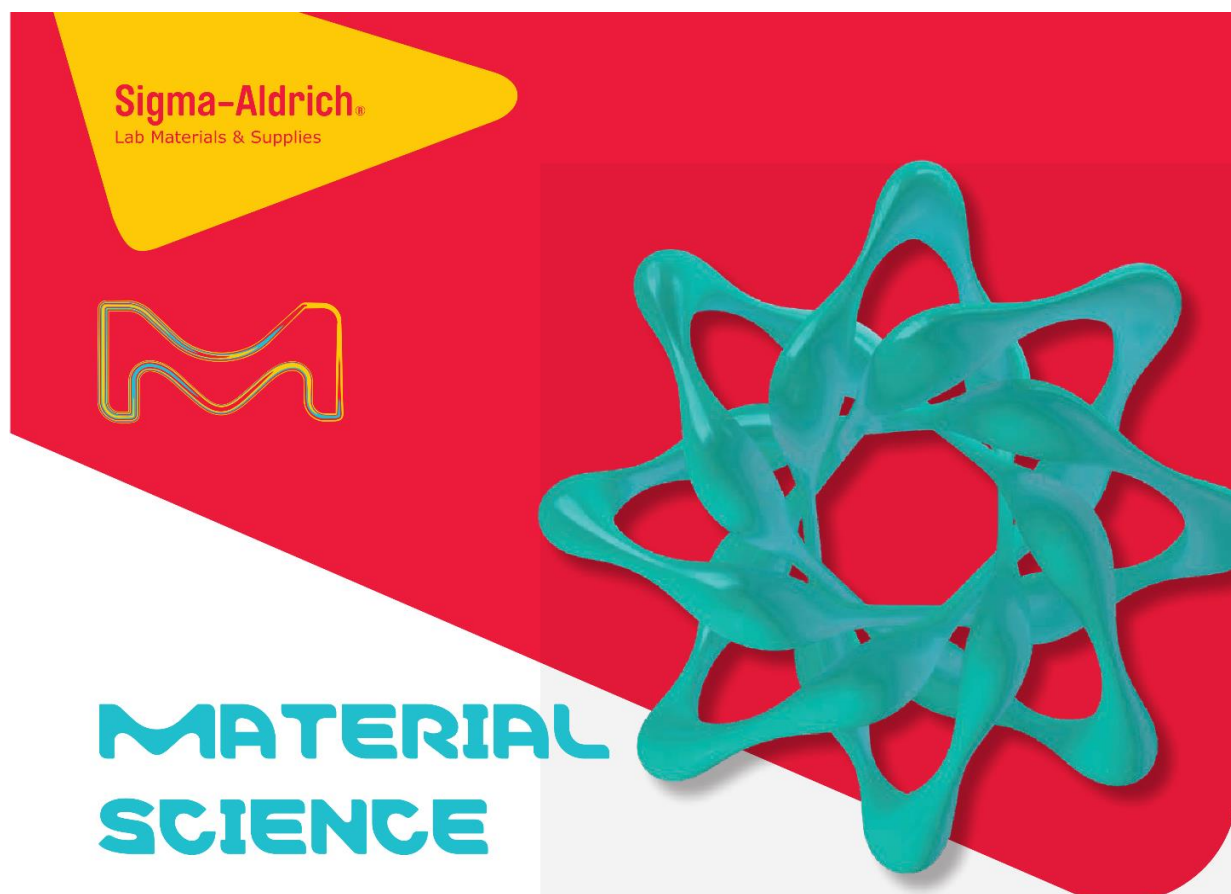
Taking our expertise in chemical analysis from the laboratory to industrial production sites, our colleagues at Metrohm Process Analytics, develop a wide range of rugged process analyzers for online process and industrial monitoring in a variety of industries.

3. ELECTROCHEMISTRY FOR RESEARCH AND DEVELOPMENT

Metrohm Autolab, based in the Netherlands, and **Metrohm DropSens**, based in Spain, develop and produce a comprehensive portfolio of instrumentation for electrochemistry, from high-quality potentiostat/galvanostats to customized screen-printed electrodes and accessories.

4. HANDHELD AND PORTABLE RAMAN SPECTROSCOPY ANALYZERS

These instruments are engineered and produced by two Metrohm subsidiaries in the USA: **Metrohm Raman** (Laramie, WY) and **B&W Tek** (Plainsboro, NJ). These instruments can be used for the identification of thousands of substances, such as illicit substances, hazardous materials, and drugs, as well as for the identification of raw materials in the production process.



Material Science portfolio & focus area



Visit us

merck-lifescience.com.vn

Merck Vietnam Company

Hotline: (084) 28 38 420 117

Email: MVN_LSMarketing@merckgroup.com

MERCK



MERCK

3-D printing better batteries

3-D Printable Inks for Energy Products make battery design faster, more flexible, more efficient and lower cost.

NEW!

R&D 100 Winners for 2022 are announced!

3-D Printable Inks for Energy Products of Merck won an R&D Top 100 Award in the Mechanical / Materials category.

This renowned worldwide science and innovation competition received entries from a dozen different countries. This year's esteemed judging panel included nearly 50 well-respected industry professionals from across the world.



Sigma-Aldrich®
Lab Materials & Supplies

MATERIAL MATTERS™

Special publications for Material Science

Register to receive Material Matters™ quarterly by scanning here:



The life science business of Merck operates as
MilliporeSigma in the U.S. and Canada.



AUTHOR INDEX

- A. Ata, 56
 A. Kuwabara, 91
 A. R. N. Hanna, 56
 A. T. M. N. Islam, 56
 Akari Onaka, 163
 Åkerman, 178
 Akihide Kuwabara, 44
 Akio Fukushima, 83
 Akira Masago, 112
 Akito Daido, 76
 Alexander S. Samardak, 76
 Alexey V. Ognev, 76
 Amane Morimura, 166
 An Bang Ngac, 97, 107, 185
 Anatoli Popov, 68
 Andreas Honecker, 85
 Andrzej Suchocki, 68
 Angelo Papageorgiou, 116
 Anh Son Pham, 123
 Anh Tuan Thanh Pham, 190
 Anh-Kiet Le, 122
 Anh-Quan Hoang, 122, 133
 Anh-Tuan Le, 140
 Anh-Tuyen Luu, 133
 Apoorva Sood, 79
 Asuka Ochi, 155
 Atsutomo Nakamura, 120
 B. Lake, 56
 B. W. Lee, 175
 Bach Huong Giang, 182
 Bach Thang Phan, 137
 Bach Thanh Son, 135, 148
 Bạch Thanh Son, 173
 Bae Ho Park, 75, 121, 167, 188, 189, 195
 Binh Hai Nguyen, 196
 Bo Wha Lee, 99
 Branislav Kunca, 61
 Brian J. Kirby, 65
 Bui Dinh Hoi, 201
 Bui Dinh Tu, 115, 170, 191
 Bui Duc Tri, 104
 Bui Nguyen Quoc Trinh, 142, 183
 Bui Thanh Tung, 50, 134
 Cao Phuong An, 129
 Ch. Thurn, 56
 Chang-woo Cho, 65
 Chansoo Yoon, 121, 167, 189, 195
 Chanyong Hwang, 74
 Chanyoung Hwang, 65
 Cheol Gi Kim, 177
 Chia-Chun Wei, 108
 Chu Duc Trinh, 50
 Chul-Hong Park, 65
 Chung-Li Dong, 114
 Chun-Liang Lin, 109
 Chuong V. Nguyen, 202
 Cong Doanh Sai, 97, 123
 Cong Thanh Bach, 169, 173
 Cuong Q. Nguyen, 174, 202
 Cz. Kapusta, 178
 Dahyun Kang, 54
 Daisuke Kobayashi, 161
 Dang Co Nguyen, 145
 Dang Duc Dung, 170
 Dang Khoa Nguyen, 43
 Dang Thanh Tran, 172
 Dang Thi My Nga, 142
 Dang Thi Thanh Thuy, 192
 Dang-Co Nguyen, 126
 Dao The Nam, 136
 Der-Hsien Lien, 111
 Dinh Lam Nguyen, 187
 Dinh Nguyen Ngoc, 171
 Dinh Tu Bui, 95, 145, 150
 Dinh Van Hai, 177
 Dinh-Tu Bui, 126
 Dmitrii B. Berezin, 147
 Do Hung Manh, 168
 Do Hong Minh, 183
 Do Khanh Tung, 168
 Do Quang Loc, 50, 192
 Do Thao Anh, 137
 Do Thi Huong Giang, 176, 177
 Do Trung Kien, 192
 Dong-Hyun Kim, 179
 Dong-Myeong Shin, 45
 Dong-Sing Wu, 79
 Dooyong Lee, 65
 Doukyun Kim, 65
 Duc Cuong Nguyen, 95, 127, 147
 Duc Hieu Nguyen, 180
 Duc Nguyen-Manh, 199
 Duc Thang Nguyen, 136
 Duy Hiep Nguyen, 180
 Duy Huy Nguyen, 169
 Duy-Khanh Pham, 122, 133
 E. Tamura, 66
 Ekkes Bruck, 48
 Elvira Paz, 194
 Fu-Gow Tarntair, 79
 Fuma Samejima, 181
 Fumitoshi Iga, 64
 G. S. Matthijs Jansen, 71
 G.L. Myronchuk, 68
 Genta Hayashi, 92
 Giang Huong Bach, 169
 Guy Stephens, 116
 Gwangtaek Oh, 188
 H. Kimura, 158
 H. Manh Dinh, 178
 H. Mori, 66
 H. N. Nhat, 175
 H. Nam Pham, 83
 H. Nomura, 66, 156

H. Yamamoto, 158	Jaebeom Lee, 69, 96, 140, 184
Ha Duc Chu, 138	Jakob Walowski, 194
Ha Thi Phuong Thao, 129	James Wang, 116, 193
Haeyong Kang, 65	Jeehoon Kim, 59
Hai Hoang, 78	Je-Geun Park, 195
Hajime Yamamoto, 58	Jenh-Yih Juang, 63
Hanh Kieu Thi Ta, 137	JeongEun Oh, 188
Harutaka Saito, 164	Jeonghyo Kim, 140
Heongkyu Ju, 110	Jessiel Saron Gueriba, 53
Hidekazu Ikeno, 102, 155, 198	Jin Young Kim, 70
Hideki Narita, 76	Jisoo Choi, 54
Hidenobu Murata, 102, 157	Jisung Lee, 65
Hikari Shinya, 112	Jiunn-Yuan Lin, 100
Hirofumi Tanaka, 94	Jiwoong Kim, 65
Hiroshi Nakamura, 53	Jozef Marcin, 61
Hiroyuki Tomita, 83	Jun Kue Park, 65
Hitoshi Fujii, 92	Jungmok Yang, 54
Hitoshi Kubota, 83	Jun-Ho Lee, 110
Ho Anh Tam, 176, 177	Junhyeok Bang, 179
Ho Khac Hieu, 78	K. Emoto, 66
Ho Ngoc Nam, 112	K. Hashimoto, 66
Ho Won Jang, 52	K. Inagaki, 98
Hoa Thi Lai, 190	K. Matsunaga, 89
Hoang Le, 116	K. Tung Do, 83, 178
Hoang Nam Nhat, 105, 182	Kaiyuan Yao, 197
Hoang Trang Nguyen, 127	Katsuhiko Suzuki, 92, 112, 119, 164
Hoang Tung Do, 128	Katsuyuki Matsunaga, 120
Hoang Van Huy, 129, 139, 149	Kazuma Midorikawa, 144
Hong Ky Vu, 172	Kazuma Ogushi, 92
Hong Phan Ngoc, 193	Kazunori Sato, 92, 112, 119, 164
Hong Tuan Nguyen, 116, 193	Kazuyuki Hirose, 161
Hong-Phuc Pham, 126	Kei Nakayama, 51
Hua Chiang Wen, 47	Kei Yakushiji, 83
Huan Tran, 93	Keiichi Koyama, 57, 151, 153, 159, 163, 165
Hung Ba Tran, 103	Khanh Tung Do, 172
Hung Manh Do, 172	Kien Cuong Dao, 136
Huong Thi Thu Le, 130	Kiminori Washika, 53
Huu-Quang Nguyen, 69, 96, 184	Kohki Takahashi, 151, 153
Huy Hoang Do, 123, 128	Kota Nakamoto, 151
Huy Tiep Nguyen, 150, 180	Kota Ryota Kobayashi, 153
Hyegyong Kim, 65	Koun Shirai, 86
Hyung Kook Kim, 121	La Thi Ngoc Mai, 142, 183
Hyung-Kook Kim, 45	Larissa. A. Maiorova, 136, 147
I. Hamada, 98	Le M. Duc, 202
I. Kézsmárki, 56	Le Thi Hong Lien, 200
I. Svito, 178	Le Thi Hong Phong, 168
I. Yamada, 158	Le Thi Huong, 135, 148
I.E. Barchiy, 68	Le Thi Thu Huong, 131, 135, 148, 173
Ikuya Yamada, 102, 152, 154, 155, 157, 160, 162, 166	Le Van Lich, 176, 177
Ippo Aoki, 154	Le Van Vu, 105, 173, 182
Isaac Oda-Bayliss, 157	Le-Hang Dang, 122
Ivan Skorvanek, 168	Lieu Nguyen Thi, 133
Ivan Škorvánek, 61	Linh Ho Thuy Nguyen, 125
J. Hyodo, 91	Linh Trung Nguyen, 145
J. Kasiuk, 178	Long Bien Le, 180
J. Przewoźnik, 178	Luana Benetti, 194
J. Zimmermann, 56	Luc Huy Hoang, 134
Jae Hyuck Jang, 65	Luong Thi Minh Thuy, 192
	Luong Trung Kien, 170

Luu Manh Quynh, 50, 104, 129, 139, 149	Nguyen Duy Thien, 105, 173, 182
M. Azuma, 158	Nguyen Hai Binh, 170, 191
M. Fukuda, 158	Nguyen Hai Pham, 97, 107, 185
M. Goto, 66, 156	Nguyen Hoang Luong, 50, 104
M. Lang, 56	Nguyen Hoang Nam, 50, 104, 139, 149
M. Winkler, 56	Nguyen Huu Duc, 176, 177
Mai Ha Hoang, 127, 136, 147	Nguyen Huy Cong, 191
Manami Goto, 152, 160	Nguyen Huy Dan, 170
Manh Xuan Vu, 196	Nguyen Huy Khan, 191
Manh-Huong Phan, 177	Nguyen Huy Ngoc, 170
Manh-Thuong Nguyen, 88	Nguyen Kien-Cuong, 186
Mark De Guire, 124	Nguyen Kieu Chang, 134
Markus Muenzenberg, 194	Nguyen Le Thi, 179
Markus Niederberger, 184	Nguyen N. Hieu, 174
Mary Clare Escaño, 90	Nguyen Ngoc Dinh, 105, 182, 183
Masahiko Tani, 90	Nguyen Ngoc Dinh, 173
Masahira Onoue, 163	Nguyen Ngoc Tuan, 200
Masako Ogura, 92	Nguyen Phuong Hoai Nam, 115
Masanobu Shiga, 64	Nguyen Quang Bau, 203
Masashi Akabori, 80	Nguyen Quang Hoa, 105, 173, 182
Masashi Ikegami, 161	Nguyen Quang Minh, 129
Masato Yoshiya, 87, 197	Nguyen Quoc Khanh, 149
Masaya Oshita, 157	Nguyen Thanh Binh, 131, 135, 148
Megumi Higashi, 198	Nguyen Thanh Tung, 72
Mi Jung Lee, 195	Nguyen Thi Mai Huong, 131, 135, 148, 173
Michal Piasecki, 68	Nguyen Thi Ngoc, 176, 177
Michihisa Koyama, 90	Nguyen Thi Thanh Nhan, 203
Mikhail Brik, 49	Nguyen Thi Thanh Van, 104
Mikhail G. Brik, 68	Nguyen Thi Thu Ha, 139
Minh Hieu Ho, 147	Nguyen Thi Thuy, 191
Minh Huy Dinh Dang, 125	Nguyen Thi Van Anh, 50, 106
Minh Nhat Dang, 116, 193	Nguyen Tran Truc Phuong, 137
Minh Phuong Le, 141, 143	Nguyen Trong Tinh, 131, 135, 148, 173
Minjeong Shin, 195	Nguyen Trung Hieu, 168
Minori Goto, 83	Nguyen Tuan Canh, 115
Miyoshi Fukumoto, 83	Nguyen V. Hieu, 202
Moongyu Jang, 54	Nguyen Van Loi, 142, 183
Moriharu Nagano, 159	Nguyen Van Tuan, 176, 177
My Ngoc Duong, 63	Nguyen Van Viet, 182
My-Chi Thi Nguyen, 69, 96	Nhat Linh Nguyen, 128
N. T. Dang, 175	Nhu Hoa Thi Tran, 137
Nadezhda M. Berezina, 147	Nhu Quynh Diep, 47
Nam Nhat Hoang, 145	Niem Tu Nguyen, 169
Nam-Nhat Hoang, 126	Noboru Miyata, 65
Naoki Masuyama, 102	Nur Ellina Annisa Salehuddin, 53
Naoki Ogi, 181	O.Y. Khyzhun, 68
Naoyuki Shibayama, 161	Oskar I. Koifman, 136
Neeraj Kumar, 65	P. Eibisch, 56
Ngo Tran, 99	P. Lunkenheimer, 56
Ngoc An Nguyen, 95, 138	Peter Švec, 61
Ngoc Quang Tran, 132	Pham Duc Thang, 170
Ngoc Xuan Dat Mai, 137, 146	Pham Nguyen Hai, 139
Ngoc-Anh Nguyen, 122	Pham Thi Minh Hanh, 78
Ngoc-Quyen Tran, 122	Pham Thi Thanh, 170
Nguyen Dang Co, 170	Pham Thi Thu Huong, 50
Nguyen Dang Phu, 134	Pham Van Thanh, 182, 192
Nguyen Dinh Nam, 203	Pham Van Thuan, 176
Nguyen Duc Cuong, 115	Phan Thi Thuy, 131, 135, 148
Nguyen Duy Phuong, 142	Phan Xuan Thien, 148

Phi Thi Huong, 50, 104, 149	Tahereh Sadat Parvini, 194
Phuc Dinh Dao, 180	Tahta Amrillah, 63
Phuong Hoai Nam Nguyen, 95	Taisei Takaoka, 165
Phuong Hoang Tran, 125	Takahiro Moriyama, 76
Phuong-Tung Nguyen, 122, 133	Takao Kotani, 119, 164
Q. Ngan Pham, 83	Takashi Kimura, 81
Quang Thuan Nguyen, 180	Takeshi Seki, 77
R. Ishikawa, 66, 156	Takuro Harada, 64
Ray-Hua Horng, 79	Takuya Takahashi, 64
Reisho Onodera, 163	Tan Le Hoang Doan, 117, 125, 146, 199
Ricardo Ferreira, 194	Tatsuaki Hirata, 118
Rie Y. Umetsu, 153, 159	Tatsuki Watanabe, 83
Rosalie Hocking, 116	Tatsumi Kawafuchi, 53
Ruey-Bin Yang, 99	Tatsuya Kawae, 64
Ryo Ishikawa, 51	Tatsuya Yokoi, 120
Ryo Kawarazaki, 76	Teruo Ono, 76
Ryohei Nishioka, 87	Tetsuya Fukushima, 112
Ryohei Oonaga, 161	Than Thi Nguyen, 110
Ryota Kobayashi, 151, 159	Thang Bach Phan, 146, 190
Ryusuke Hisatomi, 76	Thang Phan Bach, 199
S. C. Yu, 175	Thanh Binh Nguyen, 141
S. Chillal, 56	Thanh Huong Nguyen, 172
S. Fujii, 91	Thanh N. Pham, 98
S. Hartmann, 56	Thanh Tra Vu, 47
S. Kamiyama, 158	Thanh Tung Bui, 180
S. Miki, 66, 156	The Nam Dao, 138, 147
Sachiko Hiromoto, 144	The Thanh Luan Nguyen, 180
Sai Cong Doanh, 192	The-Long Phan, 126
Saikiran Kosame, 110	Thi BichNgoc Vu, 123
Scott A. Wade, 116	Thi Dieu Thuy Ung, 128
Sehwan Song, 65	Thi Ha Tran, 107, 141, 143, 185
Sena Hoshino, 120	Thi Hoa Hoang, 138
Seong-Cho Yu, 179	Thi Huong Giang Do, 95
SeoYul Lim, 188	Thi Huong Hue Hoang, 123, 128
Shin-Ichiro Kuroki, 118	Thi Huyen Trang Bui, 141
Shinpei Fujii, 165	Thi Kim Chi Tran, 128
Shiuan Huei Lin, 113	Thi Minh Thuy Nguyen, 123, 128
Shogo Kawaguchi, 162	Thi Ngoc Anh Mai, 187
Shuichi Okabe, 92	Thi Ngoc Anh Nguyen, 172
Shunsuke Yagi, 102, 155, 157	Thi Ngoc Anh Tran, 123
Singh Jitendra Pratap, 79	Thi Quynh XuanLe, 128
Sogo Asakura, 155	Thi Thanh Van Nguyen, 123
Sohwi Kim, 121	Thi Thao Vu, 95, 127, 136, 138, 147
Son Thanh Bach, 130	Thi Thu Hien Pham, 128
Ssu Kuan Wu, 47	Thi Thu Hoai Duong, 123
Stefan Petrov, 113	Thi Thu Thuy Bui, 136
Sungkyun Park, 65	Thi Thuong Huyen Tran, 123, 128
Sungmin Lee, 195	Thi Thuy Nguyen, 118
Surinder Singh, 116	Thi Thuy Quynh Tran, 145
SusumuFujii, 87	Thi-Lieu Nguyen, 122
Susumu Fujii, 197	Thi-Phuong Le, 122
T. Huong Nguyen, 83, 178	Tho Duc Nguyen, 82
T. L. Phan, 175	Thomas G. Pattison, 116
T. Nakamura, 158	Thong Nguyen-Minh Le, 199
T. Nishikubo, 158	Thu Le Thi Anh, 171
T. Watanabe, 156	Thuy Thi Phan, 130
T. Yokoi, 89	Tien Loi Do, 127
T.N. Anh Nguyen, 83, 178	Tien Quang Nguyen, 90, 112
Ta NgocBach, 137, 168	Tim Boehnert, 194

Toan Dang, 84	Vo T.T. Vi, 174
Toan Nguyen The, 199	Vu Dinh Lam, 177
Toan T. Nguyen, 46 Cancel	Vu Duong, 106
Tomofumi Hara, 87	Vu Hong Ky, 168
Tomoyuki Terai, 92	Vu Ngoc Tuoc, 200
Tomoyuki Yamamoto, 67, 144, 161, 181	Vu Nguyen Thuc, 176
Tran Anh Tuan, 203	Vu Thi Thao, 115
Tran Cong Than, 124	Vu Xuan Manh, 170, 191
Tran Doan Huan, 200	Vuong Van Hiep, 105, 173, 182
Tran Minh Duc, 195	W.-B. Wu, 178
Tran Nhu Chi, 134	Wang Wencong, 157
Tran P.T. Linh, 174	Wataru Norimatsu, 73
Tran Thi Hai, 78	Wataru Sekimoto, 87
Tran Thi Hong, 104	Way-Faung Pong, 62
Tran Thi Ngoc Anh, 173	Wen-Bin Jian, 108
Tran Van Hiep, 170, 191	Wilson Agerico Diño, 53
Tran VinhThang, 173	Woohyeon Ryu, 167
Trang Nguyen-Thuy, 199	Wu-Ching Chou, 47
Trang Thi Thu Nguyen, 125	Xuan Tung Nguyen, 95
Tri Duc Luong, 127	Y. Hamamoto, 98
Trinh Duc Chu, 196	Y. Morikawa, 98
Trung Thanh Le, 145	Y. Okazaki, 158
Truong Son Nguyen, 128	Y. Oshima, 89
Tsubasa Teramoto, 64	Y. Saito, 56
Tsutomu Miyasaka, 161	Y. Shimizu, 91
Tu Dinh Bui, 196	Y. Suzuki, 66, 156
Tuan Anh Le, 138	Y. Yamazaki, 91
Tuan Canh Nguyen, 95	Yee Sin Ang, 202
Tung Thanh Bui, 196	Yeeun Kim, 54
Tung-Han Wu, 108	Yeong-Ah Soh, 65
U. Tutsch, 56	Yoichi Shiota, 76
V. Thanh Chu, 83	Yoon-Hwae Hwang, 45
Van Cuong Giap, 172	Yoshifuru Mistui, 163
Van Dong Nguyen, 138	Yoshifuru Mitsui, 57, 151, 153, 159
Van Tan Tran, 107, 140, 141, 143, 185	Yoshifuru Mitui, 165
Van Thanh Pham, 123, 141, 143	Yoshishighe Suzuki, 83
Van-Duong Dao, 140	Youichi Yanase, 76
Van-Hai Dinh, 176	Yoyo Hinuma, 101
Van-Hiep Vuong, 126	Yu Miyazawa, 161
Van-Huong Tran, 127	Yu Oshima, 120
Van-Phu Vu, 97	Yuhei Ikeda, 76
Van-Toan Le, 133	Yuichi Okazaki, 102
Van-Tuan Hoang, 140	Yu-ichiro Matsushita, 103
Vera Marinova, 113	Yushi Fujita, 102
Viet Cuong Le, 150	Yusuke Nanba, 90
Viet Dung Nguyen, 145	Yusuke Nojima, 102
Viet Thanh Tung Bui, 138	Yuta Kato, 152, 160
Viet Tuyen Nguyen, 97, 107, 141, 143, 185	Yuta Kizawa, 160, 162
Vinh Cao Tran, 190	Yuta Miyasaka, 76
Vinh-Tan Do, 126	